Chemical properties of continental aerosol transported over the Southern Ocean : Patagonian and Namibian sources

Zihan Qu

Université Pierre et Marie Curie

Ecole doctorale 129 – Sciences de l'environnement de l'Ile-de-France

Laboratoire Inter-universitaire des Systèmes Atmosphériques (LISA) UMR 7583

CNRS UPD UPEC

Chemical properties of continental aerosol transported over the Southern Ocean: Patagonian and Namibian sources

Par Zihan QU

Thèse de doctorat de Géochimie

Dirigée par Rémi LOSNO et Émilie JOURNET

Présentée et soutenue publiquement le 25 Janvier 2016

Devant un jury composé de :

Président : Damien CARDINAL, Professeur, UPMC, LOCEAN

Rapporteur : Aloys BORY, Maître de Conférences, Univ. Lille 1, LOG

Rapporteur : Gaël LE ROUX, Chargé de recherche CNRS, EcoLab

Examinateur : Gilles BERGAMETTI, Directeur de recherche CNRS, LISA

Examinateur : Jérôme GAILLARDET, Professeur, UPD, IPGP

Directeur de thèse : Rémi LOSNO, Professeur, UPD, IPGP

Co-directrice de thèse : Émilie JOURNET, Maître de conférences, U-PEC, LISA

Remerciements

J'adresse mes premiers remerciements à Rémi LOSNO et Émilie JOURNET pour la direction de ma thèse pendant trois ans. Rémi LOSNO montre toujours sa confiance pendant les travaux de recherche, sa tolérance à nos arguments et parfois mes caprices, sa patience et ses encouragements pendant la direction rigoureuse. Émilie JOURNET, étant co-directrice de ma thèse, est toujours là en donnant ses conseils constructifs sur l'avancement de thèse et de rédaction d'article et de manuscrit.

Pendant toute ma thèse, j'ai été très heureux de connaitre Fabrice MONNA et Yves BALKANSKI qui ont fait partie de mes comités de thèse. En plus de ses conseils de déroulement de thèse, je voudrais remercier Fabrice pour sa formation en statistiques. Les discussions avec Fabrice étaient toujours détendues et agréables. Je remercie Yves BALKANSKI pour ses suggestions avec réflexions rigoureuses, ses stimulations et ses encouragements. Je remercie aussi Yann SIVRY pour son soutien pendant les trois ans. Yann pense toujours à plus long terme et me donne des conseils constructifs. Mes remerciements vont aussi à Gilles BERGAMTTI qui m'a donné également des suggestions qui me dirigent dans mes travaux.

De nombreux travaux ont été faits en collaboration internationale avec le CEILAP UMI CNRS-CONICET IFAECI, Argentine. Je voudrai remercier particulièrement Daniela BULNES, Lidia OTERO, Eduardo Jaime QUEL, Pablo RISTORI et Jacobo SALVADOR.

Je tiens aussi à remercier Jean Paul QUISEFIT pour sa formation et ses aides continues sur les mesures de SFX. Je remercie également la contribution d'Alexie HEIMBURGER. Sandra LAFON, je la remercie pour sa formation d'émission de poussière désertique, ainsi que ses soutiens continus sur mes missions d'enseignement à l'IUT. Depuis le master SGE, je suis très heureux de connaître Julie VINCENT qui reçoit également mes remerciements pour ses encouragements pour mes études, les recherches et le temps qu'on a travaillé ensemble. Pendant la thèse, j'ai rencontré beaucoup d'étudiants génials. À cette occassion, je voudrais remercier particulièrement Damien GUINOISEAUX, Jialan WANG, Zongling REN, Yasmine KOUHAIL, etc...

Pendant ma thèse, j'ai bénéficié des conditions de travail très avantageuses sous les aides sympathiques de Sylvain TRIQUET, Servane CHEVALLIER, et Elisabeth BON NGUYEN au LISA, et de Hassiba LAZAR, Laure CORDIER et Mickael THARAUD à l'IPGP. Je voudrais les remercier pour leurs soutiens à cette occasion.

Je voudrais remercier également Hervé LE TREU, Jean-Louis COLLIN et tous les autres membres du comité d'école, qui m'accueillirent en tant que doctorant à l'ED129. Je remercie Laurence TOUCHON qui m'a répondu toujours et m'a beaucoup aidé sur les affaires administratives. Je voudrais remercier Gilles BERGAMETTI à nouveau et Patrice COLL pour leur soutient continu au LISA et Marc BENEDETTI pour son accueil et ses soutiens à l'IPGP pendant ma thèse.

À cette occasion, je donne aussi mes remerciements à mes amis chinois Da HUO, Yujie QIAO, Siyu ZHANG, Haixiao LI, Yong AI, Xin GAO, etc... Je les remercie pour m'avoir accompagné pendants les années passées.

En final, je voudrai remercier du fond du cœur Mme Ha TRAN du LISA, qui m'a fait connaitre ma femme Yan TAN. Yan, je te remercie. Je te remercie pour ton soutient continu qui me calme et m'encourage dans la fin de thèse. La thèse est une période très heureuse en étant le début de la vie avec toi.

Financements ayant contribués à la thèse :

Le déroulement de cette thèse bénéfice en premier du contrat doctoral de l'École Doctorale 129, Université Pierret et Marie Curie, et puis le contrat de l'Institut de Physique du Globe de Paris (IPGP). Les travaux réalisés dans cette thèse ont été commencés avec le programme "**DFP**" (Dust From Patagonia, 2012 - 2015) financé par CNRS/INSU LEFE/CHAT et le programme "**Poussière de Patagonie**" de l'IDEX-SPC. Mon travail bénéfice aussi de financement du programme "**ASAR**" (ECOS-Sud) sous la collaboration internationale du CEILAP UMI CNRS-CONICET IFAECI à Buenos Aires, Argentine.

Table of content

Introduction

According to the recent IPCC assessment report AR5 of Working Group 1, the concentration of atmospheric CO_2, one of the most concerned greenhouse gases, continues increasing as predicted by different emission scenarios. Natural land and ocean sinks approximately remove 55% of the anthropogenic CO_2, and about half of the CO_2 uptake is realized by the ocean (IPCC, 2013). Atmospheric CO_2 is firstly absorbed by the ocean through the gas exchange and then converted into dissolved inorganic carbon (DIC) which includes carbonic acid, bicarbonate and carbonate ions in seawater (Raven and Falkowski, 1999; Sarmiento et al., 1992). This process is known as "solubility pump". Then the DIC can be transformed into organic materials with the "biological pump" (Chisholm and Morel, 1991; IPCC, 2013; Volk and Hoffert, 1985).

During primary production in the euphotic zone near the ocean surface, dissolved nutrients (e.g. NO^{3-}, PO^{4-}, $Si(OH)_4$, and micronutrients) and DIC are fixed into particulate organic materials (carbohydrates, lipids, and proteins) through photosynthesis of marine phytoplankton. After the formation of particulate organic carbon (POC) during primary production, the metabolic processes in the upper ocean remineralize the majority of POC and release CO_2 back into seawater. Some portion of POC, however, sinks out of the euphotic zone into deep water where the carbon is sequestrated for long term in deep waters and sediments (Honjo et al., 2008; De La Rocha and Passow, 2014). The biological pump transporting the carbon from the surface ocean to the deep ocean interior is a critical process to decrease the CO_2 concentration in surface seawater and consequently the concentration of CO_2 in the atmosphere (Archer and Jokulsdottir, 2014).

The consumption of DIC and macronutrients by phytoplankton in surface seawater is relatively fixed at a molar proportion of 106C : 16N : 1P, which is known as "Redfield Ratios" (Redfield, 1958; Redfield, 1934). Micronutrients such as Fe, Ca and Mn are indispensable as well to form enzymes, pigments and structural materials (De La Rocha and Passow, 2014). Since the biological pump is based on the photosynthesis of phytoplankton, the operation of biological pump is primarily limited by the availability of light and nutrients including macronutrients and micronutrients (Martin and Fitzwater, 1988; Martin et al., 1990; de Baar et al., 1995).

The subarctic north Pacific, the east equatorial Pacific, and the Southern Ocean are known as the three major High Nutrient Low Chlorophyll (HNLC) regions. The HNLC regions are characterized by high concentration of nitrate and low concentration of chlorophyll (Chisholm and Morel, 1991; Coale, 1991; de Baar et al., 1995; Boyd, 2002; Moore et al., 2001; Martin and Fitzwater, 1988). As shown in Figure 1, surface seawater in Southern Ocean has much higher concentrations of nitrate, as well as phosphate and silicate (World Ocean Atlas 2013) than in the North Atlantic Ocean, whereas the concentration of Chlorophyll in the Southern Ocean is relatively lower. Thus, considering the abundance of macronutrients in the HNLC Southern Ocean, the biological pump is not operating at its full capacity (De La Rocha and Passow, 2014).

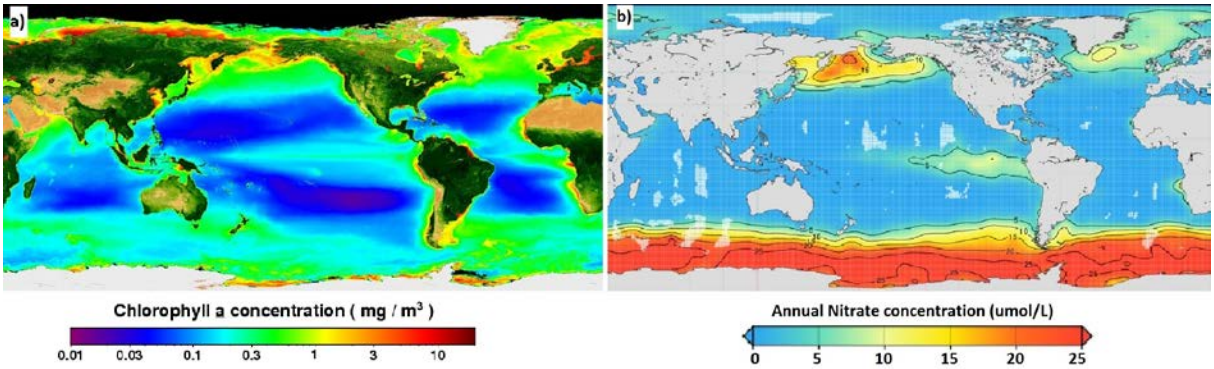

Figure 1 : a) Average chlorophyll *a* concentration in surface seawater; b) Annual nitrate concentration in surface seawater.

Source: a) NASA SeaWiFs, b) World Ocean Atlas 2013

Natural observations, numerous enrichment experiments and modeling studies indicated that the supply of micronutrients limits the primary production in Southern Ocean and other HNLC regions as well (Blain et al., 2007; Boyd et al., 2007; Boyd et al., 2000; Boyd, 2002; de Baar et al., 1995; Martin et al., 1990; Moore et al., 2001; Park et al., 2010; Takeda, 1998). For example, de Baar et al. (1995) observed that the upwelling of iron-rich deep waters in the southern branch of the Antarctic circumpolar current could sustain a moderate primary production while the iron-rich jet of the polar front induced a biomass production an order of magnitude stronger and trigger phytoplankton blooms. Kerguelen is an archipelago located in the center of the Southern Ocean. Supply of iron and major nutrients from iron-rich deep water to surface water sustains the phytoplankton bloom over the Kerguelen Plateau (Blain et al., 2007). After the proposition of “iron hypothesis”, Martin et al. (1990) conducted iron enrichment experiments in the incubation bottles with Antarctic

waters and found that the addition of iron promoted the uptake of nitrates. Coale (1991) demonstrated that additions of Cu, Mn, and Zn may also increase the marine biomass. In situ mesoscale iron addition experiments were then widely performed in the world ocean, such as the **IronEX** in the equatorial Pacific Ocean (Coale et al., 1998; Martin et al., 1994), the **SOIREE** (Southern Ocean Iron-RElease Experiment) in the Southern Ocean (Boyd et al., 2000; Boyd and Law, 2001), **SEEDS** (Subarctic Pacific iron Experiment for Ecosystem Dynamics Study) in the subarctic Pacific (Takeda and Tsuda, 2005). The **SOIREE** experiment added acidified $FeSO_4$ into the polar waters of the Southern Ocean and induced a phytoplankton bloom persisting more than 40 days and a ten percent drawdown of surface CO_2 (Boyd and Law, 2001; Boyd et al., 2000). These mesoscale iron enrichment experiments clearly demonstrate the limitation of primary production by iron supply and most of the experiments caused significant lowering of CO_2 concentration in surface waters (Boyd et al., 2007; Boyd et al., 2000; Watson et al., 2000). Overall, although the Southern Ocean has the highest concentration of unused surface macronutrients, the development of primary production in Southern Ocean is limited by the relatively insufficient supply of micronutrients such as Fe, Mn, etc (Coale, 1991; de Baar et al., 1995; Martin and Fitzwater, 1988; Morel et al., 1991).

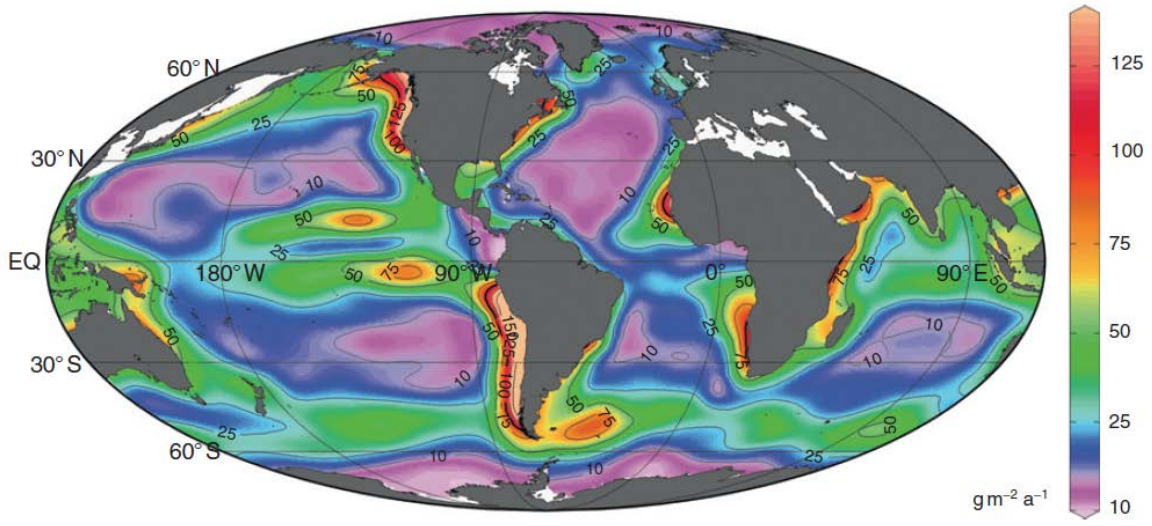

Figure 2 : Annual average export flux of particulate organic carbon (POC).
Source: modified from Schlitzer (2000) by Hüneke and Henrich (2011).

Despite the limitation of the biological pump by inadequate micronutrients supply, the Southern Ocean acts as a major sink of carbon dioxide (Takahashi et al., 2009; Arrigo et al.,

2008). Figure 2 illustrates a modeling result of the annual average export flux of particulate organic carbon in World Ocean (Schlitzer, 2000). The export flux of POC varies greatly with oceanic regions. At a global scale, the three HNLC regions including the Southern Ocean, the subarctic north Pacific and the east equatorial Pacific export substantial amount of POC. According to the modelling results, the Southern Ocean south of 30°S contributes more than 30% of the global particulate organic carbon to the ocean interior (Schlitzer, 2002), making the Southern Ocean an important carbon sink.

In natural conditions, three processes supply micronutrients to the surface seawater in the open ocean: 1) vertical advection from the deep ocean; 2) eddy diffusion induced transport from deep water; 3) atmospheric deposition of mineral aerosol (Duce and Tindale, 1991; de Baar et al., 1995). Both the contributions from deep waters and atmospheric deposition to natural fertilization vary with oceanic regions. In the Southern Ocean, upwelling of iron-rich deep waters leads to higher concentrations of chlorophyll in surface seawater in areas such as Antarctic coastal regions (de Baar et al., 1995) and Kerguelen Plateau (Blain et al., 2007), as shown in Figure 1. Higher concentration of chlorophyll could also be observed in downwind areas of the three continental regions (South America, Southern Africa and Australia) in the Southern Hemisphere (Figure 1), suggesting the biological impact of atmospheric deposition of mineral aerosol that originates from the three continental sources of Southern Hemisphere (Li et al., 2008). Mineral aerosols, also called dust, are emitted mainly from arid or semi-arid continental regions due to the wind-driven soil erosion. Mineral aerosols are mainly composed of aluminosilicate minerals and contain micronutrients such as Fe and Mn. Deposition of mineral aerosol into seawater hence deliver the micronutrients to marine ecosystem. Tagliabue et al. (2014) calculated the iron input to surface ocean from deep water (9.5~33.2 $\mu mol.m^{-2}.yr^{-1}$) in regions of Southern Ocean far from the landmass. By comparing this result to the deposition flux, which is far below 20 $\mu mol.m^{-2}.yr^{-1}$, measured indirectly by Wagener et al. (2008), Tagliabue et al. (2014) stated that the iron input from deep water is much higher than iron deposition. However, more recent studies (Heimburger et al. 2012, Chance et al., 2015; Grand et al., 2015) demonstrated that the computation of deposition flux by Wagener et al. (2008) based on short-term shipboard aerosol concentration measurements seriously underestimated the atmospheric deposition flux of mineral aerosol, which should be more than one order of magnitude higher for marine ecosystem in the South Atlantic and west Southern Indian Ocean. Although further studies are required to determine the input of micronutrients from deep waters and atmospheric deposition, mineral aerosol deposition

appears to be an important source of micronutrients for remote marine ecosystems in the South Atlantic and southern Indian Ocean. Furthermore, considering the extensive surface area of Southern Ocean and the large inventory of unused macronutrients, the atmospheric mineral aerosol deposition can disproportionately enhance the primary production in the Southern Ocean (Mahowald et al., 2005; Boyd et al., 2007).

Emission inventories of trace elements from mineral aerosol source regions depend on the emission inventory and elemental composition of mineral aerosol (Zhang et al., 2015). After deposition into the seawater, only a fraction of mineral particles is bioavailable and could be ultimately assimilated by phytoplankton. Assessment of bioavailability of trace elements in mineral aerosol is hence indispensable to evaluate the supply of bioavailable micronutrients to marine ecosystem.

In the past two decades, numerous modeling studies have been carried out to quantify the contribution of mineral aerosol from dust source regions to the Southern Ocean. For example, modeling study of Li et al. (2008) focused on the Southern Ocean and provided for the first time substantial information about the dust emission and deposition inventories. Johnson et al. (2010) modeled the outflow of mineral aerosol from Patagonia (South America) to the South Atlantic Ocean. However, field measurements of mineral aerosol concentration in source regions, which are important to compare and calibrate dust models (Cakmur et al., 2006; Li et al., 2008), are poorly conducted in subantarctic region. The measurements in Cape Grim conducted in 1990s is the only data available closing source areas in the Southern Hemisphere and were widely adapted in previous modeling studies. Respecting to the important role of Southern Ocean in global biogeochemical cycle, more field measurements closing source areas are strongly required to fulfill the necessity of model calibration in order to better quantify the emission inventory of mineral aerosol in the Southern Ocean.

To quantify the emission inventories of micronutrients associated with mineral aerosol, knowledge about the elemental composition of aerosol is indispensable. In a modelling study, Zhang et al. (2015) determined the elemental composition based on a global mineral data set and a soil data set to quantify the emission of micronutrients. This method disregards the large variability of elemental composition within each mineral and within each soil type, as clarified by the authors. Measurements of the elemental composition of mineral aerosol will be useful to better quantify the emission of micronutrients, especially when a larger dataset is available.

Similar to concentration and elemental composition of mineral aerosol, bioavailability of mineral aerosol in source regions of subantarctic regions was rarely studied. Previous measurements in this region have focused on the transported aerosol or depositions (e.g. Baker et al., 2006; Heimburger et al., 2013; Winton et al., 2015). Zhang et al. (2015) estimated the solubility, as a proxy of bioavailability, based on the global mineral data set and solubility previously measured on pure minerals. Hence, measurements of bioavailability on aerosol in source regions not only complete and improve our understanding on the bioavailability of mineral aerosol in Southern Ocean but also provide the opportunity to quantify the emission inventories of bioavailable micronutrients through dust modeling studies.

The object of this thesis is to investigate the relevant characteristics of the mineral aerosols from source regions in subantarctic regions, including the atmospheric concentration, the factors controlling the emission, the chemical composition, and the bioavailability of mineral aerosol.

In the following chapters, Chapter 1 will present our current understanding on the dust cycle in Southern Ocean and the chemical properties of dust including elemental composition and elemental solubility that will affect the bioavailability of dust. Chapters from 2 to 4 present three parts of work in this thesis with a focus on Patagonia and Namibia. Each chapter introduces in detail the experimental methodology adapted, the results obtained and the discussion developed. The main contents of each chapter are presented under the form of article draft with supplementary information, allowing reading separately each research topics with complete information in this PhD work. Chapters from 2 to 4 will introduce the three topics following the structure below:

- Chapter 2 presents a continuous aerosol sampling study from November 2011 to August 2014 in Río Gallegos, southern Patagonia. A time series of atmospheric dust concentration is obtained and the regulation mechanism resulting in the temporal pattern is discussed.
- Chapter 3 presents our investigation into the spatial variability of source dust elemental compositions in Patagonia and Namibia. This part of work contributes directly to the database of elemental composition in source areas.

- Chapter 4 presents the elemental solubility measurements on source dust. Study of solubility helps to estimate the potential bioavailability of trace elements for the marine ecosystem in open-ocean.

Chapter 5 "Conclusions and Prospects" firstly restates the different research aspects of this work. Results and conclusions previously obtained are then integrated to discuss further implications of our research finds in the frame of dust biogeochemical cycles. The section of prospect discusses firstly the shortness of our research. With respect to the results and conclusions, future research needs and recommendations are proposed at the end of Chapter.

Bibliography

Archer, D., and Jokulsdottir, T.: 8.10 - Biological Fluxes in the Ocean and Atmospheric pCO2, in: Treatise on Geochemistry (Second Edition), edited by: Turekian, H. D. H. K., Elsevier, Oxford, 281-292, 2014.

Arrigo, K. R., van Dijken, G., and Long, M.: Coastal Southern Ocean: A strong anthropogenic CO2 sink, Geophysical Research Letters, 35, L21602, 10.1029/2008GL035624, 2008.

Baker, A. R., Jickells, T. D., Witt, M., and Linge, K. L.: Trends in the solubility of iron, aluminium, manganese and phosphorus in aerosol collected over the Atlantic Ocean, Marine Chemistry, 98, 43-58, 10.1016/j.marchem.2005.06.004, 2006.

Blain, S., Quéguiner, B., Armand, L., Belviso, S., Bombled, B., Bopp, L., Bowie, A., Brunet, C., Brussaard, C., Carlotti, F., Christaki, U., Corbière, A., Durand, I., Ebersbach, F., Fuda, J.-L., Garcia, N., Gerringa, L., Griffiths, B., Guigue, C., Guillerm, C., Jacquet, S., Jeandel, C., Laan, P., Lefèvre, D., Lo Monaco, C., Malits, A., Mosseri, J., Obernosterer, I., Park, Y.-H., Picheral, M., Pondaven, P., Remenyi, T., Sandroni, V., Sarthou, G., Savoye, N., Scouarnec, L., Souhaut, M., Thuiller, D., Timmermans, K., Trull, T., Uitz, J., van Beek, P., Veldhuis, M., Vincent, D., Viollier, E., Vong, L., and Wagener, T.: Effect of natural iron fertilization on carbon sequestration in the Southern Ocean, Nature, 446, 1070-1074, 10.1038/nature05700, 2007.

Boyd, P. W., Watson, A. J., Law, C. S., Abraham, E. R., Trull, T., Murdoch, R., Bakker, D. C. E., Bowie, A. R., Buesseler, K. O., Chang, H., Charette, M., Croot, P., Downing, K., Frew, R., Gall, M., Hadfield, M., Hall, J., Harvey, M., Jameson, G., LaRoche, J., Liddicoat, M., Ling, R., Maldonado, M. T., McKay, R. M., Nodder, S., Pickmere, S., Pridmore, R., Rintoul, S., Safi, K., Sutton, P., Strzepek, R., Tanneberger, K., Turner, S., Waite, A., and Zeldis, J.: A mesoscale phytoplankton bloom in the polar Southern Ocean stimulated by iron fertilization, Nature, 407, 695-702, 10.1038/35037500, 2000.

Boyd, P. W., and Law, C. S.: The Southern Ocean Iron RElease Experiment (SOIREE)—introduction and summary, Deep Sea Research Part II: Topical Studies in Oceanography, 48, 2425-2438, http://dx.doi.org/10.1016/S0967-0645(01)00002-9, 2001.

Boyd, P. W.: The role of iron in the biogeochemistry of the Southern Ocean and equatorial Pacific: a comparison of in situ iron enrichments, Deep Sea Research Part II: Topical Studies in Oceanography, 49, 1803-1821, 10.1016/S0967-0645(02)00013-9, 2002.

Boyd, P. W., Jickells, T., Law, C. S., Blain, S., Boyle, E. A., Buesseler, K. O., Coale, K. H., Cullen, J. J., Baar, H. J. W. d., Follows, M., Harvey, M., Lancelot, C., Levasseur, M., Owens, N. P. J., Pollard, R., Rivkin, R. B., Sarmiento, J., Schoemann, V., Smetacek, V., Takeda, S., Tsuda, A.,

Turner, S., and Watson, A. J.: Mesoscale Iron Enrichment Experiments 1993-2005: Synthesis and Future Directions, Science, 315, 612-617, 10.1126/science.1131669, 2007.

Cakmur, R. V., Miller, R. L., Perlwitz, J., Geogdzhayev, I. V., Ginoux, P., Koch, D., Kohfeld, K. E., Tegen, I., and Zender, C. S.: Constraining the magnitude of the global dust cycle by minimizing the difference between a model and observations, Journal of Geophysical Research: Atmospheres, 111, n/a-n/a, 10.1029/2005JD005791, 2006.

Chance, R., Jickells, T. D., and Baker, A. R.: Atmospheric trace metal concentrations, solubility and deposition fluxes in remote marine air over the south-east Atlantic, Marine Chemistry, http://dx.doi.org/10.1016/j.marchem.2015.06.028, 2015.

Chisholm, S. W., and Morel, F. M. M.: What controls phytoplankton production in nutrient-rich areas of the open sea?, American Society of Limnology and Oceanography Symposium, 22-24 February 1991, San Marcos, California, Preface, Limnology and Oceanography, 36, U1507-U1511, 1991.

Coale, K. H.: Effects of Iron, Manganese, Copper, and Zinc Enrichments on Productivity and Biomass in the Subarctic Pacific, Limnology and Oceanography, 36, 1851-1864, 10.2307/2837719, 1991.

Coale, K. H., Johnson, K. S., Fitzwater, S. E., Blain, S. P. G., Stanton, T. P., and Coley, T. L.: IronEx-I, an in situ iron-enrichment experiment: Experimental design, implementation and results, Deep Sea Research Part II: Topical Studies in Oceanography, 45, 919-945, http://dx.doi.org/10.1016/S0967-0645(98)00019-8, 1998.

de Baar, H. J. W., de Jong, J. T. M., Bakker, D. C. E., Löscher, B. M., Veth, C., Bathmann, U., and Smetacek, V.: Importance of iron for plankton blooms and carbon dioxide drawdown in the Southern Ocean, Nature, 373, 412-415, 10.1038/373412a0, 1995.

De La Rocha, C. L., and Passow, U.: 8.4 - The Biological Pump, in: Treatise on Geochemistry (Second Edition), edited by: Turekian, H. D. H. K., Elsevier, Oxford, 93-122, 2014.

Duce, R. A., and Tindale, N. W.: Atmospheric transport of iron and its deposition in the ocean, Limnology and Oceanography, 36, 1715-1726, 10.4319/lo.1991.36.8.1715, 1991.

Grand, M. M., Measures, C. I., Hatta, M., Hiscock, W. T., Buck, C. S., and Landing, W. M.: Dust deposition in the eastern Indian Ocean: The ocean perspective from Antarctica to the Bay of Bengal, Global Biogeochemical Cycles, 29, 357-374, 10.1002/2014GB004898, 2015.

Hüneke, H., and Henrich, R.: Chapter 4 - Pelagic Sedimentation in Modern and Ancient Oceans, in: Developments in Sedimentology, edited by: Heiko, H., and Thierry, M., Elsevier, 215-351, 2011.

Heimburger, A., Losno, R., Triquet, S., Dulac, F., and Mahowald, N.: Direct measurements of atmospheric iron, cobalt, and aluminum-derived dust deposition at Kerguelen Islands, Global Biogeochemical Cycles, 26, GB4016, 10.1029/2012GB004301, 2012.

Heimburger, A., Losno, R., and Triquet, S.: Solubility of iron and other trace elements in rainwater collected on the Kerguelen Islands (South Indian Ocean), Biogeosciences, 10, 6617-6628, 10.5194/bg-10-6617-2013, 2013.

Honjo, S., Manganini, S. J., Krishfield, R. A., and Francois, R.: Particulate organic carbon fluxes to the ocean interior and factors controlling the biological pump: A synthesis of global sediment trap programs since 1983, Progress in Oceanography, 76, 217-285, http://dx.doi.org/10.1016/j.pocean.2007.11.003, 2008.

IPCC: Climate Change 2013: The Physical Science Basis. Contribution of Working Group I to the Fifth Assessment Report of the Intergovernmental Panel on Climate Change, Cambridge University Press, Cambridge, United Kingdom and New York, NY, USA, 1535 pp., 2013.

Johnson, M. S., Meskhidze, N., Solmon, F., Gassó, S., Chuang, P. Y., Gaiero, D. M., Yantosca, R. M., Wu, S., Wang, Y., and Carouge, C.: Modeling dust and soluble iron deposition to the South Atlantic Ocean, Journal of Geophysical Research: Atmospheres, 115, D15202, 10.1029/2009JD013311, 2010.

Li, F., Ginoux, P., and Ramaswamy, V.: Distribution, transport, and deposition of mineral dust in the Southern Ocean and Antarctica: Contribution of major sources, Journal of Geophysical Research: Atmospheres, 113, 10.1029/2007JD009190, 2008.

Mahowald, N. M., Baker, A. R., Bergametti, G., Brooks, N., Duce, R. A., Jickells, T. D., Kubilay, N., Prospero, J. M., and Tegen, I.: Atmospheric global dust cycle and iron inputs to the ocean, Global Biogeochemical Cycles, 19, GB4025, 10.1029/2004GB002402, 2005.

Martin, J. H., and Fitzwater, S. E.: Iron deficiency limits phytoplankton growth in the north-east Pacific subarctic, Nature, 331, 341-343, 1988.

Martin, J. H.: Glacial-interglacial CO2 change: The Iron Hypothesis, Paleoceanography, 5, 1–13, 10.1029/PA005i001p00001, 1990.

Martin, J. H., Fitzwater, S. E., and Gordon, R. M.: Iron deficiency limits phytoplankton growth in Antarctic waters, Global Biogeochemical Cycles, 4, 5-12, 10.1029/GB004i001p00005, 1990.

Martin, J. H., Coale, K. H., Johnson, K. S., Fitzwater, S. E., Gordon, R. M., Tanner, S. J., Hunter, C. N., Elrod, V. A., Nowicki, J. L., Coley, T. L., Barber, R. T., Lindley, S., Watson, A. J., Van Scoy, K., Law, C. S., Liddicoat, M. I., Ling, R., Stanton, T., Stockel, J., Collins, C., Anderson, A., Bidigare, R., Ondrusek, M., Latasa, M., Millero, F. J., Lee, K., Yao, W., Zhang, J. Z., Friederich, G., Sakamoto, C., Chavez, F., Buck, K., Kolber, Z., Greene, R., Falkowski, P., Chisholm, S. W., Hoge, F., Swift, R., Yungel, J., Turner, S., Nightingale, P., Hatton, A., Liss, P., and Tindale, N. W.: Testing the iron hypothesis in ecosystems of the equatorial Pacific Ocean, Nature, 371, 123-129, 1994.

Moore, J. K., Doney, S. C., Glover, D. M., and Fung, I. Y.: Iron cycling and nutrient-limitation patterns in surface waters of the World Ocean, Deep Sea Research Part II: Topical Studies in Oceanography, 49, 463-507, http://dx.doi.org/10.1016/S0967-0645(01)00109-6, 2001.

Morel, F. M. M., Hudson, R. J. M., and Price, N. M.: Limitation of Productivity by Trace Metals in the Sea, Limnology and Oceanography, 36, 1742-1755, 10.2307/2837711, 1991.

Park, J., Oh, I.-S., Kim, H.-C., and Yoo, S.: Variability of SeaWiFs chlorophyll-a in the southwest Atlantic sector of the Southern Ocean: Strong topographic effects and weak seasonality, Deep Sea Research Part I: Oceanographic Research Papers, 57, 604-620, http://dx.doi.org/10.1016/j.dsr.2010.01.004, 2010.

Raven, J. A., and Falkowski, P. G.: Oceanic sinks for atmospheric CO2, Plant, Cell & Environment, 22, 741-755, 10.1046/j.1365-3040.1999.00419.x, 1999.

Redfield, A. C.: On the proportions of organic derivatives in sea water and their relation to the composition of plankton, University Press of Liverpool, Liverpool, UK, 1934.

Redfield, A. C.: THE BIOLOGICAL CONTROL OF CHEMICAL FACTORS IN THE ENVIRONMENT, American Scientist, 46, 230A-221, 10.2307/27827150, 1958.

Sarmiento, J. L., Orr, J. C., and Siegenthaler, U.: A perturbation simulation of CO2 uptake in an ocean general circulation model, Journal of Geophysical Research: Oceans (1978–2012), 97, 3621-3645, 1992.

Schlitzer, R.: Applying the adjoint method for biogeochemical modeling: Export of particulate organic matter in the world ocean, in: Inverse Methods in Global Biogeochemical Cycles, edited by: Kasibhatla, P., Heimann, M., Rayner, P., Mahowald, N., Prinn, R. G., and Hartley, D. E., Geophysical Monograph Series, Amer Geophysical Union, Washington, 107-124, 2000.

Schlitzer, R.: Carbon export fluxes in the Southern Ocean: results from inverse modeling and comparison with satellite-based estimates, Deep Sea Research Part II: Topical Studies in Oceanography, 49, 1623-1644, 10.1016/S0967-0645(02)00004-8, 2002.

Tagliabue, A., Sallee, J.-B., Bowie, A. R., Levy, M., Swart, S., and Boyd, P. W.: Surface-water iron supplies in the Southern Ocean sustained by deep winter mixing, Nature Geosci, 7, 314-320, 10.1038/ngeo2101

http://www.nature.com/ngeo/journal/v7/n4/abs/ngeo2101.html#supplementary-information, 2014.

Takahashi, T., Sutherland, S. C., Wanninkhof, R., Sweeney, C., Feely, R. A., Chipman, D. W., Hales, B., Friederich, G., Chavez, F., Sabine, C., Watson, A., Bakker, D. C. E., Schuster, U., Metzl, N., Yoshikawa-Inoue, H., Ishii, M., Midorikawa, T., Nojiri, Y., Körtzinger, A., Steinhoff, T., Hoppema, M., Olafsson, J., Arnarson, T. S., Tilbrook, B., Johannessen, T., Olsen, A., Bellerby, R., Wong, C. S., Delille, B., Bates, N. R., and de Baar, H. J. W.: Climatological mean and decadal

change in surface ocean pCO2, and net sea–air CO2 flux over the global oceans, Deep Sea Research Part II: Topical Studies in Oceanography, 56, 554-577, http://dx.doi.org/10.1016/j.dsr2.2008.12.009, 2009.

Takeda, S.: Influence of iron availability on nutrient consumption ratio of diatoms in oceanic waters, Nature, 393, 774-777, 10.1038/31674, 1998.

Takeda, S., and Tsuda, A.: An in situ iron-enrichment experiment in the western subarctic Pacific (SEEDS): Introduction and summary, Progress in Oceanography, 64, 95-109, http://dx.doi.org/10.1016/j.pocean.2005.02.004, 2005.

Volk, T., and Hoffert, M. I.: Ocean Carbon Pumps: Analysis of Relative Strengths and Efficiencies in Ocean-Driven Atmospheric CO2 Changes, in: The Carbon Cycle and Atmospheric CO2: Natural Variations Archean to Present, American Geophysical Union, 99-110, 1985.

Wagener, T., Guieu, C., Losno, R., Bonnet, S., and Mahowald, N.: Revisiting atmospheric dust export to the Southern Hemisphere ocean: Biogeochemical implications, Global Biogeochemical Cycles, 22, GB2006, 10.1029/2007GB002984, 2008.

Watson, A. J., Bakker, D. C. E., Ridgwell, A. J., Boyd, P. W., and Law, C. S.: Effect of iron supply on Southern Ocean CO2 uptake and implications for glacial atmospheric CO2, Nature, 407, 730-733, 10.1038/35037561, 2000.

Winton, V. H. L., Bowie, A. R., Edwards, R., Keywood, M., Townsend, A. T., van der Merwe, P., and Bollhöfer, A.: Fractional iron solubility of atmospheric iron inputs to the Southern Ocean, Marine Chemistry, 10.1016/j.marchem.2015.06.006, 2015.

Zhang, Y., Mahowald, N., Scanza, R. A., Journet, E., Desboeufs, K., Albani, S., Kok, J. F., Zhuang, G., Chen, Y., Cohen, D. D., Paytan, A., Patey, M. D., Achterberg, E. P., Engelbrecht, J. P., and Fomba, K. W.: Modeling the global emission, transport and deposition of trace elements associated with mineral dust, Biogeosciences, 12, 5771-5792, 10.5194/bg-12-5771-2015, 2015.

Chapter 1 Background, Significance and Approaches of Research

Evaluation of the impact of mineral aerosol (or "dust") on the marine ecosystem requires a good knowledge about the dust cycle from emission to deposition and about the ultimate bioavailability of micronutrients after deposition into seawater. In this chapter, Section 1 will briefly introduce the emission mechanisms of dust and the factors affecting the emission process. Section 2 presents our current understanding on the dust cycle in the Southern Ocean from emission to deposition. Section 3 will discuss chemical properties of dust including the elemental composition and solubility that could affect the role of mineral dust as micronutrients supplier. In the Section 4, we will elaborate the questions we face for the moment and present the research strategies we have taken to improve our understanding on the supply of bioavailable micronutrients by atmospheric dust from continental sources to the Southern Ocean. Section 5 will introduce the content of following chapters.

1. Dust Emission processes

Mineral dust is emitted from soil surface by the aeolian erosion in arid or semiarid regions. Emission of mineral dust from soil surface to atmosphere could be driven by three modes (Figure 3): direct aerodynamic resuspension (Sweeney and Mason, 2013; Macpherson et al., 2008; Kjelgaard et al., 2004; Loosmore and Hunt, 2000), saltation bombardment, and aggregates disaggregation (Shao, 2008; Shao et al., 1993; Gomes et al., 1990). Under the concept of direct aerodynamic resuspension, dust particles are lifted directly from the surface by aerodynamic forces. However, for particles smaller than 20 μm, the cohesive force becomes more important and inhibits the direct resuspension of particles (Shao, 2008). Hence, dust emission due to the aerodynamic direct resuspension is generally occurred in low-magnitude but is highly frequent (Lee and Tchakerian, 1995). When the wind stress exceeds a minimum friction velocity that is known as the "threshold friction velocity", soil particles could be driven in saltation. The collision between the saltating particles and soil surface induces disaggregation of saltating soil aggregates and dust coating on saltating sand particles, or leads to dust emission by breaking the bindings between dust particles of soil surface (Gillette, 1981; Gomes et al., 1990; Shao et al., 1993). The former phenomenon is known as "disaggregation" mechanism and the later is known as "saltation bombardment" (or

"sandblasting"). Size of dust particles over the source regions generally varies from ~0.1 to 200 µm diameter with three lognormal modes. The first mode is large particles between 20-200 µm preexisting in soil. Particles in the second mode correspond to particles within 2-20 µm under the form of aggregate. The third mode is submicron mode, which is maximum in number distribution and is produced under more energetic condition (Alfaro et al., 1997; Gomes et al., 1990).

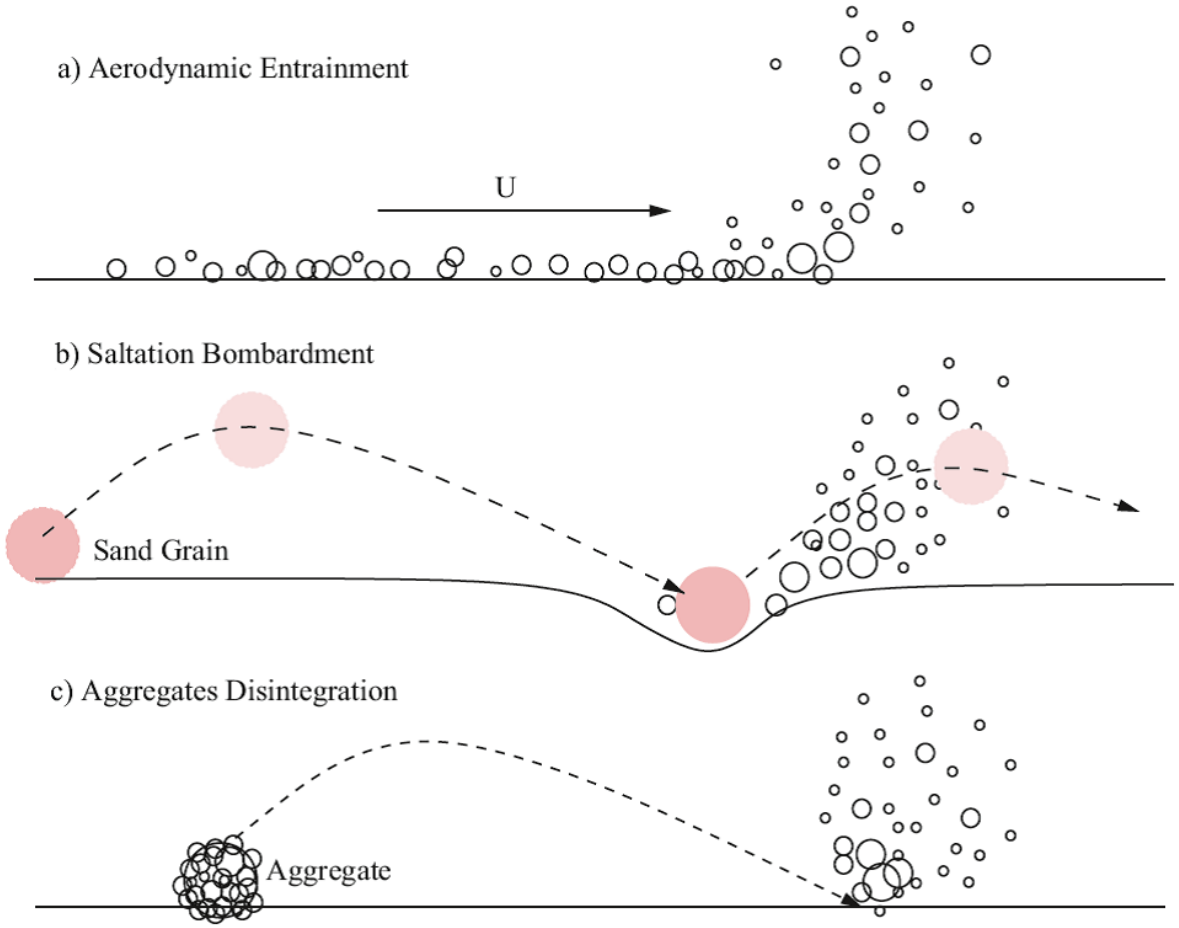

Figure 3 : Dust emission a) by direct aerodynamic resuspension, b) by saltation bombardment, and c) by aggregates disintegration.

Source: Figure 7.5 in Shao (2008)

The complex processes of dust emission depends on multiple environmental factor, such as the wind stress, the presence of non-erodible elements like vegetation and rocks, surface roughness, soil texture, soil moisture, soil mineralogy, and aggregate structure of surface soil (Gillette, 1978; Gillette, 1979). In modeling studies, dust emission flux depends generally on the wind friction velocity (Marticorena and Bergametti, 1995; Shao et al., 1993). The presence of non-erodible elements decreases the dust production by preventing the soil

surface from wind erosion and attenuating the wind momentum (Marticorena and Bergametti, 1995; Gillette, 1979). Soil texture classifies the soil particles according to the particle size distribution, and controls the availability of dust particles that are dominated by particles in clay fraction (diameter < 2 μm) and silt fraction (2~50 μm). Particles in very coarse fraction (1.0~2.0 mm) and gravel fraction (> 2 mm) are too large to be set in motion by wind. Soil containing less sand (50~1000 μm), and larger soil aggregates exhibits relatively higher threshold friction velocity (Gillette et al., 1980). Depending on the soil composition and soil texture, mineral particles can combine with organic and inorganic materials to form an aggregate structure with pore space. The soil aggregate structure strongly influences the resistance to wind erosion (Singer and Shainberg, 2004). The resistance to disruption of soil aggregates depends on the soil physical conditions such as soil moisture, aging history and chemical composition (Bronick and Lal, 2005). For example, different types of clay response differently to wetting and drying cycles, clay particles can separate from other particles during swelling and distribute more uniformly over the sand grains (Singer et al., 1992). Higher soil moisture may strengthen the cohesion forces between the soil particles with water content, thus increases the threshold velocity (Gillette et al., 1982; Ishizuka et al., 2008; Kim and Choi, 2015).

Overall, dust emission is a highly complex process controlled by a series of environmental factors, resulting high variability of dust emission in both spatial and temporal scales (Mahowald et al., 2005).

2. Sources, Transport and Deposition of Mineral Dust to the Southern Ocean

2.1. Distribution and contribution of dust sources in the Southern Ocean

2.1.1. Distribution of dust sources

Dust sources generally include desert or semi-arid desert areas, ephemeral dry lake or riverbeds, and human-disturbed land surfaces (Mahowald et al., 2003; Ginoux et al., 2012; Prospero et al., 2002). As shown in Figure 4, major dust sources in global scale are located in the following regions (Ginoux et al., 2012; Prospero et al., 2002; Li et al., 2008):

1. **North Africa**, such as Tunisia, Northeast Algeria, Eastern Libyan Desert, Egypt, Sudan, Niger, Lake Chad Basin;

2. **Middle East**, such as Arabian Peninsula;

3. **Asia**, such as Gobi desert, Tarim Basin and Takla Makan desert in China, Indian subcontinent, Pakistan Basins;

4. **North America**, such as Mojave desert in western United States;

5. **Australia**, such as the region around the Lake Eyre Basin;

6. **Southern Africa**, such as Makgadikgadi depression and pans in Botswana, Etosha pan in Namibia;

7. **South America**, including Patagonia desert, Bolivian Altiplano.

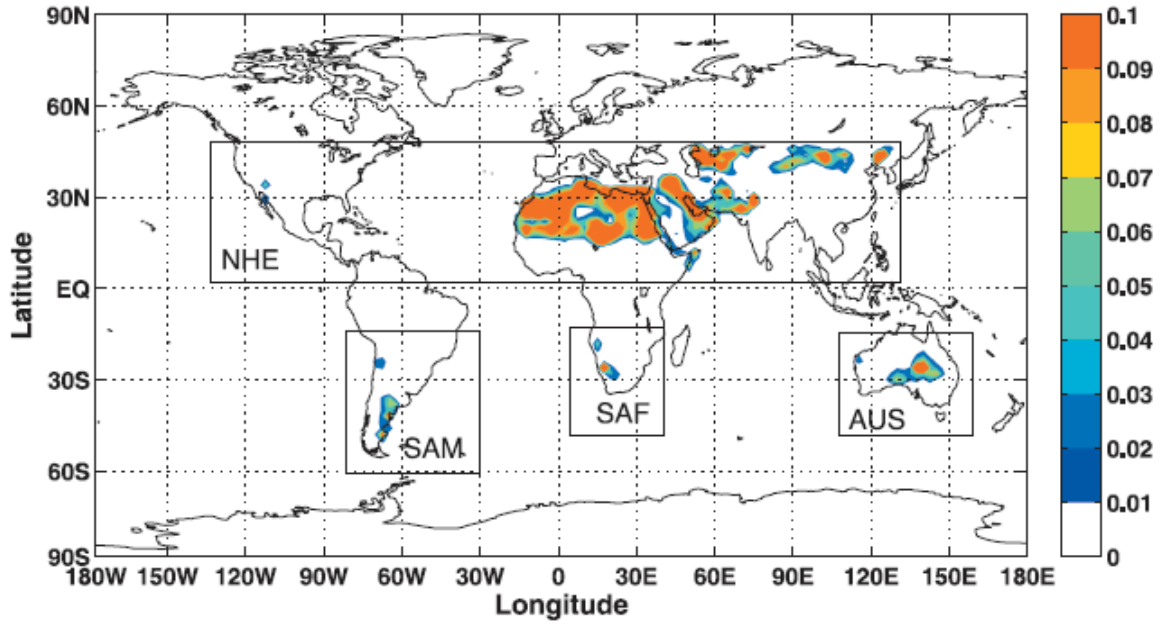

Figure 4 : Modeled average global distribution of annual dust emission (unit: $kg.m^{-2}.a^{-1}$) over 20 years from 1979 to 1998. Source: Figure 2 in Li et al. (2008)

Comparing to the dust sources in Northern Hemisphere, Southern Hemisphere sources are much smaller. According to the model-based estimations of Ginoux et al. (2004) and Li et al. (2008), North Africa and Asia contributes 65% and 25% of the global emission, respectively, whereas the Southern Hemisphere contributes only 10% of total dust emission.

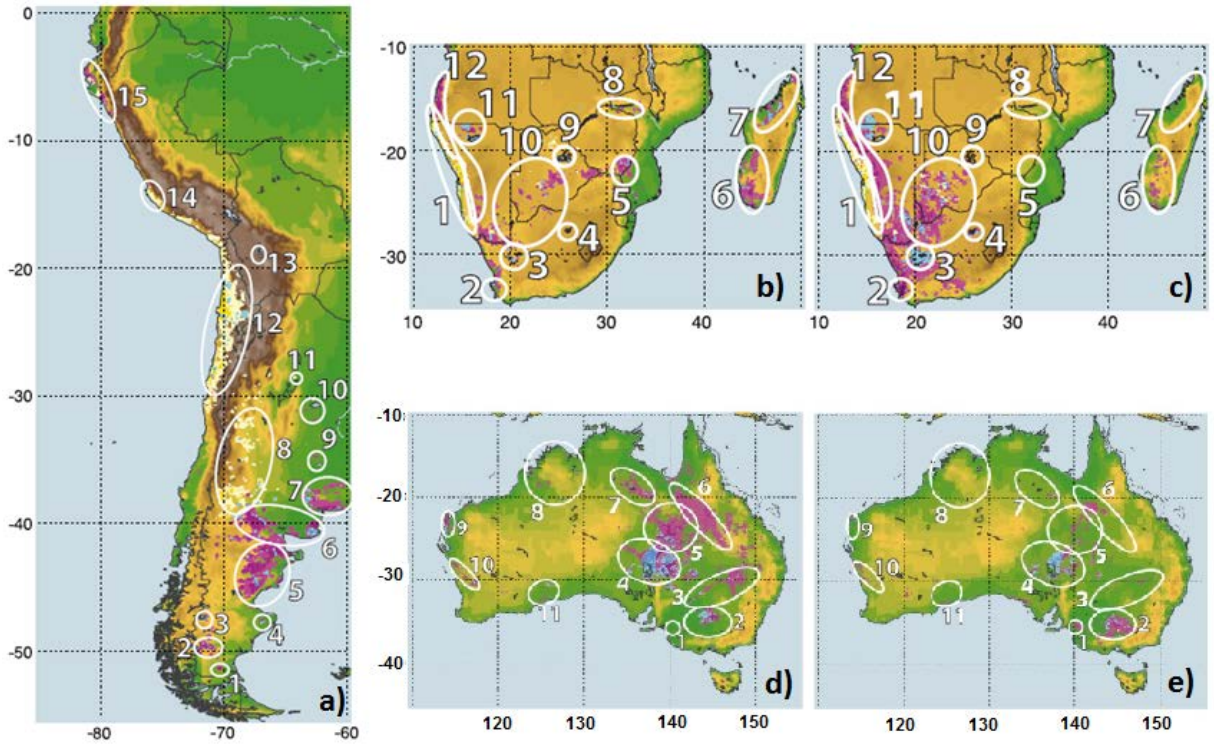

Figure 5 : Potential dust sources estimated based on MODIS Deep Blue product in a) summer (December, January, and February) in the South America; b) spring (September, October, and November) in the Southern Africa; c) summer in the Southern Africa; d) spring in the Australia; e) summer in the Australia. Source: combined with Figures 12, 13, and 14 in Ginoux et al. (2012).

In Southern Hemisphere, Southern America, Southern Africa and Australia are the three continental regions providing mineral dust deposited to the Southern Ocean. Both the global satellite data analysis of Prospero et al. (2002) and Ginoux et al. (2012) have studied the distribution of dust sources in the Southern Hemisphere. Prospero et al. (2002) used Total Ozone Mapping Spectrometer (TOMS) data to retrieve dusty days, while the study of Ginoux et al. (2012) was based on MODerate resolution Imaging Spectroradiometer (MODIS) Deep Blue aerosol products. Given that the a major uncertainty of TOMS retrivals is the sub-pixel contamination by cloud (Torres et al., 2002), the identification of dust sources in the cloudy Southern Hemisphere is particularly difficult when using TOMS data. The MODIS deep blue retrievals used by Ginoux et al. (2012) may better investigate the global dust sources distribution and also provide higher resolutions in small-scale features. Figure 5 illustrates the distribution of dust sources, as well as seasonal variability if available, in the three continental regions of Southern Hemisphere identified by Ginoux et al. (2012) based on MODIS deep blue data.

South America

Figure 5a illustrates the identified dust sources in the South America. Although in the paper of Ginoux et al. (2012) only results in austral summer were available for South America, identified source regions are in agreement with the modeling simulation of Li et al. (2008). Main dust sources in South America include four regions: the Patagonia Desert (locations 1~8 in Figure 5 a), the western Argentina (part of location 8), the Atacama Desert of Chile (location 12) and the Bolivian Altiplano (location 13). Modeling study of Johnson et al. (2010) captured most source regions except the Bolivian Altiplano. Dust sources in South America are generally associated with river basins, glacial activities and salt lakes (Ginoux et al., 2012; Prospero et al., 2002). For example, in Patagonia, dust sources in locations 1 and 4~6 are associated with river basins. Locations 2 and 3 are linked to glacial lakes.

Patagonia accounts for more than 70% of the total dust emission from South America according to the model simulation of Li et al. (2008). Johnson et al. (2010) even estimated that 95% of South American mineral dust originates from Patagonia. Gaiero et al. (2003) measured the dust deposition flux at three coastal sites (latitudes 38°S, 43°S and 45°S) in north and central Patagonia and found different seasonal patterns of dust fallout. Generally, dust activity in Patagonia is more frequent in summer, although some dust events are observed in winter, as confirmed by the modeling study of Johnson et al. (2010).

Southern Africa

Dust sources in Southern Africa include the Namib Desert along the western coast (location 1 in Figure 5b and c), the Great Escarpment of Namibia (location 12), the Kalahari Desert (location 10) including the Makgadikgadi Pan (location 9) and Etosha Pan (location 11), and the Karoo Desert (location 2~4). In Namib Desert, the dust sources are associated with dry riverbeds and saltpans instead of the Sand Sea in the south Namib Desert (Eckardt and Kuring, 2005). The Namib Desert is active during most seasons, as shown in Figure 5b and c. The Great Escarpment of Namibia, the Kalahari Desert, and the Karoo Desert are more active in summer. Dust materials in the Kalahari Desert are supplied by sediment inflows and the lake inundation activities (Bryant et al., 2007). Silt deposits are widespread on the Great Escarpment of Namibia due to the local weathering detritus and dust deposition from Kalahari Desert (Eitel et al., 2001). The easterly winds in summer activate the dust emission and result in a stronger dust emission in summer than other seasons (Figure 5b and c). Dust activity in

the Karoo Desert is associated with ephemeral lakes and land disturbance due to the long history of human occupation (Meadows, 2003; Botha et al., 2008).

Australia

Figure 5d and e show the dust sources in Australia in austral spring and summer. The region around the Lake Eyre Basin (location 4) including the Simpson Desert (location 5) are the most active and the largest dust sources in Australia. Australian dust sources are generally associated with hydrologic activities or land use. In the Lake Eyre Basin, aeolian deposits and hydrologic activities contribute respectively 37% and 60% of dust plumes (Bullard et al., 2008). In addition, Bullard et al. (2007) demonstrated that the abrasion of weathered sands with a clay coating is most important dust production mechanism in the Simpson Desert. The dust sources in the northern Australia (location 3~11) are more active in spring, particularly the regions around the Lake Eyre Basin, while dust sources in southeastern Australia (location 1~2) are more active in summer. Higher dust concentration in summer in the southeastern Australia is also confirmed by the field observations at Cape Grim (Prospero, 1996; Ginoux et al., 2001; Zender et al., 2003).

Other sources

In addition to the three continental regions above, several minor dust sources contribute to the dust input into the Southern Ocean. Bhattachan et al. (2015) suggested that the ice-free McMurdo Dry Valleys in Antarctica could be a potential source of mineral dust to the Southern Ocean. Annual melting sea ice around the Antarctic reserves mineral dust deposits in winter and releases accumulated dust materials when melts down (Winton et al., 2014; Edwards and Sedwick, 2001).

2.1.2. Contribution of dust sources in the Southern Ocean

Model simulation of Li et al. (2008) estimated that South America, Australia, and Southern Africa contribute respectively 58%, 36%, and 2% of dust deposition, respectively, into the Southern Ocean (south of 50°S). The rest 3% is contributed by the diffusion from the Northern Hemisphere. Compared to the three continental dust sources in the Southern Hemisphere, the relative contribution by the diffusion from the Northern Hemisphere is negligible at a regional scale.

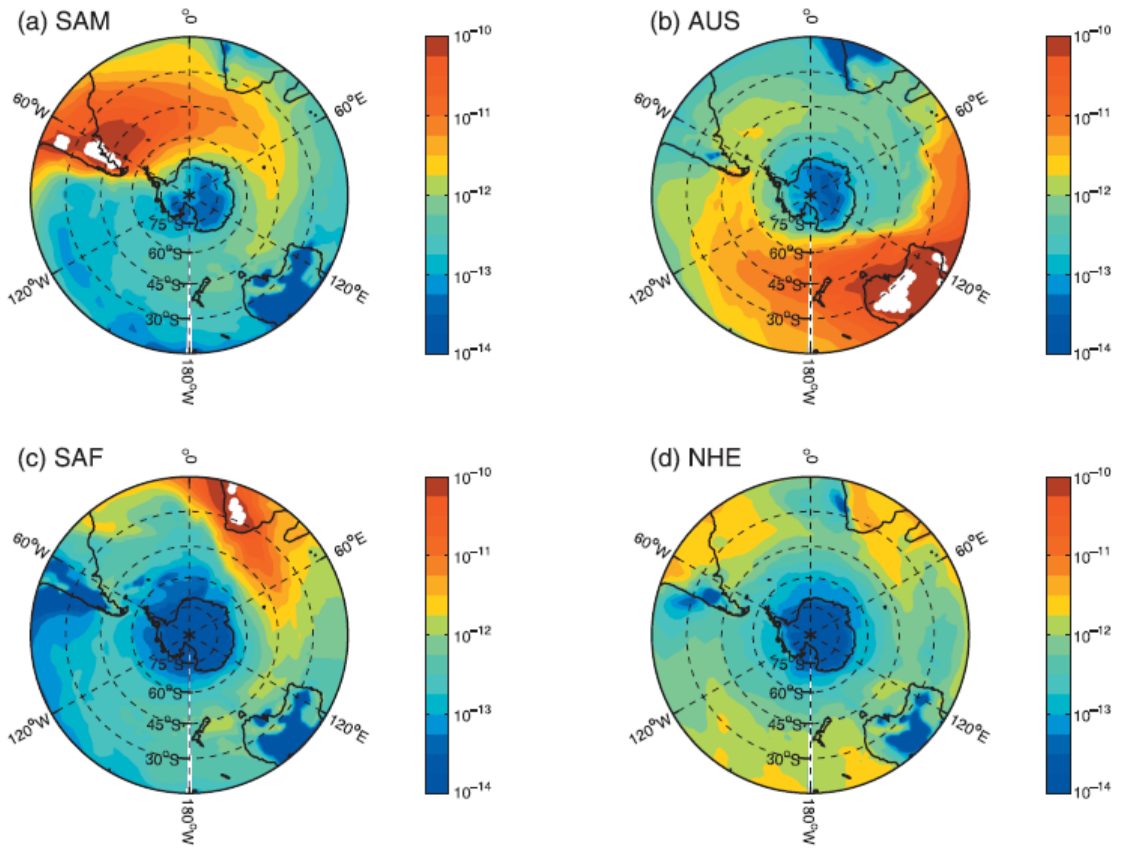

Figure 6 : Annual dust deposition in Southern Ocean and Antarctic from four individual sources, (a) South America, (b) Australia, (c) Southern Africa, and (d) diffusion from the Northern Hemisphere. Source: Figure 10 in Li et al. (2008)

The study of Li et al. (2008) also indicated that dust from South America and Australia dominates the dust deposition in polar region of the Southern Ocean, as shown in Figure 6. Australian dust dominates the deposition in the South Pacific section. Dust from Southern Africa represents relatively small amount of deposition and dominates lower latitude regions of the South Atlantic Ocean and the Indian Ocean. Dust from the South America, mostly from Patagonia, dominates the deposition in the South Atlantic section and the Indian Ocean section.

Field measurements of annual melting sea ice in previous studies quantified the contribution of this minor source to dust input in the Southern Ocean. Edwards and Sedwick (2001) estimated that the primary production supported by the melting sea ice is less than 5% in the entire seasonal sea ice zone around Antarctic. Winton et al. (2014) suggested that the accumulated dust in sea ice contribute about 15% of new primary production in the southwestern Ross Sea, Antarctica. Dust sediments in the annual sea ice acts as a minor dust source and affect only the local marine ecosystem (Chewings et al., 2014).

Dust concentration data from field observations is useful to constrain the dust emission scheme and evaluate the modeling results (Cakmur et al., 2006; Li et al., 2008), particularly in the Southern Hemisphere where satellite observation is seriously interfered by the cloudy conditions (Gasso and Stein, 2007). However, field measurements of dust concentration closing dust source areas were rarely conducted in subantarctic region, particularly compared to the good availability of experimental data for dust sources in Northern Hemisphere (e.g. Bonnet and Guieu, 2004; Formenti et al., 2003; Gelado-Caballero et al., 2012). In the study of Li et al. (2008) focusing on the dust cycle in subantarctic region, most dust concentration data used to constrain the dust emission scheme are obtained in Northern Hemisphere due to the lack of adequate data in Southern Hemisphere. The limited dust concentration data in the Southern Hemisphere are mostly located far from the dust sources except for the measurements in Cape Grim near the coast of Australia. Actually, the measurement in Cape Grim is part of surface observation network managed by the University of Miami (Prospero et al., 1989; Prospero, 1996), and is the only long-term mineral dust concentration measurement available closing dust sources in subantarctic region. This long-term dust concentration record in Cape Grim was not published but was widely used in the following modeling studies (e.g. Ginoux et al., 2001; Li et al., 2008; Zender et al., 2003). Observations at Cape Grim revealed a significant seasonal pattern with much higher dust concentration in late spring and summer in the southeastern Australia (Ginoux et al., 2001; Zender et al., 2003), while knowledge about dust concentration in other regions such as Patagonia remains poor. Field measurements of dust concentration in subantarctic region, particularly Patagonia and Namibia, are strongly required.

Overall, South America, Southern Africa and Australia are the three main sources of mineral dust deposited to the Southern Ocean. Particularly, the South America dominates the dust deposition in South Atlantic section and Patagonia is the dominant dust source in South America. Australia dominates the dust deposited into the South Pacific section. Knowledge about the dust concentration in source areas is essential to understand the strength and its temporal pattern of dust emission. Field measurements, particularly in long term, of dust concentration in dust source areas are strongly required in subantarctic region to better constrain the dust emission scheme and to further quantify the transport and deposition of dust to the Southern Ocean.

2.2. Dust transport and deposition in the Southern Ocean

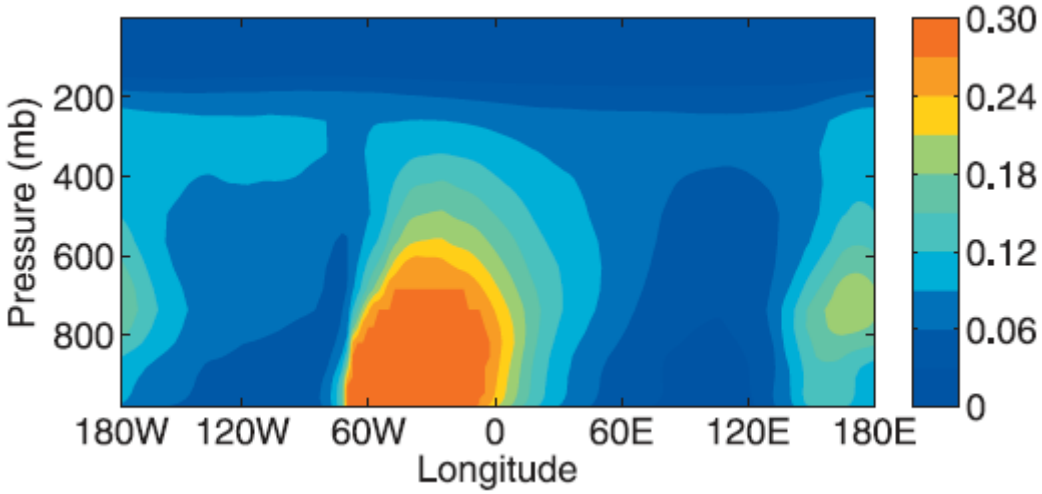

Figure 7 : Vertical distribution of the meridional mean annual dust concentration ($\mu g.m^{-3}$) over the Southern Ocean between 50°S and 75°S based on modelling results. Source: Figure 6 in Li et al. (2008)

After the emission, dust is sent to high altitude and can be transported over long distance to the open ocean. The modelling study of Li et al. (2008) simulated the vertical distribution of the meridional mean annual dust concentration ($\mu g.m^{-3}$) in the troposphere over the Southern Ocean (50°S and 75°S) (Figure 7). Maximum values are observed at 60° - 0°W and 160° - 180°E, corresponding to the longitude of South America and Australia, respectively, with an eastward shift of 30° as a result of the continuous westerly winds. The maximum dust concentration corresponding to South America is found from ground level to 600 mb, whereas the maximum dust concentration corresponding to Australia is located at high altitude between 800 mb and 600 mb, which could be explained by the long-range transport of dust emitted from Australia. Dust export from Southern Africa seems to be negligible compared to South America and Australia, according to Figure 7. Compared to the dust originated from Australia, Patagonian dust travels at low altitude over the Southern Ocean (Gasso and Stein, 2007; Johnson et al., 2011).

Dust are deposited into surface seawater by dry deposition (mostly by gravitational settling and turbulent deposition) and by wet deposition (Mahowald et al., 2005; Rosenfeld et al., 2014; Gao et al., 2003; Slinn, 1976; Textor et al., 2006). Along the atmospheric transport, large dust particles are preferentially removed by the gravitational sedimentation. Particles larger than 10 µm generally have a lifetime for a few hours and most dust particles are

deposited rapidly near the source area. Although large dust particles (>100 μm) were observed to transport for a long distance in previous studies (Betzer et al., 1988), long-range transported dust generally has a mode diameter around 2.5~3.5 μm (Schulz et al., 1998; Maring et al., 2003). Dust particles can be removed through washout process by precipitation or can act as cloud condensation nuclei (CCN) and through in-cloud scavenging (Rosenfeld et al., 2014; Berthet et al., 2010; Chate et al., 2011; Chate and Pranesha, 2004; Chate et al., 2003).

In the past decades, both field measurements and modeling studies have contributed to the quantification of mineral aerosol deposition in Southern Ocean. Wagener et al. (2008) estimated total dust deposition flux in Southern Ocean based on shipboard measurement of atmospheric aerosol concentration. Dry deposition was calculated as the product of aerosol concentration and deposition velocity. Wet deposition fluxes were derived from aerosol concentration and precipitation data by defining a fixed wet scavenging ratio (SR). Wagener et al. (2008) finally found that dust fluxes are up to two orders of magnitude lower than previous model predictions (Mahwald et al., 2005) and extrapolations of land-based measurements (Duce et al., 1991). The later studies of Heimburger et al. (2012) at Kerguelen Island (49°18'S, 70°07'E) and Chance et al. (2015) in the southeastern Atlantic Ocean sampled simultaneously atmospheric aerosol and rainwater to determine the dry deposition fluxes, wet deposition fluxes and ultimately the total deposition fluxes. The two studies found much higher deposition fluxes than those estimated by Wagener et al. (2008), and show better agreements with dust modelling results (Johnson et al., 2010; Mahowald et al., 2005; Mahowald et al., 2007). Particularly, the study of Heimburger et al. (2012) and Chance et al. (2015) indicated that he scavenging ratio (SR) used by Wagener et al. (2008) to estimate the deposition flux is too low and hence the computation of wet deposition based on atmospheric aerosol concentration seriously underestimated the wet dust deposition flux. Estimating the deposition flux from atmospheric aerosol concentration will introduce serious bias. On the other side, another study of Grand et al. (2015) estimated total dust deposition from the mixed layer concentration of dissolved aluminum (dAl) in the eastern Indian Ocean by assuming a steady state between addition of dAl due to the dissolution of atmospheric deposition and the removal of dAl via particulate scavenging. Grand et al. (2015) finally found similar total deposition flux to the modelling results of Mahowald et al. (2005) in the Southern Ocean.

However, although the measurements taking into account the contribution of wet deposition (Chance et al., 2015; Grand et al., 2015; Heimburger et al., 2012) show better agreement with previous modelling studies, discrepancies still exist between these studies. Being the only available long term time series of deposition flux in marine locations far from the dust sources in subantarctic region, the two-year measurements of dust deposition at Kerguelen and Crozet islands display a seasonal pattern with higher deposition fluxes in austral winter and spring (Heimburger et al., 2012; Heimburger et al., 2013). The time scale of sampling and the sporadic nature of dust fluxes can be a source of uncertainty and variability between observations (Grand et al., 2015).

Briefly, according to previous studies, wet deposition is the dominant mechanism to deposit atmospheric particles into the Southern Ocean. The dominant wet deposition means that most of dust particles deposited into the Southern Ocean is incorporated into rainwater, which may have further impact on the bioavailability of elements in dust for the marine ecosystem.

3. Mineral Dust as Micronutrient Supplier

For the HNLC Southern Ocean, dust deposition is supposed to be an important source of micronutrients. Hence, the key issue for the marine ecosystem is trace elements that dust contains rather than dust particles themselves. Elemental composition and bioavailability of elements are two key issues of dust that determine the amount of elements assimilated by marine ecosystem.

3.1. Elemental composition of mineral dust

As the product of wind erosion of soils, mineral dust contains several chemical elements that could be important for the biological processes of marine ecosystem. Measuring the dust elemental compositions is important to estimate the emission inventory of trace elements from dust source areas and evaluate the biological impact of dust input (Baker et al., 2003; Zhang et al., 2015).

Chemical compositions of dust can differ from its parent soil since the dust materials contain only the fine fraction of soil particles. In bulk soils, large particles, especially the sandy fraction, are dominated by quartz and calcium containing materials (e.g. calcite and

gypsum), whereas smaller particles contain clay minerals, feldspars, quartz, micas, carbonates and iron oxides (Journet et al., 2014; Schütz and Rahn, 1982). Quartz contains mainly Si; Clay minerals are mainly composed of Si and Al; Fe content is found principally in clays, feldspars and iron oxides; Ca and Mg exist mostly in gypsum, calcite and dolomite (Journet et al., 2014). The variation of chemical compositions with mineral species results in finally size dependence of elemental concentrations in desert soils (Eltayeb et al., 1993; Eltayeb et al., 2001; Castillo et al., 2008; Schütz and Rahn, 1982; Miller et al., 1972). For example, Schütz and Rahn (1982) studied African and American soils and found that elemental concentrations for most elements, except for Si, increase to the highest when the particle size decreases to 20 μm. This increase is greater in higher weathered and more winnowed soils, and is negligible in humus-rich soils. Eltayeb et al. (1993) found a nearly constant concentration of Al, K, Sr and Rb, a positive fractionation for the elements Ca, Ti, Mn, Fe, Y, and a negative fractionation for Si and Zr in aerosol fraction of Namibian soils. Therefore, both major elements and trace elements exhibit preferential partitioning with size fractions. As a result of different fractionation behavior of elements, elemental composition dust may differ from the chemical composition of parent soil.

Previous modelling studies generally take the average iron concentration of Earth's crust (3.5%) (Taylor and McLennan, 1995) as the iron content in dust (e.g. Duce and Tindale, 1991; Luo et al., 2008). However, spatial heterogeneities of dust elemental composition have been shown in former studies. For example, Formenti et al. (2008) found an average iron content equaling to 8.6 ± 0.2% (mean ± std) for local dust and 7.6 ± 0.6% for transported dust in Banizoumbou, Niger. Different iron content in dust from local source and dust from remote sources reflects regional variability of iron content. In addition, both dust sources showed much higher iron compositions than the values used by dust models. Iron composition of dust fallout measured by Gaiero et al. (2007) at four sites in Patagonian coast, despite the fact that dust deposited closing source areas is different from dust transported for long distance, also showed higher iron concentrations (4.3 ± 0.6%) than values used by models. Spatial variability of dust elemental composition must be taken into account to better evaluate the emission inventory of trace elements associated with dust.

Because dust chemical compositions are different from bulk soils and vary with the emission regions, investigations into the elemental composition of dust from sources are necessary. Considering that many active dust exist as "hot spots" in small areas, which is

quite common in the Southern Hemisphere, rather than in large homogeneous dust emission areas (Gillette, 1999), these kinds of investigations should be done at smaller scale. A database of dust elemental composition will be quite useful to evaluate the emission inventory of trace elements from dust sources and to reduce the uncertainties in dust modelling (Zhang et al., 2015).

3.2. Bioavailability of trace elements in dust

After deposited into seawater, only a fraction of trace elements in dust is bioavailable for the marine biota, where "being bioavailable" means being effective in causing a biological effect on the phytoplankton. For elements like Fe, the processes making iron bioavailable are complicated and different forms of iron are bioavailable, but all bioavailable iron are in dissolved phase including colloidal phase or soluble phase (Barbeau et al., 2001; Rich and Morel, 1990; Fitzsimmons and Boyle, 2014). Although not all forms of dissolved iron are bioavailable (Visser et al., 2003), the iron bioavailability is generally evaluated by the common known "fractional solubility" (hereafter "solubility") that is defined as the percentage ratio of dissolved amount to the total amount.

3.2.1. Factors controlling the solubility of micronutrients in mineral dust: the case of iron

For marine ecosystem, the bioavailability of micronutrients associated with dust depends on multiple factors: 1) the mineralogical composition of source dust, 2) the chemical processing history of dust during atmospheric transport, 3) the deposition process of dust into the ocean, 4) the composition of seawater (Baker and Jickells, 2006; Baker et al., 2006b; Desboeufs et al., 1999; Journet et al., 2008; Paris and Desboeufs, 2013; Gierlus et al., 2012; Losno et al., 1991; Schulz et al., 2012; Shi et al., 2012). The following content will discuss the impact of these factors with a focus on iron.

Mineralogical composition of dust may influence the solubility of elements in dust. As indicated by Journet et al. (2008), solubility of iron-containning minerals can vary by different orders of magnitude, particularly iron contained by clays generally show much higher solubility than iron (hydr-)oxide. Despite the variation of solubility among Ca-containing minerals (Krueger et al., 2004; Chou et al., 1989), some minerals such as calcium carbonate in dust can act as alkalinity buffers and neutralize the acidic conditions in cloud

droplets or rainwater during atmospheric transport (Losno et al., 1991; Loye-Pilot et al., 1986) and hence prevent the enhancement of solubility by atmospheric acid processing that is presented below.

Atmospheric processing is suggested to result in greater uncertainty of bioavailability of iron in dust (Shi et al., 2012). Previous studies generally found fractional iron solubility less than 0.5% for non-atmospheric processed dust but ranging from 0.1% to ~90% for transported aerosol (Mahowald et al., 2005; Hand et al., 2004; Chen and Siefert, 2004; Baker and Jickells, 2006; Sedwick et al., 2007; Heimburger et al., 2013a). The difference of solubility suggests an enhancement of dust solubility by atmospheric processing (Shi et al., 2012). During the atmospheric transport, dust particles can incorporate into cloud droplets as cloud condensation nuclei (CCN) or as interstitial particles (Andreae and Rosenfeld, 2008; Gierlus et al., 2012). Cloud water is an effective medium for heterogeneous chemical reactions. Nitrate and sulfate produced by the oxidation process by H_2O_2, O_3, O_2 and NO_2 acidify the cloud waters (Rosenfeld et al., 2014). Enhanced acidity of cloud water finally enhanced the elemental solubility of dust particles (Spokes and Jickells, 1995; Spokes et al., 1994; Desboeufs et al., 2001; Desboeufs et al., 2005). In addition to the acid processing in cloud, acid processing as wet particles outside cloud can also enhance the iron solubility of dust (Spokes and Jickells, 1995; Spokes et al., 1994; Desboeufs et al., 2001; Desboeufs et al., 2005; Shi et al., 2015). After the evaporation of cloud droplets, pH values of the water content in dust particles could decrease to 2 or even lower (Meskhidze et al., 2003; Zhu et al., 1992). As indicated by the recent study of Shi et al. (2015), the highly acidic wet particles outside cloud resulting from the evaporation of cloud droplets is the main process increasing readily dissolved iron during atmospheric processing. Furthermore, the exposition of dust particles to the solar ration in the presence of acidic solutions can also enhance the solubility of iron due to the photoreduction reaction (Hand et al., 2004; Fu et al., 2010) that converts the relatively insoluble Fe(III) into the more soluble Fe(II) (Kieber et al., 2005). Fu et al. (2010) found that dust in HCl solution showed higher increase of iron solubility under irradiation compared to the dark reaction.

Dry and wet deposition process can affect differently the solubility of mineral aerosol. Baker and Jickells (2006) argued that the specific surface area of mineral aerosol particles is the primary controlling factor of aerosol iron solubility. The dry deposition process removes preferentially larger particles and consequently results in higher solubility of mineral aerosol.

Dust materials could be deposited into seawater as rainwater or snow and generally show high iron solubility (Sarthou et al., 2003; Heimburger et al., 2013a; Buck et al., 2010; Buck et al., 2006; Edwards and Sedwick, 2001; Paris et al., 2011). As mentioned in the paragraph above, this high iron solubility is mainly explained by enhancement of elemental solubility due to the atmospheric processing. On the other side, previous studies observed a positive linear dependence of iron solubility on the concentration of organic ligands in simulated rainwater (Paris et al., 2011; Paris and Desboeufs, 2013). The dissolved iron could form complexes with organic ligands such as oxalic acid promotes the iron solubility in dust.

Compared to the atmospheric processing history, the physicochemical conditions of seawater have little effect on the dissolution of dust in seawater after the deposition into ocean (Fishwick et al., 2014; Aguilar-Islas et al., 2010). However, the kinetics of complexation reaction with organic and inorganic ligands ultimately controls the trace element uptake (Morel et al., 1991; Mendez et al., 2010). Previous study generally showed that colloidal iron fraction dominates the dissolved iron in seawater (Aguilar-Islas et al., 2010; Fishwick et al., 2014; Bergquist et al., 2007). The presence of Fe-binding organic ligands promotes the conversion of dissolved iron from colloidal size fraction (0.02-0.4 μm) to soluble size fraction (<0.02 μm) (Fishwick et al., 2014). The study of Hassler et al. (2011) showed that saccharides, produced by biota in surface waters, might act as organic ligands and enhance the bioavailability of iron. In addition, enhanced iron bioavailability due to the conversion from Fe(III) to Fe(II) through photoreduction are also observed in seawater (Rich and Morel, 1990; Barbeau et al., 2001).

3.2.2. Common methods of elemental solubility estimation

Elemental solubility measurements generally include a leaching procedure to extract the dissolved phase and a separation procedure to separate the dissolved phase from the particulate phase. Solubility measurements could be affected by multiple experimental parameters including the choice of leaching solvent, the time of contact between dust materials, and the separation procedure.

Table 1 summarizes several Fe solubility estimations in previous studies carried on samples of different origins or sample types including rainwater and surface snow. For aerosol samples or proxies of dust (e.g. fine fraction of soil), the choice of leach solution to measure elemental solubility depends on purposes of measurements (Shi et al., 2012).

Ultrapure deionized water is commonly used to measure the elemental solubility in solutions without affecting factors such as non-acidified cloud water (Aguilar-Islas et al., 2010; Buck et al., 2010 Winton et al., 2014). Because the buffer capacity of pure water is very limited, the pH of solutions can change to different extent resulting from the dissolution of minerals such as carbonate (Aghnatios et al., 2014). The use of weak buffers such as ammonium acetate (pH = 4.7) (Sarthou et al., 2003; Baker et al., 2006) may avoid the problem of pH modification and provide comparable results between different mineral aerosols. The pH4.7 can also simulate the dissolution at pH condition similar to rainwater. To simulate the acid processing during the atmospheric transport, previous studies often use acidified solutions and found a strong impact of pH on iron solubility (Desboeufs et al., 2005; Desboeufs et al., 1999; Baker et al., 2006b; Spokes and Jickells, 1995; Edwards and Sedwick, 2001). For example, Spokes and Jickells (1995) tested the solubility of Saharan aerosol successively under pH8, pH2, and pH5.5 and observed a variation of iron solubility from 0.1% (pH8) to 4.7 (pH2) and finally to 0.3% (pH5.5). Leaching solution could also be purified, modified or synthetic seawaters to investigate the dissolution capacity of aerosol at the pH of seawater (approximately pH8.2) and with the presence of organic ligands in marine aquatic environment (Aguilar-Islas et al., 2010; Wu et al., 2007). For samples like rainwater or meltwater of snow, dust materials they contained are already in liquid phase. Accumulated dust deposition in annual surface snow samples in oceanic region is released immediately into seawater after melting. Rainwater containing the dust materials is also ready to enter into seawater. Therefore, dissolved phase is separated immediately after the collection of rainwater (Buck et al., 2010; Heimburger et al., 2013a) or the melting of snow(Edwards and Sedwick, 2001; Winton et al., 2014).

In terms of the time of contact between dust materials and leaching solutions, “instantaneous” solubility or solubility after minutes to hours are found in different studies. For example, Baker et al. (2006) measured iron solubility after a dissolution lasting 1~2 hrs, while Buck et al. (2010) measured instantaneous solubility. Aguilar-Islas et al. (2010) measured the solubility after 1 minute, 3 minutes and 90 minutes to evaluate the impact of leaching duration.

Since the separation procedure is traditionally conducted through membrane filtration, the dissolved fraction is operationally defined as the fraction passing through the pores of membrane. As shown in Table 1, membrane filtration separation was adapted, while both the pore size and materials are quite various. Depending on the choice of authors, the pore size of

filter could be 0.45 μm, 0.4 μm or 0.2 μm, and different materials such as polycarbonate, polypropylene, cellulose and PTFE were used. Difference in pore size surely will affect the number and size of particles passing through the membrane. For the moment, the impact of membrane materials on the amount of dissolved phase passing through the filter is still unclear. On the other side, Zirkler et al. (2012) filtrated soil suspension (particles size < 3 μm) by glass fiber filter (pore size of 1.0 μm), polycarbonate filter (pore size of 1.2 μm) and cellulose nitrate filter (pore size of 1.0 μm), and found highly different concentrations of colloids (fraction < 1 μm) in the three filtrates obtained.

In support of the above discussion, methods and conditions used to measure the dust solubility could be quite various. Since the processes to be bioavailable of dust is quite complicated, solubility determined through a simple dissolution experiment does not reflect directly the bioavailability of dust. Agreements in experimental conditions such as the duration of leaching and membrane material used for filtration have never been achieved in previous studies. Fractional solubility of dust is not a term well defined. Nevertheless, several factors can be the dominating factor regulating the bioavailability of dust. For example, for pristine dust from source areas, atmospheric acid processing should be the most important process enhances the bioavailability of dust. Methods used to determine solubility must be adapted to the characteristics of dust sample and to the purpose of measurements.

Table 1: Several previous estimations of iron solubility under different experimental configuration

reference	sample type	leaching solution	filter (pore size, material)	leaching time	DFe%
Spokes and Jickells (1995)	Saharan aerosol collected by North African coast	pH2	0.2 µm, cellulose acetate	24 hrs	4.7±0.2
		pH5.5			0.3
		pH8			0.1
Aghnatios et al. (2014)	alluvial soil from Tunisia, <20 µm	ultrapure water	0.2 µm, polycarbonate	4 min	0.04
		pH5 HNO_3			0.07
		pH3 HNO_3			0.26
		pH1 HNO_3			0.93
Cwiertny et al. (2008)	Arizona test dust	pH1 HSO_4	0.2 µm, PTFE	24 hrs	15.7±0.8
		pH1 HNO_3			11.9±0.5
		pH1 HCl			13.6±0.6
Journet et al. (2008)	iron oxide/goethite, magnetite, hematite, <100 µm	pH2 HNO_3	0.2 µm, polycarbonate	60 min	0.003~0.01
	clay/illite, <100 µm				0.95~1.39
	clay/montmorillonite, <100 µm				2.6
	clay/nontronite, beidellite, <100 µm				0.34
	feldspar/oligoclase, orthoclase, <100 µm				5.25, 4.26
Wu et al. (2007)	aerosol collected over North Pacific	0.1 M HCl	0.4 µm, polycarbonate	25 - 30 hrs	7
		seawater		Instantaneous	1.1
		seawater		25 - 60 hrs	2.4-9.5
Aguilar-Islas et al. (2010)	Alaska Coastal urban aerosol	ultrapure water	0.4 µm, polycarbonate	1, 30, 90 min	1.8, 2.1, 2.3
		UV oxidized seawater			1.5, 1.7, 1.8
		UVSW+desferal			2.6, 2.8, 3.2
Baker et al. (2006)	aerosol collected over North Atlantic	NH_4Ac pH4.7	0.2 µm, cellulose acetate	1 - 2 hrs	1.4-54
	Saharan aerosol collected over North Atlantic				1.4-4.1
Buck et al. (2010)	aerosol collected over North Atlantic	ultrapure water	0.45 µm, polypropylene	Instantaneous	3~47
		seawater			1~26
	rainwater collected over North Atlantic				3.7~40
Heimburger et al. (2013a)	**rainwater** collected over Kerguelen		0.2 µm, polycarbonate	Instantaneous	51~91
Edwards and Sedwick (2001)	**surface snow** in East Antarctica		0.2 µm, PTFE	after melting	9~89
Winton et al. (2014)	**surface snow** in Ross Sea, Antarctica		0.4 µm, polycarbonate	after melting	4.12~19.93

4. Research Topics and Strategies

4.1. Research topics

Estimation of dust emission from source area in the Southern Hemisphere necessitates dust concentration data closing source areas including the level and the temporal pattern of dust concentration, which may have further application in quantification of dust emission inventory. Patagonia is suspected to be the major dust source for the Southern Ocean, while data record of dust concentration measurements in field has never been reported. The first part of this thesis aims to complete this gap and address several relevant questions:

1) Dust concentration in Patagonia: What is the dust concentration level in source area in Patagonia? How does the dust concentration vary in long term? What are the factors regulating the dust concentration level in Patagonia region?

For the dust emitted over source regions, quantity of bioavailable trace elements in dust materials depends on the elemental composition and the potential fractional solubility of dust. A database characterizing the chemical properties of the dust including elemental composition and fractional solubility by taking account of the spatial heterogeneity of dust in source regions will be quite useful to evaluate the biological impact of dust deposition. In the present work, we focused on two dust sources Patagonia and Namibia, which are important for the South Atlantic section of Southern Ocean, and tried to enrich our knowledge about the elemental composition and elemental solubility in these two dust sources by addressing questions below:

2) Elemental composition of Patagonian and Namibian dust: What are the elemental compositions, particularly Fe composition, of dust in source areas of subantarctic region? How do the elemental compositions of dust vary with geological locations? Is the elemental composition of soil representative to the elemental composition of dust? Can we use the elemental composition of soil as a surrogate of dust elemental composition?

3) Elemental solubility of Patagonian and Namibian dust: To what extent is the dust soluble after different degrees of chemical processing? How does the elemental solubility of dust vary with different types of dust sample?

4.2. Research Strategies

4.2.1. Long-term dust concentration measurements in Patagonia

Under the program "Dust From Patagonia", an aerosol sampling station was installed in Río Gallegos (69.32°W, 51.60°S). Río Gallegos is located in the east coast of south Patagonia, and the prevailing wind is the Westerly, providing the opportunity to sample dust exported from Patagonian tableland. The sampling station started to collect continuously aerosol from 29, November 2011 on a weekly basis. The sampling activity lasted for three years and was expected to improve our understanding on the temporal pattern of dust emission strength in the source areas. Collected aerosol samples were then analyzed in laboratory to determine the amount of materials collected and the atmospheric concentration of dust. Our collaborator in Argentina, CEILAP, was responsible to maintain the sampling station in Río Gallegos.

4.2.2. Spatial heterogeneity of source dust elemental compositions

Investigation into the spatial heterogeneity of dust elemental composition needs dust samples from different places. In-situ dust collection of naturally emitted dust should be the first choice to study dust at the source. However, due to the temporal variability of dust emission, sampling of naturally emitted dust from a large number of sites requires long period of dust sampling. This poses great challenges to investigate the spatial heterogeneity of source dust properties. Dust production in field or in laboratory from soil samples is an alternative to study some properties, including chemical properties, of the dust source. In this part of work, dust samples were prepared in laboratory from parent soils collected in Patagonia and Namibia. A laboratory dust generator: SyGAVib (abbreviation for "Système de Génération d'Aérosol par Vibration" in French; "aerosol generation system by vibration" in English) was used in our study. Both the dust chemical composition and soil chemical composition were determined to explore the enrichment behavior of mineral elements

from soil to dust during the dust emission. In this part of work, two dust sources: Patagonia (South America) and Namibia (Southern Africa) are considered. The two regions have different landscape and both of the two regions are important to the South Atlantic section of Southern Ocean.

4.2.3. Some aspects of the solubility of continental dust

Evaluation of dust lability was conducted on thirteen dust samples produced by SyGAVib. We adapted the sequential leaching method under decreasing pH (pure water, pH5, pH3, pH1) proposed by Aghnatios et al. (2014) to earn a relatively complete knowledge about the dissolution behavior under increasing chemical strength related to the acid processing during atmospheric transport.

Bibliography

Acosta, J. A., Martínez-Martínez, S., Faz, A., and Arocena, J.: Accumulations of major and trace elements in particle size fractions of soils on eight different parent materials, Geoderma, 161, 30-42, 10.1016/j.geoderma.2010.12.001, 2011.

Aguilar-Islas, A. M., Wu, J. F., Rember, R., Johansen, A. M., and Shank, L. M.: Dissolution of aerosol-derived iron in seawater: Leach solution chemistry, aerosol type, and colloidal iron fraction, Marine Chemistry, 120, 25-33, 10.1016/j.marchem.2009.01.011, 2010.

Alfaro, S. C., Gaudichet, A., Gomes, L., and Maillé, M.: Modeling the size distribution of a soil aerosol produced by sandblasting, Journal of Geophysical Research: Atmospheres, 102, 11239-11249, 10.1029/97JD00403, 1997.

Andreae, M. O., and Rosenfeld, D.: Aerosol–cloud–precipitation interactions. Part 1. The nature and sources of cloud-active aerosols, Earth-Science Reviews, 89, 13-41, http://dx.doi.org/10.1016/j.earscirev.2008.03.001, 2008.

Baker, A. R., Kelly, S. D., Biswas, K. F., Witt, M., and Jickells, T. D.: Atmospheric deposition of nutrients to the Atlantic Ocean, Geophysical Research Letters, 30, 2296, 10.1029/2003GL018518, 2003.

Baker, A. R., French, M., and Linge, K. L.: Trends in aerosol nutrient solubility along a west-east transect of the Saharan dust plume, Geophysical Research Letters, 33, 10.1029/2005gl024764, 2006.

Baker, A. R., and Jickells, T. D.: Mineral particle size as a control on aerosol iron solubility, Geophysical Research Letters, 33, L17608, 10.1029/2006GL026557, 2006.

Barbeau, K., Rue, E. L., Bruland, K. W., and Butler, A.: Photochemical cycling of iron in the surface ocean mediated by microbial iron(iii)-binding ligands, Nature, 413, 409-413, 10.1038/35096545, 2001.

Bergquist, B. A., Wu, J., and Boyle, E. A.: Variability in oceanic dissolved iron is dominated by the colloidal fraction, Geochimica et Cosmochimica Acta, 71, 2960-2974, 10.1016/j.gca.2007.03.013, 2007.

Berthet, S., Leriche, M., Pinty, J. P., Cuesta, J., and Pigeon, G.: Scavenging of aerosol particles by rain in a cloud resolving model, Atmospheric Research, 96, 325-336, http://dx.doi.org/10.1016/j.atmosres.2009.09.015, 2010.

Betzer, P. R., Carder, K. L., Duce, R. A., Merrill, J. T., Tindale, N. W., Uematsu, M., Costello, D. K., Young, R. W., Feely, R. A., Breland, J. A., Bernstein, R. E., and Greco, A. M.: Long-range transport of giant mineral aerosol particles, Nature, 336, 568-571, 1988.

Bhattachan, A., Wang, L., Miller, M. F., Licht, K. J., and D'Odorico, P.: Antarctica's Dry Valleys: a potential source of soluble iron to the Southern Ocean?, Geophysical Research Letters, 2015GL063419, 10.1002/2015GL063419, 2015.

Bonnet, S., and Guieu, C.: Dissolution of atmospheric iron in seawater, Geophysical Research Letters, 31, 10.1029/2003gl018423, 2004.

Botha, M. S., Carrick, P. J., and Allsopp, N.: Capturing lessons from land-users to aid the development of ecological restoration guidelines for lowland Namaqualand, Biological Conservation, 141, 885-895, 10.1016/j.biocon.2007.12.005, 2008.

Bronick, C. J., and Lal, R.: Soil structure and management: a review, Geoderma, 124, 3-22, http://dx.doi.org/10.1016/j.geoderma.2004.03.005, 2005.

Bryant, R. G., Bigg, G. R., Mahowald, N. M., Eckardt, F. D., and Ross, S. G.: Dust emission response to climate in southern Africa, Journal of Geophysical Research: Atmospheres, 112, n/a-n/a, 10.1029/2005JD007025, 2007.

Buck, C. S., Landing, W. M., Resing, J. A., and Lebon, G. T.: Aerosol iron and aluminum solubility in the northwest Pacific Ocean: Results from the 2002 IOC cruise, Geochemistry Geophysics Geosystems, 7, 10.1029/2005gc000977, 2006.

Buck, C. S., Landing, W. M., Resing, J. A., and Measures, C. I.: The solubility and deposition of aerosol Fe and other trace elements in the North Atlantic Ocean: Observations from the A16N CLIVAR/CO2 repeat hydrography section, Marine Chemistry, 120, 57-70, 10.1016/j.marchem.2008.08.003, 2010.

Bullard, J., Baddock, M., McTainsh, G., and Leys, J.: Sub-basin scale dust source geomorphology detected using MODIS, Geophysical Research Letters, 35, L15404, 10.1029/2008GL033928, 2008.

Bullard, J. E., McTainsh, G. H., and Pudmenzky, C.: Factors affecting the nature and rate of dust production from natural dune sands, Sedimentology, 54, 169-182, 10.1111/j.1365-3091.2006.00827.x, 2007.

Cakmur, R. V., Miller, R. L., Perlwitz, J., Geogdzhayev, I. V., Ginoux, P., Koch, D., Kohfeld, K. E., Tegen, I., and Zender, C. S.: Constraining the magnitude of the global dust cycle by minimizing the difference between a model and observations, Journal of Geophysical Research: Atmospheres, 111, n/a-n/a, 10.1029/2005JD005791, 2006.

Castillo, S., Moreno, T., Querol, X., Alastuey, A., Cuevas, E., Herrmann, L., Mounkaila, M., and Gibbons, W.: Trace element variation in size-fractionated African desert dusts, Journal of Arid Environments, 72, 1034-1045, 10.1016/j.jaridenv.2007.12.007, 2008.

Chance, R., Jickells, T. D., and Baker, A. R.: Atmospheric trace metal concentrations, solubility and deposition fluxes in remote marine air over the south-east Atlantic, Marine Chemistry, http://dx.doi.org/10.1016/j.marchem.2015.06.028, 2015.

Chate, D. M., Rao, P. S. P., Naik, M. S., Momin, G. A., Safai, P. D., and Ali, K.: Scavenging of aerosols and their chemical species by rain, Atmospheric Environment, 37, 2477-2484, http://dx.doi.org/10.1016/S1352-2310(03)00162-6, 2003.

Chate, D. M., and Pranesha, T. S.: Field studies of scavenging of aerosols by rain events, Journal of Aerosol Science, 35, 695-706, http://dx.doi.org/10.1016/j.jaerosci.2003.09.007, 2004.

Chate, D. M., Murugavel, P., Ali, K., Tiwari, S., and Beig, G.: Below-cloud rain scavenging of atmospheric aerosols for aerosol deposition models, Atmospheric Research, 99, 528-536, http://dx.doi.org/10.1016/j.atmosres.2010.12.010, 2011.

Chen, Y., and Siefert, R. L.: Seasonal and spatial distributions and dry deposition fluxes of atmospheric total and labile iron over the tropical and subtropical North Atlantic Ocean, Journal of Geophysical Research: Atmospheres, 109, 10.1029/2003JD003958, 2004.

Chewings, J. M., Atkins, C. B., Dunbar, G. B., and Golledge, N. R.: Aeolian sediment transport and deposition in a modern high-latitude glacial marine environment, Sedimentology, 61, 1535-1557, 10.1111/sed.12108, 2014.

Chou, L., Garrels, R. M., and Wollast, R.: Comparative study of the kinetics and mechanisms of dissolution of carbonate minerals, Chemical Geology, 78, 269-282, http://dx.doi.org/10.1016/0009-2541(89)90063-6, 1989.

Collini, E., Osores, M. S., Folch, A., Viramonte, J. G., Villarosa, G., and Salmuni, G.: Volcanic ash forecast during the June 2011 Cordón Caulle eruption, Natural Hazards, 66, 389-412, 10.1007/s11069-012-0492-y, 2013.

Desboeufs, K. V., Losno, R., Vimeux, F., and Cholbi, S.: The pH-dependent dissolution of wind-transported Saharan dust, Journal of Geophysical Research: Atmospheres, 104, 21287-21299, 10.1029/1999JD900236, 1999.

Desboeufs, K. V., Losno, R., and Colin, J. L.: Factors influencing aerosol solubility during cloud processes, Atmospheric Environment, 35, 3529-3537, http://dx.doi.org/10.1016/S1352-2310(00)00472-6, 2001.

Desboeufs, K. V., Sofikitis, A., Losno, R., Colin, J. L., and Ausset, P.: Dissolution and solubility of trace metals from natural and anthropogenic aerosol particulate matter, Chemosphere, 58, 195-203, http://dx.doi.org/10.1016/j.chemosphere.2004.02.025, 2005.

Eckardt, F. D., and Kuring, N.: SeaWiFS identifies dust sources in the Namib Desert, International Journal of Remote Sensing, 26, 4159-4167, 10.1080/01431160500113112, 2005.

Edwards, R., and Sedwick, P.: Iron in East Antarctic snow: Implications for atmospheric iron deposition and algal production in Antarctic waters, Geophysical Research Letters, 28, 3907-3910, 10.1029/2001GL012867, 2001.

Eitel, B., Dieter Blümel, W., Hüser, K., and Mauz, B.: Dust and loessic alluvial deposits in Northwestern Namibia (Damaraland, Kaokoveld): sedimentology and palaeoclimatic evidence based on luminescence data, Quaternary International, 76–77, 57-65, 10.1016/S1040-6182(00)00089-6, 2001.

Eltayeb, M. A. H., Van Grieken, R. E., Maenhaut, W., and Annegarn, H. J.: Aerosol-soil fractionation for Namib Desert samples, Atmospheric Environment. Part A. General Topics, 27, 669-678, http://dx.doi.org/10.1016/0960-1686(93)90185-2, 1993.

Eltayeb, M. A. H., Injuk, J., Maenhaut, W., and Van Grieken, R. E.: Elemental Composition of Mineral Aerosol Generated from Sudan Sahara Sand, Journal of Atmospheric Chemistry, 40, 247-273, 10.1023/A:1012272208129, 2001.

Fishwick, M. P., Sedwick, P. N., Lohan, M. C., Worsfold, P. J., Buck, K. N., Church, T. M., and Ussher, S. J.: The impact of changing surface ocean conditions on the dissolution of aerosol iron, Global Biogeochemical Cycles, 28, 1235-1250, 10.1002/2014gb004921, 2014.

Fitzsimmons, J. N., and Boyle, E. A.: Both soluble and colloidal iron phases control dissolved iron variability in the tropical North Atlantic Ocean, Geochimica et Cosmochimica Acta, 125, 539-550, http://dx.doi.org/10.1016/j.gca.2013.10.032, 2014.

Folch, A., Mingari, L., Osores, M. S., and Collini, E.: Modeling volcanic ash resuspension – application to the 14–18 October 2011 outbreak episode in central Patagonia, Argentina, Nat. Hazards Earth Syst. Sci., 14, 119-133, 10.5194/nhess-14-119-2014, 2014.

Formenti, P., Elbert, W., Maenhaut, W., Haywood, J., and Andreae, M.: Chemical composition of mineral dust aerosol during the Saharan Dust Experiment (SHADE) airborne campaign in the Cape Verde region, September 2000, Journal of Geophysical Research: Atmospheres (1984–2012), 108, 2003.

Formenti, P., Rajot, J. L., Desboeufs, K., Caquineau, S., Chevaillier, S., Nava, S., Gaudichet, A., Journet, E., Triquet, S., Alfaro, S., Chiari, M., Haywood, J., Coe, H., and Highwood, E.: Regional variability of the composition of mineral dust from western Africa: Results from the AMMA SOP0/DABEX and DODO field campaigns, Journal of Geophysical Research: Atmospheres, 113, n/a-n/a, 10.1029/2008JD009903, 2008.

Fu, H., Cwiertny, D. M., Carmichael, G. R., Scherer, M. M., and Grassian, V. H.: Photoreductive dissolution of Fe-containing mineral dust particles in acidic media, Journal of Geophysical Research: Atmospheres, 115, D11304, 10.1029/2009JD012702, 2010.

Gaiero, D. M., Probst, J.-L., Depetris, P. J., Bidart, S. M., and Leleyter, L.: Iron and other transition metals in Patagonian riverborne and windborne materials: geochemical control and transport to the southern South Atlantic Ocean, Geochimica et Cosmochimica Acta, 67, 3603-3623, 10.1016/S0016-7037(03)00211-4, 2003.

Gaiero, D. M., Brunet, F., Probst, J.-L., and Depetris, P. J.: A uniform isotopic and chemical signature of dust exported from Patagonia: Rock sources and occurrence in southern environments, Chemical Geology, 238, 107-120, 10.1016/j.chemgeo.2006.11.003, 2007.

Gao, Y., Fan, S. M., and Sarmiento, J. L.: Aeolian iron input to the ocean through precipitation scavenging: A modeling perspective and its implication for natural iron fertilization in the ocean, J. Geophys. Res.-Atmos., 108, 10.1029/2002jd002420, 2003.

Gassó, S., and Stein, A. F.: Does dust from Patagonia reach the sub-Antarctic Atlantic Ocean?, Geophysical Research Letters, 34, L01801, 10.1029/2006GL027693, 2007.

Gelado-Caballero, M. D., López-García, P., Prieto, S., Patey, M. D., Collado, C., and Hérnández-Brito, J. J.: Long-term aerosol measurements in Gran Canaria, Canary Islands: Particle concentration, sources and elemental composition, Journal of Geophysical Research: Atmospheres, 117, n/a–n/a, 10.1029/2011JD016646, 2012.

Gierlus, K. M., Laskina, O., Abernathy, T. L., and Grassian, V. H.: Laboratory study of the effect of oxalic acid on the cloud condensation nuclei activity of mineral dust aerosol, Atmospheric Environment, 46, 125-130, 10.1016/j.atmosenv.2011.10.027, 2012.

Gillette, D.: A wind tunnel simulation of the erosion of soil: Effect of soil texture, sandblasting, wind speed, and soil consolidation on dust production, Atmospheric Environment (1967), 12, 1735-1743, http://dx.doi.org/10.1016/0004-6981(78)90322-0, 1978.

Gillette, D.: Environmental factors affecting dust emission by wind erosion, Saharan dust, 71-94, 1979.

Gillette, D. A., Adams, J., Endo, A., Smith, D., and Kihl, R.: Threshold velocities for input of soil particles into the air by desert soils, Journal of Geophysical Research: Oceans, 85, 5621–5630, 10.1029/JC085iC10p05621, 1980.

Gillette, D. A.: Production of dust that may be carried great distances, Geological Society of America Special Papers, 186, 11-26, 10.1130/SPE186-p11, 1981.

Gillette, D. A., Adams, J., Muhs, D., and Kihl, R.: Threshold friction velocities and rupture moduli for crusted desert soils for the input of soil particles into the air, Journal of Geophysical Research: Oceans, 87, 9003–9015, 10.1029/JC087iC11p09003, 1982.

Gillette, D. A.: A qualitative geophysical explanation for hot spot dust emitting source regions, Contributions to Atmospheric Physics, 72, 67-77, 1999.

Ginoux, P., Chin, M., Tegen, I., Prospero, J. M., Holben, B., Dubovik, O., and Lin, S.-J.: Sources and distributions of dust aerosols simulated with the GOCART model, Journal of Geophysical Research: Atmospheres, 106, 20255–20273, 10.1029/2000JD000053, 2001.

Ginoux, P., Prospero, J. M., Torres, O., and Chin, M.: Long-term simulation of global dust distribution with the GOCART model: correlation with North Atlantic Oscillation, Environmental Modelling & Software, 19, 113-128, http://dx.doi.org/10.1016/S1364-8152(03)00114-2, 2004.

Ginoux, P., Prospero, J. M., Gill, T. E., Hsu, N. C., and Zhao, M.: Global-scale attribution of anthropogenic and natural dust sources and their emission rates based on MODIS Deep Blue aerosol products, Reviews of Geophysics, 50, RG3005, 10.1029/2012RG000388, 2012.

Gomes, L., Bergametti, G., Coudé-Gaussen, G., and Rognon, P.: Submicron desert dusts: A sandblasting process, Journal of Geophysical Research: Atmospheres, 95, 13927-13935, 10.1029/JD095iD09p13927, 1990.

Grand, M. M., Measures, C. I., Hatta, M., Hiscock, W. T., Buck, C. S., and Landing, W. M.: Dust deposition in the eastern Indian Ocean: The ocean perspective from Antarctica to the Bay of Bengal, Global Biogeochemical Cycles, 29, 357-374, 10.1002/2014GB004898, 2015.

Hand, J. L., Mahowald, N. M., Chen, Y., Siefert, R. L., Luo, C., Subramaniam, A., and Fung, I.: Estimates of atmospheric-processed soluble iron from observations and a global mineral aerosol model: Biogeochemical implications, Journal of Geophysical Research: Atmospheres, 109, n/a–n/a, 10.1029/2004JD004574, 2004.

Heimburger, A., Losno, R., Triquet, S., Dulac, F., and Mahowald, N.: Direct measurements of atmospheric iron, cobalt, and aluminum-derived dust deposition at Kerguelen Islands, Global Biogeochemical Cycles, 26, GB4016, 10.1029/2012GB004301, 2012.

Heimburger, A., Losno, R., and Triquet, S.: Solubility of iron and other trace elements in rainwater collected on the Kerguelen Islands (South Indian Ocean), Biogeosciences, 10, 6617-6628, 10.5194/bg-10-6617-2013, 2013a.

Heimburger, A., Losno, R., Triquet, S., and Nguyen, E. B.: Atmospheric deposition fluxes of 26 elements over the Southern Indian Ocean: Time series on Kerguelen and Crozet Islands, Global Biogeochemical Cycles, 27, 440-449, 10.1002/gbc.20043, 2013b.

Ishizuka, M., Mikami, M., Leys, J., Yamada, Y., Heidenreich, S., Shao, Y., and McTainsh, G. H.: Effects of soil moisture and dried raindroplet crust on saltation and dust emission, Journal of Geophysical Research: Atmospheres, 113, n/a–n/a, 10.1029/2008JD009955, 2008.

Johnson, M. S., Meskhidze, N., Solmon, F., Gassó, S., Chuang, P. Y., Gaiero, D. M., Yantosca, R. M., Wu, S., Wang, Y., and Carouge, C.: Modeling dust and soluble iron deposition to the South Atlantic Ocean, Journal of Geophysical Research: Atmospheres, 115, D15202, 10.1029/2009JD013311, 2010.

Johnson, M. S., Meskhidze, N., Kiliyanpilakkil, V. P., and Gassó, S.: Understanding the transport of Patagonian dust and its influence on marine biological activity in the South Atlantic Ocean, Atmos. Chem. Phys., 11, 2487-2502, 10.5194/acp-11-2487-2011, 2011.

Journet, E., Desboeufs, K. V., Caquineau, S., and Colin, J.-L.: Mineralogy as a critical factor of dust iron solubility, Geophysical Research Letters, 35, L07805, 10.1029/2007GL031589, 2008.

Journet, E., Balkanski, Y., and Harrison, S. P.: A new data set of soil mineralogy for dust-cycle modeling, Atmos. Chem. Phys., 14, 3801-3816, 10.5194/acp-14-3801-2014, 2014.

Kieber, R. J., Skrabal, S. A., Smith, B. J., and Willey, J. D.: Organic Complexation of Fe(II) and Its Impact on the Redox Cycling of Iron in Rain, Environmental Science & Technology, 39, 1576-1583, 10.1021/es040439h, 2005.

Kim, H., and Choi, M.: Impact of Soil Moisture on Dust Outbreaks in East Asia: Using Satellite and Assimilation data, Geophysical Research Letters, 2015GL063325, 10.1002/2015GL063325, 2015.

Kjelgaard, J. F., Chandler, D. G., and Saxton, K. E.: Evidence for direct suspension of loessial soils on the Columbia Plateau, Earth Surface Processes and Landforms, 29, 221–236, 10.1002/esp.1028, 2004.

Krueger, B. J., Grassian, V. H., Cowin, J. P., and Laskin, A.: Heterogeneous chemistry of individual mineral dust particles from different dust source regions: the importance of

particle mineralogy, Atmospheric Environment, 38, 6253-6261, 10.1016/j.atmosenv.2004.07.010, 2004.

Langmann, B.: Volcanic Ash versus Mineral Dust: Atmospheric Processing and Environmental and Climate Impacts, ISRN Atmospheric Sciences, 2013, 17, 10.1155/2013/245076, 2013.

Lee, J. A., and Tchakerian, V. P.: Magnitude and Frequency of Blowing Dust on the Southern High Plains of the United States, 1947–1989, Annals of the Association of American Geographers, 85, 684-693, 10.1111/j.1467-8306.1995.tb01820.x, 1995.

Li, F., Ginoux, P., and Ramaswamy, V.: Distribution, transport, and deposition of mineral dust in the Southern Ocean and Antarctica: Contribution of major sources, Journal of Geophysical Research: Atmospheres, 113, 10.1029/2007JD009190, 2008.

Loosmore, G. A., and Hunt, J. R.: Dust resuspension without saltation, Journal of Geophysical Research: Atmospheres, 105, 20663–20671, 10.1029/2000JD900271, 2000.

Losno, R., Bergametti, G., Carlier, P., and Mouvier, G.: Major ions in marine rainwater with attention to sources of alkaline and acidic species, Atmospheric Environment. Part A. General Topics, 25, 763-770, http://dx.doi.org/10.1016/0960-1686(91)90074-H, 1991.

Loye-Pilot, M. D., Martin, J. M., and Morelli, J.: Influence of Saharan dust on the rain acidity and atmospheric input to the Mediterranean, Nature, 321, 427-428, 1986.

Macpherson, T., Nickling, W. G., Gillies, J. A., and Etyemezian, V.: Dust emissions from undisturbed and disturbed supply-limited desert surfaces, Journal of Geophysical Research: Earth Surface, 113, n/a–n/a, 10.1029/2007JF000800, 2008.

Mahowald, N. M., Bryant, R. G., del Corral, J., and Steinberger, L.: Ephemeral lakes and desert dust sources, Geophysical Research Letters, 30, n/a–n/a, 10.1029/2002GL016041, 2003.

Mahowald, N. M., Baker, A. R., Bergametti, G., Brooks, N., Duce, R. A., Jickells, T. D., Kubilay, N., Prospero, J. M., and Tegen, I.: Atmospheric global dust cycle and iron inputs to the ocean, Global Biogeochemical Cycles, 19, GB4025, 10.1029/2004GB002402, 2005.

Mahowald, N. M.: Anthropocene changes in desert area: Sensitivity to climate model predictions, Geophysical Research Letters, 34, n/a-n/a, 10.1029/2007GL030472, 2007.

Maring, H., Savoie, D. L., Izaguirre, M. A., Custals, L., and Reid, J. S.: Mineral dust aerosol size distribution change during atmospheric transport, Journal of Geophysical Research: Atmospheres, 108, n/a–n/a, 10.1029/2002JD002536, 2003.

Marticorena, B., and Bergametti, G.: Modeling the atmospheric dust cycle: 1. Design of a soil-derived dust emission scheme, Journal of Geophysical Research: Atmospheres, 100, 16415-16430, 10.1029/95JD00690, 1995.

Meadows, M. E.: Soil erosion in the Swartland, Western Cape Province, South Africa: implications of past and present policy and practice, Environmental Science & Policy, 6, 17-28, 10.1016/S1462-9011(02)00122-3, 2003.

Mendez, J., Guieu, C., and Adkins, J.: Atmospheric input of manganese and iron to the ocean: Seawater dissolution experiments with Saharan and North American dusts, Marine Chemistry, 120, 34-43, http://dx.doi.org/10.1016/j.marchem.2008.08.006, 2010.

Meskhidze, N., Chameides, W. L., Nenes, A., and Chen, G.: Iron mobilization in mineral dust: Can anthropogenic SO2 emissions affect ocean productivity?, Geophysical Research Letters, 30, n/a-n/a, 10.1029/2003GL018035, 2003.

Miller, M. S., Friedlander, S. K., and Hidy, G. M.: A chemical element balance for the Pasadena aerosol, Journal of Colloid and Interface Science, 39, 165-176, 10.1016/0021-9797(72)90152-X, 1972.

Morel, F. M. M., Hudson, R. J. M., and Price, N. M.: Limitation of Productivity by Trace Metals in the Sea, Limnology and Oceanography, 36, 1742-1755, 10.2307/2837711, 1991.

Paris, R., Desboeufs, K. V., and Journet, E.: Variability of dust iron solubility in atmospheric waters: Investigation of the role of oxalate organic complexation, Atmospheric Environment, 45, 6510-6517, 10.1016/j.atmosenv.2011.08.068, 2011.

Paris, R., and Desboeufs, K. V.: Effect of atmospheric organic complexation on iron-bearing dust solubility, Atmos. Chem. Phys., 13, 4895-4905, 10.5194/acp-13-4895-2013, 2013.

Prospero, J. M., Uematsu, M., and Savoie, D. L.: Mineral Aerosol Transport to the Pacific Ocean, Chemical Oceanography, 187 pp., 1989.

Prospero, J. M.: The atmospheric transport of particles to the ocean, in: SCOPE-Scientific Committee on Problems of the Environment International Council of Scientific Unions, 19-52, 1996.

Prospero, J. M., Ginoux, P., Torres, O., Nicholson, S. E., and Gill, T. E.: Environmental characterization of global sources of atmospheric soil dust identified with the Nimbus 7 Total Ozone Mapping Spectrometer (TOMS) absorbing aerosol product, Reviews of Geophysics, 40, 1002, 10.1029/2000RG000095, 2002.

Rich, H. W., and Morel, F. M. M.: Availability of Well-Defined Iron Colloids to the Marine Diatom Thalassiosira weissflogii, Limnology and Oceanography, 35, 652-662, 10.2307/2837616, 1990.

Rosenfeld, D., Andreae, M. O., Asmi, A., Chin, M., de Leeuw, G., Donovan, D. P., Kahn, R., Kinne, S., Kivekäs, N., Kulmala, M., Lau, W., Schmidt, K. S., Suni, T., Wagner, T., Wild, M., and Quaas, J.: Global observations of aerosol-cloud-precipitation-climate interactions, Reviews of Geophysics, 52, 2013RG000441, 10.1002/2013RG000441, 2014.

Sarthou, G., Baker, A. R., Blain, S., Achterberg, E. P., Boye, M., Bowie, A. R., Croot, P., Laan, P., de Baar, H. J. W., Jickells, T. D., and Worsfold, P. J.: Atmospheric iron deposition and sea-surface dissolved iron concentrations in the eastern Atlantic Ocean, Deep Sea Research Part I: Oceanographic Research Papers, 50, 1339-1352, 10.1016/S0967-0637(03)00126-2, 2003.

Scasso, R. A., Corbella, H., and Tiberi, P.: Sedimentological analysis of the tephra from the 12–15 August 1991 eruption of Hudson volcano, Bulletin of Volcanology, 56, 121-132, 10.1007/BF00304107, 1994.

Schütz, L., and Rahn, K. A.: Trace-element concentrations in erodible soils, Atmospheric Environment (1967), 16, 171-176, 10.1016/0004-6981(82)90324-9, 1982.

Schulz, M., Balkanski, Y. J., Guelle, W., and Dulac, F.: Role of aerosol size distribution and source location in a three-dimensional simulation of a Saharan dust episode tested against satellite-derived optical thickness, Journal of Geophysical Research: Atmospheres, 103, 10579-10592, 10.1029/97JD02779, 1998.

Schulz, M., Prospero, J. M., Baker, A. R., Dentener, F., Ickes, L., Liss, P. S., Mahowald, N. M., Nickovic, S., García-Pando, C. P., Rodríguez, S., Sarin, M., Tegen, I., and Duce, R. A.: Atmospheric Transport and Deposition of Mineral Dust to the Ocean: Implications for Research Needs, Environmental Science & Technology, 46, 10390-10404, 10.1021/es300073u, 2012.

Sedwick, P. N., Sholkovitz, E. R., and Church, T. M.: Impact of anthropogenic combustion emissions on the fractional solubility of aerosol iron: Evidence from the Sargasso Sea, Geochemistry Geophysics Geosystems, 8, 10.1029/2007gc001586, 2007.

Shao, Y., Raupach, M. R., and Findlater, P. A.: Effect of saltation bombardment on the entrainment of dust by wind, Journal of Geophysical Research: Atmospheres, 98, 12719–12726, 10.1029/93JD00396, 1993.

Shao, Y.: Dust Emission, in: Physics and Modelling of Wind Erosion, edited by: Shao, Y., Atmospheric and Oceanographic Sciences Library, Springer Netherlands, 211-245, 2008.

Shi, Z., Krom, M. D., Jickells, T. D., Bonneville, S., Carslaw, K. S., Mihalopoulos, N., Baker, A. R., and Benning, L. G.: Impacts on iron solubility in the mineral dust by processes in

the source region and the atmosphere: A review, Aeolian Research, 5, 21-42, 10.1016/j.aeolia.2012.03.001, 2012.

Shi, Z., Krom, M. D., Bonneville, S., and Benning, L. G.: Atmospheric Processing Outside Clouds Increases Soluble Iron in Mineral Dust, Environmental Science & Technology, 49, 1472-1477, 10.1021/es504623x, 2015.

Singer, M. J., Southard, R. J., Warrington, D. N., and Janitzky, P.: Stability of Synthetic Sand-Clay Aggregates after Wetting and Drying Cycles, Soil Science Society of America Journal, 56, 1843-1848, 10.2136/sssaj1992.03615995005600060032x, 1992.

Singer, M. J., and Shainberg, I.: Mineral soil surface crusts and wind and water erosion, Earth Surface Processes and Landforms, 29, 1065-1075, 10.1002/esp.1102, 2004.

Slinn, W. G. N.: Precipitation scavenging of aerosol particles, Geophysical Research Letters, 3, 21-22, 10.1029/GL003i001p00021, 1976.

Spokes, L. J., Jickells, T. D., and Lim, B.: Solubilisation of aerosol trace metals by cloud processing: A laboratory study, Geochimica et Cosmochimica Acta, 58, 3281-3287, http://dx.doi.org/10.1016/0016-7037(94)90056-6, 1994.

Spokes, L. J., and Jickells, T. D.: Factors controlling the solubility of aerosol trace metals in the atmosphere and on mixing into seawater, Aquatic Geochemistry, 1, 355-374, 10.1007/BF00702739, 1995.

Stern, C. R.: Holocene tephrochronology record of large explosive eruptions in the southernmost Patagonian Andes, Bulletin of Volcanology, 70, 435-454, 10.1007/s00445-007-0148-z, 2008.

Sweeney, M. R., and Mason, J. A.: Mechanisms of dust emission from Pleistocene loess deposits, Nebraska, USA, Journal of Geophysical Research: Earth Surface, 118, 1460–1471, 10.1002/jgrf.20101, 2013.

Taylor, S. R., and McLennan, S. M.: The geochemical evolution of the continental crust, Reviews of Geophysics, 33, 241-265, 10.1029/95RG00262, 1995.

Textor, C., Schulz, M., Guibert, S., Kinne, S., Balkanski, Y., Bauer, S., Berntsen, T., Berglen, T., Boucher, O., Chin, M., Dentener, F., Diehl, T., Easter, R., Feichter, H., Fillmore, D., Ghan, S., Ginoux, P., Gong, S., Grini, A., Hendricks, J., Horowitz, L., Huang, P., Isaksen, I., Iversen, I., Kloster, S., Koch, D., Kirkevåg, A., Kristjansson, J. E., Krol, M., Lauer, A., Lamarque, J. F., Liu, X., Montanaro, V., Myhre, G., Penner, J., Pitari, G., Reddy, S., Seland, Ø., Stier, P., Takemura, T., and Tie, X.: Analysis and quantification of the diversities of aerosol life cycles within AeroCom, Atmos. Chem. Phys., 6, 1777-1813, 10.5194/acp-6-1777-2006, 2006.

Torres, O., Bhartia, P. K., Herman, J. R., Sinyuk, A., Ginoux, P., and Holben, B.: A Long-Term Record of Aerosol Optical Depth from TOMS Observations and Comparison to AERONET Measurements, Journal of the Atmospheric Sciences, 59, 398-413, 10.1175/1520-0469(2002)059<0398:ALTROA>2.0.CO;2, 2002.

Visser, F., Gerringa, L. J. A., Van der gaast, S. J., De baar, H. J. W., and Timmermans, K. R.: THE ROLE OF THE REACTIVITY AND CONTENT OF IRON OF AEROSOL DUST ON GROWTH RATES OF TWO ANTARCTIC DIATOM SPECIES1, Journal of Phycology, 39, 1085-1094, 10.1111/j.0022-3646.2003.03-023.x, 2003.

Wagener, T., Guieu, C., Losno, R., Bonnet, S., and Mahowald, N.: Revisiting atmospheric dust export to the Southern Hemisphere ocean: Biogeochemical implications, Global Biogeochemical Cycles, 22, GB2006, 10.1029/2007GB002984, 2008.

Winton, V. H. L., Dunbar, G. B., Bertler, N. A. N., Millet, M. A., Delmonte, B., Atkins, C. B., Chewings, J. M., and Andersson, P.: The contribution of aeolian sand and dust to iron fertilization of phytoplankton blooms in southwestern Ross Sea, Antarctica, Global Biogeochemical Cycles, 28, 2013GB004574, 10.1002/2013GB004574, 2014.

Wu, J., Rember, R., and Cahill, C.: Dissolution of aerosol iron in the surface waters of the North Pacific and North Atlantic oceans as determined by a semicontinuous flow-through

reactor method, Global Biogeochemical Cycles, 21, GB4010, 10.1029/2006GB002851, 2007.

Zender, C. S., Bian, H., and Newman, D.: Mineral Dust Entrainment and Deposition (DEAD) model: Description and 1990s dust climatology, Journal of Geophysical Research: Atmospheres, 108, n/a–n/a, 10.1029/2002JD002775, 2003a.

Zender, C. S., Newman, D., and Torres, O.: Spatial heterogeneity in aeolian erodibility: Uniform, topographic, geomorphic, and hydrologic hypotheses, Journal of Geophysical Research: Atmospheres, 108, 4543, 10.1029/2002JD003039, 2003b.

Zhang, Y., Mahowald, N., Scanza, R. A., Journet, E., Desboeufs, K., Albani, S., Kok, J. F., Zhuang, G., Chen, Y., Cohen, D. D., Paytan, A., Patey, M. D., Achterberg, E. P., Engelbrecht, J. P., and Fomba, K. W.: Modeling the global emission, transport and deposition of trace elements associated with mineral dust, Biogeosciences, 12, 5771-5792, 10.5194/bg-12-5771-2015, 2015.

Zhu, X., Prospero, J. M., Millero, F. J., Savoie, D. L., and Brass, G. W.: The solubility of ferric ion in marine mineral aerosol solutions at ambient relative humidities, Marine Chemistry, 38, 91-107, 10.1016/0304-4203(92)90069-M, 1992.

Chapter 2 Long-term dust concentration measurements in Patagonia

Introduction of Chapter

Quantification of dust concentration in source area is essential to quantify the export of dust and the input of micronutrients to the marine ecosystem. In the Southern Hemisphere, Patagonia is a major mineral dust source for the Southern Ocean. This Chapter presents our study on the temporal variability of dust concentration in southern Patagonia. Main work of this study is presented in this Chapter as submitted article entitled "**Seasonal variability and meteorological control of mineral aerosol in the south Patagonia**". Supporting information is provided in the end of Chapter for more details.

Submitted Article

Seasonal variability and meteorological control of mineral aerosol in the south Patagonia

Z. Qu[1,2], R. Losno[1,3], É. Journet[1], J. Salvador[4], D. Bulnes[4], Y. Balkanski[5], F. Monna[6], J. P. Quisefit[1], A. Heimburger[1], P. Ristori[4], and E. J. Quel[4]

[1]LISA UMR 7583, Université Paris Diderot, Université Paris Est, CNRS, 61 avenue du Général de Gaulle, 94010 Créteil Cedex, France

[2]Sorbonne Universités, UPMC Univ Paris 06, IFD, 4 Place Jussieu, 75252 Paris cedex 05, France

[3]IPGP, UMR CNRS 7154, Université Paris Diderot, SPC, 1 Rue Jussieu, 75005 Paris, France

[4]División Lidar - CEILAP - UMI-IFAECI-CNRS 3351, CITEDEF UNIDEF (MINDEF-CONICET), Villa Martelli, Buenos Aires, Argentina

[5]Laboratoire des Sciences du Climat et de l'Environnement, l'Orme des Merisiers, 91191 Gif sur Yvette Cedex, France

[6]ARTéHIS UMR 6298, Université de Bourgogne - CNRS, Dijon, France

Corresponding author: Zihan Qu (zihan.qu88@gmail.com)

Abstract

Patagonia is a major mineral dust source in the Southern Hemisphere. From November 2011 to August 2014, aerosol samples were collected weekly in Río Gallegos, south Patagonia-Atlantic Coast (69.32°W, 51.60°S). Masses of Na, Al, Si and Fe were determined by X-ray fluorescence analysis. Mineral dust concentrations were estimated from atmospheric concentrations of Si. Weekly average mineral dust concentrations in Río Gallegos vary from 0.07 to 3.68 $\mu g.m^{-3}$. Sea-salt concentrations range from 0.16 to 2.40 $\mu g.m^{-3}$. Dust concentrations during the three-year measurements revealed a seasonal pattern with lower concentrations in winter than in the other three seasons. The co-analysis with climate data (from a meteorological station and wind reanalysis) indicates that the variability in dust concentrations is not driven by the wind speed at potential source areas. The dust concentration is significantly correlated with air temperature and negatively correlated with the minimum relative air humidity. Frozen land and/or snow cover may be the cause of the continuous low dust concentration in winter. Our result suggests that alteration of surface soil moisture, rather than wind speed, is the primary regulating factor of dust emission in Patagonia. The fact that the seasonal dust concentration correlates with the variation in temperature and relative air humidity implicates a feedback of dust emission in response to short-term climate variations.

1. Introduction

Mineral dust input to the ocean is known to regulate the carbon uptake of High Nutrients Low Chlorophyll (HNLC) regions via fertilization with micronutrients such as Fe, and hence influences the global climate [*Arimoto*, 2001; *de Baar et al.*, 1995; *Jickells et al.*, 2005; *Maher et al.*, 2010; *Mahowald*, 2011; *Martin*, 1990; *Shao et al.*, 2011; *Watson et al.*, 2000]. Though dust deposition fluxes are low in the Southern Ocean [*Chisholm and Morel*, 1991; *Duce and Tindale*, 1991; *Heimburger et al.*, 2012; *Heimburger et al.*, 2013], the large area covered by the Southern Ocean and the high concentration of unused macronutrients in the surface water highlights the fertilization effect of dust input into this iron-limited oceanic region [*Boyd et al.*, 2007; *Mahowald et al.*, 2005].

Patagonia appears to be a major supplier of mineral dust to the Southern Ocean [*Iriondo*, 2000; *Johnson et al.*, 2010; *Li et al.*, 2008; *Mahowald et al.*, 2005; *Prospero et al.*, 2002]. *Li et al.* [2008] estimated that 58% of dust deposition in the Southern Ocean (south of 50°S) originates from South America, of which more than 70% is provided by Patagonia alone. *Ginoux et al.* [2012] further indicated that dust sources during the Patagonian summer are often associated with major river basins and salt lakes, such as sections of the Gallegos River in the Santa Cruz province. Using remote sensing methods and the Hybrid Single-Particle Lagrangian Integrated Trajectory model (HYSPLIT model), *Gassó et al.* [2010] and *Gassó and Stein* [2007] reported several dust events occurring between 46°S and 54°S of Patagonia. However, the frequent cloudy conditions in Patagonia disturb continuous dust event observations by satellite, continuous ground-based field studies are necessary to improve our understanding of Patagonian dust. *Gaiero et al.* [2003] measured the dust deposition flux for the first time at three coastal sites in north and central Patagonia (latitudes 38°S, 43°S and 45°S) and found seasonal patterns of dust deposition. Dust activity appears to be generally more frequent in summer, even if some events are also observed in fall and winter. However, a time series of the atmospheric dust concentrations in Patagonia has not yet been reported.

The main goal of this work is to measure mineral dust concentrations near the coast where dust from Patagonia gets exported to the Atlantic Ocean. In the results

and discussion section, we present for the first time a three-year continuous time series of atmospheric dust concentration, and sea-salt concentration as supplementary information, in Patagonia. The temporal pattern of the dust concentration and its relationship with meteorological conditions was examined in order to shed light on the potential regulating factors of dust activity in Patagonia.

2. Materials and methods

2.1. Aerosol sampling location and methods

The Laser and Applications Investigation Center (CEILAP, Argentina) set up the "Observatorio Atmosférico de la Patagonia Austral" (OAPA) station to the west of Río Gallegos (Figure 8), Argentina, to measure ozone profiles, NO_2, and solar UV radiation since 2005. The distance of OAPA from the seashore is 27 km.

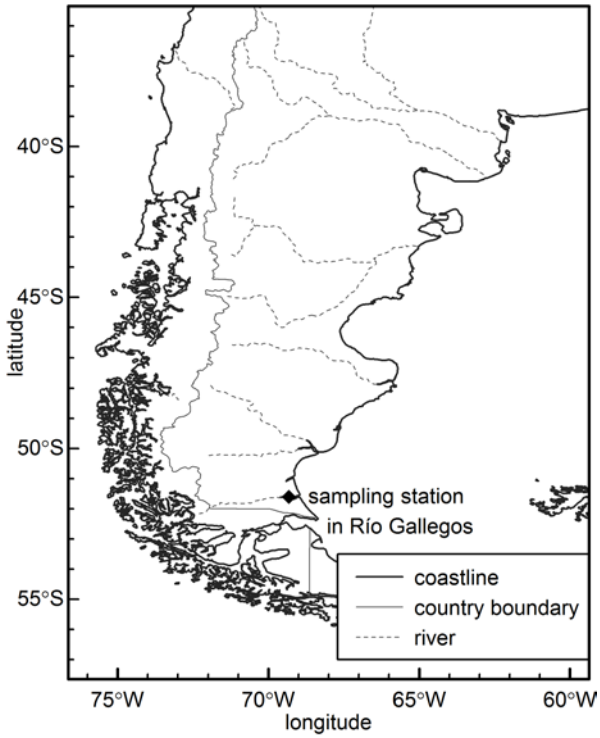

Figure 8 : Aerosols sampling location (69.32°W, 51.60°S), Río Gallegos, Patagonia.

An aerosol sampling station (69.32°W, 51.60°S) (Figure 8) was set up close to the OAPA station. The site is managed by the Argentine Ministry of Defense and its

access is strictly limited, considerably restricting possible anthropogenic influences on aerosol sampling. The nearest building is located 150 m downwind from the sampling site. The sampling station is installed in a large flat area and the nearest upwind elevation (> 100 m) is located 17 km away.

Aerosol samples were continuously collected on a weekly basis between November 2011 and August 2014, using an original aerosol collection system similar to the one described in *Heimburger et al.* [2012]: filter units were mounted downwards in a PVC pipe at a height of 2 meters above ground level (AGL) on a PVC mast. The filter units consist of a Zéfluor^{TM} PTFE Teflon membrane (0.5 µm pore size, 47 mm diameter) embedded in a polycarbonate NILU (Norwegian Institute for Air Research) open-face filter holder. The exposure area of the filters was 40 mm in diameter. Air was pumped through the filter (16 L.min^{-1}) to collect aerosol. The air volume pumped was measured with a Schlumberger gas meter. One hundred and thirty filter samples were finally obtained during the whole sampling period. Prior to aerosol collection, filters and filter storage boxes were acid-cleaned in an ISO 1 laminar flow bench located in an ISO 5 cleanroom. Zéfluor^{TM} filters were successively rinsed with sub-boiled ethanol, 2% hydrochloric acid, sub-boiled ethanol and MilliQ water. The use of ethanol helps to overcome the hydrophobic properties of Teflon. Throughout the collection period, an ultra-clean air flow unit within an isolated clean area was implemented in field to handle the loading-unloading operations of filters into filter holders. Filters were transported between the sampling tower and the field clean area using a sealed clean plastic bag to avoid contamination.

2.2. Elemental analysis

The mass of the collected elements, Na (as a reference element of marine aerosol), Al, Si and Fe (as reference elements of mineral aerosol) [*Bergametti et al.*, 1989; *Mahowald et al.*, 2008], was determined using an X-ray fluorescence (XRF) instrument (PANalytical, Epsilon 3XL). Disks measuring 15 mm in diameter were cut from Zéfluor^{TM} filters using a gasket cutter (made of Zn-Fe-Cr alloy) to adapt the disks to the size requirement of the instrument. Aerosols collected on Zéfluor^{TM} filters are considered as a “thin layer” [*Losno et al.*, 1987], which have a minimum matrix effect. Thus, the fluorescence intensity is proportional to the mass of the element present in the analyzed area. The determination of the element mass can be used to

estimate the elemental composition of the aerosol, which will be partially calculated for the mineral fraction of the collected aerosol, as presented in Sect. 2.3.

The element mass analysis was calibrated adapting the method proposed by *Quisefit and Randrianarivony* [1998]. This method consists of preparing calibration filters by depositing geo-standards on the filters. Since it is difficult to prepare homogenous geo-standard depositions on Zéfluor^{TM} filters, the calibration filters were prepared with Nuclepore^{TM} polycarbonate membranes (0.2 μm pore size). However, during XRF analyses, the background interference of the polycarbonate membrane is relatively negligible comparing to the Zéfluor^{TM} membrane due to the greater thickness of the Zéfluor^{TM} membrane (~178 μm) than the polycarbonate membrane (~11 μm). Therefore, an acid cleaned Zéfluor^{TM} disk was put behind the polycarbonate standards to produce similar interference during the calibration. Four calibration filters were prepared by depositing crushed certified reference materials (CRMs) on a polycarbonate membrane using ethanol suspension filtration: (1) pure ethanol (> 99.5%) was previously filtered through a 0.2 μm polycarbonate filter, and then distilled in a quartz sub-boiler in order to remove the possible particle and inorganic solute impurities; (2) a small portion of CRM powder (BHVO-1, basalt from the USGS, USA) was manually ground for one hour with an agate mortar to obtain fine mineral particles; (3) 10 mg of CRM powder was added into 20 mL purified ethanol within a 50 mL centrifuge tube; (4) the mixture was then processed by ultra-sonication for 5 minutes and vortex during 1 minute to obtain a suspension of fine CRM particles; (5) 3 mL of CRM suspension was diluted with 15 mL of ethanol in a 50 mL centrifuge tube, followed by a thorough vortex mixing for 1 minute; (6) 3 × 1 mL (or 6 × 1 mL) of the diluted suspension was diluted a second time with approximately 10 mL of ethanol and then slowly filtered through a polycarbonate membrane (pore size of 0.2 μm) to obtain a filter containing 250 μg (or 500 μg) CRM homogenously distributed over an area measuring 18 mm in diameter. In addition, three blank filters were prepared with the same protocol without using CRM. To check the loss of element quantity due to the dissolution of CRMs in the ethanol solution, the filtrate were first evaporated in a Teflon beaker on an electric hotplate; the dry residues were dissolved in 2 mL of nitric acid under 60°C for 2 hours, and then diluted with MilliQ water for elemental analyses by ICP-AES. The dissolution of

geo-standards in ethanol was found to be less than 0.1% for all four elements (maximum dissolution is 0.1% for Al, no dissolution detected for Na, Si and Fe).

To evaluate the accuracy of the analytical procedures, three additional filters with 500 µg GS-N (CRMs from SARM, Nancy, France) deposits were prepared directly on Zéfluor^{TM} membranes, with a deposition area measuring 42 mm in diameter, using the same protocol as the BHVO-1 standard preparation. Three to five disks were cut off from each GS-N filter and their analytical results were averaged to minimize heterogeneity issues. The mean recovery rate (mean ± SD) of the GS-N filters is 110 ± 8% for Na, 106 ± 2% for Al, 103 ± 2% for Si, and 94 ± 5% for Fe.

2.3. Chemical compositions of the crustal fraction of the aerosol

Oxygen, silicon, aluminum and iron are the four major elements in the upper continental crust. According to the upper continental crust composition in *Taylor and McLennan* [1995] (referred to as TM95), Al_2O_3, Fe_2O_3 and SiO_2, contribute 86% of the total mass of the crust. The compositions of Al_2O_3, Fe_2O_3 and SiO_2, which thus compose the major part of the crustal fraction of the collected aerosol, are calculated for each filter according to the equation below:

$$c_{i,j} = m_{i,j} / \left(m_{Al_2O_3,j} + m_{Fe_2O_3,j} + m_{SiO_2,j} \right), \qquad (1)$$

where j denotes the number of filters, i is Al_2O_3, Fe_2O_3 or SiO_2, $c_{i,j}$ is the composition for oxide i in filter j, $m_{i,j}$ is the mass of oxide i in filter j.

2.4. Air mass back trajectories

To identify the origin of the air masses and potential dust source areas, back trajectories were generated for each day of the sampling period (from November 2011 to August 2014, a period composed of 987 days in total) using the HYSPLIT model [*Draxler and Rolph*, 2015; *Rolph*, 2015]. Back trajectories were calculated using Global Data Assimilation System (GDAS) meteorological data, starting from the aerosol sampling site (51.60°S, 69.33°W) at 15:00 UTC (12:00 local time) with a start height of 500 m AGL. The hourly end point of the last six hours before arriving

the sampling site was identified to calculate the probability distribution of end points in each 0.5°× 0.5° grid of the study area (longitude: 65~75°W, latitude: 45~55°S).

2.5. Wind simulation and meteorological records

In most dust emission models, dust emission caused by wind erosion usually depends on wind speeds and land surface characteristics [*Marticorena and Bergametti*, 1995; *YP Shao et al.*, 1996]. To understand the role of wind speed in the control of dust emission over Patagonia, we co-analyzed the variability of the wind speed in the dust source areas and the measured dust concentrations.

Since observed inland wind speed data are not available in Patagonia due to the lack of meteorological stations, the European Centre for Medium-Range Weather Forecasts (ECMWF) model was used to simulate the 6-hourly average wind speed (10 m AGL) over the southern Patagonia region (resolution: 1.125°× 1.125°) for the years 2012 and 2013. Standard meteorological records in Río Gallegos, namely wind speed (W), daily surface temperature (T), daily precipitation (Prep.) and daily air relative humidity (min RH and max RH) were also obtained from the Meteorological Station at the Río Gallegos Airport (69.28°W, 51.62°S, sea level altitude: 19 m). The meteorological station is located 1.7 km to the east of the aerosol sampling station. The tableland between east of the Andes and the sampling site is a 400 km wide flat area. The surface temperature and relative humidity measured in Río Gallegos should be representative of this upwind region.

Dependence of dust concentrations on wind speed and other meteorological parameters were evaluated by correlation analysis. As their relationships might be non-linear, the non-parametric Spearman's rank test was applied to calculate the correlation coefficients. Mean values for the daily meteorological data were calculated for each sampling cycle. The mean number of days with sub-zero temperatures (n freeze) and maximum wind speed were also calculated and tested as an active variable.

3. Results and discussion

3.1. Chemical composition of the dust fraction

During the whole sampling period, 130 filters were collected. Three major elements Si, Al, and Fe were measured for the crustal fraction of the aerosols. All the 130 collected filter samples have mass of Si larger than the detection limit, while 47 less loaded samples have Al or Fe mass under the detection limit. The 47 less loaded filters were thus excluded during the composition estimation. We first assumed that the composition of Al_2O_3, Fe_2O_3, and SiO_2 in each filter add up to 100%. The average compositions ($c_i \pm$ SD) of Al_2O_3, Fe_2O_3, and SiO_2 are 13.0 ± 2.0%, 8.7 ± 1.3% and 78.3 ± 2.5%, respectively. In the upper continental crust TM95 [*Taylor and McLennan*, 1995], the compositions of Al_2O_3, Fe_2O_3, and SiO_2 adding up to 100% are 17.6%, 5.8% and 76.5%, respectively. Thus, the compositions of the three major elements in aerosol samples are similar to the upper continental crust, particularly for Si. However, the mass of the elements, such as Ca, Ti, K, Mg, in the aerosol samples were not measured in this work. According to the TM95 crust model, the total mass contributed by Al_2O_3, Fe_2O_3 and SiO_2 is 86%. In the rest of our work, we assume that the mass of the unmeasured major elements represents the same mass in the collected dust as in the TM95. A correction factor is thus applied to the previously measured composition c_i to obtain a corrected average composition of the mineral dust:

$$cc_i = c_i \times 0.86, \qquad (2)$$

where cc_i is the corrected average composition for oxide i, c_i is the average composition of i, 0.86 is the sum of Al_2O_3, Fe_2O_3 and SiO_2 compositions in the upper continental crust in *Taylor and McLennan* [1995].

The corresponding corrected average elemental compositions ($cc_i \pm SD$) of Al, Fe, and Si equaling to 5.9 ± 0.9%, 5.2 ± 0.8% and 31 ± 1%, respectively. *Gaiero et al.* [2007] studied dust depositions in Patagonia and reported dust compositions with higher Al concentration (8.2%), slightly lower Fe concentration (4.3%), and similar Si concentration (29%). Comparing to other desert regions, Patagonian dust reveals a Si/Al ratio of 5.3 in our study and 3.5 in the deposition of *Gaiero et al.* [2007], which

is close to 4.3 in Arizona dust [*Desboeufs et al.*, 2005], but is higher than 2.02 in Saharan dust [*Formenti et al.*, 2003] and 1.9 in Asian dust [*Arimoto et al.*, 2004].

3.2. Atmospheric concentration of sea salt and mineral dust

The mass of sea salt (using Na as a reference) was estimated from the mass of Na:

$$m_{sea-salt,j} = m_{Na,j} \times \left(M_{NaCl,j} / M_{Na} \right) = m_{Na,j} \times 2.54 , \qquad (3)$$

where m is the mass and M is the molar mass.

The mineral aerosol mass was estimated from the mass of Si using Eq. (4), which is relatively less variable than Al and Fe in terms of composition throughout the sampling period:

$$m_{dust,j} = m_{Si,j} / cc_{Si} = m_{Si,j} / 0.315 , \qquad (4)$$

Based on the estimated mass of the mineral dust and sea salt, atmospheric concentrations $\rho_{i,j}$ during the sampling period of filter j were calculated according to Eq. (5):

$$\rho_{i,j} = m_{i,j} / V_j , \qquad (5)$$

where $m_{i,j}$ is the collected mass of component i (dust or sea salt) in sample j, V_j is the volume of air pumped through the filter j.

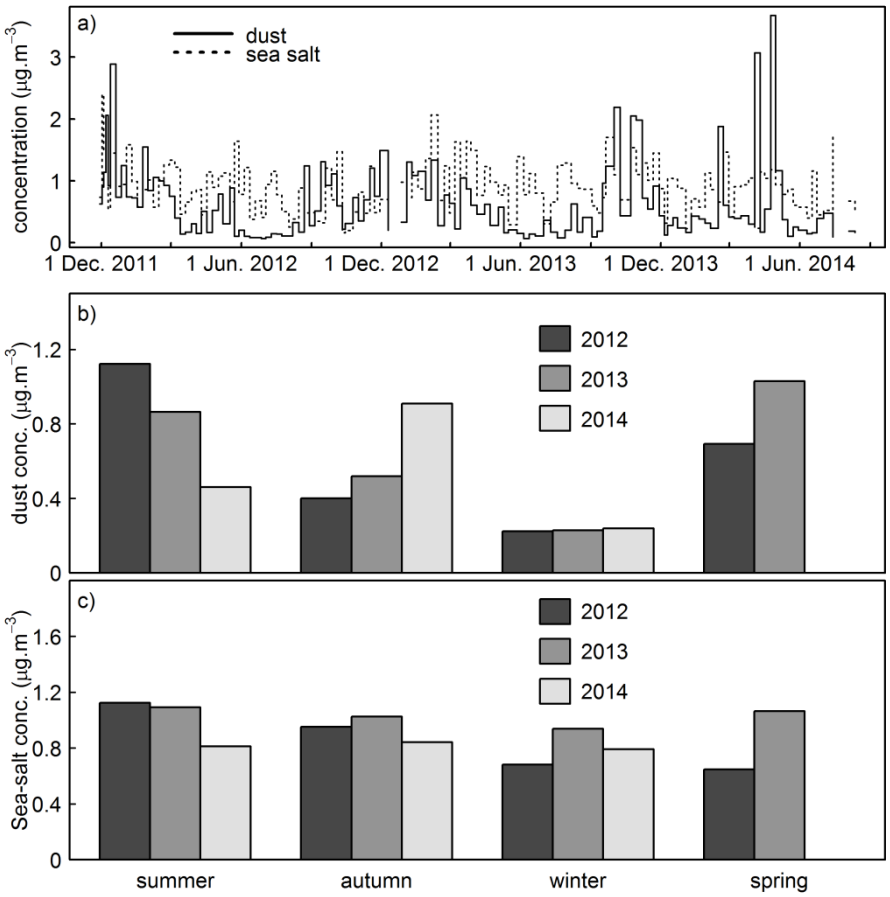

Figure 9 : a) Time series of aerosol concentrations measured in Río Gallegos. The solid line represents the concentration of the dust fraction and the dashed line is the concentration of the sea-salt fraction. b) Seasonal averaged dust concentrations for the three sampling years. Dust concentrations in winter are lower than the three other seasons. c) Seasonal averaged sea-salt concentrations for the same period.

Figure 9 illustrates the weekly mean concentrations of atmospheric dust and sea salt during the 32-month sampling period. Weekly average concentrations of sea-salt aerosol ranged from 0.16 to 2.40 $\mu g.m^{-3}$. In comparison with published sea-salt concentrations in other sites (Table 2), our measurements in Río Gallegos (mean ± SD = 0.91 ± 0.41 $\mu g.m^{-3}$) shared similar values with 1.36 ± 1.00 $\mu g.m^{-3}$ at the Dumont (66°S), 0.86 ± 0.78 $\mu g.m^{-3}$ at the Neumayer (70°S), but was quite different from 0.20 ± 0.18 $\mu g.m^{-3}$ at the Halley Bay (75°S) [*Wagenbach et al.*, 1998], 3.05 ± 2.11 $\mu g.m^{-3}$ at the Palmer (65°S, 64°W), 8.01 ± 4.88 $\mu g.m^{-3}$ at the Marsh (62°S, 58°W), and 0.368 ± 0.363 $\mu g.m^{-3}$ at the Mawson (62°S, 63°E) [*Savoie et al.*, 1993]. Dumont Station and Marsh Station are two island sampling sites with surrounding open water which could

explain the relatively higher sea-salt concentrations. Palmer station receives surface wind from open ocean and exhibited higher sea-salt concentrations than at Halley Bay and Mawson receiving surface winds from inland. In a recent study, *Xu and Gao* [2014] reported a highly variable sea-salt concentrations ranging from 0.46 to 4.9 $\mu g.m^{-3}$ over Southern Ocean and from 0.41 to 4.6 $\mu g.m^{-3}$ over coastal East Antarctica. The sea-salt concentration measured in Río Gallegos in this work was relatively lower than most measurements over the open ocean or over the coastal area, suggesting a Pacific origin of sea salt due to the westerly wind over Patagonia.

Table 2. Concentrations of sea-salt aerosol and dust in this study and in the literature.

	location	mean(± SD) or range ($\mu g.m^{-3}$)
dust		
Xu and Gao (2014)	Southern Ocean	1.0 – 3.1[a]
	coastal East Antarctica	1.7-4.0[a]
Heimburger et al. (2012)	Kerguelen	0.024 (± 0.023)[a]
Wagener et al. (2008)	Southern Ocean	0.013 (± 0.006)[a]
	southeast Pacific-Chile	3.195 (± 0.494)
Dick (1991)	Antarctic Peninsula	0.002[a]
Prospero (1996)	Cape Grim	0.1 – 3.2[a]
this study	Río Gallegos (annual)	0.07 - 3.68[b]
sea salt		
Xu and Gao (2014)	Southern Ocean	0.46 - 4.9
	coastal East Antarctica	0.41 – 4.6
Wagenbach et al. (1998)	Halley Bay, Antarctica (75°S)	0.20 (± 0.18)
	Neumayer, Antarctica (70°S)	0.86 (± 0.78)
	Dumont, Antarctica (66°S)	1.36 (± 1.00)
Savoie et al. (1993)	Palmer, Antarctica (65°S, 64°W)	3.05 (± 2.11)
	Marsh, Antarctica (62°S, 58°W)	8.01 (± 4.88)
	Mawson, Antarctica (62°S, 63°E)	0.368 (± 0.363)
this study	Río Gallegos (annual)	0.91(± 0.41)

[a]estimated using Al as a reference element and 7.7% as a reference composition.
[b]estimated using SiO_2 as a reference element and 67.3% as a reference composition.

Weekly concentrations of mineral dust ranged from 0.07 to 3.68 $\mu g.m^{-3}$ (Table 2).The mineral dust concentration (mean ± SD = 0.63 ± 0.62 $\mu g.m^{-3}$, RSD = 99%) was more variable than sea-salt aerosol (mean ± SD = 0.91 ± 0.41 $\mu g.m^{-3}$, RSD = 45%) and showed a strong temporal variability. Noticeably, during three short periods after 23 May 2012, 29 May 2013, and 29 May 2015, mineral dust concentrations decreased to low levels and remained stable for roughly three months, while sea-salt aerosol concentrations remained at high levels (Figure 9a). The constant low dust concentration from 23 May 2012 to 6 August 2012 provides a dust concentration

baseline over Patagonia around 0.11 μg.m^{-3}. Previous studies in South Hemisphere generally reported atmospheric aluminum concentrations, allowing estimations and comparisons of dust concentrations (Table 2). Being the only reported result closing to major dust source around Southern Ocean, the coastal study in Cape Grim closing to Australia and reported a dust concentration reported a monthly average dust concentration ranging from 0.1 to 3.2 μg.m^{-3} [*Prospero*, 1996], which is quite similar to our study. The rest studies are remotely located from dust sources. *Heimburger et al.* [2012] obtained a dust concentration of 0.024 ± 0.023 μg.m^{-3} on Kerguelen Island. *Wagener et al.* [2008] observed a dust concentration decreasing from 3.19 ± 0.49 μg.m^{-3} in austral summer near the Chilean coast (36°S, 75°W) to 0.013 ± 0.006 μg.m^{-3} over the Southern Ocean. *Dick* [1991] reported a extremely low dust concentration equaling to 0.002 μg.m^{-3} over the Antarctica Peninsula, suggesting a baseline of dust concentration over the Southern Ocean area. The study of *Xu and Gao* [2014] reported dust concentrations in austral summer ranging from 1.0 to 3.1 μg.m^{-3} over the Southern Ocean and from 1.7 to 4.0 μg.m^{-3} over coastal East Antarctica. In our study over the Patagonia-Atlantic coast, the upper range of the dust concentrations is similar to the concentrations measured over coastal East Antarctica and Chilean coast, whereas the lower range of dust concentrations is close to the values over the open ocean except for the measurement *Xu and Gao* [2014] over the Southern Ocean. The contrast of dust concentration under dusty condition and non-dusty condition suggests an extremely low dust emission in non-dusty periods.

3.3. Seasonal pattern of the aerosol concentration

Seasonal average concentrations of dust and sea salt were calculated from the weekly data (Figure 9b-c). As we observed in Figure 9b, dust concentration revealed a seasonal pattern throughout the sampling period. In contrast, the sea-salt concentration was less variable and did not show a seasonal pattern like dust (Figure 9c). In particular, the sea-salt concentration remained at the same level in winter as in the other seasons. During the three-year sampling, the mean seasonal dust concentrations were 0.82 ± 0.33 μg.m^{-3} (mean ± SD) in summer (December, January and February), 0.61 ± 0.27 μg.m^{-3} in autumn (March, April, and May), 0.86 ± 0.24 μg.m^{-3} in spring (September, October and November), and 0.23 ± 0.01 μg.m^{-3} in winter (June, July and August). Dust concentrations measured by *Aab et al.* [2014] at

the Pierre Auger Observatory (35°S, 69°W, Andes region) are 15 to 30 times higher, ranging from 13.1 ± 5.7 $\mu g.m^{-3}$ in spring to 7.0 ± 4.5 $\mu g.m^{-3}$ in winter. Despite concentrations that were one order of magnitude lower, the seasonality pattern observed at the Pierre Auger Observatory is similar to our study.

3.4. Meteorological dependence of seasonal dynamics of dust concentrations and emission

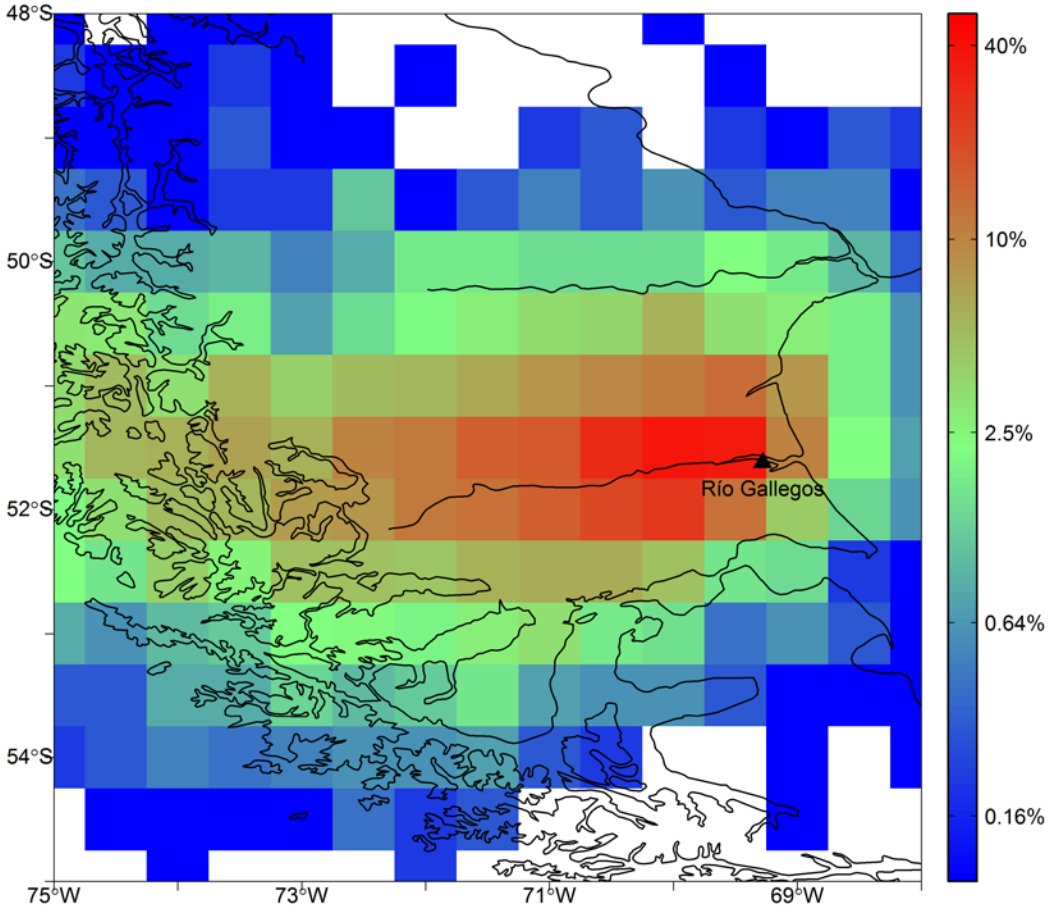

Figure 10: Distribution of the probability that the backward trajectories of air mass passed by each 0.5° × 0.5° grid of the study area (longitude: 65~75°W, latitude: 45~55°S) in the last six hours before arriving the sampling site.

Prior to explore the relationship between the meteorological condition and dust concentration, we first identified potential mineral aerosol source areas in Patagonia using the HYSPLIT back trajectory model. During the whole sampling period, more than 90% of the air masses came from west of the sampling site. Figure 10 illustrates

the probability that the back trajectories of air mass passed by each 0.5° × 0.5° grid of the study area in the last six hours before arriving the sampling site. The distribution is plotted on a logarithm scale. The probability distribution of the air mass end points demonstrates that the main potential dust sources are located in the upwind region of Patagonia within 69~72°W and 51~52°S. In this potential dust source region, the Gallegos River section (within 70~70.75°W and 51~51.75°S) is the unique identified dust source in *Ginoux et al.* [2012].

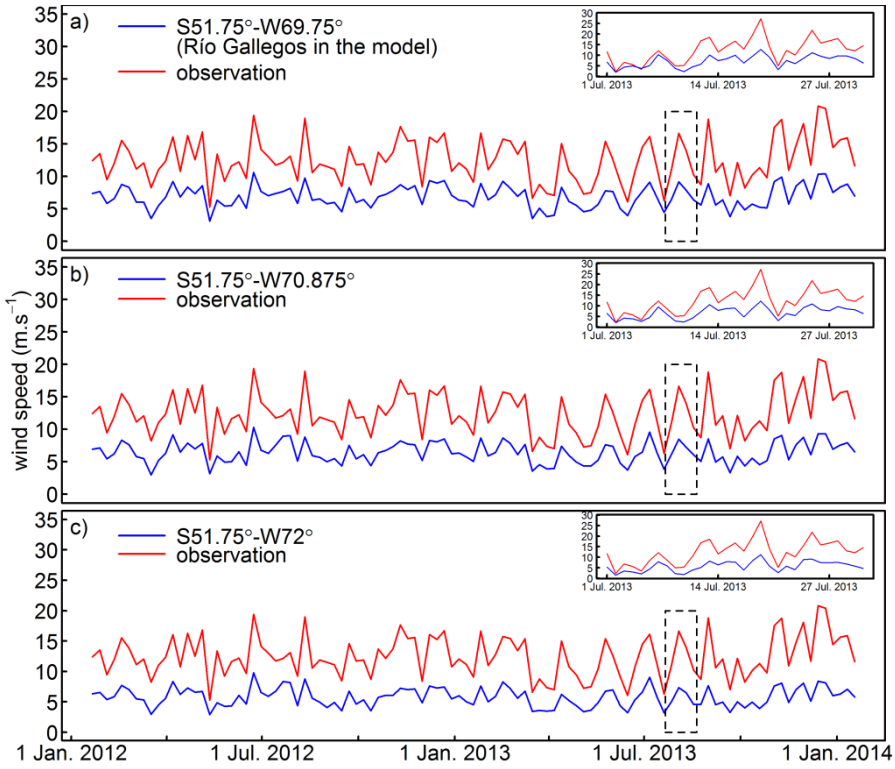

Figure 11: Time series of weekly average field measured wind speeds (red line) in Río Gallegos (69.28°W, 51.62°S) with the weekly average modelled wind speeds (blue line) in a) Río Gallegos and b-c) previously identified potential source regions (within 72°W~70°W and 51°S~52°S), during the years 2012 and 2013. Comparisons of daily average wind speeds in July 2013 (period in the dashed box) are shown in the upper right corner of each figure.

We first evaluate the dependence of dust concentration on wind speed. Figure 11 compares the weekly average field measured wind speeds (red line) in Río Gallegos (69.28°W, 51.62°S) with the weekly average modelled wind speeds (blue line) in previously identified potential source regions (within 70~72°W and 51~52°S) during the years 2012 and 2013. The upper right corner of each figure present comparisons of the daily average wind speeds in July 2013 (period in the dashed box). Though the absolute values of the wind speeds are different, which may be due to the

spatial difference and the averaging of wind data over the model grid, the simulated wind speeds in the potential source areas and the observed wind speed in Río Gallegos followed similar trend in the studied area. As shown in Figure 11, no seasonal cycles were observed for wind speed over Patagonia. The wind speed remained at the same level throughout the sampling period, including the continuous low dust concentration episodes in winter. Spearman's correlations between the dust concentration and the mean and maximum wind speed (W) are not significant (Table 3). Therefore, the recurrent high wind speed throughout the years should not be the primary regulating factor of dust emission over Patagonia.

Table 3. Spearman's rho correlations between meteorological conditions and dust concentration. Values in the top right represent the p values (two-tailed test of significance). The correlation is significant when $p < 0.05$ (bold values). Values in the bottom left are correlation coefficients.

	dust	mean Prep.	mean T	n freeze	max RH	min RH	max W	mean W
dust		0.21	**0.00**	**0.00**	**0.00**	**0.00**	0.07	0.25
mean Prep.	-0.11		0.07	0.54	**0.00**	**0.03**	0.11	0.10
mean T	**0.53**	0.16		**0.00**	**0.00**	**0.00**	**0.00**	**0.00**
n freeze	**-0.51**	-0.05	**-0.62**		**0.00**	**0.00**	**0.01**	**0.00**
max RH	**-0.36**	**0.31**	**-0.54**	**0.49**		**0.00**	**0.00**	**0.00**
min RH	**-0.59**	**0.19**	**-0.72**	**0.52**	**0.78**		**0.00**	**0.00**
max W	0.16	-0.14	**0.28**	**-0.23**	**-0.63**	**-0.45**		**0.00**
mean W	0.10	-0.14	**0.31**	**-0.30**	**-0.75**	**-0.53**	**0.84**	

The high wind speed of westerly and the independence of dust emission on wind speed make our case study easier to proceed for the rest meteorological parameters. Since the dust concentration is higher in summer and spring, the development or die off of vegetation cover should not be the cause of the seasonal trend. Dust concentration showed stronger correlations with the air temperature ($r = 0.53$), min RH ($r = -0.59$) and days of sub-zero temperatures ($r = -0.51$) than wind speed ($r = 0.16$ for max W, $r = 0.10$ for mean W). Dependencies of the dust concentration on air temperature and relative humidity are also illustrated by the similar trend of air temperature (Figure 12a) and the reverse trend of minimum air RH

(Figure 12b) regarding to the dust concentration during the sampling period. Stronger dust concentrations generally occurred in the hot and dry seasons observed in this work. In contrast, lower temperature and higher air humidity in winter, which correspond to the higher winter soil moisture reported by *Coronato and Bertiller* [1996], are associated with lower dust concentrations. The continuous low dust concentrations observed in the winter season could be also due to the frozen or snow-covered soils in the source areas [*Han et al.*, 2011; *Kang et al.*, 2013; *Micheletti et al.*, 2012]. As illustrated by Figure 12c, the days on sub-zero temperatures (n freeze) were generally consistent with the extremely low dust concentrations.

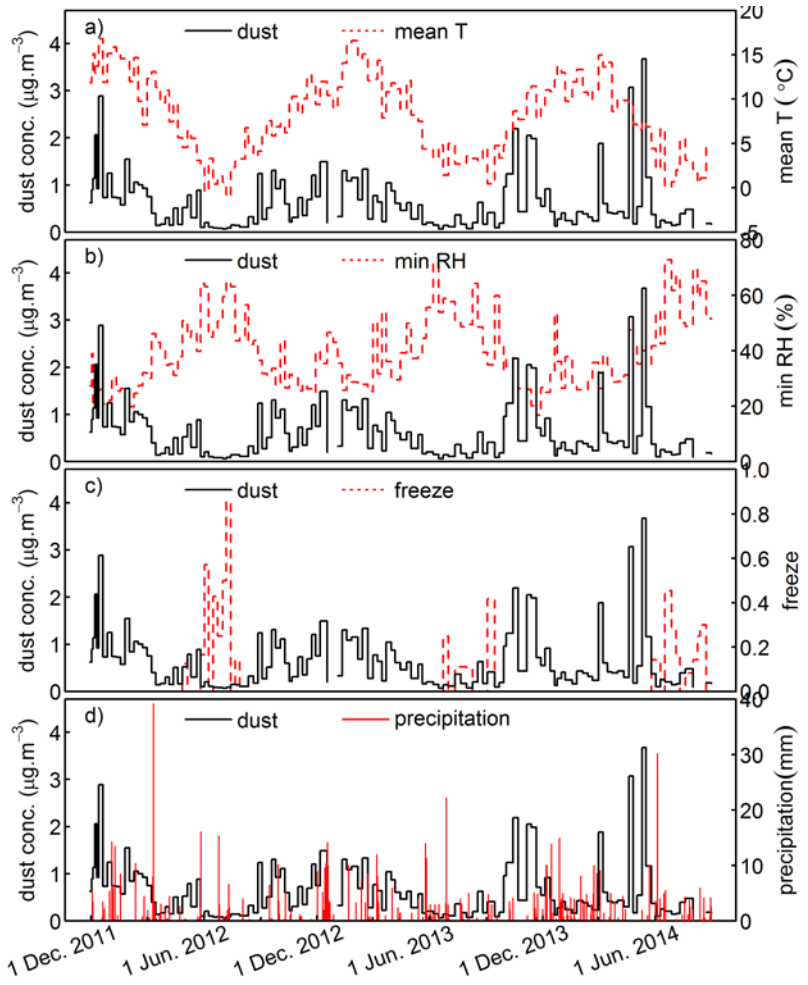

Figure 12: Time series of dust concentrations along with a) mean temperature (mean T), b) minimum RH (RH min), c) ratio of days with sub-zero temperatures (freeze) during each sampling period, d) daily precipitation amount (precipitation).

Dust emission is generally connected to the mechanisms of direct aerodynamic resuspension, saltation bombardment and sandblasting [*Gomes et al.*, 1990; *Kjelgaard et al.*, 2004; *Loosmore and Hunt*, 2000; *Macpherson et al.*, 2008; *Shao et al.*, 1993; *Sweeney and Mason*, 2013]. The emission rate of direct aerodynamic resuspension is primarily controlled by the availability of loose, fine particles [*Gillette and Chen*, 2001]. Saltation bombardment and sandblasting act as a function of wind speed and threshold friction velocity, and are triggered when the wind speed exceeds the threshold friction velocity in order to drive the saltating sand grains and aggregates [*Alfaro et al.*, 1997; *Alfaro and Gomes*, 2001; *Shao et al.*, 1993]. In terms the relations among the three mechanisms and meteorological conditions, variation of temperature and air humidity alters the soil moisture on short time scales which further changes the cohesion forces between particles and hence affects the availability of loose fine particles on soil surface [*Gillette and Chen*, 2001] and the wind erosion threshold [*Fécan et al.*, 1998; *Ravi and D'Odorico*, 2005; *Ravi et al.*, 2004]. In Patagonia, the independence of dust concentration variability on the steady high wind speed suggest that the availability of loose, fine particles on the surface instead of the transport capacity of wind is the primary factor controlling dust emission strength. In arid or semi-arid regions, soil moisture affects the cohesive forces between particles on short time scales due to the high potential evaporation [*Ravi et al.*, 2004]. Higher soil moisture increases the aggregation and crust strengths [*Ishizuka et al.*, 2008] and restricts the availability of loose, fine particles in the soil surface that could be entrained and transported. Increasing soil moisture turns Patagonia into a temporary supply-limited dust source area and inhibits the dust emission. When the surface soil is dry, more particles will be lifted up into the atmosphere.

Rain precipitation may inhibit the dust emission and the rain scavenging may decrease sharply the measured dust concentration (Chate et al., 2003; Zhao et al., 2015). As shown in Figure 12d, precipitation events are generally consistent with the transient decreases of dust concentration, particularly during strong rain events. Rain precipitation may also explain most of the abnormal dust concentration decreases regarding to the seasonal trend. Particularly, the unexpected low dust concentrations in summer 2014 were actually related to the more frequent precipitation events during that period. As a supply limited dust source, the inhibited dust emission in summer reulted in finally higher dust emission in the following autum, as indicated by the two

high dust concentrations in April 2014. Variation of precipitation resulted in an interannual variation of dust concentration.

In support of the above arguments, temperature and min RH rather than wind speed are the main meteorological factors influencing dust emissions in Patagonia. Changes in soil moisture together with ice- or snow-covered surface are likely to be the mechanism resulting in the variation in the seasonal dust concentration. Our results support the previous study of *McConnell et al.* [2007] on the ice core record of dust deposition during recent centuries in the northern Antarctic Peninsula, demonstrating that the increasing dust emission strength in Patagonia is associated with increasing air temperature and decreasing relative humidity. Variation of precipitation rate may result in interannual variations of emission strength and atmospheric concentration of dust. Seasonal dependence of dust emission strength on air temperature and relative humidity suggests an immediate response of dust concentration to climate variation, which may have further implications for the climate feedback on dust emission in Patagonia and other cold desert areas.

4. Conclusions

Continuous weekly aerosol sampling in the Patagonia-South Atlantic Coast, in Río Gallegos, from November 2011 to August 2014 reveals a seasonal variability in the mineral dust fraction, with higher concentrations in spring and summer and lower concentrations in winter. For the whole sampling period, the weekly dust concentrations measured in Río Gallegos, south Patagonia varied from 0.07 to 3.68 $\mu g.m^{-3}$, while sea-salt concentrations ranged from 0.16 to 2.40 $\mu g.m^{-3}$.

Dust emission in Patagonia followed a supply-limited mechanism rather than a transport-limited mechanism. Higher dust concentrations in summer are related to the higher aridity of the surface soil resulting from the higher temperature and associated lower minimum RH in summer. Variability of air temperature and the minimum RH, instead of the recurrent high wind speed, are demonstrated to be the primary factor responsible for the dust concentration variation in Patagonia. Frozen soil or snow cover is suggested to be responsible for the extremely low dust concentrations in

winter. Interannual variation of dust concentration is associated with the variation of precipitation rate.

Studies over remote source regions could help to better understand the wind erosion conditions and spatial/temporal dust emission pattern. However, the lack of local infrastructure poses a challenge to study dust emission inland Patagonia. These kinds of studies require automatic aerosol samplers with systematic monitoring of the aerosol concentration, size fraction, chemical composition, and meteorological conditions.

Acknowledgements

This work was supported by the CNRS INSU LEFE/CHAT financed program DFP (Dust from Patagonia) and the Franco-Argentina ECOS program. The authors thank the staff at the Río Gallegos bases for their help during the installation of the sampling station, and the Meteorological Station of Río Gallegos Airport, particularly professor Oscar Jorge Bonfili, for the meteorological data. The authors also thank Sarah Mullin for the improvement of English content. The authors gratefully acknowledge the NOAA Air Resources Laboratory (ARL) for providing the HYSPLIT Trajectory model and READY website (http://www.ready.noaa.gov) used in this publication. The analytical detail is available in supporting information. The aerosol concentration data and meteorological data are available upon request from the corresponding author.

References List

Aab, A., et al. (2014), Origin of atmospheric aerosols at the Pierre Auger Observatory using studies of air mass trajectories in South America, *Atmospheric Research*, *149*(0), 120-135, doi:http://dx.doi.org/10.1016/j.atmosres.2014.05.021.

Alfaro, S. C., A. Gaudichet, L. Gomes, and M. Maillé (1997), Modeling the size distribution of a soil aerosol produced by sandblasting, *Journal of Geophysical Research: Atmospheres*, *102*, 11239-11249, doi:10.1029/97JD00403.

Alfaro, S. C., and L. Gomes (2001), Modeling mineral aerosol production by wind erosion: Emission intensities and aerosol size distributions in source areas, *J. Geophys. Res.-Atmos.*, *106*(D16), 18075-18084, doi:10.1029/2000jd900339.

Arimoto, R. (2001), Eolian dust and climate: relationships to sources, tropospheric chemistry, transport and deposition, *Earth-Science Reviews*, *54*, 29-42, doi:10.1016/S0012-8252(01)00040-X.

Arimoto, R., X. Y. Zhang, B. J. Huebert, C. H. Kang, D. L. Savoie, J. M. Prospero, S. K. Sage, C. A. Schloesslin, H. M. Khaing, and S. N. Oh (2004), Chemical composition of atmospheric aerosols from Zhenbeitai, China, and Gosan, South Korea, during ACE-Asia, *J. Geophys. Res.-Atmos.*, *109*(D19), doi:10.1029/2003jd004323.

Bergametti, G., A.-L. Dutot, P. Buat-Ménard, R. Losno, and E. Remoudaki (1989), Seasonal variability of the elemental composition of atmospheric aerosol particles over the northwestern Mediterranean, *Tellus B*, *41B*(3), 353-361, doi:10.1111/j.1600-0889.1989.tb00314.x.

Boyd, P. W., et al. (2007), Mesoscale Iron Enrichment Experiments 1993-2005: Synthesis and Future Directions, *Science*, *315*, 612-617, doi:10.1126/science.1131669.

Chate, D. M., Rao, P. S. P., Naik, M. S., Momin, G. A., Safai, P. D., and Ali, K. (2003), Scavenging of aerosols and their chemical species by rain, *Atmospheric Environment*, 37, 2477-2484, http://dx.doi.org/10.1016/S1352-2310(03)00162-6.

Chisholm, S. W., and F. M. M. Morel (1991), What controls phytoplankton production in nutrient-rich areas of the open sea?, American Society of Limnology

and Oceanography Symposium, 22-24 February 1991, San Marcos, California, Preface, *Limnology and Oceanography*, *36*(8), U1507-U1511.

Coronato, F. R., and M. B. Bertiller (1996), Precipitation and landscape related effects on soil moisture in semi-arid rangelands of Patagonia, *Journal of Arid Environments*, *34*, 1-9, doi:10.1006/jare.1996.0088.

de Baar, H. J. W., J. T. M. de Jong, D. C. E. Bakker, B. M. Löscher, C. Veth, U. Bathmann, and V. Smetacek (1995), Importance of iron for plankton blooms and carbon dioxide drawdown in the Southern Ocean, *Nature*, *373*, 412-415, doi:10.1038/373412a0.

Desboeufs, K. V., A. Sofikitis, R. Losno, J. L. Colin, and P. Ausset (2005), Dissolution and solubility of trace metals from natural and anthropogenic aerosol particulate matter, *Chemosphere*, *58*(2), 195-203, doi:http: 10.1016/j.chemosphere.2004.02.025.

Dick, A. L. (1991), Concentrations and sources of metals in the Antarctic Peninsula aerosol, *Geochimica et Cosmochimica Acta*, *55*(7), 1827-1836, doi: 10.1016/0016-7037(91)90027-3.

Draxler, R. R., and G. D. Rolph (2015), HYSPLIT (HYbrid Single-Particle Lagrangian Integrated Trajectory) Model access via NOAA ARL READY website (http://ready.arl.noaa.gov/HYSPLIT.php). NOAA Air Resources Laboratory, Silver Spring, MD, edited.

Duce, R. A., and N. W. Tindale (1991), Atmospheric transport of iron and its deposition in the ocean, *Limnology and Oceanography*, *36*(8), 1715-1726, doi:10.4319/lo.1991.36.8.1715.

Fécan, F., B. Marticorena, and G. Bergametti (1998), Parametrization of the increase of the aeolian erosion threshold wind friction velocity due to soil moisture for arid and semi-arid areas, *Annales Geophysicae*, *17*(1), 149-157, doi:10.1007/s00585-999-0149-7.

Formenti, P., W. Elbert, W. Maenhaut, J. Haywood, and M. Andreae (2003), Chemical composition of mineral dust aerosol during the Saharan Dust Experiment (SHADE) airborne campaign in the Cape Verde region, September 2000, *Journal of Geophysical Research: Atmospheres (1984–2012)*, *108*(D18).

Gaiero, D. M., F. Brunet, J.-L. Probst, and P. J. Depetris (2007), A uniform isotopic and chemical signature of dust exported from Patagonia: Rock sources and occurrence in southern environments, *Chemical Geology*, *238*, 107-120, doi:10.1016/j.chemgeo.2006.11.003.

Gaiero, D. M., J.-L. Probst, P. J. Depetris, S. M. Bidart, and L. Leleyter (2003), Iron and other transition metals in Patagonian riverborne and windborne materials: geochemical control and transport to the southern South Atlantic Ocean, *Geochimica et Cosmochimica Acta*, *67*, 3603-3623, doi:10.1016/S0016-7037(03)00211-4.

Gassó, S., A. Stein, F. Marino, E. Castellano, R. Udisti, and J. Ceratto (2010), A combined observational and modeling approach to study modern dust transport from the Patagonia desert to East Antarctica, *Atmos. Chem. Phys.*, *10*(17), 8287-8303, doi:10.5194/acp-10-8287-2010.

Gassó, S., and A. F. Stein (2007), Does dust from Patagonia reach the sub-Antarctic Atlantic Ocean?, *Geophysical Research Letters*, *34*, L01801, doi:10.1029/2006GL027693.

Gillette, D. A., and W. Chen (2001), Particle production and aeolian transport from a "supply-limited" source area in the Chihuahuan desert, New Mexico, United States, *Journal of Geophysical Research: Atmospheres*, *106*(D6), 5267-5278, doi:10.1029/2000JD900674.

Ginoux, P., J. M. Prospero, T. E. Gill, N. C. Hsu, and M. Zhao (2012), Global-scale attribution of anthropogenic and natural dust sources and their emission rates based on MODIS Deep Blue aerosol products, *Reviews of Geophysics*, *50*, RG3005, doi:10.1029/2012RG000388.

Gomes, L., G. Bergametti, G. Coudé-Gaussen, and P. Rognon (1990), Submicron desert dusts: A sandblasting process, *Journal of Geophysical Research: Atmospheres*, *95*, 13927-13935, doi:10.1029/JD095iD09p13927.

Han, L., A. Tsunekawa, and M. Tsubo (2011), Effect of frozen ground on dust outbreaks in spring on the eastern Mongolian Plateau, *Geomorphology*, *129*(3–4), 412-416, doi:http://dx.doi.org/10.1016/j.geomorph.2011.03.005.

Heimburger, A., R. Losno, S. Triquet, F. Dulac, and N. Mahowald (2012), Direct measurements of atmospheric iron, cobalt, and aluminum-derived dust deposition at

Kerguelen Islands, *Global Biogeochemical Cycles*, *26*(4), GB4016, doi:10.1029/2012GB004301.

Heimburger, A., R. Losno, S. Triquet, and E. B. Nguyen (2013), Atmospheric deposition fluxes of 26 elements over the Southern Indian Ocean: Time series on Kerguelen and Crozet Islands, *Global Biogeochemical Cycles*, *27*(2), 440-449, doi:10.1002/gbc.20043.

Iriondo, M. (2000), Patagonian dust in Antarctica, *Quaternary International*, *68–71*, 83-86, doi:10.1016/S1040-6182(00)00035-5.

Ishizuka, M., M. Mikami, J. Leys, Y. Yamada, S. Heidenreich, Y. Shao, and G. H. McTainsh (2008), Effects of soil moisture and dried raindroplet crust on saltation and dust emission, *Journal of Geophysical Research: Atmospheres*, *113*, doi:10.1029/2008JD009955.

Jickells, T. D., et al. (2005), Global Iron Connections Between Desert Dust, Ocean Biogeochemistry, and Climate, *Science*, *308*, 67-71, doi:10.1126/science.1105959.

Johnson, M. S., N. Meskhidze, F. Solmon, S. Gassó, P. Y. Chuang, D. M. Gaiero, R. M. Yantosca, S. Wu, Y. Wang, and C. Carouge (2010), Modeling dust and soluble iron deposition to the South Atlantic Ocean, *Journal of Geophysical Research: Atmospheres*, *115*, D15202, doi:10.1029/2009JD013311.

Kang, J.-Y., T. Y. Tanaka, M. Mikami, and S.-C. Yoon (2013), A numerical study of the effect of frozen soil on dust emission during an East Asian dust event in December 2009, *Asia-Pacific Journal of Atmospheric Sciences*, *49*(1), 57-65.

Kjelgaard, J. F., D. G. Chandler, and K. E. Saxton (2004), Evidence for direct suspension of loessial soils on the Columbia Plateau, *Earth Surface Processes and Landforms*, *29*, 221–236, doi:10.1002/esp.1028.

Li, F., P. Ginoux, and V. Ramaswamy (2008), Distribution, transport, and deposition of mineral dust in the Southern Ocean and Antarctica: Contribution of major sources, *Journal of Geophysical Research: Atmospheres*, *113*, doi:10.1029/2007JD009190.

Loosmore, G. A., and J. R. Hunt (2000), Dust resuspension without saltation, *Journal of Geophysical Research: Atmospheres*, *105*, 20663–20671, doi:10.1029/2000JD900271.

Losno, R., G. Bergametti, and G. Mouvier (1987), Determination of optimal conditions for atmospheric aerosol analysis by X-ray-fluorescence, *Environmental Technology Letters*, *8*(2), 77-86.

Macpherson, T., W. G. Nickling, J. A. Gillies, and V. Etyemezian (2008), Dust emissions from undisturbed and disturbed supply-limited desert surfaces, *Journal of Geophysical Research: Earth Surface*, *113*, doi:10.1029/2007JF000800.

Maher, B. A., J. M. Prospero, D. Mackie, D. Gaiero, P. P. Hesse, and Y. Balkanski (2010), Global connections between aeolian dust, climate and ocean biogeochemistry at the present day and at the last glacial maximum, *Earth-Science Reviews*, *99*, 61-97, doi:10.1016/j.earscirev.2009.12.001.

Mahowald, N. (2011), Aerosol Indirect Effect on Biogeochemical Cycles and Climate, *Science*, *334*(6057), 794-796, doi:10.1126/science.1207374.

Mahowald, N., et al. (2008), Global distribution of atmospheric phosphorus sources, concentrations and deposition rates, and anthropogenic impacts, *Global Biogeochemical Cycles*, *22*(4), GB4026, doi:10.1029/2008GB003240.

Mahowald, N. M., A. R. Baker, G. Bergametti, N. Brooks, R. A. Duce, T. D. Jickells, N. Kubilay, J. M. Prospero, and I. Tegen (2005), Atmospheric global dust cycle and iron inputs to the ocean, *Global Biogeochemical Cycles*, *19*, GB4025, doi:10.1029/2004GB002402.

Marticorena, B., and G. Bergametti (1995), Modeling the atmospheric dust cycle: 1. Design of a soil-derived dust emission scheme, *Journal of Geophysical Research: Atmospheres*, *100*(D8), 16415-16430, doi:10.1029/95JD00690.

Martin, J. H. (1990), Glacial-interglacial CO2 change: The Iron Hypothesis, *Paleoceanography*, *5*, 1–13, doi:10.1029/PA005i001p00001.

McConnell, J. R., A. J. Aristarain, J. R. Banta, P. R. Edwards, and J. C. Simões (2007), 20th-Century doubling in dust archived in an Antarctic Peninsula ice core parallels climate change and desertification in South America, *Proceedings of the National Academy of Sciences of the United States of America*, *104*(14), 5743-5748, doi:10.1073/pnas.0607657104.

Micheletti, M. I., L. G. Murruni, M. E. Debray, M. Rosenbusch, M. Graf, G. Ávila Cadena, P. Vitale, J. Davidson, and H. Somacal (2012), Elemental analysis of aerosols collected at the Pierre Auger Cosmic Ray Observatory with PIXE technique

complemented with SEM/EDX, *Nuclear Instruments and Methods in Physics Research Section B: Beam Interactions with Materials and Atoms*, *288*(0), 10-17, doi: 10.1016/j.nimb.2012.07.022.

Prospero, J. M. (1996), The atmospheric transport of particles to the ocean, *SCOPE-Scientific Committee on Problems of the Environment International Council of Scientific Unions*, 19-52.

Prospero, J. M., P. Ginoux, O. Torres, S. E. Nicholson, and T. E. Gill (2002), Environmental characterization of global sources of atmospheric soil dust identified with the Nimbus 7 Total Ozone Mapping Spectrometer (TOMS) absorbing aerosol product, *Reviews of Geophysics*, *40*, 1002, doi:10.1029/2000RG000095.

Quisefit, J. P., and E. Randrianarivony (1998), Validation de la méthode d'étalonnage en couche mince par utilisation de géostandards déposés sur filtres pour l'analyse élémentaire par SFX, *Le Journal de Physique IV*, *08*, Pr5-359-Pr355-367, doi:10.1051/jp4:1998545.

Ravi, S., and P. D'Odorico (2005), A field-scale analysis of the dependence of wind erosion threshold velocity on air humidity, *Geophysical Research Letters*, *32*(21), L21404, doi:10.1029/2005GL023675.

Ravi, S., P. D'Odorico, T. M. Over, and T. M. Zobeck (2004), On the effect of air humidity on soil susceptibility to wind erosion: The case of air-dry soils, *Geophysical Research Letters*, *31*(9), L09501, doi:10.1029/2004GL019485.

Rolph, G. D. (2015), Real-time Environmental Applications and Display sYstem (READY) Website (http://ready.arl.noaa.gov). NOAA Air Resources Laboratory, Silver Spring, MD.

Savoie, D. L., J. M. Prospero, R. J. Larsen, F. Huang, M. A. Izaguirre, T. Huang, T. H. Snowdon, L. Custals, and C. G. Sanderson (1993), Nitrogen and sulfur species in Antarctic aerosols at Mawson, Palmer Station, and Marsh (King George Island), *Journal of Atmospheric Chemistry*, *17*(2), 95-122, doi:10.1007/BF00702821.

Shao, Y., M. Raupach, and J. Leys (1996), A model for predicting aeolian sand drift and dust entrainment on scales from paddock to region, *Soil Research*, *34*(3), 309-342, doi:http://dx.doi.org/10.1071/SR9960309.

Shao, Y., M. R. Raupach, and P. A. Findlater (1993), Effect of saltation bombardment on the entrainment of dust by wind, *Journal of Geophysical Research: Atmospheres*, *98*, 12719–12726, doi:10.1029/93JD00396.

Shao, Y., K.-H. Wyrwoll, A. Chappell, J. Huang, Z. Lin, G. H. McTainsh, M. Mikami, T. Y. Tanaka, X. Wang, and S. Yoon (2011), Dust cycle: An emerging core theme in Earth system science, *Aeolian Research*, *2*, 181-204, doi:10.1016/j.aeolia.2011.02.001.

Sweeney, M. R., and J. A. Mason (2013), Mechanisms of dust emission from Pleistocene loess deposits, Nebraska, USA, *Journal of Geophysical Research: Earth Surface*, *118*, 1460–1471, doi:10.1002/jgrf.20101.

Taylor, S. R., and S. M. McLennan (1995), The geochemical evolution of the continental crust, *Reviews of Geophysics*, *33*, 241-265, doi:10.1029/95RG00262.

Wagenbach, D., F. Ducroz, R. Mulvaney, L. Keck, A. Minikin, M. Legrand, J. S. Hall, and E. W. Wolff (1998), Sea-salt aerosol in coastal Antarctic regions, *Journal of Geophysical Research: Atmospheres*, *103*(D9), 10961-10974, doi:10.1029/97JD01804.

Wagener, T., C. Guieu, R. Losno, S. Bonnet, and N. Mahowald (2008), Revisiting atmospheric dust export to the Southern Hemisphere ocean: Biogeochemical implications, *Global Biogeochemical Cycles*, *22*, GB2006, doi:10.1029/2007GB002984.

Watson, A. J., D. C. E. Bakker, A. J. Ridgwell, P. W. Boyd, and C. S. Law (2000), Effect of iron supply on Southern Ocean CO2 uptake and implications for glacial atmospheric CO2, *Nature*, *407*, 730-733, doi:10.1038/35037561.

Xu, G., and Y. Gao (2014), Atmospheric trace elements in aerosols observed over the Southern Ocean and coastal East Antarctica, *Polar Research*, doi:10.3402/polar.v33.23973.

Zender, C. S., H. Bian, and D. Newman (2003), Mineral Dust Entrainment and Deposition (DEAD) model: Description and 1990s dust climatology, *Journal of Geophysical Research: Atmospheres*, *108*, doi:10.1029/2002JD002775.

Zhao, S., Yu, Y., He, J., Yin, D., and Wang, B. (2015), Below-cloud scavenging of aerosol particles by precipitation in a typical valley city, northwestern China,

Atmospheric Environment, 102, 70-78,
http://dx.doi.org/10.1016/j.atmosenv.2014.11.051.

Supporting Information for the article

The supporting information presents firstly the analytical detail of XRF analysis in Text S1. The analytical conditions are listed in Table S1. Calibration lines are illustrated in Figure S1. Table S2 further present the detail of calibration result of certified reference materials.

XRF measurement conditions and calibration lines

XRF analyses were all conducted using the set-up conditions displayed in Table S1 (Table 4). As showed in Figure S1 (Figure 13), least square linear regression slopes of intensity versus deposited mass were calculated for each analyzed element. Blank filters were produced to subtract background influences during the measurements. The instrument stability was checked time-to-time using the measured intensities of calibration geostandard. During a three days long analysis, the variability (RSD) of measured intensities was found to be 0.2% for Al, Fe and Si, and 4% for Na.

Table 4 : XRF measurements conditions.

elements[a]	tension (V)	current (µA)	tube filter	mediu m	time (s)	detector mode
Na, Al, Si	10	40	none	Helium	600	high resolution
Fe	40	100	Al-200	Helium	600	normal

[a]: all elements were measured with Kα emission line.

The XRF apparatus irradiates only a 0.50 cm² ellipse (6 mm×12 mm) of the filter. To determine the total mass present on sample surfaces larger than 12 mm, a surface correction factor calculated with the followed equation is applied to the previously measured mass value:

$$f = \left[diameter\left(sample\right) / diameter\left(calibration\right) \right]^2 \qquad \text{(S1)}$$

In this work, since the diameter of calibration standards is 18 mm, f= 4.94 for aerosol filter samples with an exposed surface of 40 mm diameter and f= 5.44 for the GSN geostandard filters (diameter= 42 mm).

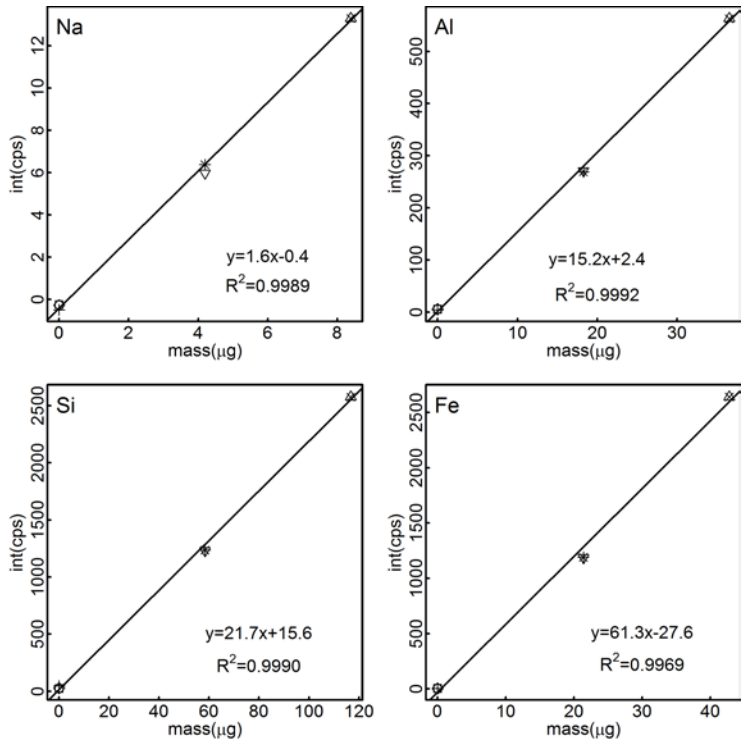

Figure 13 : Calibration curves of Na, Al, Si and Fe. Calibration standards were prepared by deposition of BHVO-1 on polycarbonate filters. A clean ZéfluorTM disk was put in the back of each PC filters to get similar interference background to ZéfluorTM samples. Each calibration was done with seven calibration samples (3 blanks, 2 filters with 250 µg CRMs, and 2 filters with 500 µg CRMs).

Table 5 : Measurement results of Zéfluor™ filters with GS-N certified reference materials.

	Na	Al	Si	Fe
mass (µg)				
detection limit	0.3	1.9	3	0.4
GS-N01a	16	40	153	11
GS-N01b	16	41	158	11
GS-N01c	15	42	162	12
GS-N01d	18	47	176	19
GS-N01	16	43	162	13
GS-N02a	17	44	170	12
GS-N02b	18	48	184	14
GS-N02c	15	39	150	11
GS-N02d	15	41	154	11
GS-N02e	16	41	158	11
GS-N02	16	43	163	12
GS-N03a	15	41	158	13
GS-N03b	14	38	147	11
GS-N03c	13	37	142	11
GS-N03	14	38	149	12
mean±SD	15.4±1.5	41.3±3.4	158±12	12.3±2.3
certified values	13.9±0.7	38.8±0.9	154±2	13±2
recovery rate (%)				
mean±SD	110±8	106±2	103±2	94±5

Conclusions of Chapter 2

The three-year continuous dust concentration measurement in the Patagonia-South Atlantic Coast is the first long-term time series obtained closing dust source regions in Patagonia. Throughout the sampling period, the weekly dust concentrations measured in Río Gallegos, south Patagonia varied from 0.07 to 3.68 $\mu g.m^{-3}$.

Our results reveal a seasonal variability of dust concentration, with higher concentrations in spring and summer and lower concentrations in winter. Variability of air temperature and the minimum relative humidity, instead of the recurrent high wind speed, are demonstrated to be the primary factor controlling the dust concentration variation in Patagonia. Higher dust concentrations are supposed to be related to the higher aridity of the surface soil resulting from the higher air temperature and lower minimum RH. Frozen soil or snow cover is suggested to be responsible for the extremely low dust concentrations in winter.

Measured dust concentration in the Patagonian-South Atlantic Coast contributes to a better understanding about the dust concentration and temporal dust emission pattern from Patagonia to the Southern Ocean. The fact that the seasonal dust concentration correlates with the variation in temperature and relative air humidity implicates a feedback of dust emission in response to short-term climate variations and has further implications in further dust modeling studies.

Chapter 3 Spatial Heterogeneity of source dust compositions

Introduction of Chapter

Chemical composition of dust varies with source areas and affects the budget of micronutrient inputs. An investigation into the spatial heterogenetiy of elemental composition of dust in source areas has further applications in biogeochemical modeling studies. This Chapter presents the elemental composition and its spatial variability of soil-derived dust in two dust source areas in subantarctic regions: Patagonia and Namibia. Factors resulting in variability of elemental composition and the enrichment behavior of elements from soil to dust are also studied. An article draft entitled "**Elemental composition of dust emitted from Patagonian and Namibian soils**" present the main content of this work.

To be submitted

Elemental composition of dust emitted from Patagonian and Namibian soils

Zihan Qu et al.

Abstract

Southern America and Southern Africa are two sources of mineral dust for the South Atlantic Ocean and the Indian Ocean and affect the marine biogeochemistry with the supply of micronutrients (Fe, Mn etc.). A laboratory aerosol generator (SyGAVib) was used to produce 135 Patagonian dust samples and 17 Namibian dust samples from soil samples. Patagonian dust contains less iron than Namibian dust, presenting average Fe_2O_3 concentrations of 6.3 ± 1.8% and 8.2 ± 2.1%, respectively. In Patagonia, dust and parent soils show a similar elemental composition for most of the analyzed elements including Si, Al and Fe. Compared to the parent soils, Namibian dust samples are enriched for Al, Fe, Ca, K, Mg, Ti, Mn, Cr, Zn and Sr, but depleted in Si. Silica is the foremost cause of this elemental enrichment due to its dilution effect in quartz-rich soils from Namibia. Principal component analysis on isometric log-ratio transformed compositional data showed that Si, Al, K, Fe and Ti are highly correlated in Patagonian dust, in Namibian dust, and in the entire sample set that includes both Patagonian and Namibian dust. This suggests that the main origin of these elements in dust is aluminosilicate (clays and feldspars) in bulk soils. Ca- or Mg-containing minerals act as the main sources of variability in the dust composition. For the soil samples, three subgroups, K-Si, Mg-Fe, and Ca, explain most of the variance in the elemental composition in Patagonia and Namibia.

Key Words: Dust generation; Patagonia; Namibia; Elemental enrichment; Spatial variability

1. Introduction

Mineral dust represents the largest mass of non-sea-salt aerosols at a global scale [*Textor et al.*, 2006]. The input of mineral dust to High Nutrient Low Chlorophyll (HNLC) oceanic regions provides essential micronutrients (Fe, Si, etc.) to marine ecosystems, and can stimulate primary production, regulate oceanic carbon uptake, and finally indirectly affect the Earth's climate [*Arimoto*, 2001; *Boyd and Ellwood*, 2010; *Maher et al.*, 2010; *Mahowald*, 2011; *Martin*, 1990; *Moore et al.*, 2013; *Moore et al.*, 2000; *Watson et al.*, 2000]. The biogeochemical effect of dust input into the ocean firstly depends on the elemental composition of the dust at its source [*Schulz et al.*, 2012]. Previous measurements have shown spatial heterogeneities of dust elemental compositions [e.g. *Arimoto et al.*, 2004; *Desboeufs et al.*, 2005; *Eltayeb et al.*, 1993; *Formenti et al.*, 2003; *Gaiero et al.*, 2007], especially given that many active dust sources exit as "hot spots" in small areas rather than in large homogeneous dust emission areas [*Gillette*, 1999], investigations into the spatial variability of dust elemental compositions are essential [*Zhang et al.*, 2015].

The Southern Ocean is one of the main HNLC regions where iron depletion limits the primary production [*Boyd*, 2002; *Chisholm and Morel*, 1991; *de Baar et al.*, 1995; *Martin and Fitzwater*, 1988; *Moore et al.*, 2001]. Mineral aerosols deposited into the Southern Ocean originate mainly from the three continental regions in the Southern Hemisphere: South America, Southern Africa and Australia. According to the modeling results of *Li et al.* [2008], dust emission from South America contributes 58% of the dust deposition over the entire Southern Ocean and 90% of the dust deposition over the South Atlantic Ocean. South Africa represents a minor source of dust deposition, the impact of which is limited to the southern Atlantic and southern Indian Oceans.

Mineral dust emission by wind erosion can be driven by direct aerodynamic resuspension [*Kjelgaard et al.*, 2004; *Loosmore and Hunt*, 2000; *Macpherson et al.*, 2008; *Sweeney and Mason*, 2013], saltation bombardment, and aggregate disintegration [*Gomes et al.*, 1990; *Shao*, 2008; *Shao et al.*, 1993]. Only fine particles with a diameter less than approximately 10 μm can be lifted up to high altitudes and be transported over long distances [*Alfaro et al.*, 2003; *Schulz et al.*, 1998]. Consequently, the chemical compositions of soil-derived dust depend on the fine fraction of soil particles and as a result, the use of the soil chemical composition as a surrogate for the source dust chemical composition may cause a

systematic bias in the composition. Previous studies generally found lower concentrations of Si and higher concentrations for most of the remaining elements in fine soil particles [*Acosta et al.*, 2011; *Castillo et al.*, 2008; *Eltayeb et al.*, 2001; *Eltayeb et al.*, 1993; *Schütz and Rahn*, 1982].

In this paper, we present our investigation of the elemental composition in two dust source areas: Patagonia and Namibia. Then we discuss the spatial variability of the elemental enrichment behavior from the parent soils to the generated aerosols. To identify the main origin of variability in the elemental composition of dust, a principal component analysis was performed with the free statistical software R [*R Core Team*, 2015].

2. Study area

2.1. Patagonia Desert

Argentinian Patagonia (39°S~55°S) is located in the southern end of South America, bordered by the Atlantic Ocean to the east and the Andes to the west. The present surface is roughly 700,000 km² with a typical width ranging from 300 km to 700 km. The westerly wind, arriving from the Pacific Ocean, discharges most of the water content over the Andes and blows through Argentinean Patagonia as dry winds. The annual precipitation is less than 250 mm in most of the area [*Gassó and Stein*, 2007], except for a narrow region along the Andes representing 15% of the total area with a rainfall above 800 mm per year [*Gaiero et al.*, 2003].

The Patagonia tableland is generally covered by deep layers of gravel and clays [*Gaiero et al.*, 2007]. Volcanoes spread along the Andes (Figure 14a), such as the Hudson volcano (45°54'S, 72°58'W, Chile) and the Puyehue Volcano, delivered volcanic ash to a vast area of the Patagonia tableland [*Collini et al.*, 2013; *Scasso et al.*, 1994; *Stern*, 2008]. Previously deposited ash may be further remobilized in the atmosphere as indicated in *Langmann et al.* [2013] and *Folch et al.* [2014]. Eight main rivers (from north to south: Colorado, Negro, Chubut, Deseado, Chico, Santa Cruz, Coyle, Gallegos), descending from the foot of the Andes, flow through the tableland and drain roughly 30% of the total

Patagonian region. These rivers transport alluvial sediments which could be potential dust sources.

2.2. Namibia: Namib Desert and Kalahari Desert

The Namib Desert and Kalahari Desert are the two desert regions in Namibia (Figure 14b). The Namib Desert is a coastal desert stretching along the coast for thousands of kilometers and is the driest region located in the southern African plateau, with the Cunene River in the north, the Kuiseb River in the middle, and the Orange River in the south. In the Namib Desert, the Kuiseb River normally dries out. The land covers are highly different to the north and south of the Kuiseb River. The region north of the Kuiseb River consists mainly of gravel plains, raw mineral soils and limestone or gypsum crusts. Shifting sand dunes dominate the region south of the Kuiseb River. The main minerals are feldspar and quartz near the coast, and feldspar, garnet, monazite, opaque and ore minerals towards the interior [*Eltayeb et al.*, 1993; *McKee*, 1982]. The Kalahari Desert is found inland in the high southern African plateau. Compared to soils in the Namib Desert, soils in the Kalahari Desert contain fewer clay materials (illite, kaolinite and smectite), feldspar and gypsum, but have a higher quartz content in the soil [*Nickovic et al.*, 2012].

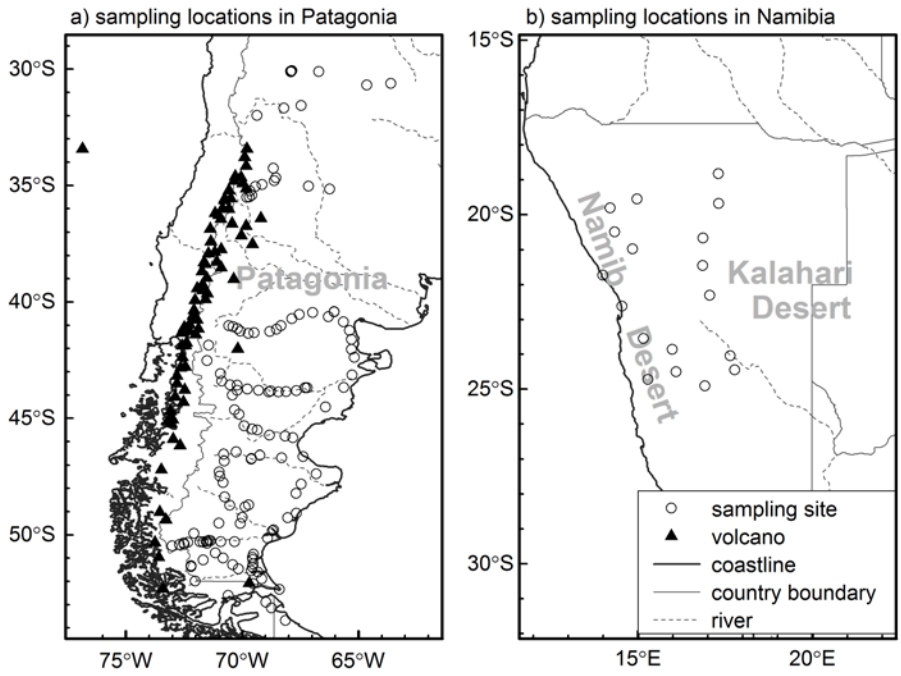

Figure 14 : Sampling locations of the top soil samples from a) Patagonia and Central West Argentina and b) the Namib Desert.

3. Materials and methods

3.1. Soil-derived aerosol generation

The in-situ collection of naturally emitted dust is probably the best way to study dust at the source. Dust collection in the field is widely used to obtain a time series on a single point but is not adapted to document the spatial variability and heterogeneity of the sources. Dust production in the field or laboratory from soil samples is an alternative way to study the source dust. *Gillette* [1978] investigated dust emission by wind erosion using a straight-line wind tunnel. *Alfaro et al.* [1997] used a wind tunnel to determine the size distribution of soil-derived aerosols due to the sandblasting process. Although the wind tunnel directly simulates the natural wind erosion process under controlled wind conditions and pedologic conditions, it is difficult to use in dust studies at a large spatial scale due to the lack of portability.

Recently, for reasons of economy in the size, portability, efficiency and ease of use, several original devices have been developed to conduct aerolization research. *Eltayeb et al.* [1993] and *Eltayeb et al.* [2001] produced aerosol from soil taken from the Namib Desert and Sahara Desert using a flow-through tunnel-type aerosol generation chamber and found a decrease in the Si content and an increase for most of the other elements such as Al and Fe in the aerosol fraction. *Alfaro et al.* [2004] and *Lafon et al.* [2014] generated desert dust by shaking soil samples in an Erlenmeyer flask. To measure the potential wind erosion and dust emission from the soil surface, *Etyemezian et al.* [2007] designed the Portable In-Situ Wind Erosion Lab (PI-SWERL): a motor-driven annular ring is placed inside an open-bottomed cylindrical chamber above the soil surface. The rotation of the annular ring induces a steady shearing force over the soil and consequently the entrainment of particles. *Salam et al.* [2006] generated aerosol by vibrating soil samples using a loudspeaker to study the ice nucleation efficiency. *Scheermeyer and Agranovski* [2009] aerosolized fungal spores with a similar method and found that the quantity of spores released is related to the vibration frequencies and that a "most efficient" frequency exists. In this work, soil-derived aerosol samples were prepared using a dust generator equipped with a loudspeaker: SyGAVib (abbreviation for "Système de Generation d'Aérosol par Vibration" in French; "aerosol generation system by vibration" in English).

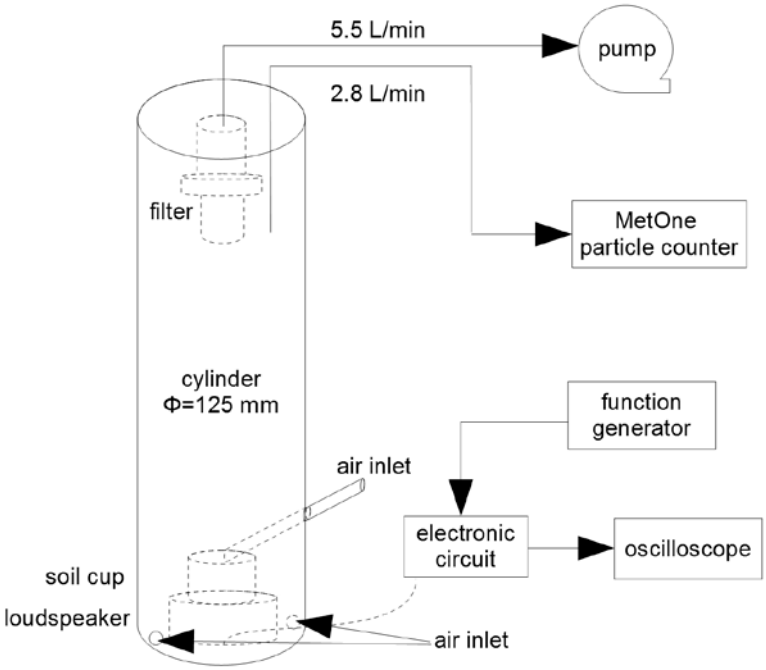

Figure 15 : SyGAVib diagram

The SyGAVib (Figure 15) uses a loud speaker to mobilize the soil particles in order to generate dust particles and carry the fine particles away with the airflow. An open-top ~20 mL polyethylene cup is fixed onto the loudspeaker membrane, 4 cm above, to avoid the possible impact of the loudspeaker's magnetic field on the magnetite particles in the soil. A 0.3 g aliquot of the soil sample added into the polyethylene cup acts as the dust emission source. The electric signal (waveform, frequency, voltage) input for the loudspeaker was regulated and monitored by a function generator/counter (MCP®, SG1639A) and an oscilloscope. The vibration of the loudspeaker mobilized the soil particles and the collisions among the particles induced disintegrations of the aggregates that emit fine particles. The dust generation cup is placed in the bottom center of an upright stainless steel cylinder measuring 125 mm in diameter. Two air inlets are positioned on the bottom side of the tube; a third inlet directing air to the top center of the soil container creates a local turbulence to strengthen the suspension of the particles. An external pump (flow rate: 5.5 $L.min^{-1}$) and an optical particle counter (flow rate: 2.8 $L.min^{-1}$) are connected to the top of the cylinder to maintain a constant upwards airflow within the system. The total ascending flow rate is approximately 8 $L.min^{-1}$, providing a vertical air velocity of 1.1 $cm.s^{-1}$. According to Stoke's steady state equations, only particles smaller than 10 µm are carried up to the top of the cylinder. The airflow destined for the pump passes through a polycarbonate filter membrane (Nuclepore®) placed in

the top of the cylinder where the generated aerosol is collected. The generation system is placed in a clean air bench hood to prevent external particle contamination. The power supplies (waveform, frequency, voltage of the electric current) to the loud speaker are monitored with an oscilloscope. The working condition of the function generator was set to 1.0 V and 100 Hz with a sine wave signal for the dust generation after evaluating the dust emission performance under different power supplies and wave shapes. Under this condition set, we observed a bimodal distribution of the aerosol volume between 0.2 μm and 10 μm which is similar to the size distribution observed by Sow et al. (2009) (Appendix 6). In the next sections, the dust samples are labeled with the prefix DP for dust from Patagonia and the prefix DN for dust from the Namib Desert.

3.2. Soil sample collection

One hundred and thirty-five topsoil samples from Patagonia (labeled with the prefix SP) (Figure 14a), taken at a depth of 0 to 2 cm and weighing approximately 200 g each, were collected during four field surveys: (1) 1-10 December 2011; (2) 29 July to 6 August 2012; (3) 16- 25 March 2013 and (4) 26 March to 3 April 2014. In 2013, 18 topsoil samples (labeled with the prefix SN) were collected from Namibia (Figure 14b). The soils were sampled in polyethylene bags (VWR®) from various land covers, such as bare land, lakesides, dry lakebeds, or volcanic ash deposits. The sampling sites were at least 50 m away from the roads. The sample bags were sealed off after the air inside them was expelled in order to limit the mobilization of the soil particles during transport. Wet soils collected during the last campaign in Patagonia were then dried by placing the opened bags in a clean airflow hood under ambient temperature for one week. All of the dry soil samples were gently sieved with 0.84 mm (20 meshes) sieves without shaking to prevent particle disintegration. In the rest of this paper, the soil samples mentioned refer to the sieved surface soils.

3.3. Elemental analysis

The elemental compositions of the bulk soils were determined by an energy dispersive X-ray fluorescence (EDXRF) instrument (PANalytical, Epsilon 3XL) using the pressed powder tablet technique (see supporting information for details). The amounts of elements collected on the aerosol filters were determined by the same instrument but using the “thin layer” method (see supporting information for details) and the elemental composition was

deduced from the elemental mass. Table 6 and Table 7 summarize the precision and accuracy respectively for the soil tablet and aerosol filter measurements.

Table 6: Measured values with certified values for the BE-N and GS-N tablets

	BE-N			GS-N		
	measured	certified	recovery rate	measured	certified	recovery rate
%wt						
SiO_2	36.7	38.2	96%	67.0	65.8	102%
Al_2O_3	9.56	10.1	95%	13.2	14.7	90%
Fe_2O_3	13.6	12.8	106%	4.04	3.75	108%
Na_2O	3.32	3.2	104%	3.37	3.77	89%
K_2O	1.37	1.4	98%	4.70	4.63	101%
CaO	14.2	13.9	102%	2.64	2.50	106%
MgO	11.3	13.2	86%	2.19	2.30	95%
TiO_2	2.48	2.61	95%	0.63	0.68	92%
P_2O_5	0.90	1.05	85%	0.11	0.28	39%
SO_3	0.07	0.08	88%	0.10	0.04	293%
ppm						
Sr	1388	1370	101%	578	570	101%
Mn	1319	1549	85%	343	434	79%
Zr	268	260	103%	217	235	92%
Rb	52	47	111%	197	185	107%
Cr	381	360	106%	55	55	100%
Zn	105	120	87%	44	48	91%
Cu	77	72	108%	22	20	109%

Table 7 : Measured values with certified values (unit: µg) for the BE-N and SDC-1 filters

	BE-N_250µg			SDC-1_500µg		
	Measured	Certified	Recover	Measured	Certified	Recover
Si	46.87	44.64	105%	151.1	153.8	98%
Al	13.04	13.32	98%	42.55	41.81	102%
Fe	25.87	22.45	115%	20.14	22.10	91%
Na	5.68	5.90	96%	7.07	7.60	93%
K	3.46	2.88	120%	12.22	12.70	96%
Ca	28.76	24.78	116%	4.96	5.00	99%
Mg	22.29	19.81	112%	6.43	5.08	127%
Ti	4.69	3.91	120%	2.66	3.03	88%
P	1.52	1.15	133%	0.10	0.35	29%
Sr	0.34	0.34	99%	0.07	0.09	81%
Mn	0.44	0.39	113%	0.38	0.44	86%
Zr	0.07	0.065	101%	0.10	0.15	71%
Cr	0.11	0.09	122%	0.02	0.03	71%
Zn	0.03	0.03	103%	0.05	0.05	94%

3.4. Principal component analysis of compositional data

Principal component analysis (PCA) is a classical and useful multivariate analysis method to explain the main origins of the variance in the data. A PCA converts variables into a new set of uncorrelated principal components (PCs) based on a covariance matrix of the dataset. The new PCs are linear combinations of the original variables and are ordered according to the variance of the variables in the original dataset that each PC explains. The first few PCs, comprising most of the variances of the original dataset, are retained in the subsequent interpretation to reduce the dimension of the multivariate dataset. One major drawback of classical PCAs is that the variance and covariance matrix of the sample are sensitive to outliers and lead to misleading results [*Filzmoser et al.*, 2009]. To reduce the influence of outliers, a robust PCA (rPCA) method was developed based on the minimum covariance determinant (MCD) method [*Filzmoser et al.*, 2009; *Rousseeuw and Driessen*, 1999]. The MCD method proposed by *Rousseeuw* [1985] finds the data subset with the lowest determinant of the covariance matrix.

The compositional data in our work is a closed system: for a given sample, the concentration values of all of the variables sum up to 100%. No single element composition is independent from the other elements due to this closed effect. For a composition of D parts, the compositional data are non-negative values and thus the dataset is constrained from 0 to the sum in the positive part of the Euclidean space with D - 1 dimensions [*Egozcue et al.*, 2003]. The compositional data in the restricted space, called simplex, followed the Aitchison geometry [*Aitchison*, 1986]. The distance between two compositions $\boldsymbol{x}$ and $\boldsymbol{y}$ in the D-part simplex is the Aitchison distance d_a (Eq. 1) instead of the Euclidean distance d_e (Eq. 2):

$$d_a = \sqrt{\sum_{i=1}^{D}\left\{\ln\left[x_i/g(x)\right]-\ln\left[y_i/g(y)\right]\right\}^2}\ \text{, for } i = 1, 2, ..., \text{D} \qquad (1)$$

$$d_e = \sqrt{\sum_{i=1}^{D}\left(x_i - y_i\right)^2}\ \text{, for } i = 1, 2, ..., \text{D} \qquad (2)$$

Classical statistical methods such as principal component analysis are designed for open systems and are generally based on Euclidean distances (Eq. 4). The direct application of the standard statistical method on closed compositional data may create spurious correlations and result in misleading results and conclusions [*Filzmoser et al.*, 2009; *Pawlowsky-Glahn et al.*, 2007]. Prior to the statistical analysis, the compositional data need to

be opened. Therefore, a log-ratio transformation is introduced to convert the compositional data into Aitchison space prior to the statistical analysis [*Buccianti and Grunsky*, 2014; *Filzmoser et al.*, 2009; *Reimann et al.*, 2012; *Wang et al.*, 2014; *Zuo et al.*, 2013].

The additive log-ratio (alr) transformation, centered log-ratio (clr) transformation, and isometric log-ratio (ilr) transformation are the three main log-ratio transformation methods. The first two methods are a one-to-one transformation developed by *Aitchison* [1986]. The alr transformation from the Aitchison simplex into Euclidean space is not isometric (i.e. angles or distances are lost) [*Egozcue et al.*, 2003] and therefore not suitable for PCA. The clr transformation (Eq. 4) divides each variable by its geometric mean. The interpretation of the clr variables is easier and more straightforward because the clr transformation converts the original variables both individually and symmetrically from Aitchison space to the new clr variables in Euclidean space, while the new clr variables add up to zero and thus the resulting data are collinear. The ilr transformation (Eq. 5) proposed by *Egozcue et al.* [2003] conducts stepwise calculations of the log-ratio of the geometric mean of the first part of the compositions to the following variable. The log ratios represent the coordinates in Euclidean space on an orthonormal basis. The ilr transformation is isometric, and free from the collinear effect of clr, and therefore allows standard multivariate analysis to be performed. However, the new ilr transformed variables are not directly connected to the original variables, rendering it difficult to interpret the statistical results. Therefore, the PCA results in ilr space are back-transformed to clr space where the results may be interpreted directly with the original variables [*Filzmoser et al.*, 2009].

$$y_i = \ln\left(x_i / x_D\right) \quad \text{for } i = 1, 2, ..., \text{D-1} \qquad (3)$$

$$y_i = \ln\left[x_i / g\left(x_1, ..., x_D\right)\right] \quad \text{for } i = 1, 2, ..., \text{D} \qquad (4)$$

$$y_i = \sqrt{\left[i/(i+1)\right]} \ln\left[g\left(x_1, ..., x_i\right) / x_{i+1}\right] \quad \text{for } i = 1, 2, ..., \text{D-1} \qquad (5)$$

The robust PCA performed on the compositional data was carried out with the "robCompositions" package in R [*Templ et al.*, 2011].

3.5. Accumulation factor and enrichment factor of dust relative to parent soil

If the whole chemical composition of the samples is known, the relative shift in the composition of a given element during dust emission from bulk soil could be quantified by calculating the accumulation factor (AF). The accumulation factor AF(x) of element x in the dust fraction with respect to the parent soil was calculated using Eq. (6) [*Acosta et al.*, 2009]:

$$AF\left(x\right) = x_{dust} / x_{soil} \qquad (6)$$

where x_{dust} and x_{soil} are the concentration of element x in the dust and its parent soil, respectively.

Previous studies usually calculate the enrichment factor (EF) to estimate the contribution to the studied samples from a specific source [*Acosta et al.*, 2011; *Eltayeb et al.*, 2001; *Ho et al.*, 2012; *Huang et al.*, 2009; *Schütz and Rahn*, 1982]. The EF of dust relative to the parent soil was calculated using Eq. (7) adapted from *Lawson and Winchester* [1979],

$$EF\left(x / E_{ref}\right) = \left(x / E_{ref}\right)_{dust} / \left(x / E_{ref}\right)_{soil} \qquad (7)$$

In the function, x represents the concentration of the element, and E_{ref} is the concentration of the reference element that should be sufficiently abundant in the sample [*Eltayeb et al.*, 2001]. In bulk soils, silicon is a major element with a high prevalence in the sand fraction due to the presence of quartz, while Al-containing minerals exist preferentially in the fine size fraction [*Acosta et al.*, 2011; *Schütz and Rahn*, 1982]. In this work, we calculated the EF relative to Al to evaluate the contribution of Al-containing minerals to the variation in the elemental composition.

4. Results and discussion

4.1. Elemental composition of soil and aerosol

In this section, we present the elemental composition of soil and aerosol in Patagonia and Namibia, with a focus on Si, which is the major component of crustal materials, and Fe for its biogeochemical properties. Dust samples were obtained for 135 soils from Patagonia and 17 soils from Namibia. No dust production was observed for soil sample SN05 (15.28° E,

24.72° S) sampled south of the Kuiseb River, Namibia, where sand dunes are the dominate landscape.

4.1.1. Element concentration of topsoil and soil-derived dust in Patagonia and Namibia

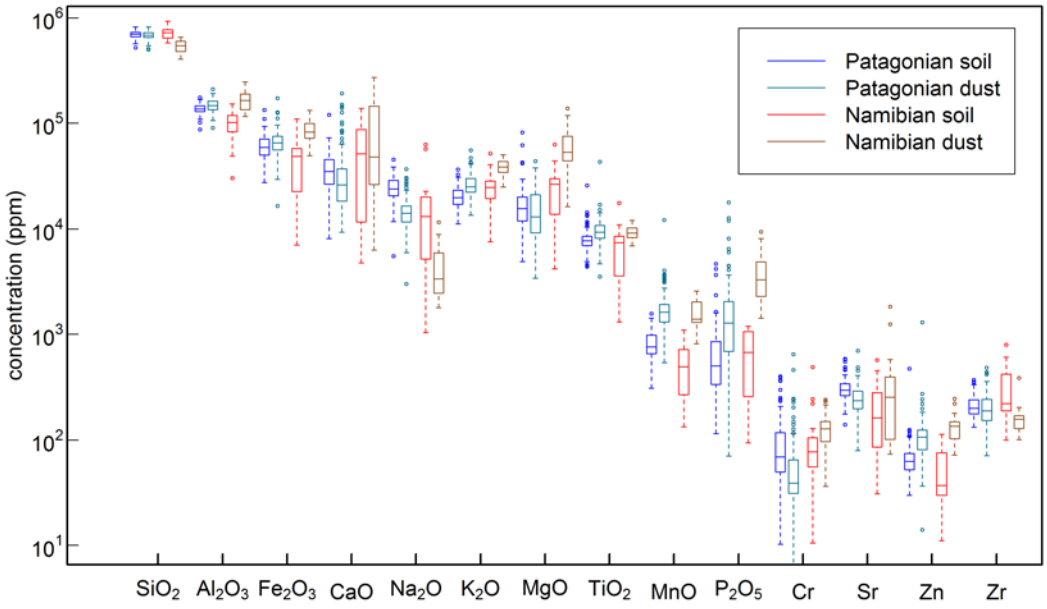

Figure 16 : Boxplot of the elemental compositions (ppm) of the topsoil and dust samples from Patagonia (n = 135) and Namibia (n = 17).

The element concentrations for soil and dust from Patagonia and Namibia are shown in Figure 16 as box-plots. Descriptive statistics of the elemental concentration are provided in the supporting information. The geometric mean SiO_2 composition (geomean ± SD) is 69 ± 5% for Patagonian soils and 72 ± 10% for Namibian soils, showing a higher variability in Namibia. For dust, the geometric mean SiO_2 composition is 68 ± 6% for Patagonia and 53 ± 8% for Namibia. The Fe_2O_3 content showed much higher variability in Namibian soils (3.9 ± 2.7%) than in Patagonian soils (5.8 ± 1.5%). Contrary to silicon, iron showed higher concentrations in Namibian dust (8.2 ± 2.1%) than in Patagonian dust (6.3 ± 1.8%). Most of the other elements showed a higher degree of concentration variability in Namibian soils than in Patagonian soils. Compared to the Patagonian dust samples, the Namibian dust samples showed higher concentrations of Al, Ca, K, Mg, P and Cr, as shown in Figure 16.

4.1.2. Spatial variation of elemental composition in regional scale

Figure 17 maps the SiO_2 concentrations in Patagonia and Namibia for the soil and dust samples. For the soil samples, higher concentrations of Si are observed in southern Patagonia (Figure 17a). Regions close to volcanoes along the Andes generally show lower SiO_2 concentrations. In addition, the sample from the Pali-Aike Volcanic Field (52.1°S, 69.7°W), shown as a dark blue point in southeastern Patagonia, has a remarkably lower concentration of Si, further implying the impacts of volcanic basalt or tephra ash on the soil composition. Patagonian dust shows a similar Si concentration and spatial pattern to the parent soils, with higher Si concentrations in southern Patagonia than in northern Patagonia (Figure 17a and c). The observed decreases in the Si concentration in dust occurred mostly on sites close to volcanos along the Andes and in one soil sample collected on a dry lakebed in northeastern Patagonia.

For the Namibian samples (Figure 17b), Kalahari Desert soils show higher SiO_2 concentrations than Namib Desert soils. Compared to the parent soils, Namibian dust is generally depleted in Si. The difference between Kalahari and Namib soils is less remarkable, which is associated with a higher quartz content in Kalahari soils [*Nickovic et al.*, 2012].

The Fe_2O_3 concentration for each sampling site in Patagonia and Namibia is shown in Figure 18. Contrary to silicon, for both soil and dust, iron generally shows lower concentrations in southern Patagonia than in northern Patagonia (Figure 18a and c). The sites close to volcanoes exhibit a relatively higher iron content. Compared to the parent soils, the dust samples are slightly enriched in iron content in most regions of Patagonia. In Namibia, the iron composition is quite variable and is generally higher in dust than in their parent soils.

Biogeochemical modeling studies usually take a fixed elemental composition to quantify elements carried by dust. For example, Fe_2O_3 concentration in the average upper continental crust composition [*Taylor and McLennan*, 1995], which equals to 5%, is adopted as the iron concentration in dust [*Luo et al.*, 2008]. However, the Fe content in dust actually varies with the source regions [*Claquin et al.*, 1999; *Gao et al.*, 2003]. As shown in our study, the average Fe_2O_3 concentration is 6.3 ± 1.8% for dust from Patagonia and 8.2 ± 2.1% for dust from Namibia. The iron concentration is similar between the dust samples and their parent soils in Patagonia, whereas it is quite different for dust and their parent soils in Namibia. This observation suggests that using the iron concentration in the soil as a surrogate

of the dust iron content has less uncertainty in Patagonia than in Namibia. The maps of the dust elemental composition help improve the knowledge about the spatial distribution of trace element contents in dust source areas and may have a further implication in biogeochemical modeling studies.

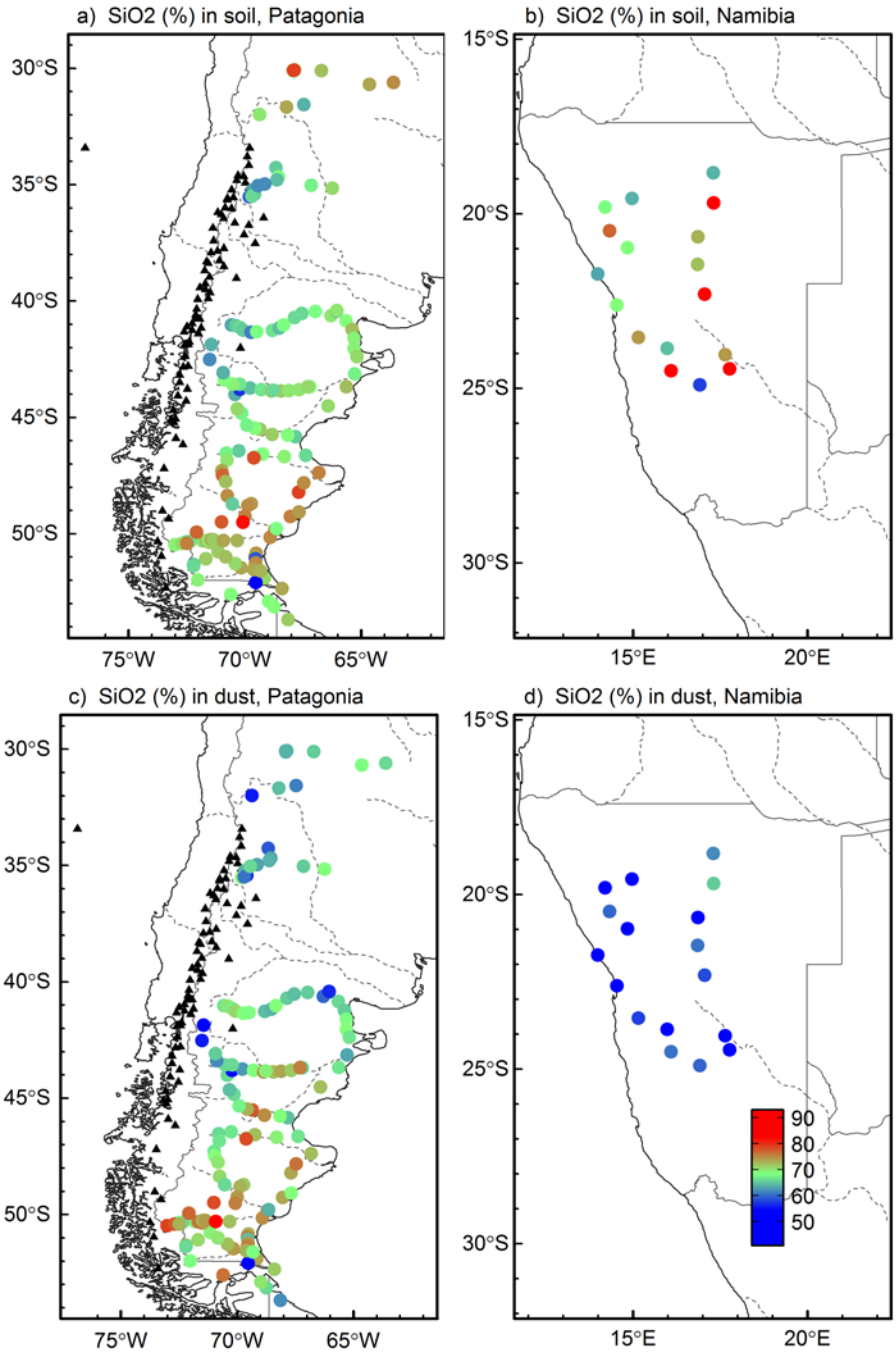

Figure 17 : SiO_2 concentration in a) Patagonian soils, b) Namibian soils, c) Patagonian dust, d) Namibian dust.

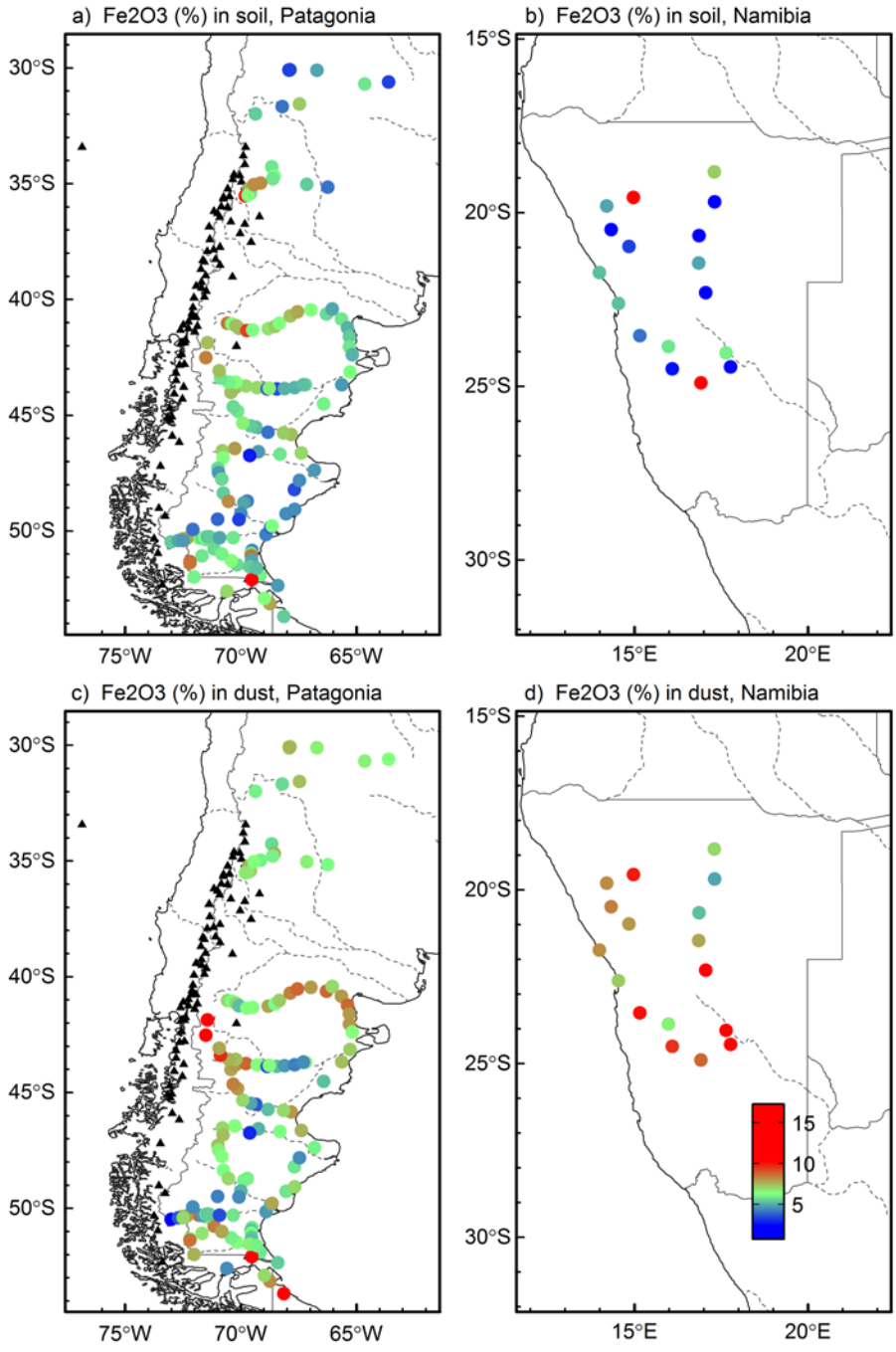

Figure 18 : Fe_2O_3 concentration in a) Patagonian soils, b) Namibian soils, c) Patagonian dust, d) Namibian dust.

4.1.3. Robust principle component analysis

To understand the origin of the variability in the elemental composition, a robust principal component analysis (rPCA) was performed on the major elements (SiO_2, Al_2O_3, Fe_2O_3, CaO, K_2O, MgO, TiO_2, MnO, and Na_2O) of soil and dust. The datasets of soil and dust were considered separately but also as an entire dataset. Three datasets were hence

obtained: a) dataset containing soil and dust (n=152×2=304), b) dataset containing only soil (n=152), and c) dataset containing only dust (n=152). As log-ratio transformations were necessary, the multivariate statistical analysis cannot be directly applied to compositional data containing zeros (below the detection limit). Both Na_2O and P_2O_5 returned zero values for more than 10% of the 152 samples in either soil dataset or dust dataset. These two elements were hence excluded prior to the rPCA. In the rest elements, CaO, K_2O and MgO showed zero values in a small proportion (<10%). Zero values of samples were replaced by 55% of the minimum detected value using the simple-subtitution replacement [*Sanford et al.*, 1993] and nonzeros were then corrected following the multiplicative replacement method proposed by *Martín-Fernández et al.* [2003].

Table 8: Percentages of variability explained by each component of the robust PCA

		PC1	PC2	PC3	PC4	PC5	PC6	PC7
soil and dust	% of variability	55.7	21.8	12.0	5.3	3.7	1.1	0.4
	cumulative %		77.5	89.4	94.8	98.5	99.6	100
soil	% of variability	46.6	26.4	14.3	6.8	4.1	1.2	0.5
	cumulative %		73.1	87.4	94.2	98.3	99.5	100
dust	% of variability	65.5	15.8	10.1	5.1	1.9	1.2	0.4
	cumulative %		81.3	91.4	96.6	98.4	99.6	100

The percentages of variability explained by each PCA component are shown in Table 8. The first two components contribute to more than 70% of the total variance in the three cases. The first component alone accounts for more than 45% of the total variance. Following the suggestion of *Aitchison and Greenacre* [2002], the results of the first two principal components are displayed as covariance biplots (Figure 19).

In the rPCA of soil and dust (Figure 19a), the first principal component (PC1) represents 55.7% of the total variance. Long arrows of Mn, Mg and Ca indicate that the three elements are the main origins of variability in the elemental composition. A noticeable observation is that dust samples are clearly distinguished from soil samples along the arrow of MnO due to the higher Mn concentration in dust samples. This observation is consistent with previous results shown in Figure 16. The noticeable difference between soil and dust also implies that the soil and dust need to be treated separately to analyze the origin of elemental composition variability.

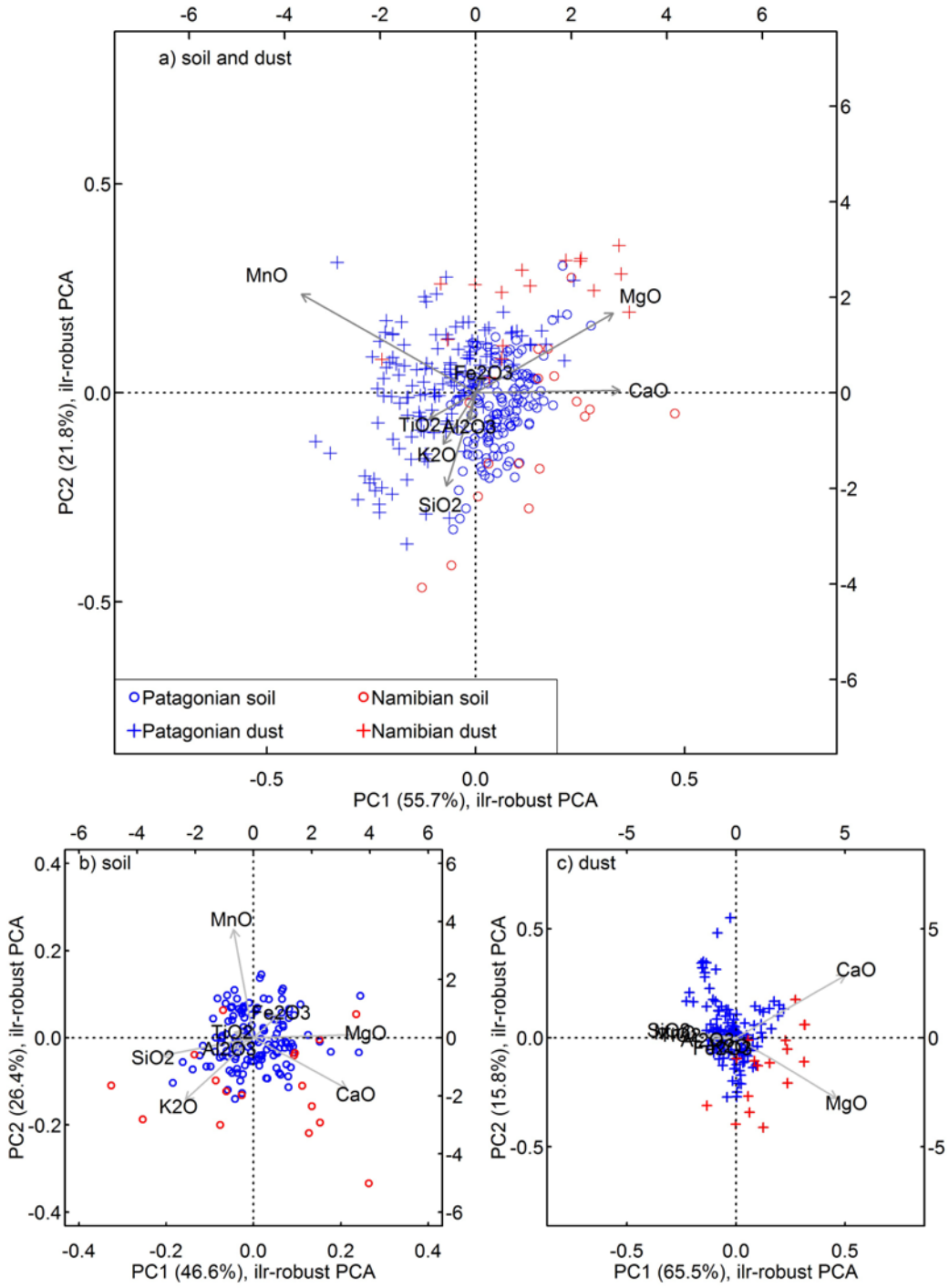

Figure 19 : Covariance biplots of the first two PCs of the robust PCA. Circle denotes soil sample and cross denotes dust sample. Blue color indicates Patagonian origin and red color indicates Namibian origin.

Figure 19b illustrates the rPCA results of soil. Ca, Mg, Mn, K and Si explain 73.1% (PC1 and PC2) of the total variance. Relatively smaller distances are observed between Si and K, and between Mg and Fe. The subgroup Si-K is located in the opposite side of Mg-Fe,

suggesting that compositions of mafic igneous rocks (rich in Mg, Fe) and felsic minerals (rich in Si, K) are critical factors leading to the variability in the elemental composition of the bulk soil. Compared to the Patagonian soil samples, Namibian soil samples show a higher variance due to the higher variability and wide concentration range of the Ca content, which is consistent with Figure 16.

For the dust samples (Figure 19c), Si, Al, K, Ti, Fe and Mn show remarkably high correlations. The first component explains 65.5% of total variance, which is mainly associated with the variability of Mg and Ca content. The variance contributed by the different types of igneous rocks in the bulk soil dramatically decreased. The high correlation between Si, Al, K and Fe suggests a main contribution of these elements in the dust fraction from aluminosilicate clays (such as kaolinite, illite, montmorillonite) and feldspars. Minerals such as quartz are unlikely to make significant contribution to the dust fraction. Conversely, the high variance contributions from Mg and Ca indicate that carbonate minerals (such as calcite, magnesite, and dolomite) are the main source of variability in the elemental composition [*Acosta et al.*, 2011; *Journet et al.*, 2014; *Nickovic et al.*, 2012; *Schütz and Rahn*, 1982]. The rPCA result of variables for the dataset containing soil and dust (Figure 19a) is actually dominated by the variability of soil (Figure 19b). The Namibian samples are clearly distinguished from the Patagonian samples due to the higher Mg concentration in the Namibian samples, which agrees well with the information provided in Figure 16.

4.2. Variation of elemental composition from bulk soil to aerosol

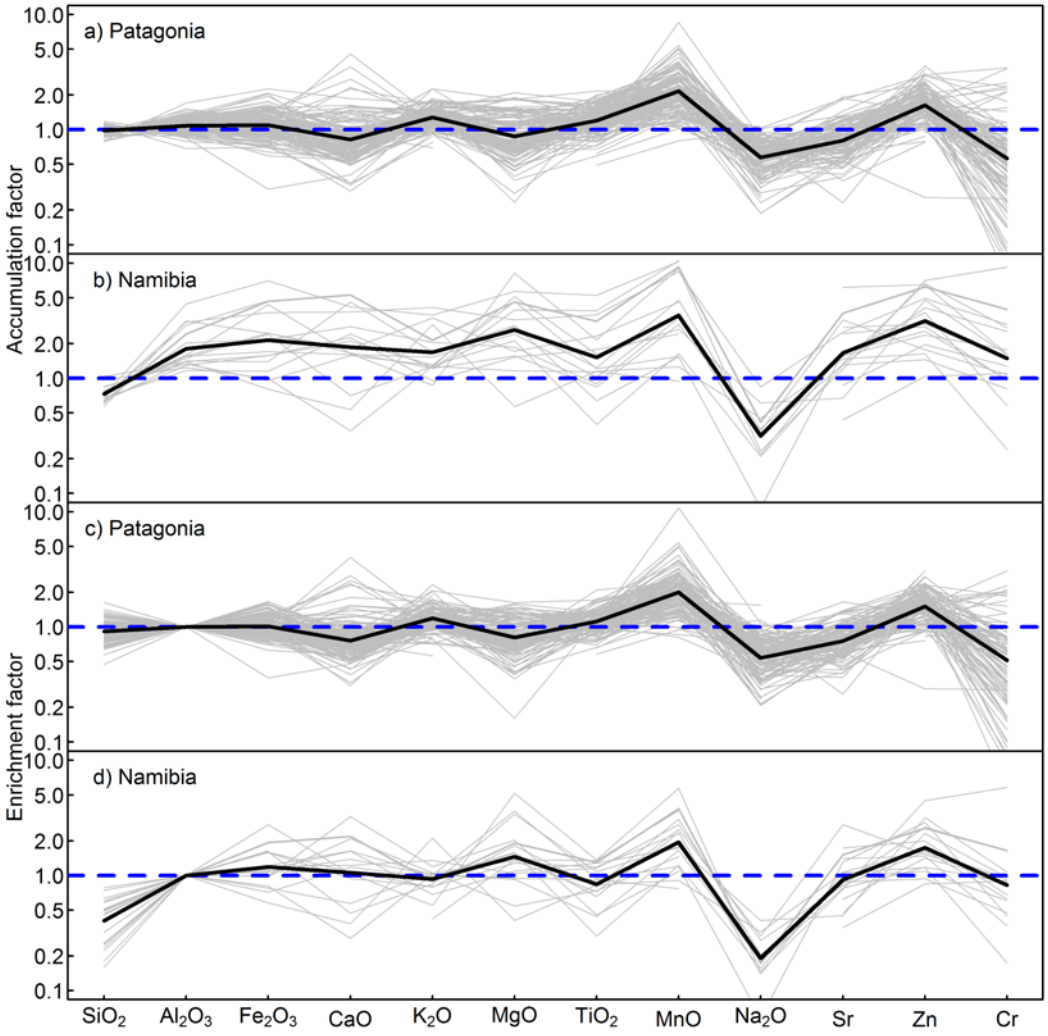

Figure 20 : Accumulation factor and enrichment factor of the elemental composition from soil to dust. a) AF in Patagonia, b) AF in Namibia, c) EF in Patagonia, d) EF in Namibia. Grey lines represent the results of the individual samples. Black lines represent the geometric average values.

Figure 20a and b illustrate the accumulation factor for the elemental composition in Patagonian and Namibian soil, respectively. P and Zr were removed due to the high proportion of values below the detection limit. The differences in the elemental compositions between topsoil and generated dust suggest a divergent variation in the elemental composition during dust emission. For the samples from Namibia, the geometric mean of the accumulation factor demonstrates lower concentrations of Si and Na in the dust fraction. The rest of the elements, i.e. Al, Fe, Ca, K, Mg, Ti, Mn, Cr. Zn and Sr, have higher concentrations in dust.

The negative fractionation of Si and the positive fractionation of Al, Fe, Ca, K, Mn and Ti observed in Namibia are in agreement with the previous studies of *Schütz and Rahn* [1982] on soils from the Sahara and Texas, *Eltayeb et al.* [1993] on Namibian soils, and *Eltayeb et al.* [2001] on Saharan soils. *Schütz and Rahn* [1982] fractionated the soil samples using dry and wet techniques into different size ranges and found that the concentrations for most of the elements, except for Si, increase with decreasing particle size down to 10-20 μm to remain nearly constant. *Eltayeb et al.* [1993] separated Namibian soils into different size fractions by dry sieving and aerosol generation coupled with a cascade impactor, and found a nearly constant concentration of Al, K, Sr and Rb, a positive fractionation for the Ca, Ti, Mn, Fe and Y, and a negative fractionation for Si in the aerosol fraction. Similarly, *Eltayeb et al.* [2001] conducted a similar study on Sahara Desert sand from Sudan and observed a negative fractionation for Si, and a positive fractionation for Al, K, Rb, Ca, Mn, Fe, Sr and Ti. These authors also found a higher concentration of Cr around 45 μm in diameter but not in the aerosol fraction. This size-dependence fractionation model is suggested to be linked to the mineral species in soil and dust. Silicon occurs mostly in the sand fraction and is dominated by quartz. The presence of quartz in bulk soil increases the Si content and dilutes the rest of the elements. Ca-containing dolomite, gypsum and calcite are present in all of the size fractions, while feldspars, micas, and clay minerals contain almost all of the elements and occur mostly in the fine particle fractions [*Acosta et al.*, 2011; *Journet et al.*, 2014; *Nickovic et al.*, 2012; *Schütz and Rahn*, 1982]. In our study, the dust fraction mainly originates from clay materials, Ca-containing materials and Mg-containing materials. The calculated enrichment factor relative to Al (Figure 20d) revealed that Fe, Ca and K exhibit a similar enrichment behavior to Al, whereas Si is highly depleted relative to Al. This is in accordance with the PCA results, which indicate that certain elements, i.e. Al, Fe, K, are the main elements contributed by clay minerals. The low values of EF(Si/Al) in the Namibian samples reveal the presence of a high concentration of quartz materials in the Namibian soil samples. The size fractionation of the soil during aerosol generation reduced the dilution effect of quartz and resulted in the negative fractionation of Si and positive fractionation of the remaining elements.

For the samples from Patagonia, the Si, Al, Fe, Ca, Mg and Sr concentrations are generally similar in both soil and aerosol. The AF value shows lower concentrations of Na and Cr and higher concentrations of K, Ti, Mn, and Zn. The calculated EF showed similar values to AF, indicating a stable Si/Al ratio during dust emission from the parent soils. Since

Patagonia is generally covered by clays and is less rich in quartz and calcite, the fractionation mode in Namibia resulting from the quartz dilution effect is not observed in Patagonia.

5. Conclusion

To investigate the chemical composition of source dust emitted from Patagonia and Namibia, 135 Patagonian dust samples and 17 Namibian dust samples were generated from soil samples collected in arid regions using a laboratory aerosol generator. The elemental compositions of aerosols and bulk soils determined by XRF analysis demonstrate a spatial variation in the elemental compositions.

The average Fe_2O_3 concentration is $6.3 \pm 1.8\%$ for dust from Patagonia and $8.2 \pm 2.1\%$ for dust from Namibia. Patagonian mineral dust generally possesses a lower concentration of Fe but a higher concentration of Si than Namibian mineral dust. At a regional scale, southern Patagonia tends to emit dust with a higher Si content than northern Patagonia, resulting in an inverse trend for the other elements. Iron-rich aerosol hot spots are found in the vicinity of the volcanoes.

A principal component analysis under the form of biplots demonstrates that the Si, Al, K, Fe and Ti contents in dust samples primarily originate from the aluminosilicate clays and feldspars in the bulk soils. Ca- or Mg containing minerals (such as calcite, magnesite, and dolomite) are the main origin of variability in the dust composition.

Calculations of the accumulation factor and enrichment factor (relative to Al) revealed a different elemental fractionation behavior between the Patagonian and Namibian samples. The Namibian samples show Si, Na and Zr depletion in the dust, but an enrichment for the other elements including Al, Fe, Ca, K, Mg, Ti, P, Mn, Cr, Zn and Sr. Silica is the foremost cause of elemental fractionation due to the dilution effect of quartz and results in dramatic Si depletion for dust produced from quartz-rich soils in Namibia. In Patagonia, except for the depletion of Na and Cr in dust, and the enrichment of Mn and Zn, the remaining elements show similar elemental composition patterns in dust and in the parent soils. Furthermore, the calculated accumulation factor provides a resolution to estimate the dust elemental composition from the soil elemental composition. The determined elemental composition of the dust and its variability, as well as the accumulation factor will have further implications in future biogeochemical modelling studies in the subantarctic region.

Acknowledgements

This work benefited from the financial support of CNRS INSU LEFE/CHAT program DFP (Dust from Patagonia) and the Franco-Argentina ECOS program. The authors thank Sarah Mullin for the improvement of English content. The analytical details, including the soil tablet preparation and “thin layer” analysis for the aerosol samples, are available in the supporting information. Descriptive statistics of the elemental composition of topsoil and dust, and the calculated accumulation factor and enrichment factor are also provided in the supporting information.

References List

Ackerman, A. S., O. B. Toon, D. E. Stevens, A. J. Heymsfield, V. Ramanathan, and E. J. Welton (2000), Reduction of Tropical Cloudiness by Soot, *Science*, *288*, 1042-1047, doi:10.1126/science.288.5468.1042.

Acosta, J. A., A. F. Cano, J. M. Arocena, F. Debela, and S. Martínez-Martínez (2009), Distribution of metals in soil particle size fractions and its implication to risk assessment of playgrounds in Murcia City (Spain), *Geoderma*, *149*(1–2), 101-109, doi:10.1016/j.geoderma.2008.11.034.

Acosta, J. A., S. Martínez-Martínez, A. Faz, and J. Arocena (2011), Accumulations of major and trace elements in particle size fractions of soils on eight different parent materials, *Geoderma*, *161*, 30-42, doi:10.1016/j.geoderma.2010.12.001.

Aitchison, J. (1986), *The statistical analysis of compositional data*, 416 pp., Chapman & Hall, Ltd. London.

Aitchison, J., and M. Greenacre (2002), Biplots of Compositional Data, *Journal of the Royal Statistical Society. Series C (Applied Statistics)*, *51*(4), 375-392, doi:10.2307/3592616.

Alfaro, S. C., A. Gaudichet, L. Gomes, and M. Maillé (1997), Modeling the size distribution of a soil aerosol produced by sandblasting, *Journal of Geophysical Research: Atmospheres*, *102*, 11239-11249, doi:10.1029/97JD00403.

Alfaro, S. C., A. Gaudichet, J. L. Rajot, L. Gomes, M. Maillé, and H. Cachier (2003), Variability of aerosol size-resolved composition at an Indian coastal site during the Indian Ocean Experiment (INDOEX) intensive field phase, *Journal of Geophysical Research: Atmospheres*, *108*, 4235, doi:10.1029/2002JD002645.

Alfaro, S. C., S. Lafon, J. L. Rajot, P. Formenti, A. Gaudichet, and M. Maillé (2004), Iron oxides and light absorption by pure desert dust: An experimental study, *Journal of Geophysical Research: Atmospheres*, *109*, doi:10.1029/2003JD004374.

Arimoto, R. (2001), Eolian dust and climate: relationships to sources, tropospheric chemistry, transport and deposition, *Earth-Science Reviews*, *54*, 29-42, doi:10.1016/S0012-8252(01)00040-X.

Arimoto, R., X. Y. Zhang, B. J. Huebert, C. H. Kang, D. L. Savoie, J. M. Prospero, S. K. Sage, C. A. Schloesslin, H. M. Khaing, and S. N. Oh (2004), Chemical composition of atmospheric aerosols from Zhenbeitai, China, and Gosan, South Korea, during ACE-Asia, *J. Geophys. Res.-Atmos.*, *109*(D19), doi:10.1029/2003jd004323.

Boyd, P. W. (2002), The role of iron in the biogeochemistry of the Southern Ocean and equatorial Pacific: a comparison of in situ iron enrichments, *Deep Sea Research Part II: Topical Studies in Oceanography*, *49*, 1803-1821, doi:10.1016/S0967-0645(02)00013-9.

Boyd, P. W., and M. J. Ellwood (2010), The biogeochemical cycle of iron in the ocean, *Nature Geosci, 3*(10), 675-682, doi:10.1038/ngeo964.

Buccianti, A., and E. Grunsky (2014), Compositional data analysis in geochemistry: Are we sure to see what really occurs during natural processes?, *Journal of Geochemical Exploration*, *141*(0), 1-5, doi:10.1016/j.gexplo.2014.03.022.

Castillo, S., T. Moreno, X. Querol, A. Alastuey, E. Cuevas, L. Herrmann, M. Mounkaila, and W. Gibbons (2008), Trace element variation in size-fractionated African desert dusts, *Journal of Arid Environments*, *72*, 1034-1045, doi:10.1016/j.jaridenv.2007.12.007.

Chisholm, S. W., and F. M. Morel (1991), What controls phytoplankton production in nutrient-rich areas of the open sea?, American Society of Limnology and Oceanography Symposium, 22-24 February 1991, San Marcos, California, Preface, edited, AMER SOC Limnology and Oceanography 810 EAST 10TH ST, LAWRENCE, KS 66044-8897.

Claquin, T., M. Schulz, and Y. J. Balkanski (1999), Modeling the mineralogy of atmospheric dust sources, *Journal of Geophysical Research: Atmospheres*, *104*(D18), 22243-22256, doi:10.1029/1999JD900416.

Collini, E., M. S. Osores, A. Folch, J. G. Viramonte, G. Villarosa, and G. Salmuni (2013), Volcanic ash forecast during the June 2011 Cordón Caulle eruption, *Natural Hazards*, *66*, 389-412, doi:10.1007/s11069-012-0492-y.

de Baar, H. J. W., J. T. M. de Jong, D. C. E. Bakker, B. M. Löscher, C. Veth, U. Bathmann, and V. Smetacek (1995), Importance of iron for plankton blooms and carbon dioxide drawdown in the Southern Ocean, *Nature*, *373*, 412-415, doi:10.1038/373412a0.

Desboeufs, K. V., A. Sofikitis, R. Losno, J. L. Colin, and P. Ausset (2005), Dissolution and solubility of trace metals from natural and anthropogenic aerosol particulate matter, *Chemosphere*, *58*(2), 195-203, doi:10.1016/j.chemosphere.2004.02.025.

Egozcue, J. J., V. Pawlowsky-Glahn, G. Mateu-Figueras, and C. Barceló-Vidal (2003), Isometric Logratio Transformations for Compositional Data Analysis, *Mathematical Geology*, *35*(3), 279-300, doi:10.1023/A:1023818214614.

Eltayeb, M. A. H., J. Injuk, W. Maenhaut, and R. E. Van Grieken (2001), Elemental Composition of Mineral Aerosol Generated from Sudan Sahara Sand, *Journal of Atmospheric Chemistry*, *40*(3), 247-273, doi:10.1023/A:1012272208129.

Eltayeb, M. A. H., R. E. Van Grieken, W. Maenhaut, and H. J. Annegarn (1993), Aerosol-soil fractionation for Namib Desert samples, *Atmospheric Environment. Part A. General Topics*, *27*(5), 669-678, doi:10.1016/0960-1686(93)90185-2.

Etyemezian, V., G. Nikolich, S. Ahonen, M. Pitchford, M. Sweeney, R. Purcell, J. Gillies, and H. Kuhns (2007), The Portable In Situ Wind Erosion Laboratory (PI-SWERL): A new method to measure PM10 windblown dust properties and potential for emissions, *Atmospheric Environment*, *41*, 3789-3796, doi:10.1016/j.atmosenv.2007.01.018.

Filzmoser, P., K. Hron, and C. Reimann (2009), Principal component analysis for compositional data with outliers, *Environmetrics*, *20*(6), 621-632, doi:10.1002/env.966.

Folch, A., L. Mingari, M. S. Osores, and E. Collini (2014), Modeling volcanic ash resuspension – application to the 14–18 October 2011 outbreak episode in central Patagonia, Argentina, *Nat. Hazards Earth Syst. Sci.*, *14*, 119-133, doi:10.5194/nhess-14-119-2014.

Formenti, P., W. Elbert, W. Maenhaut, J. Haywood, and M. Andreae (2003), Chemical composition of mineral dust aerosol during the Saharan Dust Experiment (SHADE) airborne campaign in the Cape Verde region, September 2000, *Journal of Geophysical Research: Atmospheres (1984–2012)*, *108*(D18).

Gaiero, D. M., F. Brunet, J.-L. Probst, and P. J. Depetris (2007), A uniform isotopic and chemical signature of dust exported from Patagonia: Rock sources and occurrence in southern environments, *Chemical Geology*, *238*, 107-120, doi:10.1016/j.chemgeo.2006.11.003.

Gaiero, D. M., J.-L. Probst, P. J. Depetris, S. M. Bidart, and L. Leleyter (2003), Iron and other transition metals in Patagonian riverborne and windborne materials: geochemical control

and transport to the southern South Atlantic Ocean, *Geochimica et Cosmochimica Acta*, *67*, 3603-3623, doi:10.1016/S0016-7037(03)00211-4.

Gao, Y., S. M. Fan, and J. L. Sarmiento (2003), Aeolian iron input to the ocean through precipitation scavenging: A modeling perspective and its implication for natural iron fertilization in the ocean, *J. Geophys. Res.-Atmos.*, *108*(D7), doi:10.1029/2002jd002420.

Gassó, S., and A. F. Stein (2007), Does dust from Patagonia reach the sub-Antarctic Atlantic Ocean?, *Geophysical Research Letters*, *34*, L01801, doi:10.1029/2006GL027693.

Gillette, D. (1978), Tests with a portable wind tunnel for determining wind erosion threshold velocities, *Atmospheric Environment (1967)*, *12*, 2309-2313, doi:10.1016/0004-6981(78)90271-8.

Gillette, D. A. (1999), A qualitative geophysical explanation for hot spot dust emitting source regions, *Contributions to Atmospheric Physics*, *72*(1), 67-77.

Gomes, L., G. Bergametti, G. Coudé-Gaussen, and P. Rognon (1990), Submicron desert dusts: A sandblasting process, *Journal of Geophysical Research: Atmospheres*, *95*, 13927-13935, doi:10.1029/JD095iD09p13927.

Graf, H.-F. (2004), The Complex Interaction of Aerosols and Clouds, *Science*, *303*, 1309-1311, doi:10.1126/science.1094411.

Hansen, J., M. Sato, and R. Ruedy (1997), Radiative forcing and climate response, *Journal of Geophysical Research: Atmospheres*, *102*, 6831-6864, doi:10.1029/96JD03436.

Ho, H. H., R. Swennen, V. Cappuyns, E. Vassilieva, and T. Van Tran (2012), Necessity of normalization to aluminum to assess the contamination by heavy metals and arsenic in sediments near Haiphong Harbor, Vietnam, *Journal of Asian Earth Sciences*, *56*, 229-239, doi:10.1016/j.jseaes.2012.05.015.

Huang, S., J. Tu, H. Liu, M. Hua, Q. Liao, J. Feng, Z. Weng, and G. Huang (2009), Multivariate analysis of trace element concentrations in atmospheric deposition in the Yangtze River Delta, East China, *Atmospheric Environment*, *43*, 5781-5790, doi:10.1016/j.atmosenv.2009.07.055.

Johnson, M. S., N. Meskhidze, F. Solmon, S. Gassó, P. Y. Chuang, D. M. Gaiero, R. M. Yantosca, S. Wu, Y. Wang, and C. Carouge (2010), Modeling dust and soluble iron deposition to the South Atlantic Ocean, *Journal of Geophysical Research: Atmospheres*, *115*, D15202, doi:10.1029/2009JD013311.

Journet, E., Y. Balkanski, and S. P. Harrison (2014), A new data set of soil mineralogy for dust-cycle modeling, *Atmos. Chem. Phys.*, *14*, 3801-3816, doi:10.5194/acp-14-3801-2014.

Kjelgaard, J. F., D. G. Chandler, and K. E. Saxton (2004), Evidence for direct suspension of loessial soils on the Columbia Plateau, *Earth Surface Processes and Landforms*, *29*, 221–236, doi:10.1002/esp.1028.

Koren, I., Y. J. Kaufman, L. A. Remer, and J. V. Martins (2004), Measurement of the Effect of Amazon Smoke on Inhibition of Cloud Formation, *Science*, *303*, 1342-1345, doi:10.1126/science.1089424.

Lafon, S., S. C. Alfaro, S. Chevaillier, and J. L. Rajot (2014), A new generator for mineral dust aerosol production from soil samples in the laboratory: GAMEL, *Aeolian Research*, *15*, 319-334, doi:http://dx.doi.org/10.1016/j.aeolia.2014.04.004.

Langmann, B. (2013), Volcanic Ash versus Mineral Dust: Atmospheric Processing and Environmental and Climate Impacts, *ISRN Atmospheric Sciences, 2013*, 17, doi:10.1155/2013/245076.

Lawson, D. R., and J. W. Winchester (1979), A standard crustal aerosol as a reference for elemental enrichment factors, *Atmospheric Environment (1967)*, *13*(7), 925-930, doi:http://dx.doi.org/10.1016/0004-6981(79)90003-9.

Li, F., P. Ginoux, and V. Ramaswamy (2008), Distribution, transport, and deposition of mineral dust in the Southern Ocean and Antarctica: Contribution of major sources, *Journal of Geophysical Research: Atmospheres*, *113*, doi:10.1029/2007JD009190.

Loosmore, G. A., and J. R. Hunt (2000), Dust resuspension without saltation, *Journal of Geophysical Research: Atmospheres*, *105*, 20663–20671, doi:10.1029/2000JD900271.

Losno, R., G. Bergametti, and G. Mouvier (1987), Determination of optimal conditions for atmospheric aerosol analysis by X-ray-fluorescence, *Environmental Technology Letters*, *8*(2), 77-86.

Luo, C., N. Mahowald, T. Bond, P. Y. Chuang, P. Artaxo, R. Siefert, Y. Chen, and J. Schauer (2008), Combustion iron distribution and deposition, *Global Biogeochemical Cycles*, *22*(1), n/a-n/a, doi:10.1029/2007GB002964.

Macpherson, T., W. G. Nickling, J. A. Gillies, and V. Etyemezian (2008), Dust emissions from undisturbed and disturbed supply-limited desert surfaces, *Journal of Geophysical Research: Earth Surface*, *113*, n/a–n/a, doi:10.1029/2007JF000800.

Maher, B. A., J. M. Prospero, D. Mackie, D. Gaiero, P. P. Hesse, and Y. Balkanski (2010), Global connections between aeolian dust, climate and ocean biogeochemistry at the present day and at the last glacial maximum, *Earth-Science Reviews*, *99*, 61-97, doi:10.1016/j.earscirev.2009.12.001.

Mahowald, N. (2011), Aerosol Indirect Effect on Biogeochemical Cycles and Climate, *Science*, *334*(6057), 794-796, doi:10.1126/science.1207374.

Martín-Fernández, J. A., C. Barceló-Vidal, and V. Pawlowsky-Glahn (2000), Zero Replacement in Compositional Data Sets, in *Data Analysis, Classification, and Related Methods*, edited by H. L. Kiers, J.-P. Rasson, P. F. Groenen and M. Schader, pp. 155-160, Springer Berlin Heidelberg, doi:10.1007/978-3-642-59789-3_25.

Martín-Fernández, J. A., C. Barceló-Vidal, and V. Pawlowsky-Glahn (2003), Dealing with Zeros and Missing Values in Compositional Data Sets Using Nonparametric Imputation, *Mathematical Geology*, *35*(3), 253-278, doi:10.1023/A:1023866030544.

Martin, J. H. (1990), Glacial-interglacial CO2 change: The Iron Hypothesis, *Paleoceanography*, *5*, 1–13, doi:10.1029/PA005i001p00001.

Martin, J. H., and S. E. Fitzwater (1988), Iron deficiency limits phytoplankton growth in the north-east Pacific subarctic, *Nature*, *331*(6154), 341-343.

McCormick, R. A., and J. H. Ludwig (1967), Climate Modification by Atmospheric Aerosols, *Science*, *156*(3780), 1358-1359, doi:10.1126/science.156.3780.1358.

McKee, E. D. (1982), Sedimentary Structures in Dunes of the Namib Desert, South West Africa, *Geological Society of America Special Papers*, *188*, 1-2, doi:10.1130/SPE188-p1.

Miller, R. L., and I. Tegen (1998), Climate Response to Soil Dust Aerosols, *Journal of Climate*, *11*, 3247-3267, doi:10.1175/1520-0442(1998)011<3247:CRTSDA>2.0.CO;2.

Moore, C. M., et al. (2013), Processes and patterns of oceanic nutrient limitation, *Nature Geosci, 6*(9), 701-710, doi:10.1038/ngeo1765

Moore, J. K., M. R. Abbott, J. G. Richman, and D. M. Nelson (2000), The southern ocean at the Last Glacial Maximum: A strong sink for atmospheric carbon dioxide, *Global Biogeochemical Cycles, 14*, 455-475, doi:10.1029/1999GB900051.

Moore, J. K., S. C. Doney, D. M. Glover, and I. Y. Fung (2001), Iron cycling and nutrient-limitation patterns in surface waters of the World Ocean, *Deep Sea Research Part II: Topical Studies in Oceanography*, *49*(1–3), 463-507, doi:http://dx.doi.org/10.1016/S0967-0645(01)00109-6.

Nickovic, S., A. Vukovic, M. Vujadinovic, V. Djurdjevic, and G. Pejanovic (2012), Technical Note: High-resolution mineralogical database of dust-productive soils for atmospheric dust modeling, *Atmos. Chem. Phys.*, *12*(2), 845-855, doi:10.5194/acp-12-845-2012.

Pawlowsky-Glahn, V., J. J. Egozcue, and R. Tolosana Delgado (2007), Lecture notes on compositional data analysis.

Quisefit, J. P., and E. Randrianarivony (1998), Validation de la méthode d'étalonnage en couche mince par utilisation de géostandards déposés sur filtres pour l'analyse élémentaire par SFX, *Le Journal de Physique IV*, *08*, Pr5-359-Pr355-367, doi:10.1051/jp4:1998545.

R Core Team (2015). R, A language and environment for statistical computing. R Foundation for Statistical Computing, Vienna, Austria. URL http://www.R-project.org/.

Reimann, C., P. Filzmoser, K. Fabian, K. Hron, M. Birke, A. Demetriades, E. Dinelli, and A. Ladenberger (2012), The concept of compositional data analysis in practice — Total major element concentrations in agricultural and grazing land soils of Europe, *Science of The Total Environment*, *426*(0), 196-210, doi: 10.1016/j.scitotenv.2012.02.032.

Rousseeuw, P. J. (1985), Multivariate estimation with high breakdown point, *Mathematical statistics and applications*, *8*, 283-297.

Rousseeuw, P. J., and K. V. Driessen (1999), A Fast Algorithm for the Minimum Covariance Determinant Estimator, *Technometrics*, *41*(3), 212-223, doi:10.1080/00401706.1999.10485670.

Salam, A., U. Lohmann, B. Crenna, G. Lesins, P. Klages, D. Rogers, R. Irani, A. MacGillivray, and M. Coffin (2006), Ice Nucleation Studies of Mineral Dust Particles with a New Continuous Flow Diffusion Chamber, *Aerosol Science and Technology*, *40*, 134-143, doi:10.1080/02786820500444853.

Sanford, R., C. Pierson, and R. Crovelli (1993), An objective replacement method for censored geochemical data, *Mathematical Geology*, *25*(1), 59-80, doi:10.1007/BF00890676.

Scasso, R. A., H. Corbella, and P. Tiberi (1994), Sedimentological analysis of the tephra from the 12–15 August 1991 eruption of Hudson volcano, *Bulletin of Volcanology*, *56*, 121-132, doi:10.1007/BF00304107.

Schütz, L., and K. A. Rahn (1982), Trace-element concentrations in erodible soils, *Atmospheric Environment (1967)*, *16*, 171-176, doi:10.1016/0004-6981(82)90324-9.

Scheermeyer, E., and I. E. Agranovski (2009), Design and evaluation of a new device for fungal spore aerosolization for laboratory applications, *Journal of Aerosol Science*, *40*, 879-889, doi:10.1016/j.jaerosci.2009.06.003.

Schulz, M., Y. J. Balkanski, W. Guelle, and F. Dulac (1998), Role of aerosol size distribution and source location in a three-dimensional simulation of a Saharan dust episode tested against satellite-derived optical thickness, *Journal of Geophysical Research: Atmospheres*, *103*, 10579-10592, doi:10.1029/97JD02779.

Shao, Y. (2008), Dust Emission, in *Physics and Modelling of Wind Erosion*, edited by Y. Shao, pp. 211-245, Springer Netherlands, doi:10.1007/978-1-4020-8895-7_7.

Shao, Y., M. R. Raupach, and P. A. Findlater (1993), Effect of saltation bombardment on the entrainment of dust by wind, *Journal of Geophysical Research: Atmospheres*, *98*, 12719–12726, doi:10.1029/93JD00396.

Sow, M., S. C. Alfaro, J. L. Rajot, and B. Marticorena (2009), Size resolved dust emission fluxes measured in Niger during 3 dust storms of the AMMA experiment, Atmos. Chem. Phys., 9(12), 3881-3891, doi:10.5194/acp-9-3881-2009.

Stern, C. R. (2008), Holocene tephrochronology record of large explosive eruptions in the southernmost Patagonian Andes, *Bulletin of Volcanology*, *70*, 435-454, doi:10.1007/s00445-007-0148-z.

Sweeney, M. R., and J. A. Mason (2013), Mechanisms of dust emission from Pleistocene loess deposits, Nebraska, USA, *Journal of Geophysical Research: Earth Surface*, *118*, 1460–1471, doi:10.1002/jgrf.20101.

Taylor, S. R., and S. M. McLennan (1995), The geochemical evolution of the continental crust, *Reviews of Geophysics*, *33*, 241-265, doi:10.1029/95RG00262.

Templ, M., K. Hron, and P. Filzmoser (Eds.) (2011), *robCompositions: an R-package for robust statistical analysis of compositional data*, 341-355 pp., John Wiley & Sons, Chichester (UK).

Textor, C., et al. (2006), Analysis and quantification of the diversities of aerosol life cycles within AeroCom, *Atmos. Chem. Phys.*, *6*, 1777-1813, doi:10.5194/acp-6-1777-2006.

Van der Weijden, C. H. (2002), Pitfalls of normalization of marine geochemical data using a common divisor, *Marine Geology*, *184*, 167-187, doi:10.1016/S0025-3227(01)00297-3.

Wang, W., J. Zhao, and Q. Cheng (2014), Mapping of Fe mineralization-associated geochemical signatures using logratio transformed stream sediment geochemical data in eastern Tianshan, China, *Journal of Geochemical Exploration*, *141*(0), 6-14, doi:http://dx.doi.org/10.1016/j.gexplo.2013.11.008.

Watson, A. J., D. C. E. Bakker, A. J. Ridgwell, P. W. Boyd, and C. S. Law (2000), Effect of iron supply on Southern Ocean CO2 uptake and implications for glacial atmospheric CO2, *Nature*, *407*, 730-733, doi:10.1038/35037561.

Zhang, Y., et al. (2015), Modeling the global emission, transport and deposition of trace elements associated with mineral dust, *Biogeosciences*, *12*(19), 5771-5792, doi:10.5194/bg-12-5771-2015.

Zuo, R., Q. Xia, and H. Wang (2013), Compositional data analysis in the study of integrated geochemical anomalies associated with mineralization, *Applied Geochemistry*, *28*(0), 202-211, doi:http://dx.doi.org/10.1016/j.apgeochem.2012.10.031.

Supporting Information for the article

Soil tablets preparation and measurement

Prior to the chemical analysis, tablets of soil samples were prepared. Approximately 10 g of soil samples were firstly ground into fine particles by a planetary ball mill (Planetary Mono Mill PULVERISETTE 6 classic line, FRITSCH, Germany), equipped with an 80 mL tungsten carbide grinding bowl and 25 g of 15 mm tungsten carbide grinding balls, at a revolution speed of 500 rpm for 5 minutes. Five grams of soil powder were then mixed thoroughly with 0.9 g wax ($C_{38}H_{76}N_2O_2$) and the mixture was then compressed into 32 mm diameter tablets under 20 tons of pressure. The addition of wax will strengthen the cohesion of the soil particles, and furthermore provides a similar spectral interference of the organic materials for its relatively greater mass compared to the soil containing organic material. Two certified reference materials (CRMs) tablets (GS-N as granite and BE-N as basalt, provided by SARM, Nancy) were prepared and analyzed with the same process to check the analysis technique and the calibration of the method.

The calibration was done with a series of CRM tablets prepared in addition and an integrated "Omnian" algorithm with the aim to better fit the calibration to the samples with different matrices. Table 6 compares the measured values with the certified values for the CRM samples. Si, Al, Fe, Na, K, Ca, Mg, Ti, Cr, Cu, Zn, Sr, Zr, and Rb have a recovery between 86% and 111%. The measured P, S and Mn values agree less well with the certified values, particularly in GS-N, which might be due to the low abundance of these elements in the GS-N standard. The composition results include some contribution from organic material and water present in the collected soils. The elemental composition of the dry mineral fraction of the soil was determined by dividing the mass of the elements in each sample by the total mass of the major elements expressed as oxides (Na_2O, MgO, Al_2O_3, SiO_2, P_2O_5, K_2O, CaO, TiO_2, MnO, Fe_2O_3).

Soil-derived aerosol analysis: the "thin layer method"

Mineral dust samples were collected on Nuclepore® polycarbonate filter membranes and analyzed using EDXRF. During aerosol generation, the amount of aerosol deposited on the filter was limited to less than 1000 μg on a surface measuring 28 mm in diameter. Aerosol particles collected on the filter membrane form a "thin layer" [*Losno et al.*, 1987]. The matrix

effect (absorption and secondary fluorescence) of the XRF analysis for the thin layer samples is highly restricted and the measured fluorescence intensity is proportional to the mass of the element. One requirement for the calibration standard preparation is that the layer's thickness should be restricted [*Wätjen and Cavé*, 1996]. The calibration filters were prepared by adapting the method proposed by *Quisefit and Randrianarivony* [1998]. This method deposits CRM particles on a membrane filter by filtrating an ethanol suspension containing CRM powder:

(1) pure ethanol (> 99.5%) was previously filtered through a 0.2 μm polycarbonate filter, and then distilled in a quartz sub-boiler in order to remove the possible particle and inorganic solute impurities;

(2) a small portion of the geo-standard is manually ground for one hour with an agate mortar to obtain fine mineral particles;

(3) 10 mg of the CRM powder was added into 20 mL purified ethanol in a 50 mL centrifuge tube;

(4) the mixture was then processed by ultra-sonication for 5 minutes and vortexed during 1 minute to obtain a suspension of the fine CRM particles;

(5) 3 mL of the CRM suspension was diluted with 15 mL of ethanol in a 50 mL centrifuge tube, followed by a thorough vortex mixing for 1 minute;

(6) 3 × 1 mL (or 6 × 1 mL) of the diluted suspension was diluted a second time with approximately 10 mL of ethanol and then slowly filtered through a polycarbonate membrane (pore size of 0.2 μm) to obtain a filter containing 250 μg (or 500 μg) of the CRM homogenously distributed over an area measuring 18 mm in diameter.

(7) three blank filters were prepared with the same protocol without using CRMs.

The dissolution of the geo-standards in ethanol was shown to be less than 0.5% for most of the elements, according to a subsequent ethanol filtrates analysis by ICP-AES. Exceptions include 3.8%~14.57% of K in SDC-1 found in the ethanol filtrates. The certified values of K were thus corrected with the dissolution factor to be used in the calibration processes.

The EDXRF analysis for the aerosol samples was conducted in a Helium gas medium. Two measurement conditions were used for the X-ray tube during: an accelerating voltage of 15 kV and a tube current of 80 μA with a filter of Ti for the light elements; an accelerating voltage of 35 kV and a tube current of 120 μA with an Al filter (thickness of 200 μm) for the

heavy elements (K-Zr). The elemental composition of the mineral fraction of the aerosol was determined by dividing the mass of the elements in each sample by the total mass of the major elements expressed as oxides (Na_2O, MgO, Al_2O_3, SiO_2, P_2O_5, K_2O, CaO, TiO_2, MnO, Fe_2O_3).

Measurement results of the geo-standard filters (Table 7) show good agreement for Na, Al, Si and Zn in both BE-N and SDC-1. Fe, K and Ca show better agreement in the measurement of SDC-1, while Mg, Sr and Zr show better agreement in the BE-N measurement. Mn, Ti and Cr were determined with less accuracy in both BE-N and SDC-1. Analytical result of P clearly deviated from the certified values for SDC-1 due to the low abundance of P in geostandard.

Table 9 : Descriptive statistics for the elemental compositions* of topsoil and dust from Patagonia (n = 135) and Namibia (n = 17).

	SiO_2	Al_2O_3	Fe_2O_3	CaO	Na_2O	K_2O	MgO	TiO_2	P_2O_5	MnO	Cr	Zn	Sr	Zr
Patagonia Soil (SP)									**81****		**4**			
geomean	69	14	5.8	3.4	2.4	2.0	1.5	0.78	0.05	0.08	76	63	295	206
geoSD	5	1.5	1.5	1.4	0.6	0.4	0.7	0.18	0.05	0.02	51	21	70	44
0.05	62	12	3.6	1.8	1.5	1.5	0.8	0.54	0.01	0.04	31	42	190	152
median	70	14	5.9	3.5	2.4	2.0	1.6	0.77	0.05	0.08	69	63	293	200
0.95	77	16	8.4	6.0	3.4	2.8	2.6	1.13	0.28	0.12	242	104	407	298
Patagonia Dust (DP)					**16**		**13**		**31**		**22**	**11**	**26**	**42**
geomean	68	15	6.3	2.8	1.4	2.5	1.4	0.93	0.12	0.17	45	103	237	193
geoSD	6	2	1.8	1.7	0.5	0.6	0.8	0.24	0.12	0.07	35	46	76	69
0.05	58	12	4.3	1.3	0.8	1.6	0.5	0.65	0.02	0.09	14	55	147	116
median	68	15	6.5	2.6	1.4	2.5	1.3	0.94	0.13	0.16	39	106	236	189
0.95	77	19	8.8	8.9	2.5	3.8	3.0	1.30	0.58	0.35	214	172	375	339
Namib Soil (SN)				**1**	**3**				**13**					
geomean	72	9	3.9	3.5	1.0	2.3	2.0	0.59	0.05	0.04	82	42	148	262
geoSD	10	4	2.7	4.0	1.2	1.1	1.5	0.37	0.05	0.03	69	26	120	147
0.05	62	5	1.7	0.7	0.2	1.0	0.6	0.27	0.01	0.02	28	19	50	123
median	72	10	4.8	5.1	1.3	2.5	2.6	0.74	0.07	0.05	77	37	162	222
0.95	89	14	11	12.0	5.9	4.3	4.8	1.2	0.12	0.10	292	89	475	644
Namib Dust (DN)					**6**				**1**					**2**
geomean	53	16	8.2	5.6	0.4	3.8	5.3	0.89	0.35	0.15	121	131	245	156
geoSD	8	4	2.1	6.4	0.2	0.8	3.2	0.16	0.19	0.05	55	42	233	51
0.05	41	12	5.2	1.1	0.2	2.6	2.0	0.69	0.19	0.09	76	79	77	104
median	54	16	8.3	4.8	0.3	3.8	5.3	0.92	0.33	0.14	127	135	253	158
0.95	63	24	11	25.4	1.0	4.8	12.3	1.18	0.84	0.23	233	227	1361	259

*: The elemental compositions are normalized to the total major oxide composition. Major elements in wt.% and trace elements in ppm.
**: numbers in bold are number of zeros in each regional dataset.

Table 10 : Geometric mean accumulation and enrichment factors (Al is used as the reference element and the parent soil as the reference material) in Patagonian and Namibian mineral aerosol with respect to the parent soil.

	AF	EF(x/Al)	EF(x/Si)	AF	EF(x/Al)	EF(x/Si)
	Patagonia			*Namibia*		
Si	0.98	0.9±0.1	1	0.73	0.4±0.1	1
Al	1.08	1	1.1±0.1	1.8	1	2.5±0.5
Fe	1.1	1.0±0.1	1.1±0.2	2.13	1.2±0.2	2.9±0.9
Ca	0.82	0.8±0.1	0.8±0.2	1.85	1.1±0.3	2.5±1.0
Na	0.57	0.5±0.1	0.6±0.1	0.31	0.2±0.0	0.4±0.1
K	1.28	1.2±0.1	1.3±0.1	1.67	0.9±0.1	2.3±0.5
Mg	0.88	0.8±0.1	0.9±0.2	2.62	1.5±0.4	3.6±1.2
Ti	1.2	1.1±0.1	1.2±0.2	1.52	0.8±0.2	2.1±0.7
P	2.94	2.8±0.9	3.0±1.0	9.61	6.9±2.5	12.1±4.3
Mn	2.16	2.0±0.3	2.2±0.4	3.49	1.9±0.5	4.8±1.8
Cr	0.56	0.5±0.2	0.6±0.2	1.48	0.8±0.3	2.0±0.8
Zn	1.63	1.5±0.2	1.7±0.3	3.14	1.7±0.4	4.3±1.3
Sr	0.81	0.8±0.1	0.8±0.1	1.66	0.9±0.2	2.3±0.7
Zr	0.91	0.8±0.1	0.9±0.1	0.68	0.4±0.1	0.9±0.2

Conclusions of Chapter 3

The present part of work documents the elemental composition of topsoil and dust in two dust source regions: Patagonia and Namibia. Average Fe_2O_3 concentration is 6.3±1.8% for dust in Patagonia and 8.2±2.1% for dust from Namibia. Patagonian mineral dust generally possesses a lower concentration of Fe but a higher concentration of Si than Namibian mineral dust.

At a regional scale, elemental compositions including iron content of dust vary with sampling locations. South Patagonia tends to emit dust with higher Si content than North, resulting in an inverse trend for other elements such as iron. In Namibia, iron composition is quite variable. Si, Al, K, Fe and Ti contents in dust samples primarily originate from the aluminosilicate clays and feldspars in the bulk soils. Ca- or Mg-containing minerals (such as calcite, magnesite, and dolomite) are the main origins of variability of dust composition.

Elemental compositions were different in various degrees between dust and parent soil. Iron concentrations are generally similar between the dust samples and their parent soils in Patagonia, which is not the case in Namibia. Namibian dust sample generally shows much higher iron concentration than its parent soil. Using iron concentration of soil as a surrogate of dust iron content pose less uncertainty in Patagonia than in Namibia. Silica is the foremost cause of elemental fractionation due to the dilution effect of quartz and results in a dramatic Si depletion for dust produced from quartz-rich soils in Namibia.

Biogeochemical modeling studies usually take a Fe_2O_3 concentration of 5% from the average upper continental crust composition [*Taylor and McLennan*, 1995] as the iron concentration in dust. However, the Fe content in dust actually varies with source regions, as shown in our study. The database of dust elemental composition and accumulation factor contribute to a better knowledge of the spatial distribution of trace element contents in dust source areas. The calculated accumulation factor also provides a resolution to estimate the dust elemental composition from soil elemental composition. Knowledge about the elemental composition in source dust may help to

estimate the amount of trace elements in dust emitted and have direct implication in further biogeochemical modeling studies in the subantarctic region.

Chapter 4 Contribution to Bioavailability Study of Mineral Dust from Patagonia and Namibia

Introduction of Chapter

After the deposition of dust into the open ocean, the impact of mineral dust on the marine biogeochemistry depends on the bioavailability of trace elements in dust materials. Assement of elemental bioavailability generally takes "fractional solubility" as a proxy. This chapter presents the experimental studies we have done to measure elemental solubility in source dust materials. Considering that atmospheric acid processing is a critical factor affecting elemental solubility in source dust, dissolution experiments were conducted under decreasing pH aiming to evaluate the variation of elemental solubility under increasing chemical strength. Given the fact that the traditional membrane filtration method can retain colloids on the membrane, separation of dissolved phase including colloids from insoluble phase is realized by centrifugation in our study. The main work and results obtained are presented under the form of an article draft entitled "**Investigation of pH-dependence of elemental solubility of mineral dust from Patagonia and Namibia by sequential leaching and centrifugation separation**".

To be submitted

Investigation of pH-dependence of elemental solubility of mineral dust from Patagonia and Namibia by sequential leaching and centrifugation separation

Zihan Qu et al.

Abstract

Patagonia and Namibia are two main mineral dust sources supplying bioavailable micronutrients to the South Atlantic section of Southern Ocean. Quantification of fractional solubility is essential to evaluate the biological impact of dust deposition on marine ecosystem. In this work, elemental solubility was measured for laboratory-produced Patagonian and Namibian dust following a sequential leaching procedure. Dissolved fraction, operationally defined as <0.2 μm fraction, was separated by centrifugation separation method. Elemental solubility increased with decreasing pH from pure water to pH1. Geometric mean iron solubility is 2.6 ± 1.0% (geomean ± SD) in pure water, 3.6 ± 1.2% at pH5, 4.5 ± 1.4% at pH3, and 6.7 ± 1.8% at pH1. Solubility of Al, Si, Ti, Zn, Ca, K, Mg, Mn, Sr and Ba were also determined. Calcium-rich dust, probably due to the presence of carbonate, showed higher solubility for more soluble elements namely Ca, K, Mg, Mn, Sr and Ba. Compared to previous measurements using filtration method, centrifugation method showed much higher solubility values for elements namely Fe and Al, while less difference was found for Ca, Mg, Mn, and Ba. The disagreement of iron and aluminum solubility between the two separation methods is most likely due to the overestimation resulting from experimental bias in centrifugation and the underestimation of colloidal size fraction by filtration method that stops the colloids on membrane. Further studies are strongly required to investigate the particle size distribution in dissolved fraction separated by centrifugation method and filtration method.

1. Introduction

For surface waters in remote oceanic regions, dust deposition is considered to be an important source of trace elements [*Fung et al.*, 2000; *Moore et al.*, 2001] that can affect the marine primary productivity and further oceanic carbon uptake [*Duce et al.*, 1991; *Duce and Tindale.*, 1991]. In HNLC (High Nutrient Low Chlorophyll) regions such as Southern Ocean, depletion of trace elements such as iron and manganese in surface seawater limits the primary production [*Blain et al.*, 2007; *Boyd*, 2002; *Boyd et al.*, 2007; *Boyd and Law*, 2001; *Boyd et al.*, 2000; *de Baar et al.*, 1995; *Martin et al.*, 1990; *Moore et al.*, 2001; *Watson et al.*, 2000]. A major uncertainty to evaluate the biological effects of dust input is the bioavailability of trace elements carried by dust [*Mahowald et al.*, 2005, 2009; *Sholkovitz et al.*, 2012]. Dust deposited into the Southern Ocean originates mainly from Patagonia, Australia and Southern Africa [*Li et al.*, 2008] while its chemical properties including the potential elemental bioavailability are barely known. Bioavailability of elements such as Fe in mineral aerosol could be measured by cellular Fe uptake experiment [e.g. *Achilles et al.*, 2003; *Schmidt and Hutchins*, 1999]. Chemical dissolution techniques, which are widely used [e.g. *Aguilar-Islas et al.*, 2010; *Bonnet and Guieu*, 2004; *Sedwick et al.*, 2007; *Spokes and Jickells*, 1995; *Winton et al.*, 2014; *Zhuang et al.*, 1992], cannot measure directly the elemental bioavailability but use the fractional solubility of elements as a proxy of bioavailability [*Shi et al.*, 2012].

Fractional solubility exhibits a great variability depending on aerosol types and atmospheric processing history [*Aghnatios et al.*, 2014; *Aguilar-Islas et al.*, 2010; *Bonnet and Guieu*, 2004; *Hsu et al.*, 2010; *Maring and Duce*, 1987; *Spokes and Jickells*, 1995; *Zhuang et al.*, 1992]. Solubility measured during dissolution experiments depends firstly on the extractant/solvent used [*Shi et al.*, 2012]. Former dust solubility studies have used various extraction solutions to measure elemental solubility for different purposes. Ultrapure deionized water is the simplest leaching solution commonly used to measure the solubility in non-acidified water [*Aguilar-Islas et al.*, 2010; *Buck et al.*, 2013; *Hsu et al.*, 2010; *Sedwick et al.*, 2007; *Winton et al.*, 2014]. Since pure water has no buffering capacity, dissolution of dust samples can change the pH of solutions [*Desboeufs et al.*, 2001; *Paris et al.*, 2011] and hence the obtained results are difficult to compare. The uses of buffers such as ammonium

acetate (pH = 4.7) [*Sarthou et al.*, 2003; *Baker et al.*, 2006a,b] or formate acetate (pH = 4.5) [*Chen and Siefert*, 2004], which simulate the acidified condition of rainwater, avoid the pH alteration issued during dissolution experiments. To take into account the impact of complexation with ligands during dissolution in seawater, previous studies used purified or synthetic seawater as extractant [*Aguilar-Islas et al.*, 2010; *Bonnet and Guieu*, 2004; *Buck et al.*, 2013; *Wu et al.*, 2007]. *Bonnet and Guieu* [2004] and *Buck et al.* [2013] used filtered seawater. Dissolution experiments conducted by *Aguilar-Islas et al.* [2010] with different leaches showed lower dissolution rate of iron in UV oxidized seawater than in UV oxdized seawater with deferoxamine that binds free iron, hightlighting the effect of iron-binding ligands. During atmospheric transport, dust particles undergo acid processing in cloud water in which pH values could decrease to 2 or even lower after evaporation of cloud droplets, resulting in an increase of potential solubility [*Zhu et al.*, 1992; *Meskhidze et al.*, 2003]. Acidified solution could be used as extractant to study the potential solubility of dust during atmospheric transport [*Desboeufs et al.*, 1999; *Desboeufs et al.*, 2001; *Desboeufs et al.*, 2005; *Edwards and Sedwick*, 2001; *Journet et al.*, 2008; *Maring and Duce*, 1987; *Spokes and Jickells*, 1995; *Shi et al.*, 2011; *Zhuang et al.*, 1992].

The bioavailable fraction of elements like iron mainly contain ionic fraction and colloids including nanoparticles [*Shi et al.*, 2012]. In practical measurements of aerosol solubility, the "dissolved" fraction is traditionally separated from the particulate fraction by membrane filtration methods for its portability, simplicity and low cost [*Morrison and Benoit*, 2001]. Hence, the "dissolved" fraction is operationally defined as the fraction passing through the membrane, with a pore size of 0.45 μm or 0.2 μm, and contains ionic species as well as colloids. However, *Buffle and Leppard* [1995a,b], *Morrison and Benoit* [2001] and *Zirkler et al.* [2012] indicated that filtration separation underestimates the amount of colloidal material due to the artifacts of membrane including pore clogging, adsorption and self-coagulation of colloids at the membrane surface. Amounts of colloid-bound elements such as Al, Si or Fe in dissolved phase are hence affected [*Castilho et al.*, 1996; *Zirkler et al.*, 2012]. *Gimbert et al.* [2005] found that, comparing to filtration, centrifugation method recovers more materials in colloidal size fraction (<0.2 μm or <0.45 μm).

The present work aims to determine the solubility of elements including iron and manganese in dust from the two source regions around the South Atlantic section of Southern Ocean: Patagonia and Namibia. We adapted a sequential leaching method, proposed by *Aghnatios et al.* [2014], with increasing acidity from pure water to pH1 (pure water, pH5, pH3 and pH1) to determine the pH-dependent solubility, and the centrifugation method to separate the dissolved fraction.

2. Materials and methods

2.1. Mineral aerosol samples

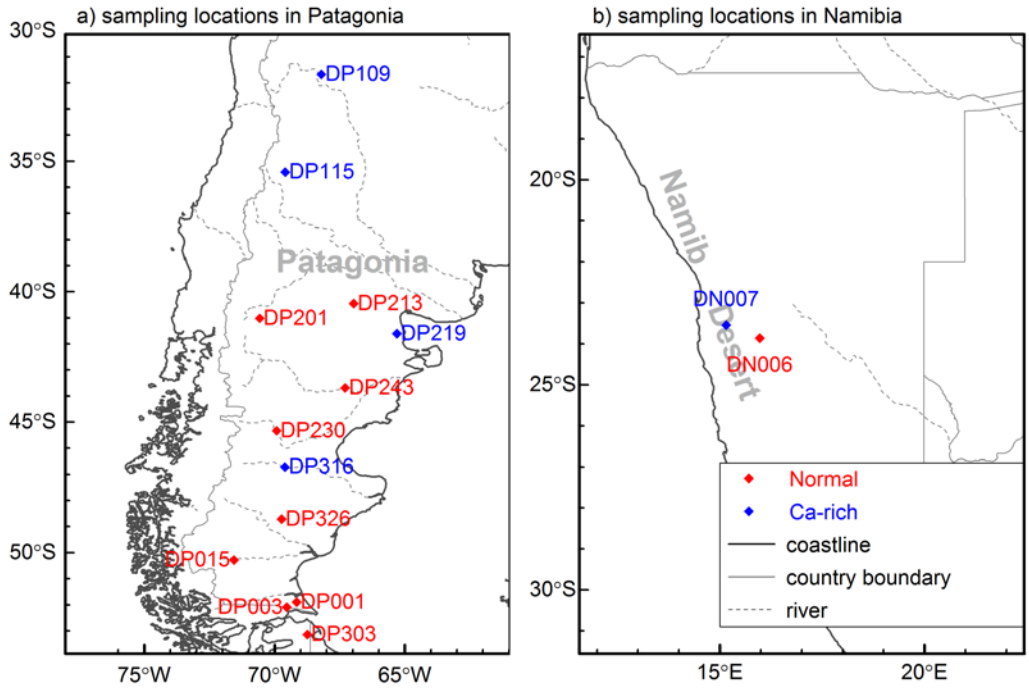

Figure 21 : Sampling locations in a) Patagonia, b) Namibia. Blue points indicate samples highly enriched in Ca. Red points indicate samples not enriched in Ca.

From the year 2011 to 2014, surface soil materials were sampled from Patagonian Desert and Namib Desert. Fifteen mineral aerosol samples (thirteen from Patagonia and two from Namibia, as shown in Figure 21 and Table 11) containing particles less than 12 µm were prepared from their parent soils using a laboratory aerosol generation device SyGAVib (Système de Génération d'Aérosol par Vibration) described in [*Qu et al.*, submitted]. Briefly, during the aerosol generation process, parent soil samples were first mobilized in a vibrating cup fixed on a loudspeaker. Airflow passed over the vibrating cup and carried emitted fine particles upwardly

through a decanter tube. Fine particles with aerodynamic diameter less than 12 μm were collected on a 0.45 μm ultraclean Nuclepore™ polycarbonate filter. A METONE™ laser particle counter estimates the aerosol mass to limit the dust load on the filter less than 2000 μg.

Table 11: Locations of samples, mass of Al and Ca on each filter (unit: ng) and enrichment factor (Ca/Al) relative to Taylor and McLennan [1995].

Ident	Coordinate	Al	Ca	EF(Ca/Al)	dust type
DP001	W69.15, S51.89	83093	15338	0.49	normal
DP003	W69.53, S52.09	298184	69201	0.62	normal
DP015	W71.55, S50.28	5844	1976	0.91	normal
DP109	W68.20, S31.66	771	1262	4.38	Ca-rich
DP115	W69.58, S35.41	16245	22421	3.70	Ca-rich
DP201	W70.57, S41.02	8908	2008	0.60	normal
DP213	W66.96, S40.45	6588	2883	1.17	normal
DP219	W65.30, S41.61	2501	2960	3.17	Ca-rich
DP230	W69.91, S45.33	11245	3763	0.90	normal
DP243	W67.29, S43.68	20494	6278	0.82	normal
DP303	W68.74, S53.14	14343	3779	0.71	normal
DP316	W69.60, S46.71	5403	4769	2.37	Ca-rich
DP326	W69.72, S48.71	12480	2656	0.57	normal
DN006	E15.97, S23.85	20699	8095	1.05	normal
DN007	E15.15, S23.54	8133	24019	7.92	Ca-rich

2.2. Dissolution experiments of aerosol sample

The aerosol sample filter was put in an ultraclean (see supporting information for ultraclean protocol) 50 mL polyethylene graduated conical centrifuge tube to proceed a twelve-step sequential leaching under four pH (pure water, pH5, pH3, pH1) suggested by *Aghnatios et al.* [2014].

Figure 25 (in supporting information) schematizes in detail the twelve-step-leaching experiments. In the first step, 40 mL ultra pure water was added into the 50 mL centrifuge tube. The dust suspension was shaken on a rotating bed (40 rpm) for 10~12 min and then centrifuged for 5 min at 6000 rpm (3984 g). A detail description about the centrifugation is presented in sect. 2.3. The centrifuge tube was taken out from the centrifuge carefully to avoid resuspension of particles. A micropipette was then immediately inserted just below the water surface to sample 10 mL supernatant into a graduated 15 mL ultra-clean polyethylene centrifuge tube. To proceed to the next leaching step, another 10 mL leaching solution was added into the 50 mL

centrifuge tube containing dust suspension. The first three leaching steps used pure water (pH=5.87~6.01) and the following nine steps used diluted Romil-UpA™ nitric acid to obtain leaching solutions with constant or increasing acidity (three steps at pH5, three steps at pH3, and three steps at pH1), providing an ultimate leaching time equaling to one hour at each pH. The repeated leaching under each pH allows a continuous leaching with reduced possibility of saturation and reduces random errors during single dissolution. In the end of dissolution experiment for each filter, thirteen samples (three supernatants for each pH of 7, 5, 3, 1, and one residual suspension) were obtained. For each sampled supernatant, 2 mL of aliquot was set aside to measure pH values (HANNA instruments pH 211 Microprocessor pH Meter) and the rest 8 mL solutions were acidified to approximately pH1 using concentrated Romil-UpA™ ultrapure nitric acid for following elemental analysis. The residual suspensions were dried off by evaporation on a hot plate. The dry residues were then digested for 13 hours in 2 mL mixture of Romil-UpA™ HNO_3:MQ: Merk™ Ultrapur® HF (6:2:1) in completely closed 30 mL Savillex™ PFA vials under 130°C in an air oven [*Heimburger et al.*, 2013]. The vials were then passed to evaporation with 0.5 mL Romil-UpA™ H_2O_2 on a hot plate to complete the oxidation of organic materials and remove HF. Residuals were finally recovered with 1% Romil-UpA™ HNO_3 and were stored in an ultraclean polyethylene bottle. The centrifuge tubes, pipette tips, and the PFA vials were previously cleaned following the ultraclean protocol (supporting information). Two certified reference materials (CRMs) GS-N (from SARM, Nancy, France) and BHVO-1 (from USGS, USA) were subject to the same acid digestion protocol as the residues of leaching experiments to evaluate the accuracy of solid phases analytical method.

To provide comparable results to centrifugation method, the twelve-step sequential leaching were also conducted using filtration separation with polycarbonate membrane (pore size 0.2 μm). The duration of leaching was one minute for each cycle and hence three minutes for each pH for the triplicate leaching. Overall, dissolution experiments were conducted on fifteen dust samples using centrifugation separation and four extra Patagonian dust samples using filtration separation.

2.3. Centrifugation separation of suspension

Suspension of dust was centrifuged in a UNIVERSAL 320 benchtop centrifuge with an angle rotor. When rotation speed of centrifugation is defined, the centrifugation time (s) to separate the particulate fraction (>0.2 μm fraction) was determined using the following equations [*Gimbert et al.*, 2005]:

$$t = \frac{18\eta \ln(R/S)}{\omega^2 d^2 \Delta\rho} \qquad (1)$$

$$\omega = (2\pi/60) \cdot rpm \qquad (2)$$

ω is the angular velocity (rad.s^{-1}) of the rotor;

rpm is the rotational speed (revolutions per minute);

d is the threshold of particle diameter (cm), equal to 2.10^{-5} cm;

$\Delta\rho$ is the difference of density (g.cm^{-3}) between the suspension medium (1.0 g.cm^{-3} for water) and the particles (here we use 2.6 g.cm^{-3});

η is the viscosity of the suspension medium (g.cm^{-1}.s^{-1}), equal 0.01 for water at 20°C;

R is the distance (cm) from the rotation axis to the level from where the supernatant is sampled from the tube;

S is the distance (cm) from rotation axis to the suspension surface.

As indicated in the equation above, the centrifugation separation depends on the particle density. Although particle density (g.cm^{-3}) can vary from 1 for bacterial cells to approximately 6 for particles such as iron oxides, we assume that our dust samples consist of mainly aluminosilicate and the particle density is set to 2.5 [*Hassellöv et al.*, 1999]. According to the equation above, to obtain 10 mL supernatant of <0.2 μm fraction, the centrifugation lasts theoretically 4 minutes if the rotation speed of centrifuge was set at 6000 rpm (3984 g). The centrifugation time was finally set to 5 minutes to settle deeper the particles of 0.2 μm. Figure 22 illustrates the theoretical threshold of particle diameter in sampled supernatant as a function of particle density after 5 minutes centrifugation at 6000 rpm. For particles with a density larger than 2.5 g.cm^{-3}, the centrifugation set up provides a theoretical size threshold less than 0.18 μm. When particle density is smaller than 1.5 g.cm^{-3}, the

cutoff particle diameter in supernatant turns to be quite sensitive to the particle density and can reaches larger than 0.31 µm.

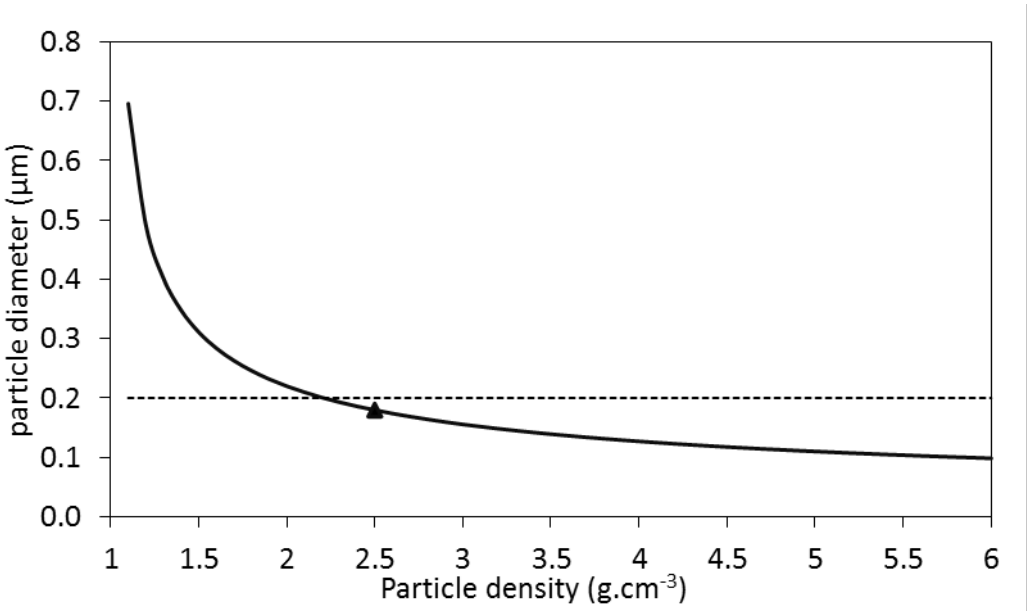

Figure 22 : Threshold of particle diameter in supernatant as a function of particle density after 5 minutes centrifugation at 6000 rpm.

2.4. Chemical analysis

Mass amounts of eleven elements in previously prepared samples were determined by ICP-AES (ARCOS, Spectro/Ametek). The repeatability and stability of the instrument was checked using filtered natural rainwater. Accuracy of elemental analysis was checked using SLRS-5 certified reference material. During the acid digestion, Si is lost under the forms of volatile SiF_4 [*Davy*, 1812; *Jarvis and Jarvis*, 1992]. Hence, mass of Si, and several other elements, collected on each filter were also determined by X-Ray Fluorescence (XRF) prior to the leaching experiments [*Qu et al.*, submitted].

Table 12 presents the analytical results of SLRS-5, as well as the results of GS-N and BHVO-1 that have underwent acid digestion (sect. 2.2). The repeatability of the ICP-AES measurement was about 0.5%. The recovery rates for elements in SLRS-5 were between 90 and 115% except for Mn (119%) and K (130%). For the digested geostandard, the recovery rates were found between 90 and 110% except for l in GS-N (66%), Ca in GS-N (71%), Mn in BHVO-1 (125%), and K in BHVO-1

(126%) and GS-N (115%). Measurement of Si by XRF is validated using GS-N (recovery rate=100%) and SDC-1 (recovery rate=101%).

Table 12: Repeatability (RSD), detection limit (DL), and analytical results of CRMs

	DL	RSD	measured values (μg/L)			certified values (μg/L)			recovery rate (%)		
	(ppb)	(%)	SLRS-5	BHVO-1	GS-N	SLRS-5	BHVO	GS-N	SLRS-5	BHVO-1	GS-N
Al	0.27	6.8	56	65445	50980	50	73035	77640	113	90	66
Ba	0.02	4.9	16	138	1428	14	139	1400	112	99	102
Ca	0.28	6.7	11774	77129	12632	10500	81475	17867	112	95	71
Fe	0.30	4.3	97	86272	24536	91.2	85542	26229	106	101	94
K	0.08	5.3	1090	5443	44325	839	4317	38436	130	126	115
Mg	0.35	8.7	2677	40427	13579	2540	43601	13870	105	93	98
Mn	0.01	4.9	5.1	1340	418	4.33	1074	379	119	125	110
Si	2.48	2.4	1899	-	-	1880	-	-	101	-	-
Sr	0.01	6.6	58	397	573	53.6	403	570	108	98	101
Ti	0.08	3.9	2.2	16943	4166	2.2	16246	4076	99	104	102
Zn	0.06	2.1	1.0	112	48	0.85	105	48	115	107	100

The fractional solubility of each element X was calculated following the Eq. 3:

$$\%DX = DX/TX \times 100\% \quad (3)$$

where %DX is the solubility of X, DX denotes the dissolved mass of X, and TX denotes the total mass of X. For each leaching step, a differential solubility and a cumulative solubility were calculated. The former one consider uniquely the mass released in the present leaching step, and the later one is the cumulative sum of previous dissolution steps and the present leaching step.

3. Results and discussion

As mentioned previously, several studies found that, compared to centrifugation method, the filtration separation underestimates the amount of materials in dissolved fraction. In this section, we will firstly compare the solubility values obtained by the two separation methods. Then we will focus on the solubility measured by centrifugation method and discuss the dissolution behaviors of mineral aerosols produced from Patagonian and Namibian soils.

Among the fifteen samples, the sample DP219 is suspected to be contaminated in Ca, according to the analytical results of XRF analysis and ICP analysis, and hence was excluded in the following statistics and discussions.

3.1. Comparison of solubility values between centrifugation and filtration

Table 13: Cumulative solubility (geomean ± SD; unit: %) under decreasing pH with centrifugation method (n=14) and filtration method (n=4)

	Centrifugation				Filtration			
	pure water	pH5	pH3	pH1	pure water	pH5	pH3	pH1
Fe	2.6±1.0	3.6±1.2	4.5±1.4	6.7±1.8	0.03±0.01	0.04±0.01	0.2±0.1	1.3±0.2
Al	2.8±1.0	3.9±1.2	5.6±1.6	9.0±2.4	<0.17	<0.34	0.4±0.3	5.1±0.4
Ti	1.5±0.5	1.7±0.6	1.9±0.7	2.8±0.9	<0.82	<0.93	<1.51	<2.08
Zn	5.8±2.4	8.9±3.0	15.3±6.2	26±8	12±5	15±7	10±7	16±7
Ca	21±11	29±12	39±14	44±15	14±2	29±3	50±4	53±4
K	8.0±3.2	9.4±3.6	12±4	15±5	13±7	16±9	21±12	26±14
Mg	10±4	13±4	16±5	17±5	9.0±1.5	13±2	16±2	18±2
Mn	17±7	22±9	28 ±10	30±11	5±1	10±2	15±2	18±2
Sr	11±8	15±9	21±10	22±11	3.9±1.2	5.7±1.3	6.6±2.2	6.6±2.2
Ba	6.8±2.4	6.8±4.0	15±6	19±7	2.3	3.8±0.5	9.9±1.6	14±2

Table 13 presents the geometric mean cumulative solubility of eleven elements obtained by centrifugation separation (fourteen dust filters) and by filtration separation (four dust filters). Comparing to filtration run, centrifugation run obtained noticeably much higher solubility of Al and Fe. Geometric mean iron solubility (geomean ± SD) increased from 2.6 ± 1.0% in pure water to 6.7 ± 1.8% at pH1 in centrifugation run, and from 0.03 ± 0.01% to 1.3 ± 0.2% in filtration run. Similarly, when pH decreased from pure water to pH1, aluminum solubility increased from 2.8 ± 1.0% to 9.0 ± 2.4% in centrifugation run, and from <0.17% to 5.1 ± 0.4% in filtration run. More acidic conditions result in higher solubility in centrifugation run and less remarkable differences between the solubility values of two separations.

On the other side, in centrifugation run and filtration run, Ca solubility was 21 ± 11% and 14 ± 2% in pure water, 29 ± 12% and 29 ± 3% at pH5, 39 ± 14% and 50 ± 4% at pH3, 44 ± 15% and 53 ± 4% at pH1, respectively. Potassium showed even higher solubility in filtration run than in centrifugation run. Discrepancy of elemental solubility obtained by the two separations varies with elements. Elements that are more soluble, such as Ca, Mg and K, tend to show less difference between solubility values obtained by the two separation methods.

In the contents below, we tried to uncover the potential reasons leading to the remarkable different values of iron and aluminum solubility between the two separations. An evident shortness of the comparison experiments is the much longer duration of leaching in centrifugation than in filtration. The total leaching time at each

pH was 60 min for centrifugation runs and 3 min for filtration runs. Hence, we first assess the difference of Fe (and Al) solubility values contributed by leaching duration. According to the study of dissolution kinetics carried out by *Desboeufs et al.* [1999] on loess sample (diameter <20 μm) from Cape Verde, the Fe solubility measured at pH5 after 60 min dissolution was 5 times larger than three-minute dissolution. *Aguilar-Islas et al.* [2010] found a factor less than two between dissolutions shorter than 1 min and dissolutions lasting 90 min in ultrapure water. In our study, the leaching duration might explain the less remarkable different solubility measured at pH1 between centrifugation and filtration. However, in pure water, leaches of pH5 and pH3, centrifugation separation obtained Fe solubility extremely larger than filtration separation. The duration of leaching contributed little to the highly different solubility in solutions at high pH.

Besides the different leaching time, the remarkable different solubility of Fe and Al between the two separation methods could be related to the two following occasions: (1) experimental bias in centrifugation; (2) artefact of membrane in filtration method.

(1) *Experimental bias in centrifugation*

The much higher solubility of iron and aluminum obtained by the centrifugation run suggests a higher concentration of Fe- and Al-containing materials in supernatants compared to concentrations measured in the filtrate recovered in the filtration run.

During the centrifugation process, lighter particles exhibiting larger cutoff sizes and particles less dense than water can even float on the surface of suspension, which increase ultimately the measured solubility for elements contained in light particles. For example, the existence of lighter particles such as organic particles (approximately 1.5 $g.cm^{-3}$) in the dust samples can lead to higher measured solubility of Fe in centrifugation separation if iron is contained in these particles. On the contrary, some particles such as iron oxide, have higher density (> 5 $g.cm^{-3}$), which will result in a lower cutoff size for these particles and decreases the measured solubility in centrifugation run. Hence, with respect to cutoff size of centrifugation,

variability of particle density in dust samples can introduce bias of measured solubility.

Larger particles (>0.2 μm) could also exist in supernatant due to the resuspension of particles after the centrifugation and before the supernatant sampling, which might result in higher measured solubility. In the twelve-step leaching for fourteen dust samples, large proportion of dissolved iron was released in the first leaching step in pure water for all dust samples. However, resuspension of particles should be unpredictable throughout the sequential leaching experiments. Considering the number of dust samples we have tested, resuspension of particles could not explain the high proportion of dissolved iron in pure water. Nevertheless, the size distribution and the elemental composition of particulate materials in the supernatant should be investigated in further studies.

(2) *Artefact of membrane in filtration method*

Buffle and Leppard [1995b] indicate that adsorption of colloids on the membrane and self-coagulations of colloids during filtration process reduce the amount of materials passing through the membrane. *Gimbert et al.* [2005] found that the filtration technique recovers less colloidal materials than the centrifugation method. *Zirkler et al.* [2012] demonstrated that filtration preferentially underestimates the amounts of mineral colloids and colloid-bound elements in suspension. Hence, retention of Fe- and Al-containing colloids could be a potential reason resulting in the discrepancy of iron and aluminum solubility between the two separation methods. Moreover, more acidic conditions dissolve iron in the colloids and thus convert more iron into dissolved phase [*Shi et al.*, 2015], which could explain the smaller differences of measured iron solubility between the two separation methods in the case of the most acidic leaching. In addition, the two separation methods give similar Ca solubility. Since Ca-containing materials are more soluble than Fe-containing materials, the proportion of Ca in colloidal particles is smaller and the two types of separation affect less the Ca in soluble phase. Hence, less difference occurs between the two separation methods.

According to the discussion above, the existence of light Fe- and Al-containing particles in supernatant and the underestimation of colloidal materials by

filtration method due to the artefact of the membrane are the most likely reasons resulting in relatively higher solubility obtained with the centrifugation method for the fourteen dust samples. Although the reasons leading to the different measured solubility of Fe and Al remain uncertain, these preliminary results showed that the choice of the separation method has a significant impact on the solubility measurement.

3.2. Variation of solubility with elements and its dependence on pH

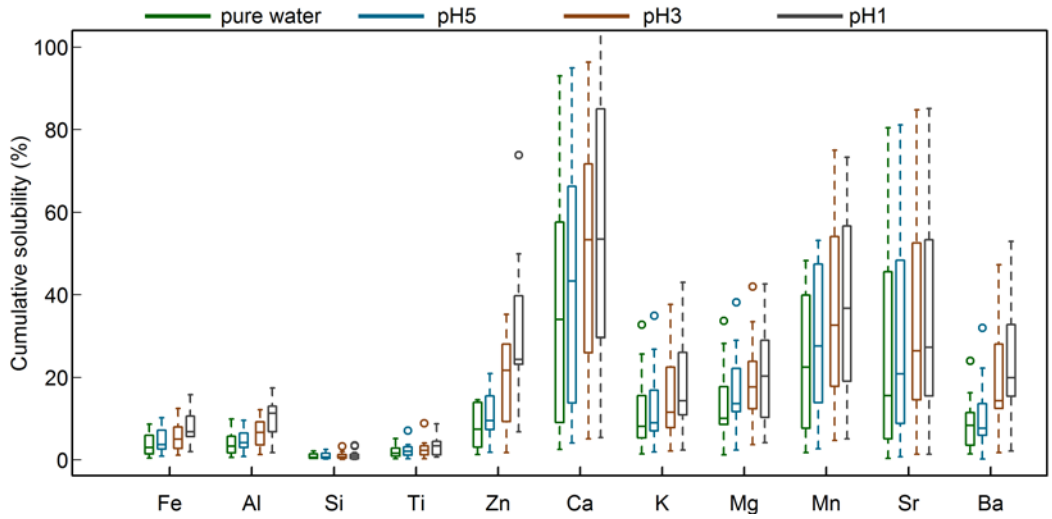

Figure 23 : Boxplot of cumulative solubility under decreasing pH of eleven elements for fourteen samples (two Namibian dust samples and twelve Patagonian dust samples). The bottom and top of the box presents the lower quartiles (Q1) and upper quartiles (Q3), and the band inside the box is the median value. Lines extending vertically from the boxes indicate observations within one and a half times the interquartile range (IQR) of the upper and lower quartiles. Individual circles outside the box are outliers that fall below Q1-1.5×IQR or above Q3+1.5×IQR.

Figure 23 and Table 14 (Supporting information) present the descriptive statistics of elemental solubility at four pH values for the fourteen dust samples in centrifugation run. In pure water, solubility of Fe ranged from 0.4% to 8.6%, with geometric mean solubility of 2.6 ± 1.0% (geomean ± SD). When pH decreased to 5, 3, and 1, iron solubility increased respectively to 0.8~10% (3.6 ± 1.2%), 1.1~12% (4.5 ± 1.4%), and 2.0~16% (6.7 ± 1.8%). Iron showed higher solubility in lower pH due to the higher chemical strength of more acidic leaching. In previous studies, *Aghnatios et al.* [2014] observed an iron solubility equaling to 0.04% in pure water for fine Tunisian alluvial soil, which increased to 0.07%, 0.26%, and 0.93% when pH decreased from to pH5, pH3, and pH1, respectively. *Spokes and Jickells* [1995]

studied the Saharan derived aerosol and obtained Fe solubility of 4.7 ± 0.2% at pH2 and a much lower solubility equaling to 0.3% when pH increased to 5.5.

Compared to Fe, Al (geomean: 2.8% in pure water, 3.9% at pH5, 5.6% at pH3, and 9.0% at pH1) showed slightly higher solubility, and Si and Ti showed lower solubility. While elements namely Zn, Ca, K, Mg, Mn, Sr and Ba show much higher solubility than Fe. Slightly higher solubility of Al and greatly higher solubility of Mn relative to Fe are consistent with previous observations of *Baker et al.* [2006b] (Fe: from 1.4% to 4.1%; Al: from 1.9% to 5.5%; Mn: from 50% to 64%) and *Spokes and Jickells* [1995] (Fe: 0.1% at pH8, 4.7% at pH2); Al: 0.4% at pH8, 7.1% at pH2; and Mn: 7.5% at pH8, 54 % at pH2).

Elements also showed different variation pattern of solubility when pH decreases. For example, iron and calcium showed quite different variation pattern of solubility for the two dust samples produced from the Namibian soils. In leaches of pure water, pH5, pH3 and pH1, the cumulative Ca solubility was 58%, 66%, 72% and 72%, respectively, for dust sample DN006, versus 93%, 95%, 96% and 96%, respectively, for another sample DN007. The corresponding iron solubility was 3.1%, 3.8%, 4.5% and 8.4%, versus 7.0%, 7.2%, 7.4% and 11.4%. Most of Ca were released in pure water and in leaches of pH5, whereas iron showed significant increase of solubility when pH decreased from 3 to 1. This observation is in agreement with the requirement of stronger chemical strength to dissolve iron-containing minerals compared to Ca-containing materials. Aluminum also showed similar variation pattern to iron.

3.3. Dependence of solubility on types of dust sample

Shi et al. [2011] indicated that the nature of dust might affect elemental solubility. *Krueger et al.* [2004] and *Aghnatios et al.* [2014] demonstrated that calcium-containing materials such as carbonate influence significantly the dissolution behavior of mineral particles. Particularly, *Aghnatios et al.* [2014] found higher solubility and similar dissolution behavior in sequential leachings for elements including Ba, Ca, K, Mn, Na and Sr in calcium-rich soil in Tunisia. Based on the analytical result of ICP-AES in dissolution experiments, we calculated enrichment factor (EF) of Ca relative to Al (reference element) and upper continental crust (UCC)

composition in *Taylor and McLennan* [1995] (reference material) following the equation below [*Lawson and Winchester*, 1979]:

$$EF\left(Ca/Al\right)=\left(Ca/Al\right)_{dust}/\left(Ca/Al\right)_{ref} \quad (4)$$

Calculated EF(Ca/Al) were presented in Table 11. The fourteen dust samples were thus regrouped into two classes and shown with different colors in Figure 21: normal dust, which contains ten dust samples; Ca-rich dust including DP109, DP115, DP316, and DN007.

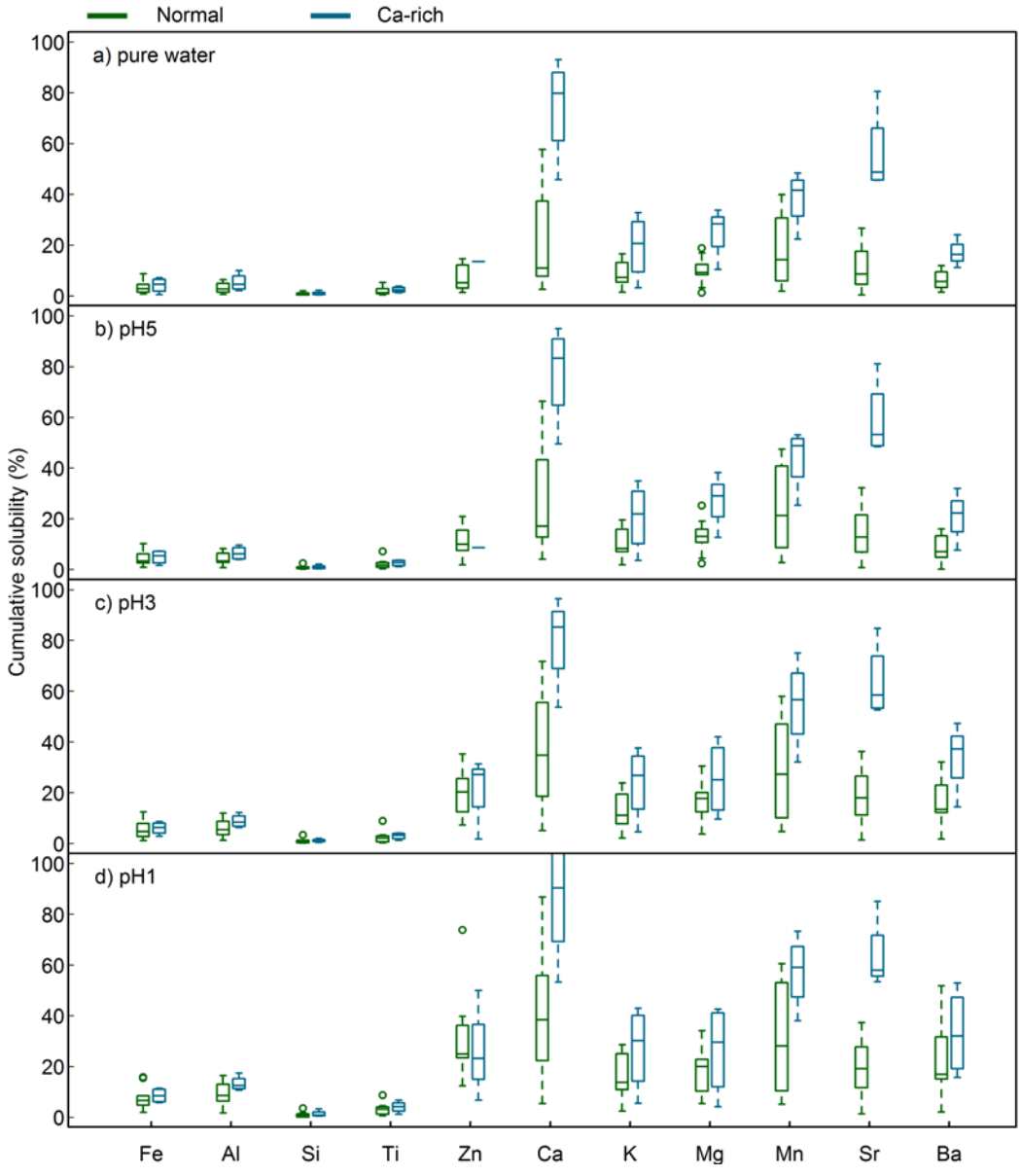

Figure 24 : Variation of solubility for normal dust (n=10) and Ca-rich dust (n=4) at different pH: a) pure water, b) pH5, c) pH3, d) pH1.

The variation of solubility as a function of dust type at each pH is displayed in Figure 24. As mentioned above, a large proportion of Ca was already dissolved in pure water and pH5. Compared to normal dust samples, Ca-rich samples showed noticeably higher solubility for those more soluble elements namely Ca, K, Mg, Mn, Sr and Ba (referred to hereafter Ca-group). Elements namely Fe, Al, Si, Ti and Zn (referred to hereafter Fe-group) were not affected by the concentration of Ca in dust samples.

Higher solubility and similar dissolution behavior for elements of Ca-group in Ca-rich dust agree well with previous observation of *Aghnatios et al.* [2014] and are supposed to due to the higher proportion of calcium-containing minerals such as calcite ($CaCO_3$) and dolomite ($CaMg(CO_3)_2$) [*Aghnatios et al.*, 2014]. *Krueger et al.* [2004] indicated that calcium carbonates dissolve largely around pH5, resulting in a higher solubility of Ca in our study. The similar dissolution behavior of Ba, K, Mn, Na, and Sr implicates a strong link or similar mineralogical form of these elements to Ca-containing minerals [*Aghnatios et al.*, 2014]. For example, barium carbonate such as witherite ($BaCO_3$) has similar dissolution rate to calcite [*Chou et al.*, 1989]. Mg can also exist as carbonate minerals such as magnesite ($MgCO_3$). *Chou et al.* [1989] indicated that the dissolution rate of magnesite is approximately four orders of magnitude lower than calcite, which might partly explain the less significant difference of Mg solubility between Ca-rich dust and normal dust. *Moreno et al.* [2006] found a close relationship between Sr and Ca in Saharan dust. Consequently, dust containing more carbonate calcium should exhibit higher solubility for elements in Ca-group than dust containing more magnesite. *Fujiwara* [1964] indicated that free and coagulated Mn^{2+} randomly distributes in calcium carbonate. Thus, the dissolution of carbonate increases simultaneously the solubility of Ca, Sr, Ba, Mg and Mn. In normal dust samples, less carbonate exists and Ca-group elements mostly present in less soluble mineralogical form such as aluminosilicate (e.g. $CaAl_2Si_2O_8$, $SrAl_2Si_2O_8$, $BaAl_2Si_2O_8$). Smaller proportion of more soluble carbonate results in finally lower fractional solubility for the elements in Ca-group.

The presence of carbonate also affects the pH of leaching solution, particularly pure water (pH=5.87~6.01), due to the neutralization by calcium carbonate. After the first leaching in pure water, pH of two samples among the fourteen dust samples,

DP115 and DN007, increased significantly to 6.4 and 6.7, respectively. DP115 (EF(Ca/Al)=3.7, m(Ca)=22421 ng) and DN007 (EF(Ca/Al)=7.92, m(Ca)=24019 ng) are rich in Ca, leading to an increase of pH in pure water. The rest two Ca-rich dust samples DP109 (EF(Ca/Al)=4.38, m(Ca)=1262 ng) and DP316 (EF(Ca/Al)=2.37, m(Ca)=4769 ng) obtained a pH value equaling to 5.6 and 5.4, respectively. Although the latter two samples are also rich in Ca, amount of Ca in these samples are too small to change significantly the pH of leaching solutions.

Although Ca content does not affect solubility of elements in Fe-group, elemental solubility differs with samples due to other types of minerals. As indicated by *Journet et al.* [2008], iron solubility varies with mineral types and iron in clay minerals is generally more soluble than iron in (hydr-)oxide. Hence, further determination of mineralogical composition is necessary to better understand the differences of elemental solubility with dust samples.

4. Conclusion

The present work investigated the elemental solubility of laboratory-produced Patagonian and Namibian dust using sequential leaching in pure water and at pH 5, 3 and 1. Dissolved fraction, operationally defined as <0.2 μm fraction, was separated by centrifugation method. Geometric mean of iron solubility was 2.6% in pure water, 3.6% at pH5, 4.5% at pH3, and 6.7% at pH1. Solubility of Al, Si, Ti, Ba, Ca, Mn, P, Sr and Zn were also determined. Solubility of elements increases with decreasing pH. Most of calcium was dissolved in first leaches in pure water and pH5, while Fe and Al showed significant increase of solubility when pH decreased from 3 to 1.

Calcium-rich dust, probably due to the presence of carbonate, showed higher solubility and similar dissolution behavior for Ca, K, Mg, Mn, Sr and Ba. Solubility of less soluble elements namely Al, Fe and Si was not affected by the proportion of calcium content and hence no significant difference of solubility was observed between normal dust and Ca-rich dust.

Method separating dissolved fraction from particulate fraction affects significantly the solubility measured. Compared to solubility determined by filtration, solubility of Fe and Al obtained with centrifugation method in this work showed

much higher solubility values in pure water and leaches of pH5. Less difference was found for more soluble elements such as Ca, K, Mg, Mn, Ba and Sr. Retention of colloids on the membrane in filtration method is suspected to be a major reason leading to the different solubility between two separation methods. Stronger dissolution of colloids in more acidic leaches reduced the difference of solubility at pH3 and pH1 between centrifugation method and filtration method.

5. Prospect

The impact of separation method on solubility measurements have emerged and grown to ask multiple questions about the relevance of centrifugal separation to the bioavailability evaluation and artefacts including experimental bias that could affect the solubility measurement when using filtration or centrifugation respectively. Further studies are strongly required to investigate the effectiveness of the two separation methods.

Experimental bias associated with particle density is also suspectable reasons resulting in the higher measured solubility in centrifugation run. In further studies aiming to compare the two separation methods for elemental solubility measurements, the size distribution of materials in filtrates (in filtration) and centrifugates (in centrifugation) should be verified. Observation by scanning electron microscope of membrane (in filtration) is also needed to study the artefact of membrane in filtration method. Since the cutoff size of particles could be adjusted depending on requirements, it is possible to investigate the fractional solubility as a function of cutoff size and find finally a more appropriate cutoff size to evaluate the bioavailability of dust.

Acknowledgements

This work is financed by the CNRS INSU LEFE/CHAT program DFP and the Franco-Argentina ECOS program. Descriptive statistics of cumulative solubility and the schema of dissolution protocol are provided in the supporting information.

References List

Achilles, K. M., T. M. Church, S. W. Wilhelm, G. I. I. I. W. Luther, and D. A. Hutchins (2003), Bioavailability of iron to Trichodesmium colonies in the western subtropical Atlantic Ocean, *Limnology and Oceanography*, *48*(6), 2250-2255, doi:10.4319/lo.2003.48.6.2250.

Aghnatios, C., R. Losno, and F. Dulac (2014), A fine fraction of soil used as an aerosol analogue during the DUNE experiment: sequential solubility in water, decreasing pH step-by-step, *Biogeosciences*, *11*(17), 4627-4633, doi:10.5194/bg-11-4627-2014.

Aguilar-Islas, A. M., J. F. Wu, R. Rember, A. M. Johansen, and L. M. Shank (2010), Dissolution of aerosol-derived iron in seawater: Leach solution chemistry, aerosol type, and colloidal iron fraction, *Marine Chemistry*, *120*(1-4), 25-33, doi:10.1016/j.marchem.2009.01.011.

Alfaro, S. C., A. Gaudichet, L. Gomes, and M. Maillé (1997), Modeling the size distribution of a soil aerosol produced by sandblasting, *Journal of Geophysical Research: Atmospheres*, *102*, 11239-11249, doi:10.1029/97JD00403.

Baker, A. R., M. French, and K. L. Linge (2006a), Trends in aerosol nutrient solubility along a west-east transect of the Saharan dust plume, *Geophysical Research Letters*, *33*(7), doi:10.1029/2005gl024764.

Baker, A. R., T. D. Jickells, M. Witt, and K. L. Linge (2006b), Trends in the solubility of iron, aluminium, manganese and phosphorus in aerosol collected over the Atlantic Ocean, *Marine Chemistry*, *98*(1), 43-58, doi:10.1016/j.marchem.2005.06.004.

Bergquist, B. A., J. Wu, and E. A. Boyle (2007), Variability in oceanic dissolved iron is dominated by the colloidal fraction, *Geochimica et Cosmochimica Acta*, *71*(12), 2960-2974, doi:10.1016/j.gca.2007.03.013.

Bonnet, S., and C. Guieu (2004), Dissolution of atmospheric iron in seawater, *Geophysical Research Letters*, *31*(3), doi:10.1029/2003gl018423.

Boyd, P. W., et al. (2007), Mesoscale Iron Enrichment Experiments 1993-2005: Synthesis and Future Directions, *Science*, *315*, 612-617, doi:10.1126/science.1131669.

Buck, C. S., W. M. Landing, and J. Resing (2013), Pacific Ocean aerosols: Deposition and solubility of iron, aluminum, and other trace elements, *Marine Chemistry*, *157*(0), 117-130, doi:10.1016/j.marchem.2013.09.005.

Buffle, J., and G. G. Leppard (1995a), CHARACTERIZATION OF AQUATIC COLLOIDS AND MACROMOLECULES .2. KEY ROLE OF PHYSICAL STRUCTURES ON ANALYTICAL RESULTS, *Environmental Science & Technology*, *29*(9), 2176-2184, doi:10.1021/es00009a005.

Buffle, J., and G. G. Leppard (1995b), Characterization of Aquatic Colloids and Macromolecules. 1. Structure and Behavior of Colloidal Material, *Environmental Science & Technology*, *29*(9), 2169-2175, doi:10.1021/es00009a004.

Castilho, P. D., R. van Faassen, and R. Moerman (1996), Differences between super-centrifuged and membrane-filtrated soil solutions obtained from bulked and non-bulked topsoils by soil centrifugation, *Fresenius J Anal Chem*, *354*(5-6), 756-759, doi:10.1007/s0021663540756.

Chou, L., R. M. Garrels, and R. Wollast (1989), Comparative study of the kinetics and mechanisms of dissolution of carbonate minerals, *Chemical Geology*, *78*(3–4), 269-282, doi:10.1016/0009-2541(89)90063-6.

Coale, K. H. (1991), Effects of Iron, Manganese, Copper, and Zinc Enrichments on Productivity and Biomass in the Subarctic Pacific, *Limnology and Oceanography*, *36*(8), 1851-1864, doi:10.2307/2837719.

Cullen, J. T., B. A. Bergquist, and J. W. Moffett (2006), Thermodynamic characterization of the partitioning of iron between soluble and colloidal species in the Atlantic Ocean, *Marine Chemistry*, *98*(2–4), 295-303, doi:10.1016/j.marchem.2005.10.007.

Cwiertny, D. M., J. Baltrusaitis, G. J. Hunter, A. Laskin, M. M. Scherer, and V. H. Grassian (2008), Characterization and acid-mobilization study of iron-containing mineral dust source materials, *Journal of Geophysical Research: Atmospheres*, *113*, n/a–n/a, doi:10.1029/2007JD009332.

Davy, J. (1812), An Account of Some Experiments on Different Combinations of Fluoric Acid, *Philosophical Transactions of the Royal Society of London*, *102*, 352-369, doi:10.2307/107324.

Desboeufs, K. V., R. Losno, and J. L. Colin (2001), Factors influencing aerosol solubility during cloud processes, *Atmospheric Environment*, *35*(20), 3529-3537, doi:10.1016/S1352-2310(00)00472-6.

Desboeufs, K. V., R. Losno, F. Vimeux, and S. Cholbi (1999), The pH-dependent dissolution of wind-transported Saharan dust, *Journal of Geophysical Research: Atmospheres*, *104*(D17), 21287-21299, doi:10.1029/1999JD900236.

Desboeufs, K. V., A. Sofikitis, R. Losno, J. L. Colin, and P. Ausset (2005), Dissolution and solubility of trace metals from natural and anthropogenic aerosol particulate matter, *Chemosphere*, *58*(2), 195-203, doi:10.1016/j.chemosphere.2004.02.025.

Duce, R. A., et al. (1991), The atmospheric input of trace species to the world ocean, *Global Biogeochemical Cycles*, *5*(3), 193-259, doi:10.1029/91GB01778.

Duce, R. A., and N. W. Tindale (1991), Atmospheric transport of iron and its deposition in the ocean, *Limnology and Oceanography*, *36*(8), 1715-1726, doi:10.4319/lo.1991.36.8.1715.

Edwards, R., and P. Sedwick (2001), Iron in East Antarctic snow: Implications for atmospheric iron deposition and algal production in Antarctic waters, *Geophysical Research Letters*, *28*(20), 3907-3910, doi:10.1029/2001gl012867.

Fitzsimmons, J. N., and E. A. Boyle (2014), Both soluble and colloidal iron phases control dissolved iron variability in the tropical North Atlantic Ocean, *Geochimica et Cosmochimica Acta*, *125*(0), 539-550, doi:10.1016/j.gca.2013.10.032.

Fujiwara, S. (1964), Investigation of Trace Impurities in Solids by Electron Paramagnetic Resonance. Distribution of Manganese in Calcium Carbonate, *Analytical Chemistry*, *36*(12), 2259-2261, doi:10.1021/ac60218a012.

Gierlus, K. M., O. Laskina, T. L. Abernathy, and V. H. Grassian (2012), Laboratory study of the effect of oxalic acid on the cloud condensation nuclei activity of mineral dust aerosol, *Atmospheric Environment*, *46*, 125-130, doi:10.1016/j.atmosenv.2011.10.027.

Gimbert, L. J., P. M. Haygarth, R. Beckett, and P. J. Worsfold (2005), Comparison of Centrifugation and Filtration Techniques for the Size Fractionation of Colloidal Material in Soil Suspensions Using Sedimentation Field-Flow Fractionation, *Environmental Science & Technology*, *39*(6), 1731-1735, doi:10.1021/es049230u.

Gleyzes, C., S. Tellier, and M. Astruc (2002), Fractionation studies of trace elements in contaminated soils and sediments: a review of sequential extraction procedures, *TrAC Trends in Analytical Chemistry*, *21*(6–7), 451-467, doi:10.1016/S0165-9936(02)00603-9.

Gomes, L., G. Bergametti, G. Coudé-Gaussen, and P. Rognon (1990), Submicron desert dusts: A sandblasting process, *Journal of Geophysical Research: Atmospheres*, *95*, 13927-13935, doi:10.1029/JD095iD09p13927.

Hassellöv, M., B. Lyvén, and R. Beckett (1999), Sedimentation Field-Flow Fractionation Coupled Online to Inductively Coupled Plasma Mass SpectrometryNew Possibilities for Studies of Trace Metal Adsorption onto Natural Colloids, *Environmental Science & Technology*, *33*(24), 4528-4531, doi:10.1021/es981334f.

Heimburger, A., R. Losno, and S. Triquet (2013), Solubility of iron and other trace elements in rainwater collected on the Kerguelen Islands (South Indian Ocean), *Biogeosciences*, *10*(10), 6617-6628, doi:10.5194/bg-10-6617-2013.

Hsu, S.-C., et al. (2010), Effects of acidic processing, transport history, and dust and sea salt loadings on the dissolution of iron from Asian dust, *Journal of Geophysical Research: Atmospheres*, *115*, doi:10.1029/2009JD013442.

Jarvis, I., and K. E. Jarvis (1992), Plasma spectrometry in the earth sciences: techniques, applications and future trends, *Chemical Geology*, *95*(1–2), 1-33, doi:10.1016/0009-2541(92)90041-3.

Journet, E., K. V. Desboeufs, S. Caquineau, and J.-L. Colin (2008), Mineralogy as a critical factor of dust iron solubility, *Geophysical Research Letters*, *35*(7), L07805, doi:10.1029/2007GL031589.

Krueger, B. J., V. H. Grassian, J. P. Cowin, and A. Laskin (2004), Heterogeneous chemistry of individual mineral dust particles from different dust source regions: the importance of particle mineralogy, *Atmospheric Environment*, *38*, 6253-6261, doi:10.1016/j.atmosenv.2004.07.010.

Lawson, D. R., and J. W. Winchester (1979), A standard crustal aerosol as a reference for elemental enrichment factors, *Atmospheric Environment (1967)*, *13*(7), 925-930, doi:10.1016/0004-6981(79)90003-9.

Li, F., P. Ginoux, and V. Ramaswamy (2008), Distribution, transport, and deposition of mineral dust in the Southern Ocean and Antarctica: Contribution of major sources, *Journal of Geophysical Research: Atmospheres*, *113*, doi:10.1029/2007JD009190.

Losno, R., G. Bergametti, P. Carlier, and G. Mouvier (1991), Major ions in marine rainwater with attention to sources of alkaline and acidic species, *Atmospheric Environment. Part A. General Topics*, *25*(3–4), 763-770, doi:10.1016/0960-1686(91)90074-H.

Mahowald, N., S. Albani, J. F. Kok, S. Engelstaeder, R. Scanza, D. S. Ward, and M. G. Flanner (2014), The size distribution of desert dust aerosols and its impact on the Earth system, *Aeolian Research*, *15*(0), 53-71, doi:10.1016/j.aeolia.2013.09.002.

Maring, H. B., and R. A. Duce (1987), The impact of atmospheric aerosols on trace metal chemistry in open ocean surface seawater, 1. Aluminum, *Earth and Planetary Science Letters*, *84*(4), 381-392, doi:10.1016/0012-821X(87)90003-3.

Martin, J. H., S. E. Fitzwater, and R. M. Gordon (1990), Iron deficiency limits phytoplankton growth in Antarctic waters, *Global Biogeochemical Cycles*, *4*(1), 5-12, doi:10.1029/GB004i001p00005.

Meskhidze, N., W. L. Chameides, A. Nenes, and G. Chen (2003), Iron mobilization in mineral dust: Can anthropogenic SO2 emissions affect ocean productivity?, *Geophysical Research Letters*, *30*(21), doi:10.1029/2003GL018035.

Moore, J. K., S. C. Doney, D. M. Glover, and I. Y. Fung (2001), Iron cycling and nutrient-limitation patterns in surface waters of the World Ocean, *Deep Sea Research Part II: Topical Studies in Oceanography*, *49*(1–3), 463-507, doi: 10.1016/S0967-0645(01)00109-6.

Moreno, T., X. Querol, S. Castillo, A. Alastuey, E. Cuevas, L. Herrmann, M. Mounkaila, J. Elvira, and W. Gibbons (2006), Geochemical variations in aeolian mineral particles from the Sahara–Sahel Dust Corridor, *Chemosphere*, *65*, 261-270, doi:10.1016/j.chemosphere.2006.02.052.

Morrison, M. A., and G. Benoit (2001), Filtration Artifacts Caused by Overloading Membrane Filters, *Environmental Science & Technology*, *35*(18), 3774-3779, doi:10.1021/es010670k.

Paris, R., K. V. Desboeufs, and E. Journet (2011), Variability of dust iron solubility in atmospheric waters: Investigation of the role of oxalate organic complexation, *Atmospheric Environment*, 45(36), 6510-6517, doi:10.1016/j.atmosenv.2011.08.068.

Paris, R., and K. V. Desboeufs (2013), Effect of atmospheric organic complexation on iron-bearing dust solubility, *Atmos. Chem. Phys.*, *13*(9), 4895-4905, doi:10.5194/acp-13-4895-2013.

Schmidt, M. A., and D. A. Hutchins (1999), Size-fractionated biological iron and carbon uptake along a coastal to offshore transect in the NE Pacific, *Deep Sea Research Part II: Topical Studies in Oceanography*, *46*(11–12), 2487-2503, doi:http://dx.doi.org/10.1016/S0967-0645(99)00073-9.

Schulz, M., et al. (2012), Atmospheric Transport and Deposition of Mineral Dust to the Ocean: Implications for Research Needs, *Environmental Science & Technology*, *46*, 10390-10404, doi:10.1021/es300073u.

Sedwick, P. N., E. R. Sholkovitz, and T. M. Church (2007), Impact of anthropogenic combustion emissions on the fractional solubility of aerosol iron: Evidence from the Sargasso Sea, *Geochemistry Geophysics Geosystems*, *8*, doi:10.1029/2007gc001586.

Shi, Z., et al. (2011), Influence of chemical weathering and aging of iron oxides on the potential iron solubility of Saharan dust during simulated atmospheric processing, *Global Biogeochemical Cycles*, *25*(2), doi:10.1029/2010GB003837.

Shi, Z., M. D. Krom, T. D. Jickells, S. Bonneville, K. S. Carslaw, N. Mihalopoulos, A. R. Baker, and L. G. Benning (2012), Impacts on iron solubility in the mineral dust by

processes in the source region and the atmosphere: A review, *Aeolian Research*, *5*, 21-42, doi:10.1016/j.aeolia.2012.03.001.

Shi, Z., M. D. Krom, S. Bonneville, and L. G. Benning (2015), Atmospheric Processing Outside Clouds Increases Soluble Iron in Mineral Dust, *Environmental Science & Technology*, *49*(3), 1472-1477, doi:10.1021/es504623x.

Spokes, L. J., and T. D. Jickells (1995), Factors controlling the solubility of aerosol trace metals in the atmosphere and on mixing into seawater, *Aquatic Geochemistry*, *1*, 355-374, doi:10.1007/BF00702739.

Taylor, S. R., and S. M. McLennan (1995), The geochemical evolution of the continental crust, *Reviews of Geophysics*, *33*, 241-265, doi:10.1029/95RG00262.

Turekian, K. K., and J. L. Kulp (1956), The geochemistry of strontium, *Geochimica et Cosmochimica Acta*, *10*(5), 245-296, doi:10.1016/0016-7037(56)90015-1.

Watson, A. J., D. C. E. Bakker, A. J. Ridgwell, P. W. Boyd, and C. S. Law (2000), Effect of iron supply on Southern Ocean CO2 uptake and implications for glacial atmospheric CO2, *Nature*, *407*, 730-733, doi:10.1038/35037561.

Winton, V. H. L., G. B. Dunbar, N. A. N. Bertler, M. A. Millet, B. Delmonte, C. B. Atkins, J. M. Chewings, and P. Andersson (2014), The contribution of aeolian sand and dust to iron fertilization of phytoplankton blooms in southwestern Ross Sea, Antarctica, *Global Biogeochemical Cycles*, *28*(4), 2013GB004574, doi:10.1002/2013GB004574.

Wu, J., R. Rember, and C. Cahill (2007), Dissolution of aerosol iron in the surface waters of the North Pacific and North Atlantic oceans as determined by a semicontinuous flow-through reactor method, *Global Biogeochemical Cycles*, *21*(4), GB4010, doi:10.1029/2006GB002851.

Zender, C. S., H. Bian, and D. Newman (2003), Mineral Dust Entrainment and Deposition (DEAD) model: Description and 1990s dust climatology, *Journal of Geophysical Research: Atmospheres*, *108*, doi:10.1029/2002JD002775.

Zhu, X., J. M. Prospero, F. J. Millero, D. L. Savoie, and G. W. Brass (1992), The solubility of ferric ion in marine mineral aerosol solutions at ambient relative humidities, *Marine Chemistry*, *38*(1–2), 91-107, doi:10.1016/0304-4203(92)90069-M.

Zhu, X. R., J. M. Prospero, and F. J. Millero (1997), Diel variability of soluble Fe(II) and soluble total Fe in North African dust in the trade winds at Barbados, *Journal of Geophysical Research: Atmospheres*, *102*(D17), 21297-21305, doi:10.1029/97JD01313.

Zhuang, G., Z. Yi, R. A. Duce, and P. R. Brown (1992), Chemistry of iron in marine aerosols, *Global Biogeochemical Cycles*, *6*, 161–173, doi:10.1029/92GB00756.

Zirkler, D., F. Lang, and M. Kaupenjohann (2012), "Lost in filtration"—The separation of soil colloids from larger particles, *Colloids and Surfaces A: Physicochemical and Engineering Aspects*, *399*, 35-40, doi:10.1016/j.colsurfa.2012.02.021.

Supporting Information

Table 14: Descriptive statistics of cumulative elemental solubility (unit: %) of dust samples (n=14).

	Fe	Al	Si	Ti	Zn	Ca	K	Mg	Mn	Sr	Ba
geometric mean											
pure water	2.6	2.8	0.7	1.5	5.8	21	8.0	10	17	11	6.8
pH5	3.6	3.9	0.7	1.7	8.9	29	9.4	13	22	15	6.8
pH3	4.5	5.6	0.6	1.9	15	39	12	16	28	21	15
pH1	6.7	9.0	0.6	2.8	26	44	15	17	30	22	19
geometric SD											
pure water	1.0	1.0	0.22	0.5	2.4	11	3.2	3.9	7	8	2.4
pH5	1.2	1.2	0.27	0.6	3.0	12	3.6	4	9	9	4.0
pH3	1.4	1.6	0.32	0.7	6	14	4	5	10	10	6
pH1	1.8	2.4	0.34	0.9	8	15	5	5	11	11	7
median											
pure water	2.9	3.3	0.53	1.6	7.4	34	8.1	10.0	22	16	8.4
pH5	3.7	4.2	0.62	2.1	9.5	43	9.0	14	28	21	7.6
pH3	5.0	6.6	0.62	2.3	22	53	12	18	33	26	14
pH1	6.8	11	0.78	3.4	24	53	14	20	37	27	20
min											
pure water	0.4	0.6	0.32	0.3	1.2	2.5	1.4	1.2	1.7	0.3	1.4
pH5	0.8	0.8	0.20	0.2	1.8	4.1	1.9	2.3	2.7	0.7	0.1
pH3	1.1	1.2	0.07	0.3	1.7	5.0	2.1	3.7	4.7	1.3	1.8
pH1	2.0	1.7	0.10	0.6	6.8	5.4	2.4	4.1	5.1	1.3	2.1
max											
pure water	8.6	9.9	2.1	5.2	15	93	33	34	48	80	24
pH5	10	9.6	2.5	7.1	21	95	35	38	53	81	32
pH3	12	12	3.3	8.9	35	96	38	42	75	85	47
pH1	16	17	3.5	8.7	74	114	43	43	73	85	53

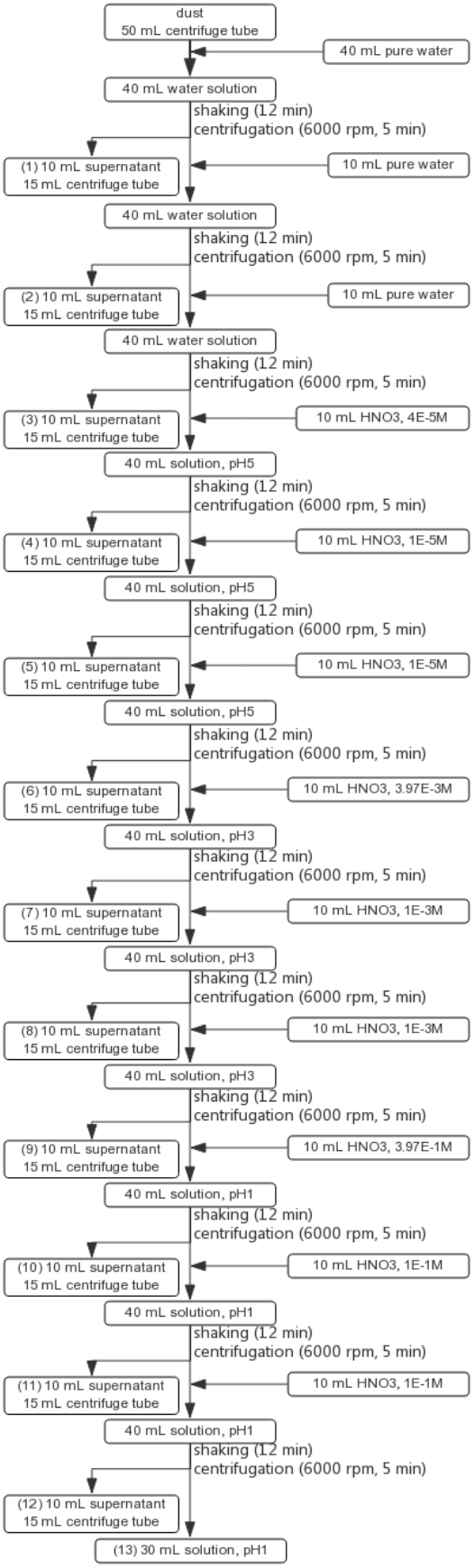

Figure 25 : Schema of dissolution experiments at four pH (pure water, pH5, pH3, pH1) coupled with centrifugation separation.

Conclusions of Chapter 4

The present work investigated the elemental solubility of laboratory-produced Patagonian and Namibian dust using sequential leaching in pure water and at pH 5, 3 and 1. Higher acidity resulted in generally larger elemental solubility. Iron and aluminum dissolve more rapidly when pH decreases from 3 to 1, while Ca tends to dissolve most of its content in first leaches. High Ca content leads to higher solubility of Ba, Ca, K, Mn and Sr, which is probably due to the presence of carbonate. Solubility of less soluble elements namely Al, Fe and Si was not affected by the Ca content.

Values of solubility obtained by centrifugation method are much higher for less soluble elements such as Fe, whereas elements like Ca are less affected. Retention of colloids on the membrane in filtration method is a major reason resulting in the different solubility between two separation methods, which could be reduced by stronger dissolution of colloids in more acidic leaches.

Experimental bias in centrifugation method is also needed to be checked in further studies by measuring the particle size distribution in dissolved fraction. This kind of study and the evaluation of membrane artefact are already in planning with Professor Zongbo SHI from University of Birmingham who possesses advantageous facilities to study the nanoparticles, and will greatly help to understand methodological issues. Nevertheless, bioavailability assessment experiments using phytoplankton cultures are necessary to test the relevance of filtration and centrifugation methods.

Conclusions and prospects

This experiments-based study was set out to contribute to the quantification of the emission of mineral dust and bioavailable micronutrients from source areas in subantarctic region. The study investigated the relevant characteristics of the mineral aerosols from source regions in subantarctic, including the dust concentration, the factors controlling the dust emission, the chemical composition, and the bioavailability of dust, to answer a series of questions:

1) *The dust concentration in Patagonia*. What is the dust concentration level in source area in subantarctic region? How does the dust concentration vary in long term? What are the factors regulating the dust concentration level in source area in subantarctic region?

2) *The elemental composition of dust in Patagonia and Namibia.* What are the elemental compositions, particularly Fe composition, of dust in source areas of subantarctic region? How do the elemental compositions of dust vary with geological locations? Is the elemental composition of soil representative to the elemental composition of dust? Can we use the elemental composition of soil as a surrogate of dust elemental composition?

3) *The elemental solubility of dust in Patagonia and Namibia.* To what extent is the dust soluble after different degrees of chemical processing? How does the elemental solubility of dust vary with different types of dust sample?

1. Principal results

The dust concentration in Patagonia

The three-year dust samplings in Patagonia-South Atlantic Coast revealed weekly average dust concentrations ranging from 0.07 to 3.68 $\mu g.m^{-3}$ in the border of South Patagonia. A seasonal pattern was observed with persistently low dust concentrations in winter. However, the wind speed in Patagonia was recurrently high and could not explain the seasonal variability of dust concentration. The trend of dust concentrations was in parallel with decreasing air relative humidity and increasing air temperatures. Dust emission strength in source area is hence assumed to be controlled by surface soil moisture. In addition, frozen

soil or snow cover is suggested to be responsible for the extremely low dust concentrations in winter.

The elemental composition of dust in Patagonia and Namibia

Laboratory measurements of dust elemental compositions for two dust source regions, Patagonia and Namibia, demonstrate a spatial heterogeneity of dust elemental composition in subantarctic region. Patagonian mineral dust generally possesses lower concentration of Fe than Namibian mineral dust. At a regional scale, elemental compositions including iron content of dust vary with locations. South Patagonia tends to emit dust with higher Si content than North, resulting in an inverse trend for the rest elements. Contents of Si, Al, K, Fe and Ti in dust originate mainly from minerals such as aluminosilicate clays and feldspars. Ca- or Mg-containing minerals (such as calcite, magnesite, and dolomite) are the main origins of variability in dust composition. Discrepancies of elemental composition were observed to different extent between dust and parent soil. Iron concentrations are similar between the dust samples and their parent soils in Patagonia, whereas are quite different between dust and parent soils in Namibia. Silica is the foremost cause of elemental fractionation due to the dilution effect of quartz and results in a dramatic Si depletion for dust produced from quartz-rich soils in Namibia. Using iron concentration in soil as a surrogate of dust iron content poses less uncertainty in Patagonia than in Namibia.

The elemental solubility of dust in Patagonia and Namibia

Elemental solubility was measured for laboratory-produced Patagonian and Namibian dust following a sequential leaching procedure. Dissolved fraction, operationally defined as <0.2 μm fraction, was separated by centrifugation separation method. Elemental solubility increases with decreasing pH from pure water to pH1. Geometric mean iron solubility is 2.3 ± 1.0% (geomean ± SD) in pure water, 3.4 ± 1.1% at pH5, 4.3 ± 1.3% at pH3, and 6.3 ± 1.8% at pH1. Solubility of Al, Si, Ti, Zn, Ca, K, Mg, Mn, Sr and Ba were also determined. Calcium-rich dust, probably due to the presence of carbonate, showed higher solubility of Ca, K, Mg, Mn, Sr and Ba. Compared to previous measurements using filtration method, centrifugation method showed much higher solubility values for elements namely Fe and Al, while less difference was found for Ca, Mg, Mn, and Ba. The disagreement of iron and aluminum solubility between the two separation methods is most likely due to experimental bias in centrifugation and retention of colloids on membrane in filtration.

2. Implications of results

Poor availability of dust concentration records in source areas of subantarctic region limits our understanding of dust cycle and modelling study in this region. As no such measurements in Patagonia were reported before, our measurements of dust concentration in the Patagonian-South Atlantic Coast provides the first time series of dust concentration in Patagonia and contributes to a better understanding of the dust export level and temporal dust emission pattern from Patagonia to the Southern Ocean. The time series obtained could be used to for the calibration of dust emission models in Patagonia. The fact that the seasonal dust concentration correlates with the variation in temperature and relative air humidity implicates a feedback of dust emission in response to short-term climate variations, which has further implications in parameterization of dust production model to evaluate the dust export from Patagonia to the Southern Ocean.

Elemental composition of dust is essential information to evaluate the input of micronutrients to open ocean from continental dust source areas. Although it's commonly known that elemental composition of dust varies with regions, biogeochemical modeling studies usually take a Fe_2O_3 concentration of 5% from the average upper continental crust composition as the iron concentration in dust due to the poor availability of measurement data. Our measurements contribute a database of elemental composition of dust in Namibia and Patagonia. The calculated accumulation factor also provides a resolution to estimate the dust elemental composition from soil elemental composition. The database of dust elemental composition and accumulation factor contribute to a better knowledge of the spatial distribution of trace element contents in dust source areas and may help to estimate the amount of trace elements in export dust flux and have further implication in biogeochemical modeling studies of dust in the subantarctic region.

Information of the potential elemental solubility of dust may help to estimate the potential amount of bioavailable trace element for the marine ecosystem in open-ocean. Our measurements of solubility using centrifugation method show high discrepancies with previous measurements using filtration separation. Retention of colloids on membrane in filtration separation reflects artefacts of membrane during the filtration procedure. Since the reasons resulting in the disagreement remain uncertain, solubility values obtained in this study need to be verified in further studies. The disagreement between the solubility obtained by centrifugation and filtration initials the investigation of the impact of separation method on

dust solubility measurements and the relevance of separation method to the bioavailability of dust.

3. Research limitation and prospects

The present thesis measured atmospheric dust concentration in the Patagonian-South Atlantic Coast. Considering the large extent along the longitude and the spatial heterogeneity of topography of Patagonian Desert, and the lack of dust concentration data in southern Africa, more dust sampling studies are required to shed light on the spatial variation of dust concentration in source areas and to better constrain dust models. Lack of local infrastructure to sustain a dust sampling station poses challenges to study dust emission in interior of Patagonia and other remote dust sources. Automatic aerosol samplers with simultaneous monitoring of the aerosol concentration, size fraction, chemical composition, and meteorological conditions are required. Measurement of vertical distribution of atmospheric dust, by LIDAR for example, is also helpful to better evaluate the dust export from source regions.

Since we have assumed that the dust emission strength in Patagonia is primarily regulated by the soil moisture instead of wind speed, modelling study is required in this region to compare the measured dust concentration with modelling results and to test the sensitivity of modeled dust emission to the soil moisture variation in Patagonia. The CEILAP station in Río Gallegos is a part of AERONET network. AERONET data is hence available for the aerosol-sampling period in this thesis. A comparison study between AERONET data and dust concentration data can potentially enhance our understanding on the dust concentration level and temporal pattern in Patagonia.

The elemental composition regulates the amount of trace elements in dust emitted. Our investigation into the Patagonian and Namibian dust has revealed a spatial heterogeneity of dust elemental composition. Australia is also important another major dust source for the Southern Ocean, particularly for the South Pacific section of the Southern Ocean. An extended investigation into the dust elemental composition in Australia will provide a more complete database of dust in Southern Hemisphere. On the other side, the mineralogical composition affects the solubility of dust as indicated by Journet et al., [2007].

Mineralogical composition of dust is a critical property that affects the bioavailability of elements in dust. In this work, we have observed the effect of Ca content on the solubility of soluble elements such as Ca, Mg and Mn, which is assumed to be associated with the concentration of carbonate. Measurements of mineralogical composition could help to better understand the variability of elemental solubility observed in our study. This kind of measurements could be done with techniques such as X-ray diffraction (XRD) or scanning electron microscopy (SEM).

In this work, the elemental solubility was measured using centrifugation separation method. Our attempts revealed remarkably higher solubility values when we separated the dissolved fraction using centrifugation separation instead of filtration separation. Possible underestimation of solubility in filtration due to the artefact of membrane and potential experimental bias in centrifugation separation are supposed to be the major reasons and need to be evaluated as a top priority. Investigations into the particle size distribution in dissolved fraction obtained by the two separation methods and the artefact of membrane in filtration are already in planning with Professor Zongbo SHI from University of Birmingham. Lastly, bioavailability assessments using phytoplankton cultures are necessary to test the relevance of filtration and centrifugation methods.

The three-year dust concentration record in Patagonia, the database of elemental composition and elemental solubility of source dust for Patagonia and Namibia are a substantial contribution to the knowledge about dust cycle in subantarctic region. At the same time, we have emphasized the association between the temporal pattern of dust concentration and soil moisture in source areas, the spatial heterogeneity of dust elemental composition, and the impact of Ca content on elemental solubility. Despite the limitation of our research, the obtained results of this work will benefit further evaluation of emission inventories of dust and bioavailable trace elements from dust sources to the Southern Ocean.

Appendix

Appendix 1. Super clean protocol

The super clean protocol aims to clean vessels and other experimental materials through removing the particle materials and extracting absorbed contaminants. Generally, this protocol consists of a cleaning procedure in normal ambiance and a further cleaning in clean room of class ISO5 (Appendix 2).

In normal ambiance:

1. Wash the materials with common detergent and rinsed successively with tap water and reverse osmosis purified water for five times;
2. Soak for at least 24 hours in 2% Decon® detergent then rinsed with purified water for five times;
3. If materials are not made of Teflon: soak for at least 24 hours in 2% hydrochloric acid (analytical grade, Merck) then rinsed with purified water for five times; If materials are made of Teflon: soak for at least 24 hours in 10% nitric acid (analytical grade, Merck) followed by rinsing with purified water for five times, then soak in 10% hydrochloric acid (analytical grade, Merck) followed by rinsing with purified water for five times;

In clean room (ISO 5):

4. Wash the materials with MilliQ (18 $M\Omega.cm^{-1}$) water for five times;
5. Soak for at least 24 hours in 2% hydrochloric acid (Suprapur®, Merck) then rinsed with MilliQ water five times;
6. Dry the materials in the ISO 1 laminar flow hood individually.
7. For Teflon vials, acid digestion with 3 mL pure nitric acid (Suprapur®, Merck) under 130°C in an air oven for >3 hours.

Appendix 2. Classification of cleanroom (ISO 14644-1)

The table below presents the classification of cleanroom according to the ISO 14644-1. Clean rooms we have used in this work are in accord with ISO5.

Number of Particles per Cubic Meter by Micrometer Size

CLASS	0.1 µm	0.2 µm	0.3 µm	0.5 µm	1 µm	5 µm
ISO1	10	2				
ISO2	100	24	10	4		
ISO3	1000	237	102	35	8	
ISO4	10000	2370	1020	352	83	
ISO5	100000	23700	10200	3520	832	29
ISO6	1000000	237000	102000	35200	8320	293
ISO7				352000	83200	2930
ISO8				3520000	832000	29300
ISO9				35200000	8320000	293000

Appendix 3. XRF instrument (PANalytical, Epsilon 3XL) and XRF analysis

The determination of the element mass allows estimating the elemental composition of the aerosol and the atmospheric concentration of aerosol. The mass of the collected elements, Na (as a reference element of marine aerosol), Al, Si and Fe (as reference elements of mineral aerosol) [*Bergametti et al.*, 1989; *Mahowald et al.*, 2008], was determined using a X-ray fluorescence (XRF) instrument (PANalytical, Epsilon 3XL) (Figure 26a). Disks measuring 15 mm in diameter were cut from Zéfluor™ filters using a gasket cutter (made of Zn-Fe-Cr alloy) to adapt the disks to the size requirement of the instrument (Figure 26b and c).

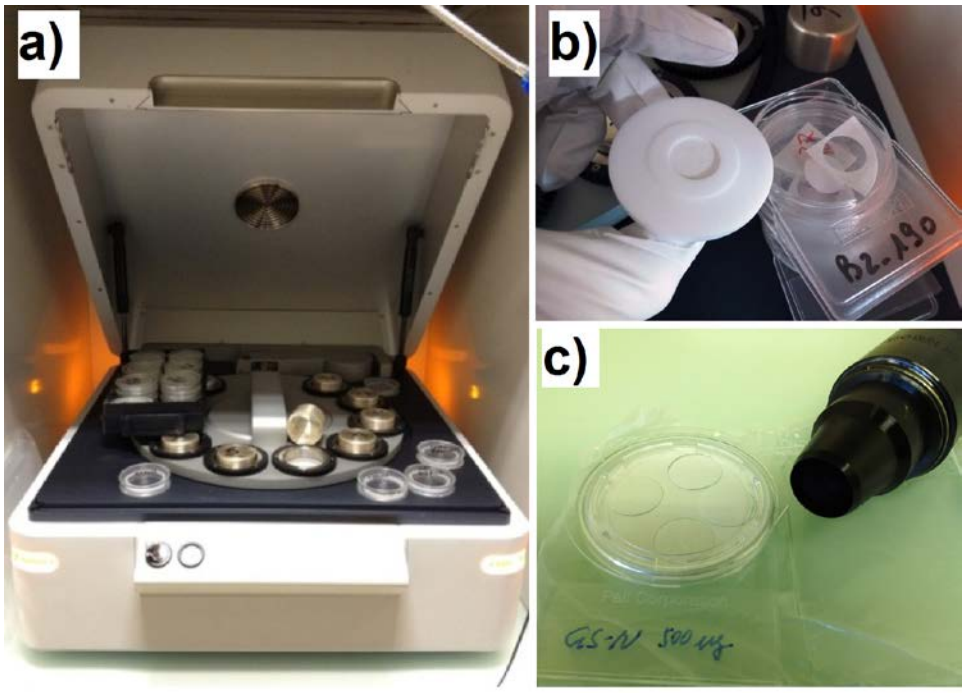

Figure 26 : a) XRF instrument (PANalytical, Epsilon 3XL), b) the supporter of filter disk, c) the Zéfluor membrane (47 mm) and gasket cutter (15 mm) (Remark: the GS-N membrane was prepared by geo-standard deposition and several sub-samples were cut off and analyzed by XRF to check the calibration accuracy).

Appendix 4. Illustration of aerosol sampling station in Río Gallegos, Patagonia

The main photo illustrates the sampling station and its location. The sampling location was located in a flat area closing to the east border of Patagonia. The case intergratting the air pumping system and gas flowmeter were placed in the downwind direction of sampling tower. The photo in the upper right corner illustrates the Zéfluor filter collecting the aerosol.

Location of sampling site in Río Gallegos:

Longitude:69.32°W

Latitude: 51.60°S

Altitude: 2 m AGL

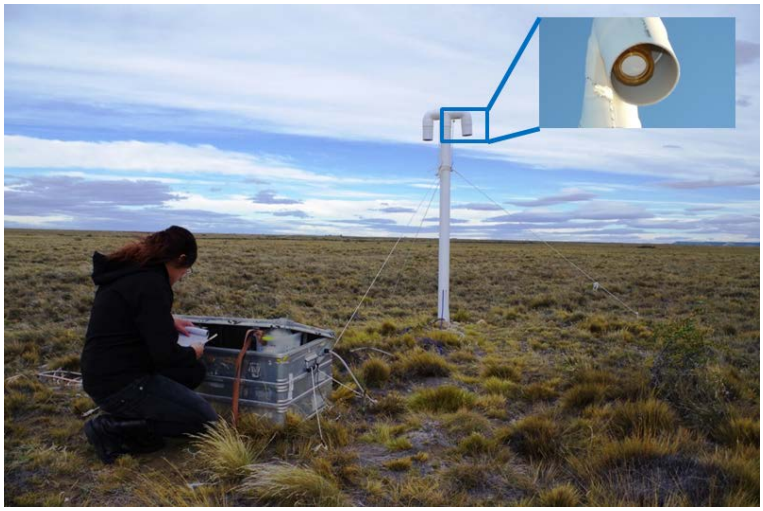

Appendix 5. Atmospheric concentration of Si, Al, Fe, Na, dust and sea salt measured in Río Gallegos

Atmospheric concentration of the collected mineral dust and sea salt is derived from the atmospheric concentration of Si (Si%=31.5% in dust) and Na (Na%=39.3% in NaCl).

unit: $\mu g.m^{-3}$

start date	end date	Al	Si	Fe	dust	Na	NaCl
2011/11/29	2011/12/2		0.197	0.023	0.625	0.289	0.735
2011/12/2	2011/12/4		0.284	0.041	0.903	0.942	2.396
2011/12/4	2011/12/7	0.053	0.358	0.049	1.138	0.582	1.480
2011/12/7	2011/12/10	0.131	0.649	0.126	2.062	0.646	1.644
2011/12/10	2011/12/13	0.046	0.291	0.043	0.924	0.215	0.546
2011/12/13	2011/12/20	0.220	0.908	0.163	2.885	0.571	1.453
2011/12/20	2011/12/27	0.041	0.231	0.051	0.734	0.359	0.913
2011/12/27	2012/1/3	0.082	0.393	0.047	1.247	0.371	0.944
2012/1/3	2012/1/10	0.037	0.233	0.033	0.741	0.623	1.583
2012/1/10	2012/1/17	0.037	0.229	0.035	0.727	0.389	0.990
2012/1/17	2012/1/24	0.028	0.181	0.028	0.574	0.228	0.581
2012/1/24	2012/1/31	0.106	0.488	0.077	1.549	0.338	0.860
2012/1/31	2012/2/7	0.049	0.266	0.038	0.844	0.400	1.017
2012/2/7	2012/2/14	0.075	0.333	0.055	1.058	0.227	0.576
2012/2/14	2012/2/21	0.070	0.315	0.057	1.002	0.400	1.017
2012/2/21	2012/2/28	0.060	0.292	0.052	0.929	0.494	1.256
2012/2/28	2012/3/6	0.040	0.237	0.033	0.752	0.526	1.338
2012/3/6	2012/3/13	0.018	0.126	0.020	0.400	0.481	1.222
2012/3/13	2012/3/20		0.044	0.007	0.139	0.183	0.464
2012/3/20	2012/3/28		0.054	0.006	0.171	0.260	0.661
2012/3/28	2012/4/3		0.096	0.015	0.305	0.322	0.819
2012/4/3	2012/4/10		0.047	0.004	0.151	0.337	0.858
2012/4/10	2012/4/17	0.033	0.160	0.025	0.508	0.178	0.454
2012/4/17	2012/4/24		0.052	0.008	0.165	0.450	1.145
2012/4/24	2012/5/2	0.031	0.165	0.027	0.525	0.352	0.894
2012/5/2	2012/5/8	0.048	0.249	0.040	0.790	0.423	1.075
2012/5/8	2012/5/17	0.012	0.096	0.014	0.305	0.443	1.128
2012/5/17	2012/5/23	0.058	0.279	0.042	0.887	0.262	0.666
2012/5/23	2012/5/29		0.033		0.104	0.645	1.641
2012/5/29	2012/6/5		0.064	0.006	0.205	0.307	0.782
2012/6/5	2012/6/12		0.033		0.106	0.478	1.216
2012/6/12	2012/6/19		0.027		0.086	0.149	0.380
2012/6/19	2012/6/27		0.026	0.002	0.083	0.267	0.679
2012/6/27	2012/7/3		0.021		0.068	0.162	0.411

start date	end date	Al	Si	Fe	dust	Na	NaCl
2012/7/3	2012/7/10		0.029		0.091	0.370	0.942
2012/7/10	2012/7/17		0.047	0.003	0.148	0.454	1.156
2012/7/17	2012/7/24		0.045	0.006	0.144	0.305	0.776
2012/7/24	2012/8/2		0.035	0.005	0.111	0.199	0.506
2012/8/2	2012/8/7		0.035		0.111	0.099	0.253
2012/8/7	2012/8/15	0.021	0.104	0.014	0.329	0.151	0.384
2012/8/15	2012/8/22		0.055	0.006	0.175	0.349	0.888
2012/8/22	2012/8/29	0.093	0.390	0.072	1.241	0.189	0.481
2012/8/29	2012/9/5	0.012	0.086	0.010	0.275	0.191	0.486
2012/9/5	2012/9/13	0.033	0.162	0.019	0.515	0.138	0.351
2012/9/13	2012/9/19	0.099	0.412	0.071	1.309	0.126	0.321
2012/9/19	2012/9/27	0.063	0.291	0.049	0.926	0.474	1.204
2012/9/27	2012/10/4	0.084	0.350	0.063	1.113	0.272	0.693
2012/10/4	2012/10/11	0.031	0.188	0.028	0.597	0.579	1.472
2012/10/11	2012/10/15		0.069	0.005	0.221	0.064	0.163
2012/10/15	2012/10/25	0.018	0.098	0.012	0.311	0.078	0.198
2012/10/25	2012/11/1	0.044	0.230	0.027	0.731	0.196	0.498
2012/11/1	2012/11/8	0.014	0.111	0.015	0.353	0.321	0.817
2012/11/8	2012/11/16	0.047	0.218	0.031	0.693	0.187	0.476
2012/11/16	2012/11/22	0.072	0.380	0.050	1.207	0.487	1.238
2012/11/22	2012/11/29	0.041	0.236	0.028	0.750	0.192	0.488
2012/11/29	2012/12/10	0.115	0.470	0.084	1.493	0.276	0.702
2012/12/10	2012/12/20		0.063	0.010	0.202	0.443	1.127
2012/12/20	2012/12/27				pump failure		
2012/12/27	2013/1/3	0.014	0.104	0.016	0.331	0.386	0.982
2013/1/3	2013/1/10	0.096	0.411	0.068	1.305	0.287	0.730
2013/1/10	2013/1/18	0.072	0.342	0.059	1.088	0.449	1.142
2013/1/18	2013/1/28	0.081	0.363	0.063	1.154	0.343	0.872
2013/1/28	2013/2/4	0.032	0.216	0.024	0.688	0.536	1.362
2013/2/4	2013/2/13	0.082	0.420	0.069	1.334	0.812	2.064
2013/2/13	2013/2/21		0.088	0.010	0.279	0.270	0.686
2013/2/21	2013/2/28	0.046	0.243	0.044	0.773	0.489	1.244
2013/2/28	2013/3/7	0.041	0.201	0.034	0.640	0.190	0.483
2013/3/7	2013/3/14		0.071	0.010	0.227	0.641	1.631
2013/3/14	2013/3/22	0.072	0.329	0.058	1.045	0.414	1.053
2013/3/22	2013/3/28	0.057	0.275	0.052	0.872	0.645	1.640
2013/3/28	2013/4/5	0.039	0.191	0.035	0.608	0.585	1.489
2013/4/5	2013/4/15	0.028	0.145	0.030	0.462	0.301	0.766
2013/4/15	2013/4/22	0.037	0.197	0.041	0.625	0.485	1.233
2013/4/22	2013/5/3	0.016	0.088	0.016	0.281	0.385	0.980
2013/5/3	2013/5/10	0.033	0.181	0.034	0.575	0.304	0.773
2013/5/10	2013/5/16		0.052	0.008	0.164	0.367	0.932
2013/5/16	2013/5/27	0.010	0.065	0.013	0.207	0.114	0.291

start date	end date	Al	Si	Fe	dust	Na	NaCl
2013/5/27	2013/6/5		0.047	0.012	0.150	0.548	1.395
2013/6/5	2013/6/12		0.021	0.003	0.068	0.306	0.777
2013/6/12	2013/6/20		0.045	0.007	0.143	0.439	1.118
2013/6/20	2013/7/1		0.035	0.006	0.113	0.316	0.805
2013/7/1	2013/7/10	0.022	0.115	0.018	0.365	0.121	0.309
2013/7/10	2013/7/19		0.054	0.008	0.171	0.259	0.659
2013/7/19	2013/7/29		0.024	0.004	0.078	0.492	1.251
2013/7/29	2013/8/6		0.064	0.013	0.203	0.506	1.288
2013/8/6	2013/8/14	0.043	0.198	0.040	0.630	0.380	0.966
2013/8/14	2013/8/21		0.054	0.009	0.172	0.347	0.883
2013/8/21	2013/9/2	0.025	0.130	0.025	0.413	0.340	0.865
2013/9/2	2013/9/9		0.030	0.006	0.094	0.235	0.599
2013/9/9	2013/9/16		0.059	0.011	0.188	0.189	0.481
2013/9/16	2013/9/20	0.057	0.303	0.059	0.963	0.287	0.730
2013/9/20	2013/10/1	0.093	0.390	0.076	1.238	0.670	1.704
2013/10/1	2013/10/9	0.166	0.689	0.137	2.189	0.432	1.098
2013/10/9	2013/10/23	0.026	0.137	0.020	0.437	0.273	0.693
2013/10/23	2013/10/30	0.142	0.646	0.107	2.052	0.605	1.538
2013/10/30	2013/11/7	0.144	0.624	0.110	1.984	0.434	1.103
2013/11/7	2013/11/14	0.039	0.226	0.034	0.719	0.507	1.289
2013/11/14	2013/11/21	0.025	0.172	0.025	0.547	0.397	1.011
2013/11/21	2013/11/29	0.054	0.289	0.051	0.918	0.571	1.452
2013/11/29	2013/12/6	0.017	0.137	0.017	0.436	0.345	0.878
2013/12/6	2013/12/10		0.040	0.006	0.128	0.124	0.316
2013/12/10	2013/12/17		0.088	0.012	0.280	0.409	1.040
2013/12/17	2013/12/23	0.014	0.128	0.017	0.407	0.403	1.026
2013/12/23	2014/1/3	0.010	0.076	0.011	0.242	0.346	0.881
2014/1/3	2014/1/10		0.052	0.007	0.166	0.091	0.231
2014/1/10	2014/1/20	0.024	0.136	0.020	0.432	0.278	0.708
2014/1/20	2014/1/28	0.018	0.121	0.029	0.384	0.226	0.575
2014/1/28	2014/2/4		0.100	0.017	0.316	0.443	1.127
2014/2/4	2014/2/14		0.074	0.012	0.236	0.338	0.858
2014/2/14	2014/2/21	0.140	0.592	0.115	1.881	0.258	0.656
2014/2/21	2014/2/28	0.037	0.191	0.039	0.607	0.576	1.464
2014/2/28	2014/3/7	0.020	0.131	0.025	0.416	0.165	0.420
2014/3/7	2014/3/16	0.019	0.124	0.019	0.393	0.356	0.905
2014/3/16	2014/3/26	0.026	0.137	0.024	0.437	0.369	0.938
2014/3/26	2014/4/3	0.014	0.095	0.016	0.301	0.411	1.045
2014/4/3	2014/4/10	0.233	0.966	0.173	3.070	0.092	0.234
2014/4/10	2014/4/16		0.055	0.008	0.174	0.450	1.144
2014/4/16	2014/4/24	0.034	0.172	0.034	0.546	0.410	1.043
2014/4/24	2014/4/30	0.283	1.155	0.216	3.672	0.465	1.182
2014/4/30	2014/5/9	0.083	0.366	0.068	1.164	0.369	0.938

start date	end date	Al	Si	Fe	dust	Na	NaCl
2014/5/9	2014/5/16	0.017	0.117	0.021	0.372	0.307	0.782
2014/5/16	2014/5/23		0.033	0.005	0.104	0.341	0.868
2014/5/23	2014/5/30		0.080	0.014	0.254	0.239	0.607
2014/5/30	2014/6/10	0.009	0.065	0.015	0.206	0.227	0.576
2014/6/10	2014/6/17		0.046	0.024	0.146	0.157	0.400
2014/6/17	2014/6/23		0.050	0.011	0.160	0.456	1.160
2014/6/23	2014/7/2	0.023	0.125	0.022	0.397	0.178	0.453
2014/7/2	2014/7/14	0.033	0.151	0.029	0.479	0.207	0.526
2014/7/14	2014/7/21		0.030	0.008	0.096	0.693	1.762
2014/7/21	2014/7/25			pump failure			
2014/7/25	2014/8/4			pump failure			
2014/8/4	2014/8/12		0.059	0.010	0.186	0.265	0.673
2014/8/12	2014/8/21		0.053	0.010	0.167	0.190	0.483

Appendix 6. Dust generation by SyGAVib: the condition set

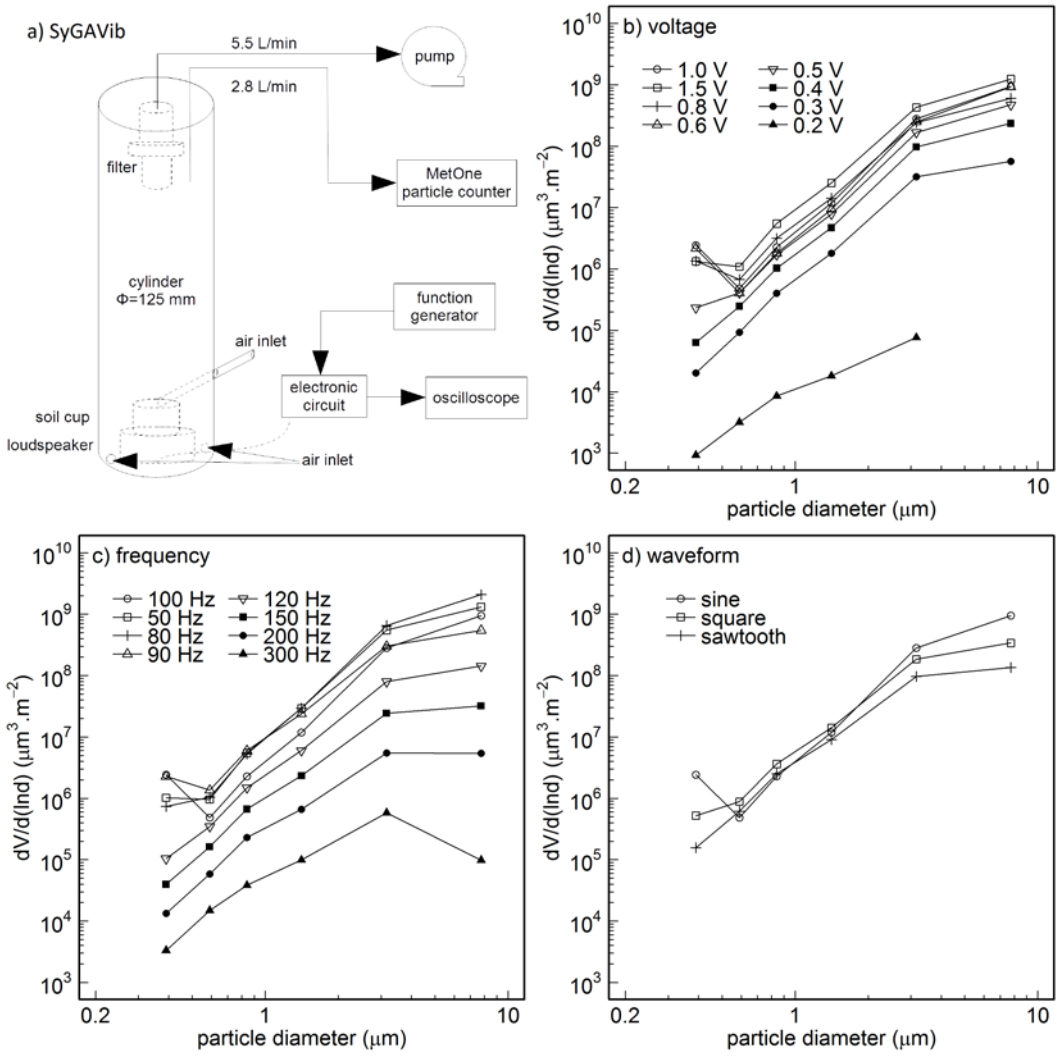

Figure 27 : a) Schema of SyGAVib and size resolved particle volume as a function of working conditions: b) voltage, c) frequency, d) waveform of vibration.

Trials were conducted to evaluate the dust emission performance under different power supplies, with the same soil (SP203). Since the motion scale of particles relates directly with the momentum transmitted by the vibrating cup, experiments were firstly conducted under voltage inputs ranging from 0 V (no emission detected) to 1.5 V, 100 Hz and sinus current. Figure 27b presents the time-averaged size distribution of dust emission for adequate length of time (0.2 V-896 min, 0.25 V-378 min, 0.3 V-121 min, 0.4 V-19 min, 0.6 V-8 min, 1 V-6 min, and 1.5 V-4 min). The emission rate increases with the energy of vibration and reaches steady state at 0.6-1.0 V. Another phenomenon is the relative increase of sub-micron particles as power increases, which suggests more effective disaggregation of coarse particles.

During the aerosol generation, the voltage was set at 1.0 V to assure a stronger soil disaggregation and dust emission.

After the input voltage is determined, experiments were conducted to evaluate the influence of current frequency on the aerosol generation with sinus current (Figure 27c). Results shows that frequencies lower than 120 Hz induce more particles releases. Tests under 90 Hz and 100 Hz are more efficient for both total aerosol emission and sub-micro particles emission. Thus the frequency of 100 Hz was finally conserved to process the aerosol generation.

Experiments under different signal wave form (Figure 27d) shows that, under 1.0 V and 100 Hz, the three different waves generated approximately the same amount of particles, while sinusoidal signal is more efficient to release both the sub-micro and coarse particles than square wave and saw-tooth wave. An applicable condition is defined: the speaker is driven at 1.0 V and 100 Hz, about 0.3 g soil sample is placed in the container, to produce the aerosol.

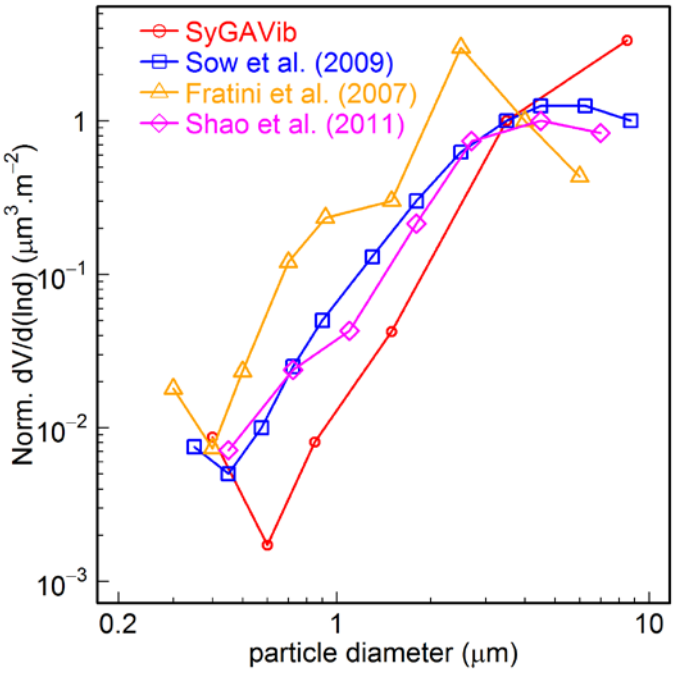

Figure 28 : Normalized volume size distribution as a function of particle diameter (µm). Values are normalized to the channel between 3.5 and 4.5 µm. Measurements of Sow et al. (2009), Fratini et al. (2007) and Shao et al. (2011) were made in Niger, China, and Australia, respectively.

Figure 28 compared the volume size distribution of aersol generated by SyGAVib to the in fied measurements of dust size distribution in Niger, China, and Australia. Volume size distribution generally shows a bimodal distribution of the aerosol volume between 0.2 μm and 10 μm: one coarse mode centered between 2 to 5 μm and a finer mode between 0.3 to 0.5 μm, as shown in Figure 28. The size distribution of dust generated by SyGAVib is similar to field observations. Hence, the dust generated by SyGAVib under the determined condition set generally captured the size charateristics of dust emitted by the naturally occuring eolian erosion.

Appendix 7. Map of elemental composition for a) Patagonian soils, b) Namibian soils, c) Patagonian dust, d) Namibian dust.

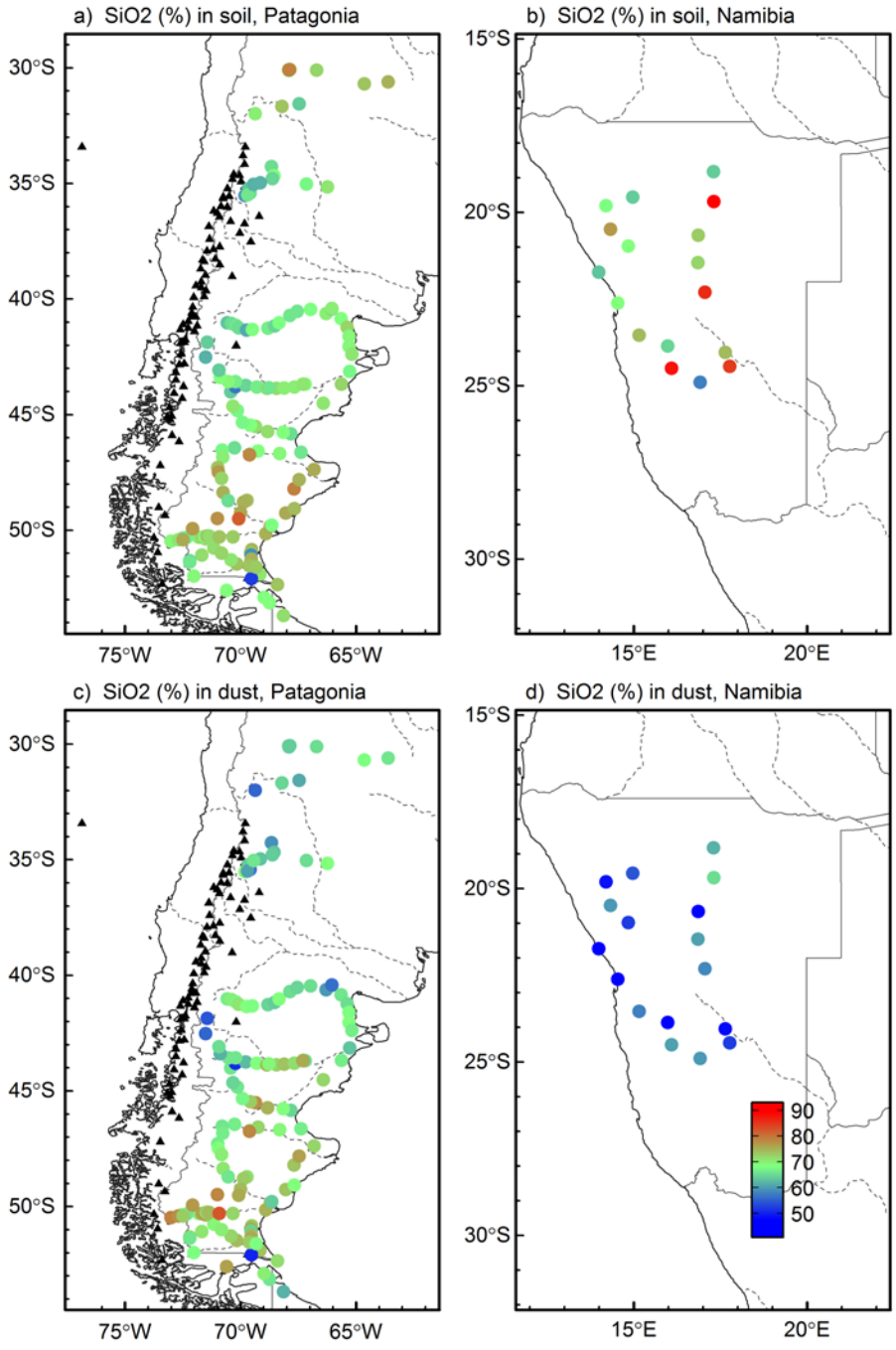

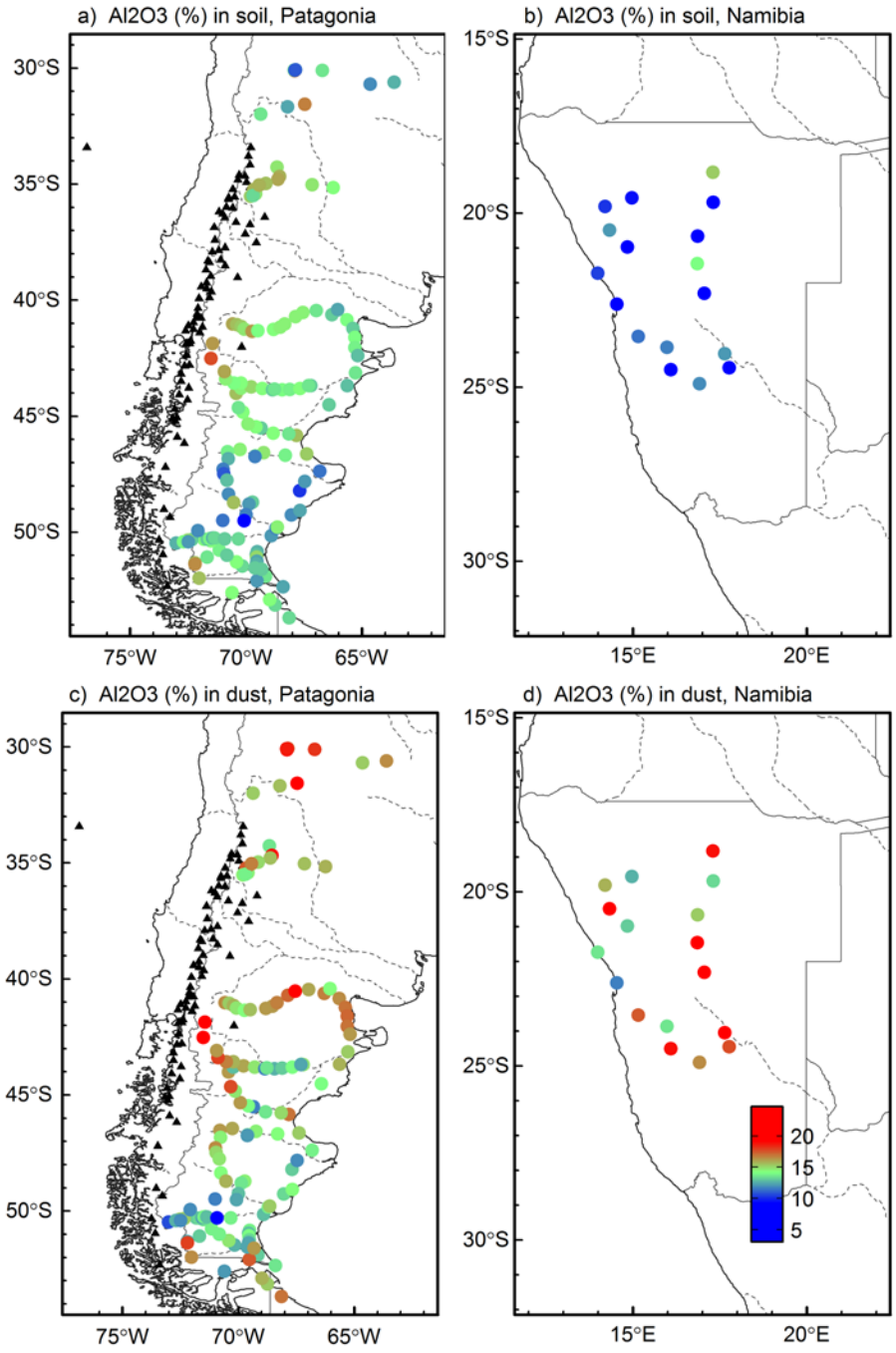
a) Al2O3 (%) in soil, Patagonia
b) Al2O3 (%) in soil, Namibia
c) Al2O3 (%) in dust, Patagonia
d) Al2O3 (%) in dust, Namibia
30°S
35°S
40°S
45°S
50°S
75°W
70°W
65°W
15°S
20°S
25°S
30°S
15°E
20°E
20
15
10
5

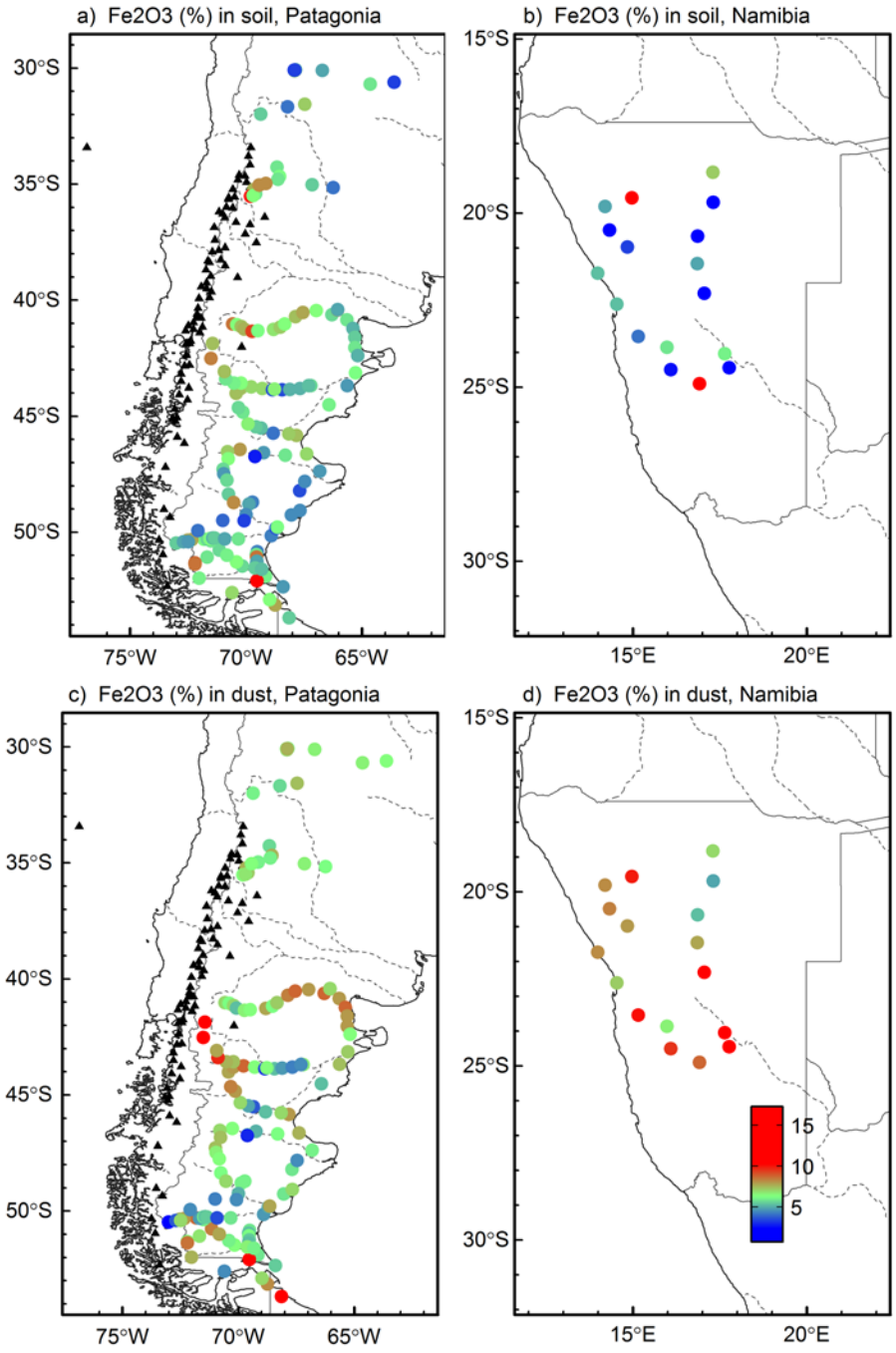
a) Fe2O3 (%) in soil, Patagonia
b) Fe2O3 (%) in soil, Namibia
c) Fe2O3 (%) in dust, Patagonia
d) Fe2O3 (%) in dust, Namibia
30°S
35°S
40°S
45°S
50°S
75°W
70°W
65°W
15°S
20°S
25°S
30°S
15°E
20°E
15
10
5

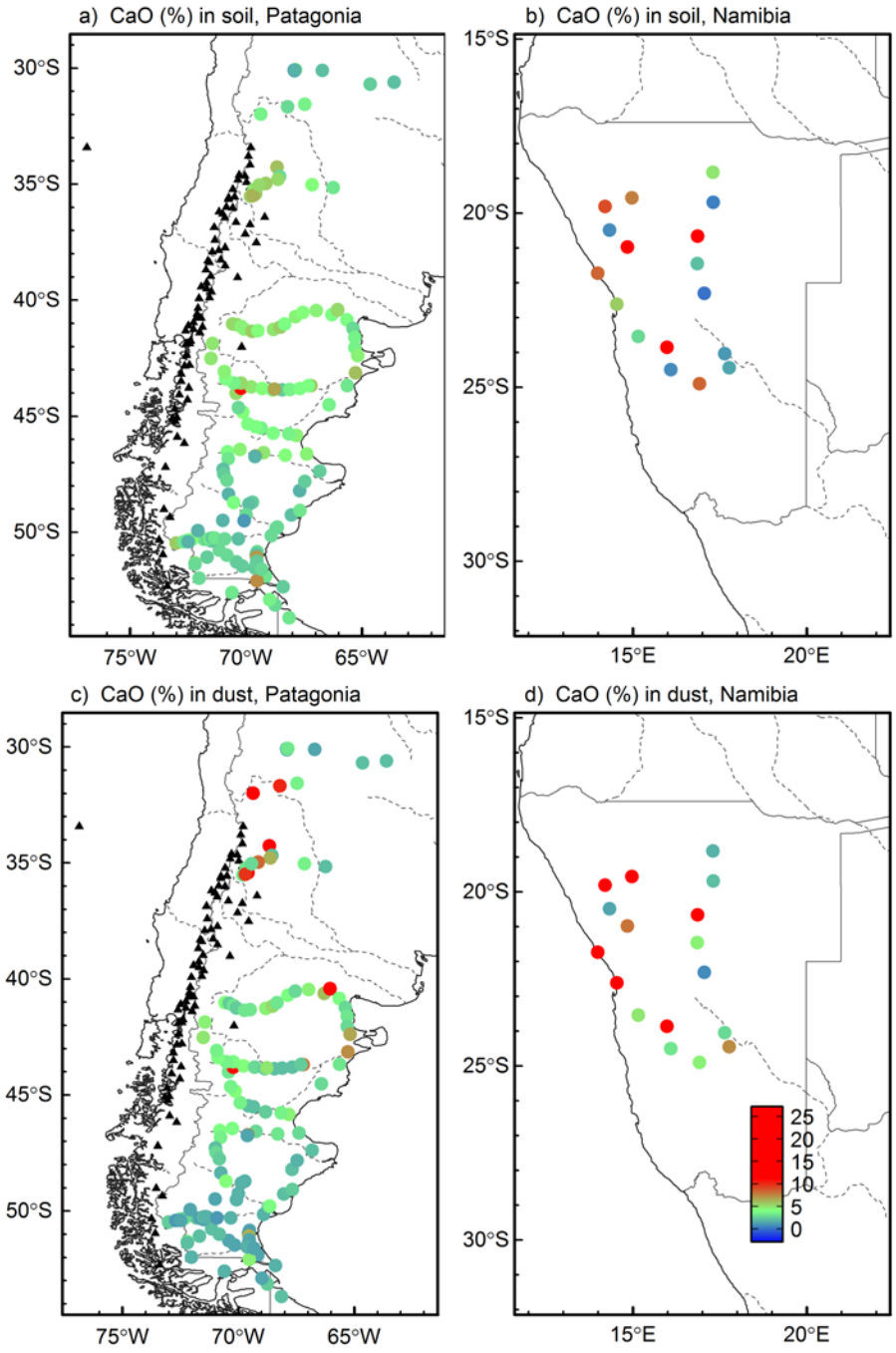
a) CaO (%) in soil, Patagonia
b) CaO (%) in soil, Namibia
c) CaO (%) in dust, Patagonia
d) CaO (%) in dust, Namibia
30°S
35°S
40°S
45°S
50°S
75°W
70°W
65°W
15°S
20°S
25°S
30°S
15°E
20°E
25
20
15
10
5
0

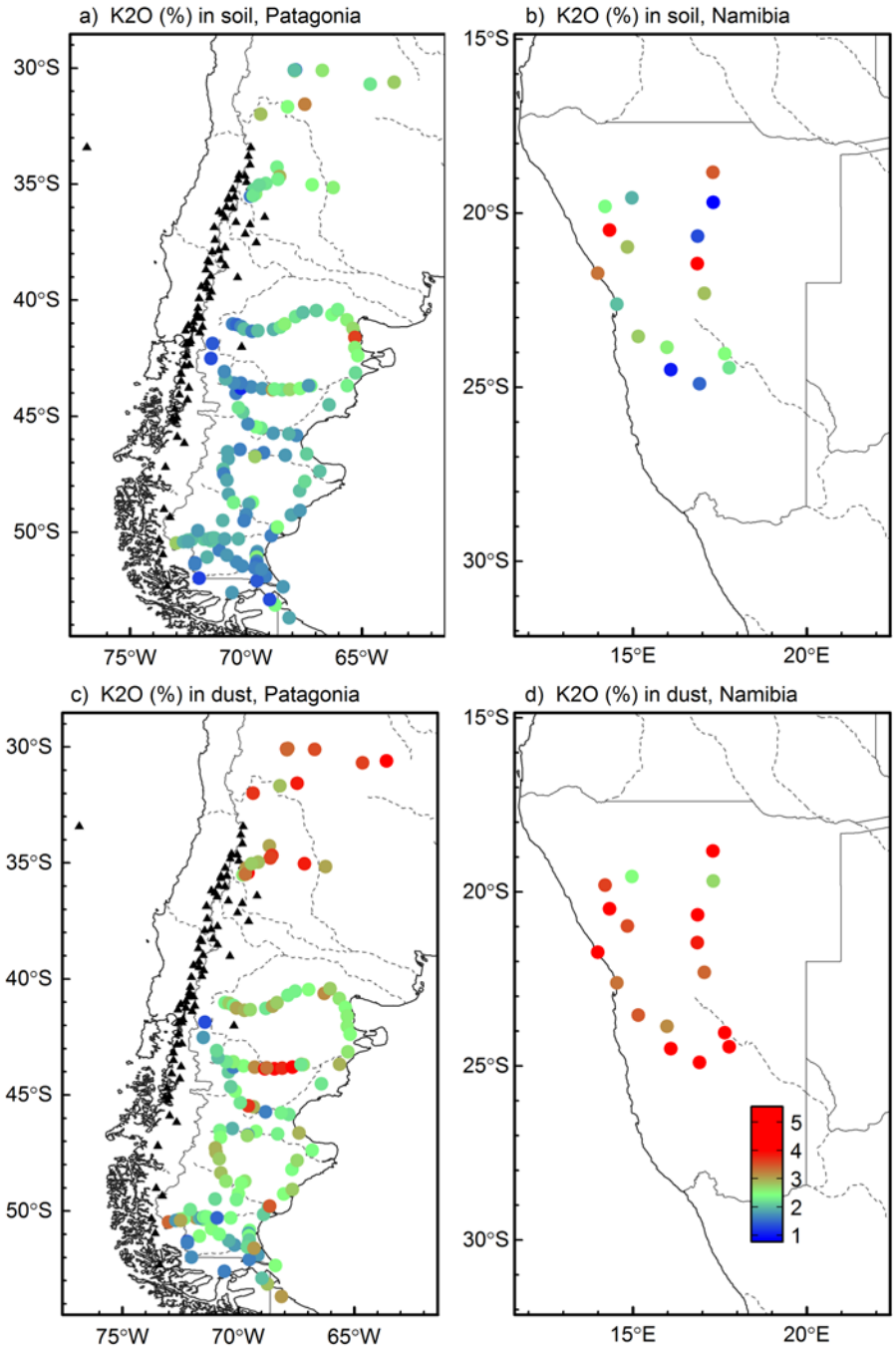
a) K2O (%) in soil, Patagonia
b) K2O (%) in soil, Namibia
c) K2O (%) in dust, Patagonia
d) K2O (%) in dust, Namibia
30°S
35°S
40°S
45°S
50°S
75°W
70°W
65°W
15°S
20°S
25°S
30°S
15°E
20°E
5
4
3
2
1

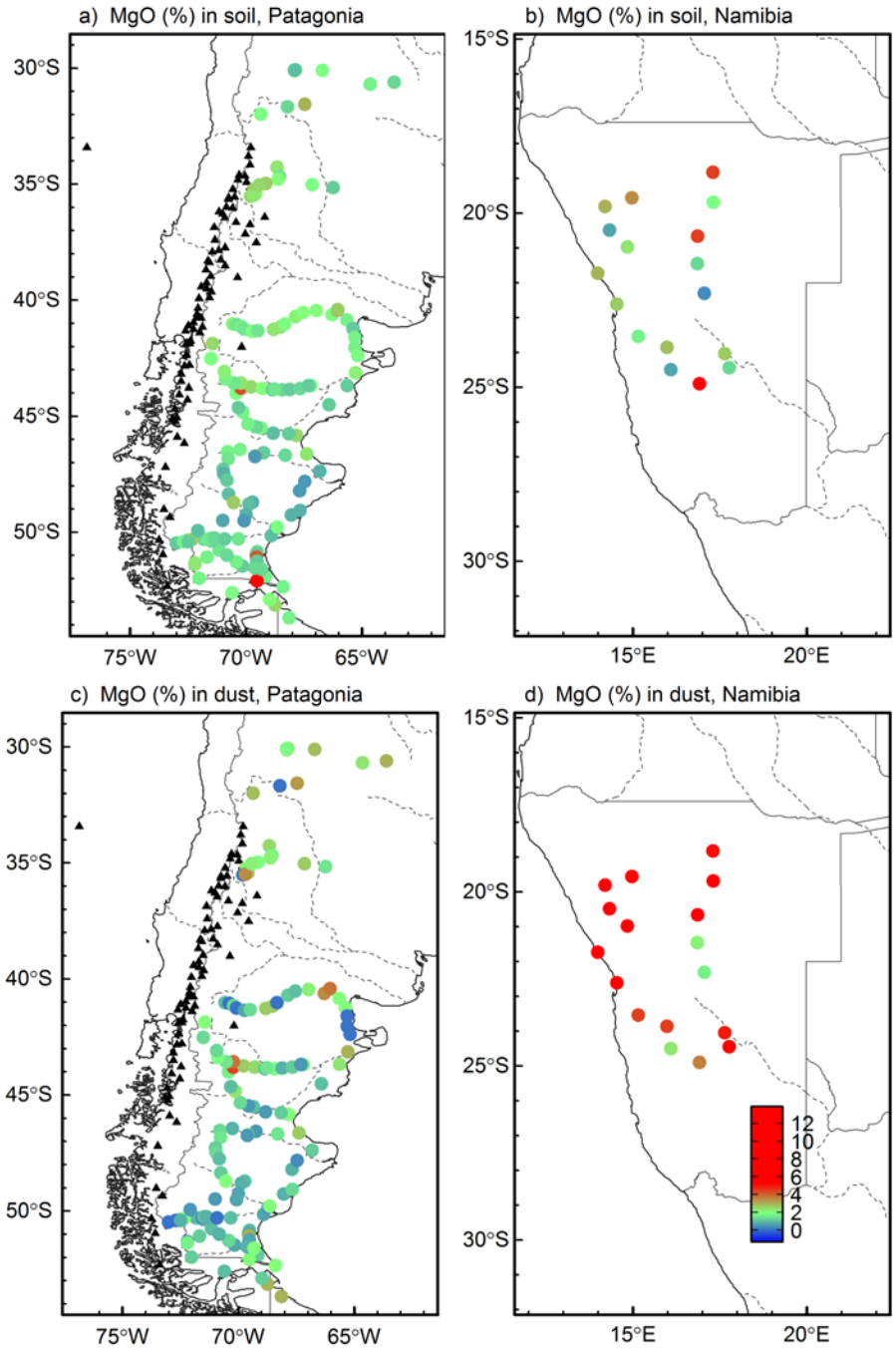
a) MgO (%) in soil, Patagonia
b) MgO (%) in soil, Namibia
c) MgO (%) in dust, Patagonia
d) MgO (%) in dust, Namibia
30°S
35°S
40°S
45°S
50°S
75°W
70°W
65°W
15°S
20°S
25°S
30°S
15°E
20°E
12
10
8
6
4
2
0

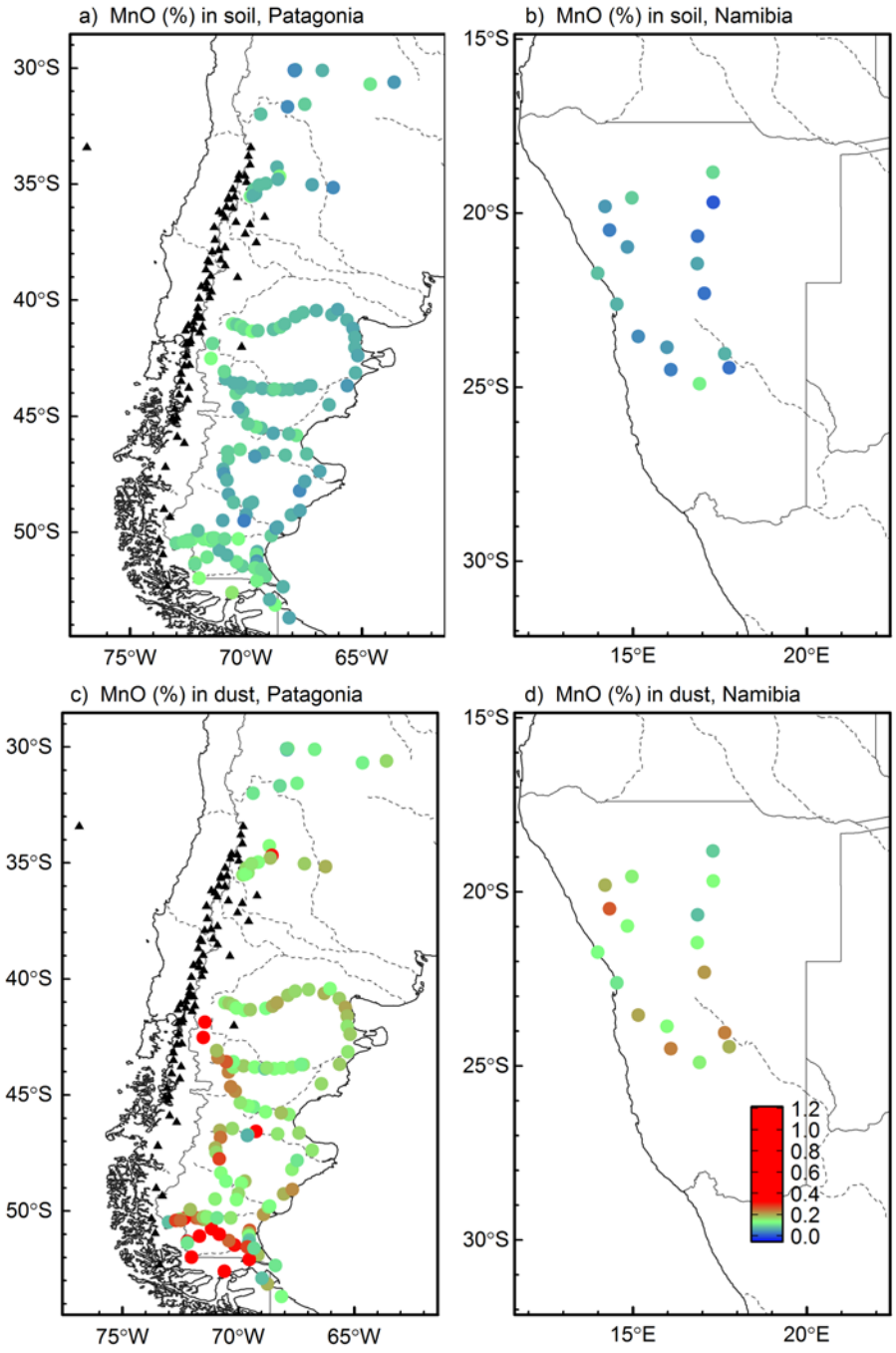
a) MnO (%) in soil, Patagonia
b) MnO (%) in soil, Namibia
c) MnO (%) in dust, Patagonia
d) MnO (%) in dust, Namibia
30°S
35°S
40°S
45°S
50°S
75°W
70°W
65°W
15°S
20°S
25°S
30°S
15°E
20°E
1.2
1.0
0.8
0.6
0.4
0.2
0.0

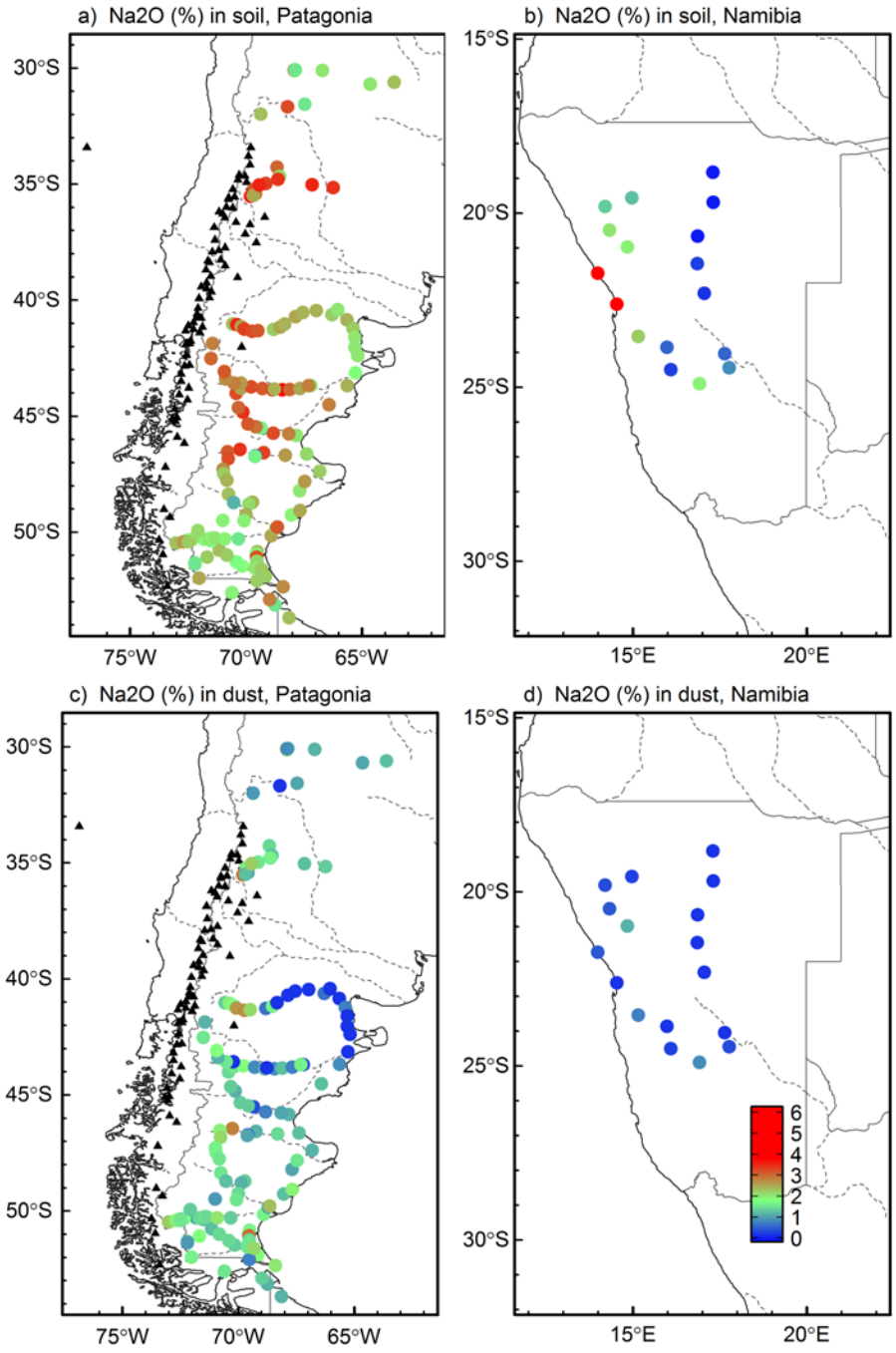
a) Na2O (%) in soil, Patagonia
b) Na2O (%) in soil, Namibia
c) Na2O (%) in dust, Patagonia
d) Na2O (%) in dust, Namibia
30°S
35°S
40°S
45°S
50°S
75°W
70°W
65°W
15°S
20°S
25°S
30°S
15°E
20°E
6
5
4
3
2
1
0

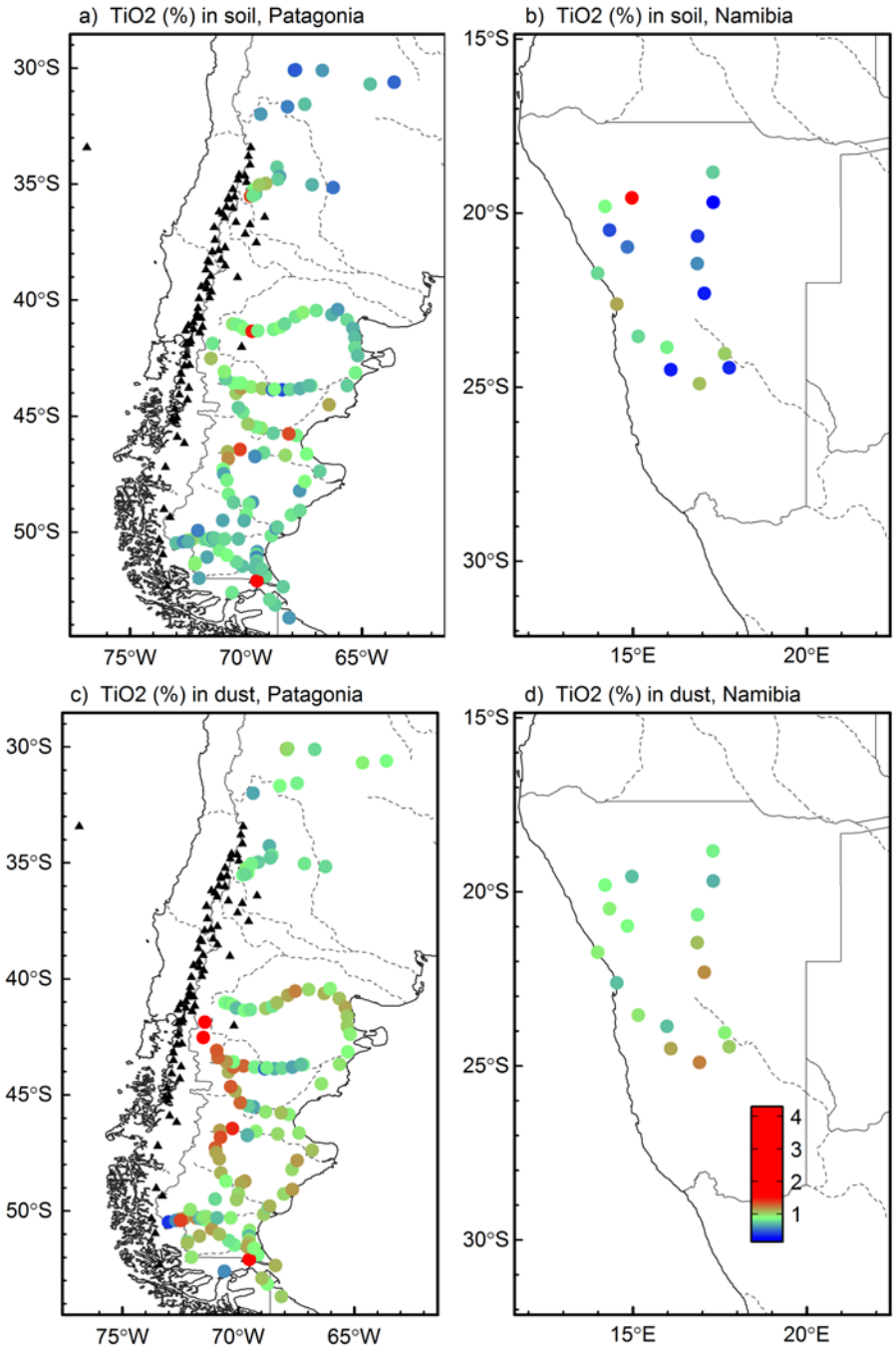
a) TiO2 (%) in soil, Patagonia
b) TiO2 (%) in soil, Namibia
c) TiO2 (%) in dust, Patagonia
d) TiO2 (%) in dust, Namibia
30°S
35°S
40°S
45°S
50°S
75°W
70°W
65°W
15°S
20°S
25°S
30°S
15°E
20°E
4
3
2
1

Appendix 8. Elemental concentration in soils (SP: Soil from Patagonia; SN: Soil from Namibia)

unit: oxide in %, trace elements in ppm

	SiO_2	Al_2O_3	Fe_2O_3	CaO	Na_2O	K_2O	MgO	TiO_2	P_2O_5	MnO	Cr	Zn	Sr	Zr
SP001	71.0%	13.6%	5.94%	3.12%	2.20%	1.63%	1.59%	0.76%	<	0.10%	129	58	351	164
SP002	73.5%	12.4%	4.68%	2.38%	2.69%	1.77%	1.68%	0.74%	0.06%	0.07%	63	63	250	167
SP003	52.6%	12.1%	13.43%	7.29%	2.26%	1.44%	8.21%	2.58%	0.47%	0.12%	401	123	580	245
SP004	73.4%	13.2%	5.58%	2.40%	1.79%	1.69%	1.14%	0.70%	<	0.08%	135	62	308	185
SP005	70.6%	14.4%	6.39%	2.55%	1.77%	1.74%	1.68%	0.78%	<	0.10%	91	69	320	228
SP006	71.3%	13.8%	5.69%	2.78%	2.36%	1.65%	1.53%	0.84%	<	0.07%	103	56	262	206
SP007	71.8%	14.2%	5.89%	2.21%	1.73%	2.11%	1.21%	0.71%	0.07%	0.11%	298	69	264	218
SP008	70.3%	14.2%	6.19%	3.08%	1.83%	2.06%	1.38%	0.81%	0.08%	0.11%	54	76	327	229
SP009	67.0%	13.2%	7.77%	4.21%	2.16%	2.01%	2.60%	0.98%	0.16%	0.11%	235	75	288	149
SP010	66.1%	15.0%	7.81%	3.79%	1.75%	2.01%	2.48%	0.94%	0.09%	0.10%	242	81	369	196
SP011	69.3%	12.5%	5.43%	5.69%	2.35%	2.76%	1.13%	0.72%	0.16%	0.10%	79	99	552	256
SP012	70.9%	14.1%	4.93%	3.20%	2.60%	1.95%	1.61%	0.59%	<	0.11%	117	64	341	192
SP013	75.3%	12.2%	4.59%	1.84%	2.27%	1.88%	1.14%	0.67%	0.08%	0.11%	42	74	233	191
SP014	72.1%	13.1%	5.74%	2.80%	1.89%	2.01%	1.52%	0.73%	0.07%	0.11%	55	66	285	198
SP015	69.3%	14.1%	6.42%	3.61%	2.00%	1.97%	1.66%	0.81%	0.06%	0.12%	187	77	353	198
SP016	70.4%	13.7%	6.21%	3.20%	2.05%	1.98%	1.55%	0.81%	0.07%	0.12%	66	66	317	219
SP017	74.4%	12.5%	5.09%	2.09%	1.83%	1.94%	1.41%	0.61%	<	0.10%	65	54	228	239
SP018	71.7%	13.4%	5.50%	3.09%	2.05%	1.99%	1.40%	0.75%	0.05%	0.10%	54	65	323	216
SP019	73.5%	13.2%	4.90%	2.71%	1.92%	1.88%	1.13%	0.75%	0.04%	0.09%	39	54	325	257
SP020	72.8%	13.3%	5.90%	2.21%	1.55%	1.92%	1.46%	0.71%	<	0.12%	100	67	222	200
SP021	74.5%	12.5%	4.35%	2.64%	2.29%	1.76%	1.24%	0.62%	<	0.07%	75	43	301	183
SP022	73.5%	12.9%	5.78%	2.20%	1.87%	1.72%	1.13%	0.81%	<	0.11%	208	58	277	254
SP023	59.0%	14.9%	8.56%	6.94%	3.22%	2.55%	4.15%	0.57%	0.08%	0.11%	156	104	364	143
SP024	74.7%	12.3%	4.96%	2.28%	2.12%	1.70%	1.10%	0.77%	0.04%	0.05%	77	44	264	242
SP025	74.6%	12.5%	4.95%	2.40%	2.16%	1.56%	1.10%	0.72%	<	0.06%	64	54	289	204

	SiO_2	Al_2O_3	Fe_2O_3	CaO	Na_2O	K_2O	MgO	TiO_2	P_2O_5	MnO	Cr	Zn	Sr	Zr
SP026	73.3%	13.1%	5.48%	2.30%	2.07%	1.64%	1.34%	0.71%	0.04%	0.10%	133	78	278	178
SP027	73.2%	12.8%	5.44%	2.56%	2.18%	1.69%	1.33%	0.71%	<	0.09%	367	56	301	200
SP028	71.9%	13.1%	5.95%	2.77%	2.24%	1.75%	1.32%	0.86%	0.03%	0.07%	120	55	295	207
SP029	71.8%	13.5%	5.78%	2.52%	2.18%	1.92%	1.57%	0.66%	0.06%	0.10%	390	67	279	201
SP030	64.7%	15.6%	8.73%	4.74%	1.51%	1.55%	2.05%	0.91%	0.37%	0.14%	110	126	392	173
SP031	65.7%	16.5%	8.59%	2.82%	1.53%	1.59%	2.22%	0.92%	0.10%	0.10%	61	86	331	196
SP032	69.3%	15.4%	6.12%	2.94%	2.52%	1.26%	1.67%	0.64%	0.14%	0.14%	48	60	373	132
SP033	68.9%	14.2%	7.08%	3.23%	1.94%	1.77%	1.88%	0.80%	0.24%	0.16%	143	104	312	143
SP034	72.8%	13.0%	5.35%	2.69%	2.26%	1.71%	1.34%	0.75%	<	0.09%	56	56	313	213
SP302	71.5%	13.3%	5.45%	3.18%	2.37%	1.86%	1.64%	0.62%	<	0.06%	63	42	317	158
SP303	68.6%	13.3%	7.85%	2.86%	1.55%	2.36%	2.54%	0.73%	0.09%	0.13%	122	108	271	149
SP304	68.9%	14.2%	6.38%	3.59%	2.79%	1.33%	2.01%	0.75%	<	0.07%	72	60	370	179
SP101	73.3%	11.8%	5.83%	2.41%	2.00%	2.22%	1.59%	0.70%	<	0.11%	111	66	188	332
SP102	74.7%	12.6%	3.35%	2.24%	2.30%	2.80%	1.39%	0.49%	<	0.04%	43	43	300	204
SP103	72.1%	13.6%	4.93%	2.11%	2.08%	2.65%	1.82%	0.60%	<	0.06%	53	63	264	286
SP104	74.0%	11.3%	5.08%	4.25%	1.87%	1.47%	1.42%	0.53%	<	0.07%	175	41	185	195
SP105	67.0%	16.8%	7.09%	1.38%	1.83%	2.73%	2.32%	0.84%	<	0.04%	104	81	242	253
SP106	75.1%	13.7%	3.17%	0.81%	3.06%	1.95%	1.58%	0.61%	<	0.03%	44	44	176	243
SP107	79.2%	10.9%	3.31%	1.60%	1.54%	1.98%	0.96%	0.46%	<	0.04%	21	42	201	211
SP108	64.1%	16.7%	7.26%	3.51%	1.49%	3.26%	2.95%	0.70%	0.02%	0.09%	68	113	249	170
SP109	73.3%	12.2%	4.04%	2.90%	3.17%	2.44%	1.37%	0.55%	<	0.04%	31	42	292	271
SP110	70.1%	13.5%	5.39%	3.30%	2.37%	2.82%	1.78%	0.62%	<	0.07%	44	76	251	240
SP111	65.0%	14.7%	5.92%	5.99%	3.00%	2.31%	2.21%	0.74%	<	0.06%	85	74	489	192
SP112	68.0%	15.8%	6.21%	2.72%	2.14%	2.92%	1.41%	0.65%	0.03%	0.13%	53	474	305	232
SP113	64.3%	16.0%	5.83%	5.34%	3.43%	2.31%	2.02%	0.73%	<	0.06%	52	63	460	188

	SiO_2	Al_2O_3	Fe_2O_3	CaO	Na_2O	K_2O	MgO	TiO_2	P_2O_5	MnO	Cr	Zn	Sr	Zr
SP114	61.7%	15.4%	8.07%	5.64%	3.35%	2.20%	2.54%	1.03%	0.03%	0.08%	61	81	405	192
SP115	65.6%	14.8%	5.93%	5.58%	2.78%	2.54%	2.02%	0.72%	0.04%	0.07%	55	65	393	164
SP116	63.2%	15.7%	7.62%	4.69%	3.11%	2.17%	2.55%	0.85%	0.06%	0.08%	72	92	368	174
SP117	58.8%	15.3%	10.99%	5.54%	3.85%	1.56%	2.50%	1.36%	0.13%	0.11%	70	109	397	159
SP118	66.2%	13.3%	6.43%	6.14%	2.52%	2.26%	2.30%	0.79%	0.02%	0.07%	42	63	358	200
SP119	61.8%	15.7%	8.14%	5.16%	3.50%	2.14%	2.48%	1.01%	<	0.08%	62	82	412	196
SP120	67.2%	14.7%	5.49%	4.05%	3.47%	2.46%	1.86%	0.68%	<	0.06%	42	63	376	177
SP121	70.9%	14.4%	4.02%	3.03%	3.44%	2.52%	1.11%	0.53%	0.02%	0.04%	20	51	336	153
SP201	69.4%	13.6%	5.50%	2.95%	4.54%	2.32%	0.84%	0.73%	<	0.08%	<	81	181	262
SP202	62.9%	15.9%	8.57%	5.32%	2.36%	1.65%	2.14%	0.94%	0.04%	0.12%	97	75	290	150
SP203	65.4%	15.5%	6.51%	5.20%	3.49%	1.47%	1.48%	0.83%	<	0.08%	83	72	320	176
SP204	65.7%	15.3%	7.47%	4.67%	2.49%	1.71%	1.71%	0.82%	<	0.10%	150	86	278	214
SP205	65.5%	14.9%	7.48%	4.39%	3.32%	1.99%	1.48%	0.88%	<	0.10%	30	81	264	203
SP206	60.8%	16.2%	9.37%	5.48%	3.17%	1.60%	1.79%	1.44%	0.13%	0.13%	115	84	471	199
SP207	68.0%	14.0%	6.25%	4.14%	3.13%	2.02%	1.53%	0.84%	<	0.08%	41	72	286	215
SP208	66.8%	14.3%	6.75%	4.93%	2.21%	1.93%	2.23%	0.82%	0.02%	0.08%	152	76	348	174
SP209	64.5%	14.6%	7.24%	5.61%	2.57%	2.21%	2.23%	0.89%	0.04%	0.09%	118	75	331	182
SP210	67.7%	14.5%	6.39%	3.88%	2.45%	2.57%	1.74%	0.77%	<	0.07%	118	75	333	161
SP211	65.9%	14.5%	7.35%	4.54%	2.52%	2.25%	2.11%	0.80%	<	0.07%	146	62	312	156
SP212	66.0%	14.6%	7.77%	4.29%	2.38%	1.99%	1.98%	0.93%	<	0.08%	250	73	312	177
SP213	68.2%	13.6%	6.39%	4.43%	2.40%	2.11%	1.95%	0.81%	<	0.07%	176	62	311	166
SP214	70.2%	13.2%	5.63%	3.70%	2.23%	2.42%	1.87%	0.68%	<	0.07%	41	61	246	154
SP215	59.3%	13.6%	8.20%	6.95%	2.02%	2.84%	6.20%	0.80%	0.04%	0.10%	69	97	305	166
SP216	69.9%	12.4%	4.81%	5.26%	2.05%	2.33%	2.57%	0.62%	<	0.05%	98	54	315	163
SP217	68.6%	14.1%	5.90%	3.98%	2.43%	2.53%	1.69%	0.76%	<	0.07%	73	73	321	187

	SiO_2	Al_2O_3	Fe_2O_3	CaO	Na_2O	K_2O	MgO	TiO_2	P_2O_5	MnO	Cr	Zn	Sr	Zr
SP218	72.1%	13.2%	4.99%	2.78%	2.27%	2.72%	1.23%	0.69%	<	0.05%	242	53	253	189
SP219	69.1%	13.9%	5.43%	3.49%	2.02%	3.64%	1.62%	0.70%	0.01%	0.07%	63	63	230	209
SP220	69.7%	13.8%	5.92%	3.49%	2.06%	2.53%	1.66%	0.78%	<	0.07%	150	64	257	225
SP221	70.7%	12.7%	5.04%	4.49%	2.01%	2.45%	1.85%	0.70%	0.02%	0.06%	64	53	265	202
SP222	67.0%	13.6%	6.21%	6.01%	1.87%	2.19%	2.14%	0.83%	<	0.07%	148	57	274	285
SP223	72.4%	12.9%	4.76%	3.16%	2.47%	2.31%	1.22%	0.75%	<	0.05%	190	42	265	254
SP224	70.6%	13.0%	5.99%	3.31%	2.83%	2.00%	1.10%	1.12%	<	0.07%	361	52	289	258
SP225	65.4%	15.4%	7.39%	4.55%	2.04%	1.69%	2.53%	0.84%	<	0.10%	127	69	393	162
SP226	68.4%	13.4%	7.18%	3.52%	2.82%	1.95%	1.23%	1.33%	0.01%	0.08%	156	62	291	280
SP227	71.1%	14.2%	4.02%	3.84%	3.23%	1.78%	1.05%	0.74%	<	0.06%	10	41	349	195
SP228	71.6%	13.2%	5.17%	3.63%	1.59%	2.25%	1.56%	0.95%	0.02%	0.08%	33	55	371	251
SP229	69.0%	14.3%	5.42%	3.84%	2.92%	2.37%	1.27%	0.82%	0.01%	0.11%	<	66	286	209
SP230	67.4%	14.6%	6.55%	3.96%	3.08%	1.73%	1.60%	1.01%	<	0.08%	31	61	306	184
SP231	67.4%	14.3%	5.90%	4.30%	3.41%	2.08%	1.71%	0.79%	0.06%	0.08%	168	63	336	200
SP232	70.8%	13.5%	5.72%	2.77%	3.05%	2.26%	1.15%	0.73%	<	0.06%	31	41	258	258
SP233	64.0%	15.5%	7.40%	5.31%	3.23%	1.59%	1.82%	1.01%	0.04%	0.09%	42	62	375	198
SP234	56.7%	14.6%	7.47%	12.04%	2.57%	1.12%	4.25%	1.14%	0.10%	0.07%	96	72	587	180
SP235	64.6%	15.1%	7.08%	4.90%	3.20%	1.69%	2.43%	0.92%	0.04%	0.07%	62	62	382	176
SP236	66.4%	14.4%	6.98%	4.23%	3.15%	1.81%	1.91%	1.01%	<	0.07%	165	52	330	155
SP237	71.4%	13.2%	3.47%	3.97%	3.18%	3.08%	1.19%	0.45%	<	0.08%	<	42	385	177
SP238	71.3%	14.0%	3.58%	2.55%	4.52%	2.26%	1.27%	0.44%	<	0.07%	<	42	187	146
SP239	70.0%	13.8%	5.12%	3.33%	2.98%	2.69%	1.20%	0.76%	<	0.07%	30	51	283	293
SP240	70.0%	14.3%	5.01%	3.65%	2.57%	2.44%	1.37%	0.67%	<	0.07%	31	51	306	224
SP241	70.5%	13.0%	6.06%	3.26%	2.59%	2.47%	1.11%	0.90%	<	0.08%	175	51	278	319
SP242	68.4%	13.1%	5.68%	5.77%	2.06%	2.34%	1.81%	0.76%	<	0.07%	57	57	286	251

	SiO_2	Al_2O_3	Fe_2O_3	CaO	Na_2O	K_2O	MgO	TiO_2	P_2O_5	MnO	Cr	Zn	Sr	Zr
SP243	70.9%	13.6%	5.18%	3.77%	2.81%	1.81%	1.12%	0.71%	<	0.07%	42	52	364	239
SP244	66.0%	13.5%	6.56%	6.67%	2.40%	2.28%	1.56%	0.85%	0.04%	0.09%	65	54	390	260
SP245	66.6%	14.3%	6.49%	5.13%	2.61%	1.60%	2.36%	0.85%	<	0.07%	62	52	310	155
SP246	69.5%	14.0%	6.01%	3.53%	2.79%	1.74%	1.48%	0.85%	<	0.07%	41	62	258	196
SP247	68.7%	14.6%	5.85%	3.78%	2.71%	1.92%	1.59%	0.75%	<	0.06%	41	51	278	165
SP248	64.2%	16.0%	7.36%	4.63%	3.11%	1.66%	2.09%	0.91%	<	0.09%	53	84	295	158
SP249	61.9%	17.6%	8.38%	4.82%	3.00%	1.34%	1.76%	1.05%	0.42%	0.13%	68	103	308	216
SP250	64.0%	16.2%	7.31%	4.89%	2.83%	1.41%	2.38%	0.79%	0.14%	0.10%	99	88	318	154
SP305	74.9%	12.0%	4.39%	2.76%	2.52%	1.62%	0.93%	0.80%	<	0.09%	55	44	286	297
SP306	76.6%	11.5%	3.59%	2.94%	2.33%	1.61%	0.80%	0.57%	<	0.05%	32	43	267	192
SP307	68.3%	14.6%	6.28%	2.65%	3.10%	2.48%	1.85%	0.73%	0.03%	0.06%	60	72	286	179
SP308	75.8%	11.9%	4.55%	2.18%	1.93%	1.88%	0.88%	0.81%	0.02%	0.07%	32	43	214	300
SP309	74.3%	12.3%	4.44%	2.97%	2.57%	1.78%	0.84%	0.77%	<	0.06%	31	52	271	239
SP310	79.3%	10.1%	3.61%	1.73%	1.99%	2.00%	0.57%	0.62%	<	0.04%	167	33	190	212
SP311	74.9%	12.0%	4.41%	2.37%	2.61%	2.19%	0.59%	0.88%	<	0.06%	53	42	275	349
SP312	75.7%	11.3%	4.65%	2.44%	2.21%	2.03%	0.87%	0.73%	<	0.06%	41	51	214	245
SP313	65.9%	15.3%	7.03%	4.36%	2.13%	2.09%	2.26%	0.86%	<	0.07%	90	79	371	180
SP314	69.4%	13.8%	5.91%	4.05%	2.62%	1.78%	1.28%	1.00%	<	0.08%	73	63	346	262
SP315	68.6%	14.8%	4.76%	4.81%	3.36%	1.63%	1.19%	0.77%	<	0.07%	20	51	378	163
SP316	67.0%	14.1%	7.24%	6.11%	0.55%	1.40%	2.72%	0.81%	<	0.08%	39	78	273	221
SP317	78.5%	11.6%	2.73%	1.63%	1.63%	2.77%	0.49%	0.58%	<	0.04%	21	32	190	349
SP318	65.1%	14.5%	7.97%	4.35%	3.45%	1.60%	1.59%	1.37%	0.03%	0.10%	61	71	374	354
SP319	67.5%	13.8%	7.13%	3.76%	3.13%	1.85%	1.69%	1.09%	0.05%	0.08%	61	71	305	223
SP320	69.8%	12.7%	6.39%	3.25%	3.24%	1.87%	1.51%	1.18%	0.07%	0.08%	43	65	291	183
SP321	73.8%	11.7%	5.57%	2.19%	2.73%	1.99%	1.11%	0.87%	<	0.07%	31	63	209	219
SP322	76.7%	11.0%	4.59%	2.32%	2.20%	1.64%	0.91%	0.64%	<	0.05%	51	51	216	247

	SiO_2	Al_2O_3	Fe_2O_3	CaO	Na_2O	K_2O	MgO	TiO_2	P_2O_5	MnO	Cr	Zn	Sr	Zr
SP323	72.4%	12.9%	5.56%	2.84%	2.38%	1.88%	1.10%	0.82%	<	0.06%	104	62	292	239
SP324	74.7%	11.8%	5.53%	1.89%	2.31%	1.86%	1.05%	0.83%	<	0.05%	93	62	196	279
SP325	65.5%	15.5%	8.13%	3.96%	1.17%	2.29%	2.66%	0.74%	<	0.08%	104	104	208	169
SP326	74.0%	13.0%	4.22%	2.38%	2.44%	2.38%	0.91%	0.62%	<	0.07%	83	52	248	186
SP327	75.1%	12.1%	4.85%	2.15%	2.09%	1.88%	1.02%	0.79%	<	0.07%	74	63	242	274
SP328	75.5%	11.7%	4.41%	2.68%	2.39%	1.70%	0.78%	0.83%	<	0.05%	61	40	252	212
SP329	82.1%	8.7%	3.28%	1.11%	1.93%	1.61%	0.57%	0.67%	<	0.03%	90	30	140	369
SP330	77.5%	11.5%	3.92%	1.80%	1.94%	1.96%	0.75%	0.63%	<	0.06%	115	52	219	271
SP331	76.8%	11.8%	4.16%	1.84%	2.11%	1.82%	0.93%	0.54%	0.05%	0.08%	74	53	211	201
SN01	84.3%	7.4%	2.25%	1.39%	0.81%	2.21%	1.31%	0.33%	<	0.02%	32	21	86	129
SN02	58.0%	11.8%	10.96%	8.36%	1.97%	1.47%	6.29%	1.04%	0.01%	0.11%	489	83	114	187
SN03	88.1%	6.2%	2.56%	0.78%	0.28%	1.05%	0.70%	0.32%	<	0.03%	51	31	31	195
SN04	64.5%	11.7%	5.77%	11.27%	0.52%	2.58%	2.82%	0.83%	<	0.05%	128	58	571	443
SN06	74.3%	11.3%	4.06%	2.89%	2.27%	2.80%	1.58%	0.77%	<	0.04%	85	32	191	297
SN07	68.9%	8.3%	5.24%	5.46%	6.27%	1.97%	2.68%	1.10%	<	0.07%	243	35	162	799
SN08	63.1%	10.5%	5.27%	8.30%	5.68%	3.35%	2.98%	0.77%	0.09%	0.08%	223	37	346	606
SN09	68.6%	8.8%	3.33%	11.56%	1.91%	2.84%	2.34%	0.53%	<	0.05%	105	30	314	538
SN010	77.0%	12.0%	1.93%	0.74%	2.00%	5.16%	0.65%	0.43%	<	0.03%	11	21	116	222
SN011	68.4%	10.2%	4.84%	9.08%	1.38%	2.39%	2.89%	0.85%	0.04%	0.05%	105	47	279	419
SN012	64.0%	9.4%	10.47%	7.70%	1.25%	1.92%	3.44%	1.76%	<	0.09%	45	67	225	270
SN013	64.1%	15.3%	7.13%	4.81%	<	3.49%	4.37%	0.74%	<	0.10%	77	77	181	219
SN014	93.1%	3.0%	0.70%	0.48%	<	0.76%	1.86%	0.13%	<	0.01%	55	11	55	100
SN015	73.0%	4.9%	2.14%	13.86%	<	1.29%	4.41%	0.36%	<	0.02%	59	83	451	214
SN016	72.5%	14.2%	4.94%	2.02%	0.29%	4.06%	1.38%	0.58%	0.12%	0.05%	76	114	114	189
SN017	85.8%	8.3%	2.22%	<	0.10%	2.83%	0.42%	0.30%	<	0.02%	87	22	55	164
SN018	74.0%	12.2%	6.09%	0.94%	0.53%	2.45%	2.63%	1.03%	<	0.07%	76	76	65	227

Appendix 9. Elemental concentration in dust (DP: Dust from Patagonia; DN: Dust from Namibia)

unit: oxide in %, trace elements in ppm

	SiO_2	Al_2O_3	Fe_2O_3	CaO	Na_2O	K_2O	MgO	TiO_2	P_2O_5	MnO	Cr	Zn	Sr	Zr
DP001	73.8%	13.0%	5.92%	1.55%	1.80%	1.80%	1.12%	0.85%	0.18%	0.17%	41	104	218	116
DP002	71.5%	13.6%	5.48%	1.78%	2.07%	2.43%	1.95%	1.08%	0.10%	0.11%	36	105	190	156
DP003	51.1%	17.7%	17.61%	4.64%	0.71%	1.66%	1.93%	4.38%	0.32%	1.82%	129	277	494	425
DP004	74.5%	12.7%	6.36%	1.46%	1.35%	1.80%	0.71%	0.83%	0.31%	0.15%	32	115	202	132
DP005	72.0%	14.8%	6.01%	1.42%	1.48%	1.96%	1.28%	0.81%	0.24%	0.06%	47	105	180	138
DP006	69.6%	13.8%	8.32%	1.96%	1.27%	2.45%	1.07%	1.15%	0.37%	0.22%	51	136	253	200
DP007	73.5%	13.5%	6.02%	1.51%	1.23%	2.45%	0.77%	0.89%	0.18%	0.18%	28	120	256	150
DP008	69.3%	13.1%	8.84%	2.30%	1.06%	3.05%	0.87%	1.21%	0.26%	0.20%	39	166	334	231
DP009	66.1%	15.5%	7.93%	2.89%	1.70%	2.41%	2.00%	1.18%	0.35%	0.60%	44	143	259	141
DP010	67.1%	15.2%	7.66%	2.87%	1.42%	2.53%	2.06%	1.07%	0.15%	0.16%	58	130	315	147
DP011	79.3%	10.6%	1.65%	2.31%	2.28%	3.41%	<	0.35%	0.08%	<	<	77	198	<
DP012	78.0%	12.6%	3.81%	0.93%	1.98%	1.81%	<	0.57%	0.27%	0.26%	52	111	79	<
DP013	72.6%	11.8%	7.08%	1.51%	1.55%	3.02%	0.79%	1.36%	0.25%	0.21%	34	172	312	262
DP014	75.4%	13.4%	4.59%	1.39%	1.45%	1.97%	0.97%	0.68%	0.23%	0.19%	25	87	134	137
DP015	78.0%	12.1%	4.59%	1.19%	1.39%	1.73%	<	0.76%	0.23%	<	<	<	<	<
DP016	72.5%	13.7%	5.94%	1.92%	1.43%	2.44%	0.99%	1.00%	0.16%	0.14%	31	112	253	168
DP017	73.1%	14.2%	5.33%	1.63%	1.56%	2.23%	0.99%	0.84%	0.18%	0.05%	25	102	198	128
DP018	74.1%	12.9%	5.38%	1.74%	1.44%	2.42%	0.88%	0.96%	0.14%	0.09%	24	97	234	161
DP019	82.2%	9.0%	3.45%	0.93%	2.05%	1.47%	<	0.72%	0.11%	<	<	<	<	<
DP020	72.5%	13.9%	5.91%	1.83%	1.38%	2.38%	1.06%	0.92%	0.15%	0.10%	35	108	228	154
DP021	72.8%	13.7%	5.89%	1.38%	1.59%	2.36%	1.04%	0.96%	0.26%	0.16%	36	112	206	155
DP022	75.4%	12.9%	5.26%	1.11%	1.69%	1.82%	0.71%	0.91%	0.19%	0.11%	31	82	178	129
DP023	64.5%	14.0%	6.14%	6.20%	3.04%	2.41%	2.91%	0.70%	0.13%	0.14%	31	103	336	71
DP024	74.6%	13.2%	5.51%	1.42%	1.48%	2.08%	0.65%	0.97%	0.09%	0.15%	37	98	210	168
DP025	75.8%	12.3%	5.18%	1.32%	1.55%	2.07%	0.71%	1.05%	0.08%	0.14%	33	95	215	169

	SiO_2	Al_2O_3	Fe_2O_3	CaO	Na_2O	K_2O	MgO	TiO_2	P_2O_5	MnO	Cr	Zn	Sr	Zr
DP026	73.2%	12.5%	6.68%	1.82%	1.51%	2.15%	0.80%	1.10%	0.27%	0.15%	40	164	279	195
DP027	74.2%	12.8%	5.55%	1.74%	1.73%	1.98%	0.91%	0.88%	0.27%	0.23%	27	94	245	135
DP028	70.4%	13.7%	7.77%	1.94%	1.44%	2.42%	0.91%	1.06%	0.37%	0.23%	46	132	272	187
DP029	71.0%	13.1%	6.86%	2.23%	1.82%	2.48%	1.10%	1.08%	0.36%	0.19%	34	137	308	172
DP030	72.5%	12.3%	6.39%	3.52%	1.28%	1.43%	0.57%	0.79%	1.23%	0.82%	<	200	188	<
DP031	65.9%	18.0%	8.53%	2.10%	0.98%	1.65%	1.73%	1.05%	0.11%	0.45%	39	133	289	148
DP032	68.5%	16.5%	7.56%	1.68%	1.62%	1.69%	1.09%	0.96%	0.36%	0.65%	25	120	296	148
DP033	76.4%	12.2%	4.53%	1.81%	1.58%	1.63%	0.92%	0.59%	0.33%	0.30%	27	125	194	80
DP034	68.1%	16.3%	5.98%	1.44%	2.10%	3.06%	2.04%	0.90%	0.10%	0.05%	56	102	174	213
DP302	61.5%	16.9%	11.16%	2.07%	1.15%	3.05%	2.99%	1.03%	0.13%	0.15%	149	124	146	<
DP303	66.3%	15.3%	8.08%	2.34%	1.10%	2.82%	2.94%	0.90%	0.19%	0.12%	98	125	217	<
DP304	70.4%	15.7%	7.06%	1.23%	1.34%	2.02%	1.16%	1.04%	0.08%	0.31%	59	108	217	154
DP101	68.2%	15.1%	6.61%	2.14%	1.02%	3.62%	2.29%	0.91%	0.11%	<	<	171	198	<
DP102	65.8%	16.6%	6.52%	1.92%	1.19%	4.11%	2.90%	0.86%	0.16%	0.17%	43	154	235	92
DP103	65.5%	18.1%	6.56%	1.48%	1.15%	3.55%	2.75%	0.78%	0.11%	<	<	132	149	152
DP104	64.4%	17.2%	6.15%	4.02%	1.34%	3.32%	2.58%	0.82%	0.15%	<	<	128	157	119
DP105	64.2%	19.0%	7.06%	1.21%	1.89%	3.31%	2.38%	0.91%	0.05%	<	69	117	451	164
DP106	64.6%	18.5%	6.61%	1.02%	2.45%	3.50%	2.12%	1.15%	0.08%	<	78	131	323	258
DP107	63.8%	18.6%	7.51%	3.00%	0.87%	3.35%	1.76%	0.99%	0.09%	<	73	126	291	154
DP108	60.8%	19.2%	7.44%	3.45%	1.07%	3.88%	3.25%	0.83%	0.11%	<	64	151	181	116
DP109	64.9%	15.5%	5.63%	10.22%	<	2.85%	<	0.86%	0.10%	<	<	<	<	<
DP110	55.4%	15.3%	6.08%	15.04%	0.96%	3.72%	2.75%	0.64%	0.10%	0.24%	37	148	206	131
DP111	58.9%	13.7%	5.72%	14.02%	1.40%	3.01%	2.48%	0.68%	0.13%	0.36%	<	122	291	97
DP112	63.4%	19.3%	7.57%	1.96%	1.23%	3.72%	1.59%	0.80%	0.36%	0.19%	50	1307	210	160
DP113	63.8%	15.6%	6.00%	6.32%	1.60%	3.62%	2.11%	0.73%	0.18%	0.32%	<	164	246	158

	SiO_2	Al_2O_3	Fe_2O_3	CaO	Na_2O	K_2O	MgO	TiO_2	P_2O_5	MnO	Cr	Zn	Sr	Zr
DP114	63.3%	15.1%	5.98%	8.47%	1.49%	2.89%	1.89%	0.75%	0.14%	0.26%	<	241	239	162
DP115	56.6%	14.6%	7.20%	12.65%	1.05%	4.28%	2.57%	0.87%	0.15%	0.31%	33	123	323	128
DP116	63.7%	17.4%	7.63%	3.26%	1.67%	3.11%	2.11%	0.94%	0.16%	0.31%	46	169	272	190
DP117	69.4%	14.5%	6.52%	3.02%	2.97%	2.60%	<	0.84%	0.15%	<	<	112	<	<
DP118	60.7%	13.8%	6.81%	9.75%	1.25%	3.28%	3.49%	0.78%	0.13%	<	40	106	260	172
DP119	65.9%	16.7%	6.34%	2.92%	2.23%	2.80%	2.07%	0.82%	0.15%	<	<	122	216	<
DP120	65.4%	15.7%	6.60%	3.60%	1.26%	3.83%	2.67%	0.79%	0.18%	0.45%	29	158	250	166
DP121	69.1%	15.8%	6.32%	2.05%	1.36%	3.00%	1.43%	0.77%	0.19%	0.41%	<	172	188	181
DP201	71.3%	14.2%	4.68%	2.09%	3.66%	3.27%	<	0.64%	0.12%	<	80	64	118	356
DP202	66.8%	16.5%	7.06%	4.06%	1.30%	2.28%	1.02%	0.85%	0.14%	0.08%	76	83	225	223
DP203	70.2%	15.4%	6.18%	2.60%	1.94%	2.75%	<	0.82%	0.17%	<	117	<	<	483
DP204	67.6%	15.7%	7.08%	3.16%	1.76%	2.34%	1.25%	0.89%	0.17%	0.08%	50	112	172	284
DP205	71.1%	14.9%	5.23%	2.32%	2.62%	3.03%	<	0.69%	0.13%	<	65	77	<	436
DP206	68.8%	14.4%	6.52%	3.04%	2.70%	2.90%	0.65%	0.85%	0.13%	0.08%	53	94	238	332
DP207	67.8%	15.5%	6.34%	3.07%	2.18%	2.68%	1.38%	0.80%	0.18%	0.09%	140	119	<	244
DP208	64.7%	16.3%	7.75%	4.57%	0.59%	2.27%	2.66%	1.03%	0.12%	0.07%	115	104	<	<
DP209	64.2%	16.1%	6.27%	5.27%	1.60%	2.97%	2.59%	0.81%	0.19%	0.12%	107	76	210	189
DP210	69.0%	16.8%	7.24%	2.96%	<	2.78%	<	1.04%	0.20%	<	<	123	<	<
DP211	65.6%	17.3%	8.41%	3.95%	<	2.35%	1.14%	1.11%	0.17%	<	228	78	<	<
DP212	64.7%	19.1%	8.81%	2.72%	<	2.33%	1.03%	1.22%	0.16%	<	244	<	<	<
DP213	65.5%	16.1%	7.99%	4.66%	<	2.44%	2.20%	1.00%	0.16%	<	204	61	<	<
DP214	60.0%	16.7%	8.72%	6.05%	0.60%	3.15%	3.49%	1.07%	0.19%	0.11%	105	126	<	<
DP215	61.4%	15.5%	7.47%	8.51%	<	3.34%	2.72%	0.94%	0.18%	<	648	<	<	<
DP216	56.6%	14.3%	7.03%	14.47%	<	2.74%	3.78%	0.93%	0.14%	0.11%	459	<	<	<
DP217	66.1%	16.5%	7.99%	3.67%	<	2.60%	1.99%	1.04%	0.17%	0.08%	164	132	<	<

	SiO_2	Al_2O_3	Fe_2O_3	CaO	Na_2O	K_2O	MgO	TiO_2	P_2O_5	MnO	Cr	Zn	Sr	Zr
DP218	65.1%	17.0%	8.76%	2.67%	0.72%	2.50%	1.96%	1.10%	0.20%	0.07%	12	105	<	<
DP219	67.8%	17.3%	7.94%	3.16%	<	2.55%	<	1.03%	0.18%	<	244	<	<	<
DP220	68.6%	17.0%	7.94%	2.70%	<	2.57%	<	1.03%	0.15%	<	240	<	<	<
DP221	67.0%	16.4%	6.47%	6.56%	<	2.49%	<	0.92%	0.17%	<	98	<	<	<
DP222	63.6%	15.4%	7.21%	7.16%	<	2.66%	2.94%	0.89%	0.15%	0.17%	43	75	<	246
DP223	66.4%	15.8%	7.36%	3.18%	0.86%	2.93%	2.32%	0.95%	0.17%	0.08%	51	104	203	209
DP224	72.3%	14.0%	5.30%	2.81%	1.26%	2.20%	0.94%	0.96%	0.16%	0.07%	31	57	270	239
DP225	64.4%	16.8%	7.98%	4.41%	1.14%	2.24%	1.91%	0.92%	0.14%	0.03%	47	78	408	<
DP226	68.9%	15.0%	6.93%	3.41%	1.03%	2.28%	1.19%	1.04%	0.18%	0.07%	22	78	320	174
DP227	74.9%	13.5%	5.17%	2.29%	0.75%	1.64%	0.57%	0.97%	0.13%	0.02%	15	69	201	289
DP228	77.5%	11.7%	3.66%	2.15%	0.30%	2.91%	1.07%	0.65%	0.11%	0.01%	8	14	198	266
DP229	72.5%	14.1%	4.78%	2.24%	1.38%	3.66%	0.50%	0.74%	0.13%	<	36	37	<	<
DP230	67.1%	16.2%	7.03%	3.34%	1.36%	2.22%	1.27%	1.28%	0.16%	0.05%	<	65	261	299
DP231	65.8%	14.8%	7.91%	4.34%	1.18%	2.46%	2.26%	1.08%	0.22%	0.26%	28	123	340	250
DP232	64.4%	17.8%	8.46%	3.46%	1.33%	2.12%	0.94%	1.30%	0.23%	0.18%	26	80	209	<
DP233	66.1%	16.3%	7.80%	3.28%	1.43%	2.12%	1.67%	1.09%	0.23%	0.14%	33	96	154	232
DP234	50.8%	13.0%	8.02%	19.24%	1.55%	1.64%	4.39%	1.27%	0.15%	0.37%	34	103	699	188
DP235	62.6%	16.1%	8.65%	4.30%	1.85%	2.43%	2.67%	1.26%	0.17%	0.03%	71	113	237	<
DP236	68.6%	14.7%	6.49%	2.82%	0.80%	3.17%	2.43%	0.84%	0.13%	<	65	86	<	<
DP237	75.2%	11.6%	3.21%	2.54%	1.18%	4.69%	1.03%	0.47%	0.09%	0.01%	<	44	330	152
DP238	72.4%	12.6%	5.34%	1.99%	0.84%	4.19%	1.85%	0.68%	0.14%	0.02%	<	85	107	207
DP239	73.6%	13.0%	4.66%	1.98%	1.27%	3.79%	0.84%	0.75%	0.13%	<	<	44	152	211
DP240	71.7%	13.9%	4.25%	1.91%	0.73%	5.55%	1.18%	0.63%	0.14%	0.02%	9	74	119	176
DP241	73.2%	13.6%	4.46%	2.35%	1.34%	3.17%	1.01%	0.71%	0.12%	0.01%	12	66	227	184
DP242	65.3%	14.7%	6.58%	8.08%	<	2.65%	1.65%	0.84%	0.16%	0.05%	37	70	<	<

	SiO_2	Al_2O_3	Fe_2O_3	CaO	Na_2O	K_2O	MgO	TiO_2	P_2O_5	MnO	Cr	Zn	Sr	Zr
DP243	75.5%	12.4%	4.45%	2.36%	1.61%	2.27%	0.50%	0.70%	0.11%	<	6	55	245	227
DP244	69.5%	13.6%	6.38%	4.77%	<	3.31%	1.49%	0.84%	0.15%	0.06%	20	73	241	<
DP245	65.7%	15.8%	7.43%	3.83%	<	2.53%	3.68%	0.85%	0.13%	0.05%	31	67	<	<
DP246	65.7%	16.7%	7.66%	3.34%	1.50%	2.21%	1.49%	1.13%	0.26%	0.11%	28	110	255	218
DP247	61.9%	18.0%	9.65%	3.88%	1.18%	2.02%	1.83%	1.28%	0.23%	0.13%	31	119	282	238
DP248	65.5%	16.2%	7.86%	3.58%	1.80%	2.17%	1.38%	1.29%	0.18%	0.19%	52	138	229	240
DP249	56.1%	19.4%	12.69%	5.04%	1.54%	1.78%	1.32%	1.72%	0.41%	1.21%	37	222	367	436
DP250	55.0%	21.3%	12.85%	4.54%	1.15%	1.36%	1.91%	1.54%	0.34%	1.28%	67	186	351	261
DP305	75.1%	12.9%	4.69%	1.66%	1.60%	2.05%	0.71%	1.02%	0.21%	0.06%	<	70	215	<
DP306	74.8%	13.9%	4.81%	2.17%	0.90%	2.11%	0.39%	0.76%	0.15%	0.09%	43	<	<	<
DP307	64.2%	15.2%	7.70%	3.79%	2.32%	3.49%	2.04%	1.09%	0.13%	0.07%	31	107	348	199
DP308	73.3%	13.2%	5.86%	1.96%	1.21%	2.44%	0.82%	0.99%	0.19%	0.11%	16	76	217	146
DP309	68.6%	14.4%	7.01%	2.58%	1.98%	2.77%	1.30%	1.15%	0.22%	0.21%	33	121	292	303
DP310	73.8%	13.0%	5.78%	1.99%	1.05%	2.40%	0.79%	0.97%	0.14%	0.10%	35	88	225	197
DP311	76.2%	11.8%	4.50%	1.62%	1.58%	2.66%	0.34%	1.16%	0.11%	<	57	48	228	294
DP312	72.0%	13.9%	5.96%	2.21%	1.16%	2.41%	1.14%	1.04%	0.15%	0.13%	27	89	267	205
DP313	66.3%	15.3%	7.53%	2.91%	1.25%	2.96%	2.62%	0.96%	0.17%	0.06%	56	112	334	<
DP314	69.7%	14.4%	6.25%	3.29%	1.48%	2.32%	1.41%	0.97%	0.16%	0.19%	54	95	353	213
DP315	72.0%	14.6%	5.01%	2.92%	1.14%	2.50%	0.58%	0.93%	0.33%	0.14%	<	108	200	<
DP316	68.3%	13.3%	5.69%	8.35%	<	1.43%	2.14%	0.72%	0.12%	0.06%	84	97	343	<
DP317	78.5%	12.1%	2.93%	1.48%	1.08%	2.72%	0.43%	0.67%	0.06%	<	<	43	184	231
DP318	66.7%	15.9%	6.49%	3.71%	2.81%	1.95%	0.88%	1.43%	0.17%	0.06%	36	74	384	286
DP319	66.0%	16.3%	7.08%	3.70%	1.92%	2.30%	1.34%	1.13%	0.19%	0.19%	30	118	401	<
DP320	67.0%	14.7%	7.37%	3.44%	2.11%	2.44%	1.45%	1.34%	0.23%	0.22%	32	115	354	316
DP321	66.7%	16.4%	7.45%	2.22%	1.64%	2.92%	1.22%	1.30%	0.19%	0.16%	74	111	194	291
DP322	68.4%	15.0%	6.64%	2.80%	1.66%	2.92%	1.31%	1.11%	0.17%	0.13%	36	101	278	248

	SiO_2	Al_2O_3	Fe_2O_3	CaO	Na_2O	K_2O	MgO	TiO_2	P_2O_5	MnO	Cr	Zn	Sr	Zr
DP323	69.8%	14.7%	6.37%	2.47%	1.54%	2.77%	0.98%	1.10%	0.27%	0.10%	33	98	338	203
DP324	70.8%	14.4%	6.17%	1.87%	1.54%	2.84%	1.12%	1.08%	0.13%	0.09%	26	69	221	256
DP325	66.0%	15.8%	7.07%	4.27%	1.20%	2.61%	2.00%	0.90%	0.13%	0.04%	62	114	276	<
DP326	71.5%	14.5%	6.11%	1.70%	1.35%	2.60%	0.93%	1.14%	0.18%	0.08%	41	106	216	<
DP327	73.0%	13.5%	6.01%	1.70%	1.13%	2.48%	0.90%	1.12%	0.13%	0.06%	68	101	173	332
DP328	74.5%	12.9%	4.99%	1.84%	1.41%	2.44%	0.73%	0.98%	0.16%	0.07%	26	78	260	208
DP329	75.8%	12.3%	4.46%	1.73%	1.55%	2.31%	0.66%	1.03%	0.13%	0.06%	20	74	267	189
DP330	78.1%	11.6%	4.37%	1.42%	0.92%	2.17%	0.50%	0.77%	0.14%	0.04%	12	82	159	181
DP331	77.2%	11.9%	4.44%	1.28%	1.30%	2.22%	0.54%	0.95%	0.18%	0.07%	20	93	191	199
DN001	52.0%	17.8%	10.50%	7.34%	0.34%	4.75%	6.05%	1.02%	0.19%	0.26%	128	134	315	170
DN002	60.0%	16.5%	8.84%	4.46%	0.89%	4.33%	3.57%	1.21%	0.14%	0.21%	118	136	169	205
DN003	60.4%	19.0%	9.50%	2.95%	0.23%	4.35%	2.24%	1.12%	0.23%	0.23%	150	152	77	203
DN004	43.8%	13.6%	6.65%	27.33%	0.18%	3.15%	4.43%	0.70%	0.14%	0.35%	137	103	1836	170
DN006	57.8%	17.6%	10.06%	4.80%	0.72%	3.44%	4.47%	0.94%	0.20%	0.31%	216	130	254	159
DN007	44.0%	11.7%	7.30%	25.13%	<	3.33%	7.67%	0.70%	0.11%	0.82%	233	98	397	<
DN008	40.9%	13.5%	8.30%	17.53%	0.42%	4.37%	13.95%	0.93%	0.12%	0.53%	128	138	583	<
DN009	52.8%	13.3%	8.04%	8.17%	1.16%	3.60%	11.99%	0.86%	0.13%	0.95%	168	143	211	127
DN010	59.8%	19.1%	8.45%	1.21%	0.46%	4.50%	5.32%	0.93%	0.26%	0.22%	98	150	140	171
DN011	49.3%	15.8%	8.25%	14.64%	0.30%	3.64%	6.98%	0.87%	0.19%	0.75%	101	120	466	139
DN012	54.4%	12.6%	10.00%	12.16%	0.26%	2.50%	7.30%	0.70%	0.14%	0.35%	36	98	294	137
DN013	61.9%	18.8%	7.09%	1.68%	<	4.45%	5.08%	0.85%	0.09%	<	85	80	78	129
DN014	65.7%	13.3%	4.95%	1.99%	<	2.68%	10.56%	0.69%	0.14%	0.28%	90	72	344	105
DN015	41.5%	15.5%	5.26%	24.95%	<	4.30%	7.57%	0.83%	0.08%	0.35%	89	246	1249	129
DN016	60.7%	19.7%	7.81%	4.58%	<	3.86%	2.10%	1.04%	0.13%	0.44%	97	223	98	101
DN017	58.6%	23.9%	10.44%	0.63%	<	3.42%	1.64%	1.17%	0.21%	0.14%	240	145	74	158
DN018	48.1%	24.7%	13.26%	2.63%	0.19%	5.04%	4.92%	0.92%	0.23%	0.23%	134	180	102	387

Appendix 10. Coordinates of soil samples and total mass of dust generated from soil (DP: Dust from Patagonia; DN: Dust from Namibia)

Dust samples were produced from parent soil using SyGAVib. Total mass of dust collected (μg) on each filter was estimated by summing up the mass of major oxides.

	longitude	latitude	mass of dust (μg)
DP001	-69.1524	-51.8954	1445
DP002	-68.4038	-52.3520	1319
DP003	-69.5326	-52.0938	2410
DP004	-70.1661	-51.4622	1172
DP005	-70.4070	-51.2817	613
DP006	-71.1558	-50.7714	2266
DP007	-71.5080	-50.3683	1537
DP008	-71.8119	-50.2997	2797
DP009	-72.3358	-50.3231	371
DP010	-72.5170	-50.3494	768
DP011	-73.0075	-50.4738	185
DP012	-72.6984	-50.4131	225
DP013	-72.4899	-50.4117	3040
DP014	-71.6739	-50.3072	446
DP015	-71.5570	-50.2809	157
DP016	-71.5011	-50.2628	1798
DP017	-71.4334	-50.2445	652
DP018	-71.3631	-50.2556	1028
DP019	-70.9132	-50.2928	72
DP020	-70.3199	-50.2952	1846
DP021	-69.5089	-50.8381	994
DP022	-69.5556	-50.9629	784
DP023	-69.5346	-51.0719	362
DP024	-69.5266	-51.2544	1138
DP025	-69.5539	-51.3783	1831
DP026	-69.6096	-51.5496	2252
DP027	-69.3192	-51.6004	1465
DP028	-70.8214	-50.9999	2120
DP029	-71.6741	-51.0808	1977
DP030	-72.1937	-51.3210	179
DP031	-72.1997	-51.3724	1358
DP032	-72.0188	-51.9898	1474
DP033	-70.5983	-52.6030	517
DP034	-69.3263	-51.6017	1222

	longitude	latitude	mass of dust (μg)
DP101	-64.6439	-30.6872	115
DP102	-63.6158	-30.6067	531
DP103	-66.7003	-30.1022	269
DP104	-67.8667	-30.0667	258
DP105	-67.9003	-30.1158	825
DP106	-67.9136	-30.0844	1490
DP107	-67.8844	-30.0844	850
DP108	-67.4669	-31.5594	531
DP109	-68.2058	-31.6694	15
DP110	-69.3603	-31.9903	275
DP111	-68.6583	-34.2639	303
DP112	-68.5539	-34.6736	422
DP113	-68.6253	-34.7919	311
DP114	-69.1439	-34.9667	205
DP115	-69.5875	-35.4197	382
DP116	-69.6633	-35.2308	571
DP117	-69.8003	-35.5167	107
DP118	-69.6925	-35.4931	216
DP119	-69.4250	-35.0403	156
DP120	-67.1439	-35.0342	515
DP121	-66.2381	-35.1556	255
DP201	-70.5678	-41.0225	288
DP202	-70.5678	-41.0225	282
DP203	-70.4000	-41.0553	131
DP204	-70.2064	-41.1397	453
DP205	-70.0744	-41.2525	214
DP206	-69.7306	-41.3511	398
DP207	-69.4844	-41.3203	244
DP208	-68.8131	-41.2656	197
DP209	-68.5178	-41.1692	310
DP210	-68.3267	-41.0250	40
DP211	-67.8656	-40.7114	67
DP212	-67.5453	-40.5308	67
DP213	-66.9614	-40.4511	93
DP214	-66.2917	-40.6292	242
DP215	-66.0492	-40.4278	29
DP216	-66.0492	-40.4131	35
DP217	-65.6433	-40.8467	92
DP218	-65.3792	-41.2250	239
DP219	-65.3022	-41.6067	32
DP220	-65.2956	-42.0419	48
DP221	-65.1717	-42.3875	18

	longitude	latitude	mass of dust (μg)
DP222	-65.2683	-43.1389	277
DP223	-65.6275	-43.6783	401
DP224	-66.4211	-44.5156	455
DP225	-67.8247	-45.8386	188
DP226	-68.1497	-45.7683	340
DP227	-68.8225	-45.7317	323
DP228	-69.3425	-45.5111	382
DP229	-69.5636	-45.4631	168
DP230	-69.9172	-45.3314	241
DP231	-70.1369	-44.8297	510
DP232	-70.3231	-44.6386	185
DP233	-70.4186	-44.0089	298
DP234	-70.2136	-43.8006	442
DP235	-69.7811	-43.7408	210
DP236	-69.2975	-43.8033	164
DP237	-68.8478	-43.8642	484
DP238	-68.4394	-43.8683	433
DP239	-68.1072	-43.8497	325
DP240	-67.6717	-43.8069	494
DP241	-67.2858	-43.6825	485
DP242	-67.2028	-43.6861	101
DP243	-67.2928	-43.6886	357
DP244	-68.7686	-43.8328	216
DP245	-70.2172	-43.5731	155
DP246	-70.5128	-43.5703	419
DP247	-70.8772	-43.3950	518
DP248	-70.9339	-43.0817	713
DP249	-71.5108	-42.5192	1732
DP250	-71.4356	-41.8631	1221
DP302	-68.1377	-53.6865	252
DP303	-68.7419	-53.1408	326
DP304	-68.9822	-52.9016	619
DP305	-68.9032	-50.1503	356
DP306	-68.7051	-49.8238	138
DP307	-68.6506	-49.7833	654
DP308	-68.0378	-49.2643	614
DP309	-67.6711	-49.0697	811
DP310	-67.6835	-48.2126	633
DP311	-67.4646	-47.8190	498
DP312	-66.8101	-47.3741	687
DP313	-67.3842	-46.6351	321
DP314	-68.3033	-46.6822	502
DP315	-69.2337	-46.5750	157
DP316	-69.6022	-46.7158	184
DP317	-69.6079	-46.7423	572

	longitude	latitude	mass of dust (μg)
DP318	-70.2516	-46.4442	296
DP319	-70.8001	-46.5318	338
DP320	-70.7610	-46.8315	946
DP321	-70.9897	-47.2889	415
DP322	-70.9550	-47.4799	699
DP323	-70.8281	-47.7541	437
DP324	-70.7472	-48.3644	651
DP325	-70.5378	-48.7192	330
DP326	-69.7221	-48.7113	342
DP327	-69.8723	-48.7943	360
DP328	-69.9914	-49.2523	803
DP329	-70.0805	-49.5092	927
DP330	-70.9949	-49.4928	713
DP331	-72.0740	-49.9349	878
DN01	17.6431	-24.0396	539
DN02	17.7711	-24.4431	1503
DN03	16.9134	-24.9001	622
DN04	16.0920	-24.5024	562
DN05	15.2845	-24.7186	no observed dust generation
DN06	15.9781	-23.8589	599
DN07	15.1578	-23.5414	163
DN08	14.5382	-22.6157	283
DN09	13.9859	-21.7308	682
DN10	14.8437	-20.9766	571
DN11	14.3321	-20.4876	634
DN12	14.2047	-19.8080	539
DN13	14.9737	-19.5588	371
DN14	17.2997	-18.8266	622
DN15	17.3087	-19.6853	766
DN16	16.8647	-20.6619	337
DN17	16.8496	-21.4530	461
DN18	17.0574	-22.3063	842

Appendix 11. Photo of soil sampling

Sampling period of parent soils:

Patagonia (SP)
1. DP0XX: November - December 2011
2. DP1XX: July – August 2012
3. DP2XX: March 2013
4. DP3XX: March-April 2014

Namibia (SN)
5. DNXX: July – August 2013

Sampling period 1 *Patagonia*

SP001
1-Dec-2011

SP002
1-Dec-2011

SP003
3-Dec-2011

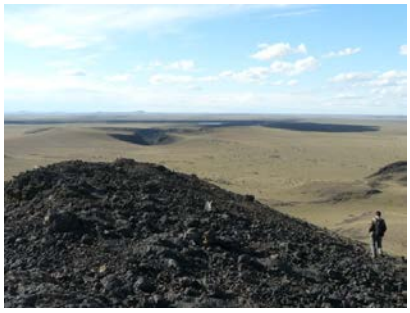

SP004
4-Dec-2011

SP005
4-Dec-2011

SP006
4-Dec-2011

SP007
4-Dec-2011

SP008
4-Dec-2011

SP009
4-Dec-2011

SP010
5-Dec-2011

SP011
5-Dec-2011

SP012
5-Dec-2011

SP013
5-Dec-2011

SP014
6-Dec-2011

SP015
6-Dec-2011

SP016
6-Dec-2011

SP017
6-Dec-2011

SP018
6-Dec-2011

SP019
6-Dec-2011

SP020
6-Dec-2011

SP021
6-Dec-2011

SP022
6-Dec-2011

SP023
6-Dec-2011

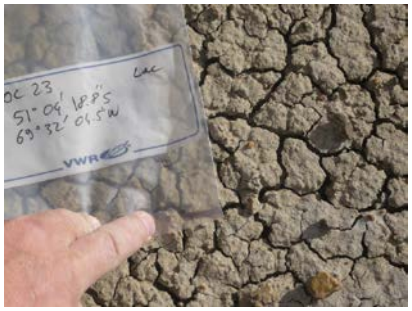

SP024
6-Dec-2011

SP025
6-Dec-2011

SP026
6-Dec-2011

SP027
28-Nov-2011

SP028
8-Dec-2011

SP029
8-Dec-2011

SP030
8-Dec-2011

SP031
8-Dec-2011

SP032
9-Dec-2011

SP033
9-Dec-2011

SP034
1-Dec-2011

Sampling period 2

Patagonia

SP101
29-Jul-2012

SP102
29-Jul-2012

SP103
29-Jul-2012

SP104
30-Jul-2012

SP105
30-Jul-2012

SP106
30-Jul-2012

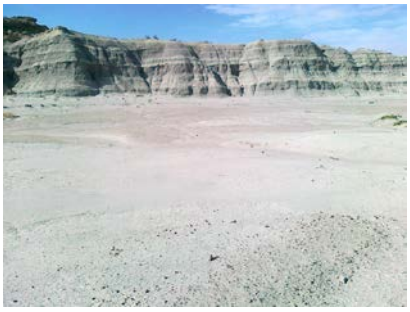

SP107
30-Jul-2012

SP108
31-Jul-2012

SP109
31-Jul-2012

SP110
1-Aug-2012

SP111
3-Aug-2012

SP112
3-Aug-2012

SP113
3-Aug-2012

SP114
3-Aug-2012

SP115
4-Aug-2012

SP116
4-Aug-2012

SP117
5-Aug-2012

SP118
5-Aug-2012

SP119
5-Aug-2012

SP120
6-Aug-2012

SP121
6-Aug-2012

Sampling period 3

Patagonia

SP201
16-Mar-2013

SP202
16-Mar-2013

SP203
16-Mar-2013

SP204
16-Mar-2013

SP205
16-Mar-2013

SP206
16-Mar-2013

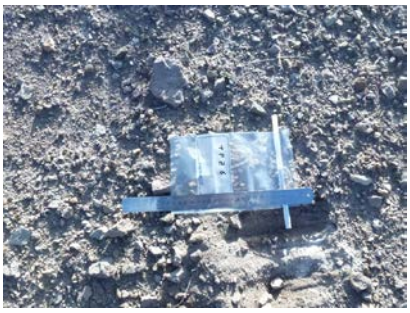

SP207
17-Mar-2013

SP208
17-Mar-2013

SP209
17-Mar-2013

SP210
17-Mar-2013

SP211
17-Mar-2013

SP212
17-Mar-2013

SP213
17-Mar-2013

SP214
17-Mar-2013

SP215
18-Mar-2013

SP216
18-Mar-2013

SP217
18-Mar-2013

SP218
18-Mar-2013

SP219
18-Mar-2013

SP220
18-Mar-2013

SP221
18-Mar-2013

SP222
20-Mar-2013

SP223
20-Mar-2013

SP224
20-Mar-2013

SP225
22-Mar-2013

SP226
22-Mar-2013

SP227
22-Mar-2013

SP228
23-Mar-2013

SP229
23-Mar-2013

SP230
23-Mar-2013

SP231
23-Mar-2013

SP232
23-Mar-2013

SP233
23-Mar-2013

SP234
23-Mar-2013

SP235
23-Mar-2013

SP236
23-Mar-2013

SP237
23-Mar-2013

SP238
23-Mar-2013

SP239
23-Mar-2013

SP240
23-Mar-2013

SP241
24-Mar-2013

SP242
24-Mar-2013

SP243
24-Mar-2013

SP244
24-Mar-2013

SP245
24-Mar-2013

SP246
24-Mar-2013

SP247
24-Mar-2013

SP248
24-Mar-2013

SP249
25-Mar-2013

SP250
25-Mar-2013

Sampling period 4

Patagonia

SP302
28-Mar-2014

SP303
29-Mar-2014

SP304
29-Mar-2014

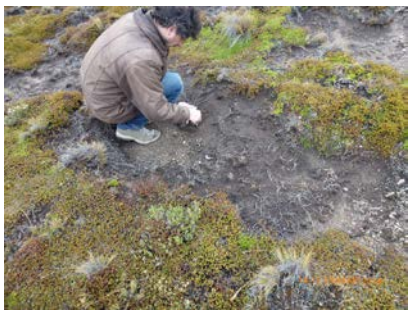

SP305
30-Mar-2014

SP306
30-Mar-2014

SP307
30-Mar-2014

SP308
31-Mar-2014

SP309
1-Apr-2014

SP310
1-Apr-2014

SP311
1-Apr-2014

SP312
1-Apr-2014

SP313
1-Apr-2014

SP314
1-Apr-2014

SP315
2-Apr-2014

SP316
2-Apr-2014

SP317
2-Apr-2014

SP318
2-Apr-2014

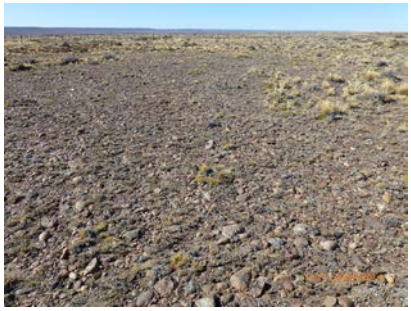

SP319
2-Apr-2014

SP320
2-Apr-2014

SP321
2-Apr-2014

SP322
2-Apr-2014

SP323
2-Apr-2014

SP324
2-Apr-2014

SP325
2-Apr-2014

SP326
3-Apr-2014

SP327
3-Apr-2014

SP328
3-Apr-2014

SP329
3-Apr-2014

SP330
3-Apr-2014

SP331
3-Apr-2014

Sampling period 5
SN01
23-Jul-2013

Namibia
SN02
25-Jul-2013

SN03
25-Jul-2013

SN04
26-Jul-2013

SN05
27-Jul-2013

SN06
29-Jul-2013

SN07
29-Jul-2013

SN08
30-Jul-2013

SN09
31-Jul-2013

SN10
2-Aug-2013

SN11
2-Aug-2013

SN12
3-Aug-2013

SN13
4-Aug-2013

SN14
7-Aug-2013

SN15
7-Aug-2013

SN16
7-Aug-2013

SN17
8-Aug-2013

SN18
8-Aug-2013

Appendix 12. Mass of elements, differential Solubility and pH after leaching

Mass of elements on each filter according to ICP-AES analysis (unit: ng)

Ident	Fe	Al	Si	Ti	Zn	Ca	K	Mg	Mn	Sr	Ba
DP001	58876	83093	496864	7198	152	15338	22467	10975	2320	317	691
DP003	282957	298184	562604	66889	596	69201	35437	50765	6613	966	1795
DP015	3788	5844	57149	523	19	1976	2010	783	340	18	62
DP109	541	771	4949	118	5	1262	2221	261	20	6	7
DP115	10215	16245	100541	1204	31	22421	9208	4124	348	81	172
DP201	4066	8908	95913	572	14	2008	4122	502	128	22	112
DP213	4326	6588	28534	534	11	2883	3089	1790	120	23	50
DP219	2833	2501	10157	585	10	2960	1031	743	91	18	22
DP230	6381	11245	75657	1128	21	3763	3565	1575	195	50	81
DP243	8795	20494	126063	1299	34	6278	7750	2062	296	92	180
DP303	10711	14343	100809	1064	33	3779	5664	3805	358	48	105
DP316	2747	5403	58775	373	7	4769	1685	1408	100	30	41
DP326	7335	12480	114301	1279	19	2656	6511	1357	318	47	129
DN006	16383	20699	160922	1518	57	8095	8371	6256	538	57	178
DN007	7282	8133	33167	603	29	24019	4516	6349	139	57	47

Differential Solubility and pH after leaching

Results of differential solubility are presented for each filter. Data of results are presented as two parts: first part for normal dust and second part for Ca-rich dust.

Normal dust

Differential solubility for DP001 (unit: %)

	pH	Fe	Al	Si	Ti	Zn	Ca	K	Mg	Mn	Sr	Ba
pH7a	4.95	1.88	1.06	0.21	0.88	4.80	6.72	4.87	6.13	5.30	3.53	2.07
pH7b	4.92	0.76	0.50	0.11	0.31	1.07	2.57	0.68	1.46	1.86	1.14	1.24
pH7c	5.28	0.21	0.11	0.00	0.18	-0.75	0.52	0.31	0.66	0.49	0.44	0.00
pH5a	4.82	0.96	0.60	0.13	0.36	2.43	3.92	0.85	2.78	3.10	2.17	1.28
pH5b	4.97	0.83	0.54	0.12	0.37	2.89	1.74	0.57	1.21	2.13	0.99	0.95
pH5c	4.99	0.44	0.26	0.06	0.21	-0.50	0.54	0.45	0.76	1.01	0.56	0.37
pH3a	3.1	-0.84	-0.40	-0.16	-0.48	3.83	9.12	0.62	2.71	1.68	4.85	5.49
pH3b	3.07	0.76	0.58	0.11	0.29	0.94	-0.01	0.77	0.67	1.28	0.58	1.32
pH3c	3.07	0.37	0.33	0.05	0.14	0.92	0.81	0.45	0.35	0.97	0.28	0.78
pH1a	1.23	0.34	1.65	0.03	0.19	3.58	1.98	2.30	0.12	-0.42	0.34	2.33
pH1b	1.22	0.47	0.43	0.03	0.29	-0.01	1.09	0.65	0.84	0.37	0.17	0.41
pH1c	1.25	1.08	0.67	0.14	0.48	3.95	0.65	0.62	1.35	1.30	0.47	0.99

Differential solubility for DP003 (unit: %)

	pH	Fe	Al	Si	Ti	Zn	Ca	K	Mg	Mn	Sr	Ba
pH7a	5.48	2.81	2.95	1.20	3.25	2.58	6.73	5.97	2.20	3.08	10.05	4.89
pH7b	5.64	0.07	-0.02	0.00	0.09	0.21	0.63	0.10	0.11	0.13	0.72	-0.15
pH7c	5.51	1.57	1.98	0.66	1.85	1.44	1.65	0.90	0.85	1.60	2.90	2.55
pH5a	5.09	-0.24	-0.46	-0.10	-0.40	0.10	2.52	0.42	0.25	-0.23	4.03	0.26
pH5b	5.17	1.06	0.89	0.37	1.23	0.75	1.53	0.70	0.55	1.03	2.74	1.70
pH5c	5.13	0.94	1.11	0.42	1.09	0.91	0.70	0.49	0.44	1.09	1.55	1.43
pH3a	3.06	-0.01	0.73	0.02	-0.14	1.31	3.61	0.84	0.24	0.10	7.86	7.76
pH3b	3.07	2.40	2.71	1.08	2.81	2.40	1.20	1.33	1.18	2.44	2.33	4.15
pH3c	3.05	-0.69	-0.68	-0.35	-0.91	-0.46	0.01	-0.15	-0.30	-0.79	0.09	0.44
pH1a	1.22	-1.09	0.82	-0.42	-1.46	0.90	1.05	0.95	-0.52	-1.47	2.13	6.58
pH1b	1.25	0.30	1.40	0.23	0.27	1.01	0.08	0.46	0.13	0.20	0.20	0.83
pH1c	1.21	1.04	2.22	0.43	1.02	1.28	0.64	0.86	0.68	1.11	0.95	1.17

Differential solubility for DP015 (unit: %)

	pH	Fe	Al	Si	Ti	Zn	Ca	K	Mg	Mn	Sr	Ba
pH7a	5.47	9.28	4.83	<	3.49	21.06	22.4	14.26	14.69	25.69	8.74	7.88
pH7b	5.6	-1.02	0.44	<	-0.85	2.17	2.5	1.14	1.72	5.22	0.63	1.19
pH7c	5.54	0.36	1.03	<	0.32	-13.47	5.8	1.06	2.28	2.64	1.40	2.75
pH5a	5.06	-1.41	-0.78	<	-1.24	25.49	12.8	0.30	2.31	6.09	1.96	2.88
pH5b	5.06	1.94	1.76	<	0.93	-1.73	1.6	1.71	2.65	3.93	2.17	1.26
pH5c	5.11	1.03	1.01	<	0.45	-13.04	-1.7	1.07	1.53	2.27	1.25	0.03
pH3a	2.94	-0.08	0.90	<	-0.05	30.22	14.5	1.95	1.66	5.00	1.71	17.22
pH3b	2.98	1.93	2.05	<	-0.61	-22.67	0.1	1.83	2.60	2.48	1.82	-3.97
pH3c	2.98	0.41	0.67	<	0.88	<	5.3	0.51	1.04	0.75	0.84	2.85
pH1a	1.07	1.16	3.08	<	-0.66	42.69	18.2	2.73	0.49	-1.01	0.38	13.33
pH1b	1.05	0.77	0.33	<	<	-32.02	-12.7	1.07	1.21	0.35	-0.30	-3.92
pH1c	1.05	1.08	1.16	<	0.88	35.11	18.0	0.90	1.97	0.95	1.59	10.24

Differential solubility for DP201 (unit: %)

	pH	Fe	Al	Si	Ti	Zn	Ca	K	Mg	Mn	Sr	Ba
pH7a	5.56	1.13	0.41	<	0.98	<	1.92	1.61	<	4.12	1.38	<
pH7b	5.6	0.02	0.13	<	-0.13	<	0.64	0.11	<	1.09	-1.04	1.22
pH7c	5.69	-0.15	0.02	<	0.00	<	0.12	0.03	<	0.58	<	0.19
pH5a	5.06	0.17	0.09	<	0.16	<	0.79	0.08	<	1.47	1.56	0.73
pH5b	5.03	-0.20	-0.08	<	-0.37	<	0.18	-0.02	<	0.25	-1.17	-1.17
pH5c	5.02	0.26	0.22	<	<	<	0.41	0.10	<	1.10	<	0.87
pH3a	2.98	0.37	0.34	<	<	<	1.08	0.28	<	1.36	2.34	0.62
pH3b	2.99	-0.21	-0.06	<	<	<	0.10	-0.12	<	0.01	-1.76	0.11
pH3c	3	0.14	0.16	<	<	<	-0.19	0.08	<	0.07	<	-0.79
pH1a	1.03	0.15	0.21	<	<	<	-0.04	0.08	<	-0.15	<	1.32
pH1b	1.02	0.21	0.16	<	<	<	-0.65	0.09	<	0.25	<	-0.99
pH1c	1.02	0.09	0.13	<	<	<	1.01	0.08	10.25	0.32	<	<

Differential solubility for DP213 (unit: %)

	pH	Fe	Al	Si	Ti	Zn	Ca	K	Mg	Mn	Sr	Ba
pH7a	5.7	1.50	1.63	<	1.25	<	35.37	7.44	5.79	17.96	14.13	6.53
pH7b	5.6	0.43	0.73	0.31	0.28	<	3.03	0.75	1.44	2.16	2.37	1.21
pH7c	5.71	0.76	1.15	0.25	0.46	<	2.78	0.79	2.39	2.50	1.53	1.85
pH5a	5.1	-0.76	-0.90	-0.36	-0.45	<	4.44	-0.37	-0.99	2.28	1.92	0.55
pH5b	5.01	0.33	0.45	<	0.19	<	1.53	0.27	1.04	1.47	0.89	1.34
pH5c	5.03	0.39	0.47	<	0.43	<	1.45	0.48	1.00	0.71	0.64	1.85
pH3a	2.98	-0.41	1.81	<	-0.17	<	6.37	1.61	-0.03	4.44	4.75	12.78
pH3b	2.99	0.37	1.15	<	0.21	<	0.12	0.30	1.33	1.16	0.23	1.16
pH3c	2.97	0.12	0.44	<	0.12	<	0.38	0.27	0.44	0.37	0.09	0.83
pH1a	1.01	0.98	4.39	<	1.00	<	-0.04	1.74	0.69	1.15	-0.11	1.51
pH1b	1.02	0.47	0.66	0.33	0.55	<	0.11	0.46	0.80	0.14	0.40	1.28
pH1c	1.01	0.61	0.62	0.09	0.61	<	0.28	0.51	1.12	1.02	-0.03	1.86

Differential solubility for DP230 (unit: %)

	pH	Fe	Al	Si	Ti	Zn	Ca	K	Mg	Mn	Sr	Ba
pH7a	5.56	1.72	1.94	<	0.93	7.36	6.88	6.97	7.99	8.50	4.04	3.12
pH7b	5.56	-0.24	-0.38	<	-0.11	-5.52	-0.13	-0.41	-0.38	0.11	-0.10	-0.41
pH7c	5.43	0.22	0.43	<	0.11	<	0.97	0.74	1.28	1.07	0.58	0.35
pH5a	5.02	0.43	0.35	<	0.16	<	2.24	0.28	2.02	2.97	1.20	0.32
pH5b	4.99	0.42	0.66	<	0.08	<	1.19	0.25	1.70	1.89	0.69	1.18
pH5c	5.02	0.06	-0.04	<	-0.04	<	1.62	0.20	0.40	0.89	0.54	0.24
pH3a	2.98	2.63	2.83	0.28	0.77	11.91	11.44	2.72	5.95	8.20	4.22	6.48
pH3b	2.97	-1.32	-1.17	-0.21	-0.34	0.66	5.61	0.16	-1.07	-2.07	-0.05	1.29
pH3c	2.98	0.85	0.93	<	0.26	-7.20	0.37	0.60	1.16	1.35	0.08	0.65
pH1a	1	0.46	1.85	0.11	0.37	7.08	-5.39	1.88	0.07	-0.78	0.00	0.00
pH1b	1.01	0.40	0.36	-0.08	0.35	4.00	0.07	0.50	0.86	0.35	0.20	0.57
pH1c	1.01	0.37	0.28	<	0.14	14.49	12.33	0.55	0.92	0.46	0.28	2.92

Differential solubility for DP243 (unit: %)

	pH	Fe	Al	Si	Ti	Zn	Ca	K	Mg	Mn	Sr	Ba
pH7a	5.69	0.62	0.34	<	0.40	<	1.40	1.13	<	0.91	0.63	<
pH7b	5.5	0.20	0.77	<	-0.06	4.96	0.74	0.08	0.94	0.22	0.20	<
pH7c	5.59	-0.18	-0.40	<	0.07	-3.72	0.36	0.21	0.28	0.61	0.02	<
pH5a	5.04	0.05	0.14	<	-0.19	<	1.37	0.49	0.59	0.51	0.61	<
pH5b	5.02	0.03	0.06	<	<	<	3.45	0.20	0.31	0.20	0.17	0.58
pH5c	4.99	0.12	0.26	<	<	9.26	1.57	0.18	0.20	0.24	0.17	-0.43
pH3a	2.97	0.09	0.32	<	0.26	9.34	3.34	1.91	0.74	1.18	1.36	1.64
pH3b	2.97	0.14	0.30	<	-0.19	3.94	1.22	0.64	0.37	0.35	0.52	1.29
pH3c	2.97	0.07	0.28	<	<	-0.74	1.54	0.49	0.25	0.49	0.35	0.18
pH1a	1.04	0.61	1.48	0.07	0.53	0.49	31.82	1.61	1.65	0.57	2.10	1.46
pH1b	1.04	0.11	0.17	0.02	0.11	2.05	-25.07	-0.05	-0.43	-0.18	-0.98	0.27
pH1c	1.04	0.20	0.20	0.03	0.12	-1.86	0.61	0.13	0.51	-0.01	0.21	0.38

Differential solubility for DP303 (unit: %)

	pH	Fe	Al	Si	Ti	Zn	Ca	K	Mg	Mn	Sr	Ba
pH7a	5.83	2.54	2.04	0.27	1.06	4.52	27.56	8.99	8.80	29.84	11.79	1.79
pH7b	5.71	1.98	1.49	0.24	0.29	1.57	5.35	1.93	3.37	5.32	2.87	1.40
pH7c	5.75	2.88	2.21	0.50	1.43	8.44	4.34	3.29	4.64	4.68	2.85	2.41
pH5a	5.04	-0.56	-0.39	-0.17	-0.63	-2.66	3.00	-0.28	-0.19	4.27	1.13	0.45
pH5b	4.99	1.00	0.82	0.16	0.45	3.23	2.18	1.43	1.69	2.21	1.18	0.45
pH5c	4.98	0.35	0.31	0.02	0.08	-6.05	0.80	0.51	0.79	1.06	0.32	0.53
pH3a	2.98	0.09	0.27	-0.05	-0.22	13.46	9.02	1.32	1.75	8.91	4.60	3.74
pH3b	2.96	0.98	1.01	0.15	0.23	-3.00	0.27	1.04	1.13	0.96	0.68	0.53
pH3c	2.91	1.13	0.96	0.15	0.30	0.82	0.50	1.17	1.87	0.69	0.97	0.84
pH1a	0.91	0.93	1.53	-0.05	0.10	1.84	-0.24	2.28	-0.39	0.17	-0.33	0.99
pH1b	0.94	2.64	1.62	0.33	0.53	0.97	0.67	2.25	3.42	1.37	1.25	1.22
pH1c	0.94	1.82	1.05	0.20	0.36	1.80	0.11	1.07	2.11	1.01	0.38	0.73

Differential solubility for DP326 (unit: %)

	pH	Fe	Al	Si	Ti	Zn	Ca	K	Mg	Mn	Sr	Ba
pH7a	5.41	2.01	1.76	<	0.59	<	10.50	5.44	8.74	17.46	5.62	4.27
pH7b	5.47	0.30	0.31	<	0.10	<	1.46	0.32	1.10	1.49	0.89	0.91
pH7c	5.47	-0.87	-0.65	<	-0.40	<	0.05	-0.45	-0.65	-0.28	-0.30	-1.40
pH5a	4.89	1.06	0.91	<	0.44	<	3.72	1.26	3.13	5.64	1.84	2.09
pH5b	4.9	-0.37	-0.27	<	-0.10	<	0.69	-0.33	0.04	0.42	0.80	-0.46
pH5c	4.89	0.81	0.82	<	0.27	<	1.68	0.79	1.83	3.43	0.65	1.68
pH3a	2.91	-0.37	-0.10	<	-0.33	<	37.43	-0.67	7.07	-3.26	6.85	1.52
pH3b	2.89	0.34	0.49	<	0.18	<	1.22	0.18	2.57	0.19	0.87	0.86
pH3c	2.91	0.07	0.19	<	-0.14	<	-17.56	1.23	-3.78	6.47	-1.99	2.98
pH1a	0.96	3.20	3.50	0.26	0.82	<	1.33	2.79	2.59	3.23	1.60	3.34
pH1b	0.98	-0.86	-0.43	-0.10	-0.22	<	-0.61	0.01	-0.48	-2.01	-0.99	-0.43
pH1c	1	0.29	0.25	0.00	0.02	<	-0.23	0.30	0.64	0.38	0.13	0.07

Differential solubility for DN006 (unit: %)

	pH	Fe	Al	Si	Ti	Zn	Ca	K	Mg	Mn	Sr	Ba
pH7a	6.09	2.21	2.37	0.20	0.64	15.81	47.45	11.21	8.62	24.99	21.35	7.75
pH7b	6.12	0.22	0.23	0.04	0.12	-0.15	7.11	0.55	1.67	3.24	2.93	-0.06
pH7c	5.94	0.66	0.64	0.08	0.12	-1.25	3.05	1.26	1.99	2.46	2.35	1.76
pH5a	5.22	0.80	0.87	0.09	0.26	10.06	5.39	2.13	2.35	5.47	3.55	3.11
pH5b	5.1	-0.04	0.04	-0.02	-0.01	-0.41	1.68	0.23	0.74	0.23	0.87	-0.17
pH5c	5.1	-0.08	0.17	0.04	0.12	-3.14	1.62	0.51	0.47	4.35	1.10	1.24
pH3a	2.95	-0.28	-0.19	-0.12	-0.17	15.59	6.08	1.29	0.48	2.19	3.96	4.09
pH3b	2.94	0.31	0.38	0.06	0.13	-1.48	-0.56	0.80	0.35	1.97	-0.33	1.28
pH3c	2.93	0.72	0.74	0.07	0.28	0.18	-0.11	1.52	0.97	2.12	0.50	1.75
pH1a	1.01	-0.04	1.28	-0.03	-0.12	2.46	-0.22	2.29	-0.50	-0.57	-0.14	0.98
pH1b	1.01	0.45	0.45	0.05	0.15	-0.20	-0.03	1.26	0.72	1.14	0.26	1.07
pH1c	1.01	3.49	2.10	0.52	1.49	2.23	0.18	2.99	4.80	5.41	0.94	3.51

Ca-rich dust

Differential solubility for DP109 (unit: %)

	pH	Fe	Al	Si	Ti	Zn	Ca	K	Mg	Mn	Sr	Ba
pH7a	5.64	1.72	1.56	<	4.76	<	39.74	3.14	<	35.60	44.42	<
pH7b	5.57	-1.29	0.40	<	-3.57	<	4.36	-0.02	<	4.22	5.09	<
pH7c	5.57	<	0.08	<	<	<	1.60	0.06	<	0.68	2.12	<
pH5a	5.01	<	0.91	<	<	<	2.39	0.17	<	2.30	2.64	<
pH5b	5.02	<	0.00	<	<	<	0.82	0.02	<	1.61	-0.18	<
pH5c	5.03	1.16	1.54	<	<	<	0.66	0.24	<	3.11	3.13	<
pH3a	2.98	-0.87	0.26	<	<	<	4.50	0.47	<	6.36	5.35	<
pH3b	2.99	2.37	2.48	<	<	<	0.02	0.60	9.30	1.97	-0.27	<
pH3c	3	-0.32	0.02	<	<	<	-0.42	-0.13	0.30	-1.81	0.57	<
pH1a	1.06	1.92	3.29	<	<	<	-0.13	0.66	-5.45	0.57	-1.10	<
pH1b	1.05	0.59	0.75	<	<	<	-0.14	0.18	<	0.07	1.07	<
pH1c	1.03	0.48	0.61	<	<	<	-0.08	0.15	<	1.98	-4.72	15.72

Differential solubility for DP115 (unit: %)

	pH	Fe	Al	Si	Ti	Zn	Ca	K	Mg	Mn	Sr	Ba
pH7a	6.36	1.84	1.98	0.31	1.14	<	61.05	28.75	7.24	34.92	37.46	18.37
pH7b	6.31	0.40	0.51	0.08	0.14	<	12.37	1.50	1.01	4.97	4.80	2.11
pH7c	6.12	0.81	0.86	0.12	0.48	<	3.04	2.51	2.18	2.84	3.47	3.52
pH5a	5.47	0.14	0.30	0.05	-0.04	<	-0.79	-0.13	0.66	3.82	-0.17	2.24
pH5b	5.31	0.70	0.76	0.12	0.34	<	3.72	1.90	2.03	2.64	2.46	4.34
pH5c	5.25	-0.35	-0.40	-0.06	-0.13	<	0.47	0.36	-0.42	0.81	0.33	1.36
pH3a	2.99	0.32	0.58	0.04	0.14	6.80	4.31	1.39	1.42	6.36	3.49	11.90
pH3b	2.98	0.71	0.83	0.13	0.24	-5.10	-0.32	0.67	1.25	1.12	0.03	1.77
pH3c	2.98	0.64	0.91	0.16	0.17	<	0.28	0.64	1.40	1.62	0.67	1.64
pH1a	1.02	0.22	2.58	-0.01	0.54	<	0.04	1.91	-0.56	0.17	-0.08	2.07
pH1b	1	0.07	0.28	-0.05	0.21	<	-0.09	0.53	0.19	0.51	-0.04	0.70
pH1c	1.02	0.87	1.49	-0.11	0.54	48.20	29.81	2.91	3.35	1.52	5.40	2.93

Differential solubility for DP219 (unit: %)

	pH	Fe	Al	Si	Ti	Zn	Ca	K	Mg	Mn	Sr	Ba
pH7a	5.6	0.44	1.65	<	<	<	4.59	9.19	3.01	6.81	2.92	<
pH7b	5.62	0.32	0.34	<	<	<	0.69	0.15	0.52	1.25	0.37	<
pH7c	5.57	-0.15	0.20	<	<	<	0.46	0.23	0.41	0.70	0.13	<
pH5a	4.99	0.41	0.71	<	<	<	1.80	0.59	1.26	2.87	1.35	8.70
pH5b	4.99	0.21	0.81	<	<	<	1.13	1.16	1.43	2.29	1.10	-1.50
pH5c	5.01	0.23	0.34	<	<	<	-0.42	-0.14	0.26	-0.37	-0.41	1.44
pH3a	2.97	0.76	2.95	<	<	<	2.38	2.54	2.22	2.81	2.13	15.84
pH3b	2.97	-0.32	0.14	<	<	<	-0.20	0.02	-0.01	0.97	-0.53	-4.13
pH3c	2.98	0.08	0.70	<	0.47	<	0.11	0.22	0.75	0.89	0.20	1.11
pH1a	1.07	0.25	3.40	<	-0.35	<	0.01	1.52	-0.03	-0.19	0.33	2.88
pH1b	1.01	0.26	0.51	<	0.46	<	-0.07	0.56	-1.83	0.03	-1.29	0.20
pH1c	1.01	0.13	0.49	<	-0.35	<	0.05	0.29	<	-0.02	<	0.06

Differential solubility for DP316 (unit: %)

	pH	Fe	Al	Si	Ti	Zn	Ca	K	Mg	Mn	Sr	Ba
pH7a	5.4	4.87	4.42	0.26	2.17	<	75.82	13.98	29.54	44.33	41.92	14.94
pH7b	5.61	0.27	0.49	0.06	0.01	<	5.32	0.78	2.82	1.53	2.49	1.14
pH7c	5.66	0.75	0.82	0.04	0.54	<	1.81	0.79	1.31	2.43	1.13	0.20
pH5a	4.94	0.85	1.13	0.08	0.76	<	1.36	0.52	2.25	2.13	2.24	5.10
pH5b	4.98	0.22	0.24	0.00	-0.48	<	0.09	0.33	0.62	1.47	0.11	-0.78
pH5c	4.92	0.25	0.67	-0.14	0.59	<	2.35	0.48	1.66	1.23	1.20	1.66
pH3a	2.89	-0.30	-0.45	<	-0.38	<	-10.83	5.83	-2.73	36.38	0.47	19.78
pH3b	2.89	0.93	1.19	<	1.21	<	0.05	2.14	0.65	2.02	0.48	3.43
pH3c	2.91	0.74	0.90	0.14	-0.62	27.10	10.43	-2.40	5.84	-16.52	3.94	-8.26
pH1a	0.95	1.62	3.28	0.05	0.67	-20.33	-0.90	0.17	-0.48	-1.31	-0.42	3.94
pH1b	0.98	0.17	0.03	0.05	-0.17	<	-0.59	0.10	0.45	-0.66	-0.35	0.86
pH1c	0.94	0.20	0.27	-0.12	0.29	<	0.09	0.20	0.71	0.26	0.12	-0.48

Differential solubility for DN007 (unit: %)

	pH	Fe	Al	Si	Ti	Zn	Ca	K	Mg	Mn	Sr	Ba
pH7a	6.7	3.61	4.48	0.98	2.03	5.12	86.60	20.06	17.49	12.68	75.98	4.90
pH7b	6.49	2.37	3.56	0.87	1.41	5.40	6.71	3.96	7.79	8.55	3.30	3.55
pH7c	6.43	1.06	1.83	0.27	0.33	2.97	-0.35	1.65	2.96	1.07	1.16	2.65
pH5a	5.63	1.08	1.69	0.40	0.66	3.01	0.28	2.20	3.40	5.91	0.55	0.85
pH5b	5.44	-1.28	-1.90	-0.48	-0.70	-7.82	0.86	-1.21	-2.76	-5.27	-0.36	-1.73
pH5c	5.27	0.36	-0.08	0.03	-0.04	<	0.82	0.18	0.09	2.44	0.50	-2.58
pH3a	2.94	1.54	2.36	0.22	2.52	10.37	1.84	3.95	4.29	4.97	3.53	6.62
pH3b	2.95	-0.65	0.83	0.19	-1.46	10.17	-0.28	0.88	1.56	1.93	0.39	0.34
pH3c	2.95	-0.68	-0.67	-0.48	-0.69	2.04	-0.13	-0.48	-1.43	-0.19	-0.29	-0.25
pH1a	1.04	4.33	4.98	1.81	2.72	-3.90	-0.94	5.00	5.10	4.52	0.06	6.37
pH1b	1	0.77	1.25	0.25	0.71	0.93	0.25	1.56	2.03	2.56	0.40	1.17
pH1c	1	-1.09	-0.89	-0.71	-0.78	-5.04	0.06	-0.39	-1.05	-1.13	-0.09	0.65

List of figures

List of tables

QU Zihan – Thèse de doctorat – Année 2015

Caractérisation chimique de l'aérosol continental transporté sur l'Océan Austral: Sources patagonienne et namibienne

Résumé :
L'aérosol minéral est un vecteur important de micronutriments pour l'océan Austral. La production primaire de l'océan Austral est limitée par un approvisionnement insuffisant de micronutriments. Patagonie (Amérique du Sud) et la Namibie (Afrique australe) sont les deux principales sources de poussière pour la section Atlantique Sud de l'océan Austral. Flux des émissions de micronutriments biodisponibles de ces deux régions régulent l'impact biologique final sur l'écosystème marin dans l'océan Atlantique Sud.
L'objet de cette thèse est d'étudier 1) la concentration atmosphérique de la poussière et de sa variation temporel en Patagonie, 2) l'hétérogénéité spatiale de composition élémentaire de poussière en Patagonie et en Namibie, et 3) la dépendance de pH de la solubilité élémentaire dans la poussière de Patagonie et de la Namibie. Ces trois aspects sont les principaux enjeux pour modéliser les inventaires des émissions de micronutriments biodisponibles à partir de sources de poussière.
Des mesures de concentration en poussière ont été menées sur la côte Atlantique de la Patagonie et montrent une variation saisonnière de la concentration de poussière avec un niveau plus bas en hiver que pour les trois autres saisons. Les données météorologiques suggèrent que cette variation saisonnière est associée à la variation de l'humidité du sol dans les zones source plutôt qu'à la vitesse du vent. Des échantillons d'aérosol minéral ont été générés à partir des sols de Patagonie et de Namibie afin d'en caractériser la composition élémentaire et la solubilité élémentaire. La composition élémentaire des poussières diffère à différents degrés de celles des sols parents, en particulier en Namibie en raison de l'effet de dilution par le quartz dans les sols. On a observé la variabilité spatiale de composition élémentaire aux échelles continentale et régionale en Patagonie et Namibie. Les variations de Ca et Mg sont les principales raisons conduisant à l'hétérogénéité spatiale de la composition élémentaire des poussières. Les solubilités élémentaires des aérosols minéraux de Patagonie et de Namibie augmentent avec l'acidité de la solution altérante. Les poussières riches en calcium présentent une solubilité plus élevée pour les éléments les plus solubles à savoir Ca, K, Mg, Mn, Sr et Ba en raison de la présence de carbonate.
Le suivi de la concentration en poussières obtenu en Patagonie peut aider à mieux en quantifier les émissions dans la région subantarctique et ainsi à mieux contraindre les modèles. La base de données que nous avons obtenue sur les poussières et leur solubilité contribue également à l'évaluation des émissions d'éléments solubles dans la région Australe.

Mots clés : aérosol minéral; micronutriment; Patagonie; Namibie; Océan Austral; concentration atmosphérique; composition élémentaire; solubilité

Chemical properties of continental aerosol transported over the Southern Ocean: Patagonian and Namibian sources

Abstract:
Mineral dust is considered to be an important supplier of micronutrient for the Southern Ocean where the primary production is limited by insufficient supply of micronutrients. Patagonia (South America) and Namibia (Southern Africa) are two main dust sources for the South Atlantic section of the Southern Ocean. Emission inventories of bioavailable micronutrients from these two regions regulate the final biological impact on marine ecosystem in the South Atlantic Ocean.
This thesis is mainly focused on the investigation of 1) the atmospheric dust concentration and its temporal pattern in Patagonia, 2) the spatial heterogeneity of dust elemental composition in Patagonia and Namibia, and 3) the pH dependence of elemental solubility in Patagonian and Namibian dust. These three aspects are the key issues to model the emission inventories of bioavailable micronutrients from dust sources.
Dust concentration measurements were conducted in Patagonia-Atlantic Coast and revealed a seasonal pattern of dust concentration with lower dust level in winter than the other three seasons. Meteorological records suggest that this seasonal pattern is associated with the variation of soil moisture in source areas rather than the recurrently high wind speed. Dust samples were generated from Patagonian and Namibian soils to investigate the elemental composition and the elemental solubility of source dust. Dust elemental composition differs to different degrees from their parents soils, particularly in Namibia due to the dilution effect of quartz in soil. Spatial variability of dust elemental composition was observed at both continental scale and regional scale in Patagonia and Namibia. Variations in Ca and Mg content are the main reasons for the spatial heterogeneity of dust elemental composition. Elemental solubility of Patagonian and Namibian dust increased with acidity of leaching solution. More soluble elements namely Ca, K, Mg, Mn, Sr and Ba showed much higher solubility in calcium-rich dust due to the presence of carbonate.
The dust concentration record obtained in Patagonia may help to better quantify the dust emission in subantarctic region and to constrain dust models. Database of dust elemental composition and elemental solubility in Patagonia and Namibia also contributes to the evaluation of emission inventories of soluble elements from dust sources to the Southern Ocean.

Keywords: Mineral dust; micronutrient; Patagonia; Namibia; Southern Ocean; atmospheric concentration; elemental composition; solubility.